

Identifying genes underlying *Fusarium* and mycotoxin susceptibility in *Brachypodium distachyon*

Elizabeth Anna Bankes-Jones

Doctor of Philosophy (PhD)

University of East Anglia (UEA)

Department of Crop Genetics, John Innes Centre

March 2021

© This copy of the thesis has been supplied on condition that anyone who consults it is understood to recognise that its copyright rests with the author and that use of any information derived therefrom must be in accordance with current UK Copyright Law. In addition, any quotation or extract must include full attribution.

Abstract

Fusarium head blight (FHB) is a widespread fungal disease of temperate, small-grain cereals. Infection leads to reduced yield and mycotoxin accumulation in grain. Chemical controls have limited effect and genetic resistances are typically quantitative and environmentally sensitive. *Brachypodium distachyon* (Bd) has been demonstrated as a model for cereal-*Fusarium* interactions and is a powerful genetic tool due to having a small, diploid genome, high recombination rate and a pan-genome sequence of 54 diverse accessions.

These Bd accessions were characterised for variation in susceptibility to FHB, flowering time, height and trichomes. A recombinant inbred line (RIL) population, ABR6 x Bd21, was characterised for susceptibility to FHB and lemma trichome phenotype. A coincident QTL for FHB resistance and absence of trichomes was identified on Bd chromosome four. It was hypothesised that trichome basal cells are exploited as points of infection for *Fusarium* species. Fine mapping refined the position of the trichome trait to a physical region containing five annotated genes in Bd21. Expression and sequence analysis identified an ATP-dependent CLP protease as the best candidate gene. CRISPR mutagenesis was unsuccessful, without which it was not possible to determine whether the relationship between FHB and trichomes is causative or pleiotropic.

Concentration dependent root elongation and inhibition in response to deoxynivalenol (DON) had been previously observed in Bd. DON sensitivity of Bd accessions was characterised using root assays. A novel root branching phenotype was identified in accession Bd2-3, and the Bd2-3 x Bd21 RIL population characterised at two DON concentrations. A region on Bd chromosome 1 was identified to be associated with DON sensitivity, refined to a region of 56 genes using bulked segregant analysis and RNAseq among which four were differentially DON-responsive between the two accessions indicating that one or more may be responsible for the observed difference in DON response.

Access Condition and Agreement

Each deposit in UEA Digital Repository is protected by copyright and other intellectual property rights, and duplication or sale of all or part of any of the Data Collections is not permitted, except that material may be duplicated by you for your research use or for educational purposes in electronic or print form. You must obtain permission from the copyright holder, usually the author, for any other use. Exceptions only apply where a deposit may be explicitly provided under a stated licence, such as a Creative Commons licence or Open Government licence.

Electronic or print copies may not be offered, whether for sale or otherwise to anyone, unless explicitly stated under a Creative Commons or Open Government license. Unauthorised reproduction, editing or reformatting for resale purposes is explicitly prohibited (except where approved by the copyright holder themselves) and UEA reserves the right to take immediate 'take down' action on behalf of the copyright and/or rights holder if this Access condition of the UEA Digital Repository is breached. Any material in this database has been supplied on the understanding that it is copyright material and that no quotation from the material may be published without proper acknowledgement.

Acknowledgements

My funding was provided by UK Research and Innovation via the Innovate UK Knowledge Transfer Network CASE program, with partnership with BASF SE.

Firstly, I would like to thank my supervisor Prof. Paul Nicholson for the opportunity, guidance, encouragement, and support, especially over the last year. I am also grateful to my secondary supervisor, Dr Matt Moscou, for many words of guidance on the project.

I will always be grateful to Nicholson and Brown groups members past and present for welcoming and helping me over the years; special thanks to Andy Steed, Martha Clarke, Marianna Pasquariello, Antoine Peraldi, Laetitia Chartrain and Rachel Goddard for sharing their expertise. I would also like to thank the following people who have helped me with the project: the JIC Horticultural services team, Martin Trick and Burkhard Steuernagel for bioinformatic assistance and guidance, Abraham Gomez Gutierrez and Asli Yalcin for guidance in BSA analysis, Andy Davis and Phil Robinson from JIC Photographic services. For allowing me to carry out nanopore sequencing: Darren Heavens for help with DNA extraction and size selection, Ned Peel for help with library preparation and sequencing and Matt Moscou for assembly of data.

I would like to thank members of the fungicide development department at BASF Limburgerhof for supporting me during a CASE placement, most notably Sylvia Luib and my supervisors Dr Egon Haden and Dr Sebastian Rohrer.

Finally, I would like to thank my fellow students, Miguel, Ben, John, Lola and Cyrielle for making my time at JIC thoroughly enjoyable. Thank you to Colwyn Thomas for encouraging my love of plant research during my previous studies at UEA. Last but not least, I am extremely grateful for the love and support of my family, and to my partner in life Ned Peel.

Abbreviations

At	<i>Arabidopsis thaliana</i>
AUDPC	area under disease progress curve
BCI	Bayes credible interval
Bd	<i>Brachypodium distachyon</i>
BLAST	basic local alignment search tool
BLUP	best linear unbiased predictor
bp	base pair
BSA	bulked segregant analysis
CER	controlled environment room
CIM	composite interval mapping
cm	centimetre
cv	cultivar
cM	centimorgan
Cq	quantitative cycle
CRISPR	clustered regularly interspaced short palindromic repeats
CTAB	cetyl trimethyl ammonium bromide
DEPC	diethyl pyrocarbonate
dH ₂ O	sterile deionised water
DNA	deoxynucleic acid
DON	deoxynivalenol
dpi	days post inoculation
EDTA	ethylenediaminetetraacetic acid
Eff	Efficiency of primer
EM	electron micrograph
EMBL-EBI	European Molecular Biology Laboratory, European Bioinformatics Institute
EtBr	ethidium bromide
F	forward
Fc	Fusarium culmorum
FHB	Fusarium head blight
FIJI	FIJI is just ImageJ
GA	gibberellic acid
GLM	generalized linear model
GO	gene ontology
GxP	genotype by phenotype (plot)
hr	hour
Hv	<i>Hordeum vulgare</i>
HYG	hygromycin resistance gene
IAA	3-indole acetic acid
INDEL	insertion or deletion
IPTG	Isopropyl β -D-1-thiogalactopyranoside
KASP	kompetitive allele specific PCR

kb	kilo base pair
L	litre
LB	Luria-Bertani
LOD	log of the odds (base 10)
M	molar
Mbp	mega base pair
MDS	multidimensional scaling
min	minute
mL	millilitre
mM	millimolar
NaN ₃	sodium azide
ng	nanogram
PacBio	Pacific Biosciences
PCR	polymerase chain reaction
PE	paired end
PT	permutation threshold
PVE	percentage variance explained
QTL	quantitative trait locus
qRT-PCR	quantitative reverse transcription polymerase chain reaction
R	reverse
REML	linear mixed model
rep	replicate
RIL	recombinant inbred line
RIN	RNA integrity number
RNA	ribonucleic acid
RNASeq	RNA sequencing
SDS	sodium dodecyl sulfate
SE	standard error
sgRNA	single guide RNA
SIM	genome scan
SNP	single nucleotide polymorphism
TIBA	triiodobenzoic acid
TILLING	targeted induced local lesions in genomes
T _m	melting temperature (°C)
TPM	transcripts per kilobase million
TSL	The Sainsbury Laboratory, Norwich
USDA	United States department of agriculture
°C	degrees Celsius
µL	microlitre
µM	micromolar

Contents

Abstract	i
Acknowledgements	ii
Abbreviations	iii
Contents	v
List of Tables	lix
List of Figures.....	xii
1 Chapter 1 - General Introduction	1
1.1 Cereal Crops.....	1
1.2 <i>Fusarium</i> Head Blight and other <i>Fusarium</i> diseases of cereals.....	1
1.3 Economic Cost.....	2
1.4 Infection, symptoms, and tissues affected.....	2
1.5 Causal species & mycotoxins.....	5
1.6 Control measures for FHB.....	7
1.6.1 Chemical controls.....	7
1.6.2 Alternative controls.....	8
1.6.3 Genetic resistance.....	9
1.7 <i>Brachypodium distachyon</i> as a model.....	10
1.7.1 <i>Brachypodium</i> as a pathosystem.....	13
1.7.2 <i>Brachypodium</i> resources.....	14
1.8 Research objectives.....	17
2 Chapter 2 - Assessing natural variation in <i>Fusarium</i> head blight susceptibility of <i>Brachypodium distachyon</i>	19
2.1 Introduction.....	19
2.1.1 Chapter aims.....	20
2.2 Methods.....	21
2.2.1 Characterisation of Bd accessions under glasshouse conditions.....	21
2.2.2 Further characterisation of a subset of Bd accessions under controlled conditions.....	24
2.3 Results.....	26
2.3.1 Characterisation of Bd accessions under glasshouse conditions.....	26
2.3.2 Further characterisation of a subset of Bd accessions under controlled conditions.....	40
2.4 Discussion.....	45
2.4.1 Natural variation of FHB susceptibility in Bd.....	45
2.4.2 FHB and Flowering time.....	46
2.4.3 FHB and Height.....	49
2.4.4 FHB and Trichomes.....	51

2.4.5	Further characterisation of a subset of Bd accessions under controlled conditions	52
3	Chapter 3 - Identification of QTL associated with FHB, height, and lemma trichome in ABR6 x Bd21	55
3.1	Introduction.....	55
3.2	Methods.....	57
3.2.1	Plant materials.....	57
3.2.2	<i>Fusarium</i> inoculation	57
3.2.3	Phenotyping	58
3.2.4	Data analysis, statistics, and QTL mapping	58
3.3	Results	61
3.3.1	Characterisation of ABR6 x Bd21 F9 for FHB susceptibility	61
3.3.2	Height distribution, and correlation with FHB	66
3.3.3	QTL mapping of ABR6 x Bd21 population	67
3.4	Discussion	76
3.4.1	Is there a genetic link between lemma trichomes and FHB?.....	76
3.4.2	Characterisation of ABR6 x Bd21	77
3.4.3	Height.....	79
3.4.4	FHB QTL	79
3.4.5	Trichome QTL	81
3.4.6	Concluding remarks.....	83
4	Chapter 4 - Fine mapping of lemma trichome as a potential FHB susceptibility trait.....	84
4.1	Introduction.....	84
4.2	Methods.....	86
4.2.1	Plant material and growth conditions	86
4.2.2	Refinement of interval – exploiting F4-5 heterozygous families.....	86
4.2.3	Expression analysis of candidate genes	90
4.2.4	Comparison of candidate regions <i>in silico</i>	94
4.2.5	Community Bd mutant materials.....	95
4.2.6	Disruption of candidate gene Bradi4g22650 using CRISPR in Bd21. 95	
4.2.7	Assessment of CRISPR lines to identify transformants (HYG) and target-site edits	101
4.3	Results	103
4.3.1	Exploiting F4-5 heterozygous families to refine candidate region....	103
4.3.2	Expression analysis of candidate genes	105
4.3.3	Comparison of Bd21, ABR6 and Bd1-1 candidate region <i>in silico</i> ... 108	
4.3.4	ABR6 and Bd1-1 orthologues of Bradi4g22650 are predicted to have truncated proteins.....	116
4.3.5	Other Bd mutant material.....	117
4.3.6	Disruption of Bradi4g22650 using CRISPR/Cas9	118

4.4	Discussion	120
4.4.1	Trichome candidate interval refined to five genes	120
4.4.2	Bradi4g22651	121
4.4.3	Bradi4g22641	122
4.4.4	Bradi4g22645	123
4.4.5	Bradi4g22637	124
4.4.6	Bradi4g22650	125
4.4.7	Concluding remarks and future work	129
5	Chapter 5 - Characterisation and mapping of DON responsive root development in <i>Brachypodium distachyon</i>.....	130
5.1	Introduction.....	130
5.1.1	Previous work.....	131
5.1.2	Chapter Aims.....	131
5.2	Methods.....	132
5.2.1	Plant materials.....	132
5.2.2	Characterisation of Bd accessions; DON responsive root development	132
5.2.3	DON head assay	133
5.2.4	Induction of Bd2-3 root branching phenotype by other compounds?	133
5.2.5	Characterisation of Bd2-3xBd21 population for DON sensitivity in roots	134
5.2.6	KASP mapping of DON root sensitivity	135
5.2.7	Bulked Segregant Analysis by Next-Generation Sequencing.....	135
5.2.8	Fine mapping of Bd1L BSA interval	137
5.2.9	RNAseq analysis of Bd2-3 and Bd21 in response to DON.....	138
5.3	Results	140
5.3.1	Brachypodium accessions vary in response/sensitivity to DON	140
5.3.2	DON sensitivity in floral tissues (Bd2-3 vs Bd21)	142
5.3.3	Do other stress treatments induce root branching in Bd2-3?.....	144
5.3.4	Characterisation of Bd2-3xBd21 population for DON sensitivity.....	145
5.3.5	Identification of region associated with DON sensitivity	150
5.3.6	Bulked segregant analysis for extreme DON sensitivity RILs of Bd2-3 x Bd21	152
5.3.7	RNAseq - analysis of Bd2-3 and Bd21 response to DON	161
5.4	Discussion	172
5.4.1	Why map a DON induced root branching phenotype in a model grass species?.....	172
5.4.2	There is natural variation in DON responsive root development in Bd	172
5.4.3	Bd2-3 and Bd21 vary in response to DON in a non-tissue-specific way	173

5.4.4	Characterisation of Bd2-3xBd21 population to DON sensitivity.....	175
5.4.5	Identification of loci associated with DON sensitivity using mapping (KASPs)	177
5.4.6	Bulked segregant analysis for extreme DON sensitivity RILs of Bd2-3 x Bd21 population identifies 56-gene candidate region.....	178
5.4.7	Genes of most interest in the Bd1L candidate interval	179
5.4.8	RNAseq for comparison of DON responsive genes in Bd21 and Bd2-3	184
5.4.9	Fine mapping of Bd1L candidate interval.....	185
5.4.10	Concluding Remarks	185
6	Chapter 6 - General Discussion.....	187
6.1	Extensive FHB resistance variability in Bd	188
6.2	No association of height with FHB	189
6.3	Major FHB effect identified on Bd4	190
6.4	Association of FHB with lemma trichomes	190
6.5	DON sensitivity	193
6.6	Major DON sensitivity effect identified on Bd1	194
	References	198
	Appendix	214

List of Tables

Table 2.1 Details of inoculation batches for glasshouse characterisation trial of diverse <i>Brachypodium</i> accessions, in chronological order. *Inoculations failed, an extra inoculation was applied	23
Table 3-1 Summary of QTL identified through the characterisation of ABR6 x Bd21 population (F9) using composite interval mapping. *PT= permutation threshold, BCI= Bayes credible interval	75
Table 3-2 <i>Brachypodium distachyon</i> genes orthologous to key trichome development in <i>Arabidopsis</i>	82
Table 4-1 KASP primers used for the genotyping of ABR6 x Bd21 F4-5 RILs. Polymorphism listed in lower case. 5' tags are F1 = VIC, F2 = FAM.....	89
Table 4-2 Reaction components for cDNA synthesis	91
Table 4-3 Reaction conditions for qPCR expression quantification of lemma trichome candidate genes	92
Table 4-4 qPCR primers used for the specific amplification of lemma trichome candidate genes	93
Table 4-5 Primers for CRISPR Level 0 sgRNA plasmid construction. sgRNA1 and sgRNA2 relate to the two target sites.	96
Table 4-6 Reaction components for Level 0 assembly. A separate reaction was prepared for each guide/target. Final reaction volumes = 25 µL	97
Table 4-7 Level 0 construction cycle conditions for Bradi4g22650 CRISPR plasmid construction using Q5 High-Fidelity DNA Polymerase	97
Table 4-8 Digestion-Ligation reaction components for assembly of Level 1 plasmids for Bradi4g22650 CRISPR	98
Table 4-9 Digestion-Ligation reaction conditions for assembly of Level 1 plasmids for Bradi4g22650 CRISPR.....	98
Table 4-10 Primers used for sequencing Level 1 and Level 2 construct vectors for disruption of Bradi4g22650 by CRISPR/Cas9	99

Table 4-11 Digestion-Ligation reaction components for assembly of Level 2 plasmids for Bradi4g22650 CRISPR	100
Table 4-12 PCR conditions for the amplification of Bradi4g22650 CRISPR target-edit sites in T ₂ transformed lines. *annealing temperature decreasing 0.5 °C per cycle for 16 cycles.	102
Table 4-13 Annotated function of trichome candidate genes and orthologues in Arabidopsis thaliana and Hordeum vulgare. *Top hit BLASTP orthologue using EnsemblPlants, assembly TAIR10 for At and IBSC_v2 for Hv. "-=" no BLAST hits	110
Table 4-14 Loci of lemma trichome candidate genes in ABR6 and Bd1-1 Brachypan-genomes. Locus for non-annotated genes were identified using BLAST (Phytozome).....	111
Table 4-15 Summary of sequence comparison and expression analysis of five Bd21 v3.1 genes annotated in candidate region for lemma trichome phenotype, between Bd21, ABR6 and Bd1-1 accessions.	115
Table 5-1 Chemical treatments and concentrations to assess stress responses of Bd2-3 root development	134
Table 5-2 Pools of Bd21xBd2-3 RILs F1-x, F7-1 used for bulked segregant analysis of DON sensitivity in Brachypodium distachyon roots.	136
Table 5-3 Genes in BSA chromosome Bd1 peak and the variants within each with bulk frequency ratio (BFR) >7 for DON sensitivity in Bd2-3xBd21 F7 high-confidence Bd21-like and Bd2-3-like pools. Bd1 position applies to Bd21v3.1 bp locus on chromosome one.....	156
Table 5-4 Genes annotated in Bd21 v3.1 within the 56 gene BSA candidate interval in association with DON sensitivity from high-confidence Bd2-3 x Bd21 RILs.....	157
Table 5-5 RNAseq data for comparison of Bd2-3 relative to Bd21, genes included have a Log ₂ fold change >1, from within the 56 gene candidate DON interval on Bd1L. FDR = false discovery rate Error! Bookmark not defined.	
Table 5-6 Genes annotated in Bd21 v3.1 in fine-mapped candidate region for DON sensitivity in Bd2-3xBd21 F7 RIL population, defined by fine-mapping	

markers Bd1L_69696725 and Bd1L_ (Bd21v2 bp nomenclature). At =
Arabidopsis thaliana 168

Table 5-7 Intragenic variants within DON sensitivity candidate interval identified from
RNAseq experiment comparing Bd21 and Bd2-3 response to DON at 6 hrs.
Locus is bp position Bd21 v3.1 chromosome 1. Variant effect position
applied to Bd21 v3.1 annotated protein 169

Table 6-1 Wheat orthologues of Bd candidate genes..... 197

List of Figures

- Figure 1-1 Life-cycle summary of *F. graminearum* (sexual stage, *Gibberella zeae*). *F. culmorum* is limited to asexual reproduction only Taken from publication: (Trail, 2009)..... 3
- Figure 1-2 Symptoms of *Fusarium* infection; A, bleached heads resulting from vasculature damage by root or stem rot; B, pink discoloration of basal nodes in stem infection, taken from publication (Scherm et al., 2013) 5
- Figure 1-3 LHS, divergence times of cereal crop species sorghum, wheat rice and model genus *Brachypodium*. WGD, whole-genome duplication. The numbers refer to the predicted divergence times measured as Myr ago; RHS, Orthologous gene relationships between *Brachypodium* and hexaploid bread wheat defined by 5,003 ESTs mapped to wheat deletion bins. Each set of orthologous relationships is represented by a band that is evenly spread across each deletion interval on the wheat chromosomes. Figure adapted from publication: International *Brachypodium* Initiative (2010)..... 12
- Figure 1-4. Comparison of wheat, *Brachypodium distachyon* and *Arabidopsis thaliana* root systems. Horizontal line represents soil level. Abbreviations: CNR, coleoptile node axile root; LNR, leaf nod axile root; PR, primary axile root;; SNR, scutella node axile root. (Catalan et al., 2014). 13
- Figure 1-5. Visual comparison of *Fusarium* head blight symptoms between wheat and *Brachypodium distachyon*. (Peraldi et al., 2011)..... 14
- Figure 1-6 Geographical distribution of *Brachypodium* germplasm collection sites, from a representation of the native range. Colour of marker described clade of origin (Gordon, Contreras-Moreira et al. 2017) 15
- Figure 2-1 *Brachypodium* tiller spray inoculated with *F. culmorum* conidial suspension. To illustrate the saturation of floral tissues during inoculation. 22
- Figure 2-2 Example *Fusarium* infection phenotypes from accessions characterised under glasshouse conditions. Accessions left-right: ABR6, ABR7, BdTR12C and Jer-1. D, arrow highlights non-spreading browning lesion. 27
- Figure 2-3 Variation in mean FHB susceptibility between inoculation batches for 2017 glasshouse spray experiment. Bars = Mean FHB percentage score at 10

dpi for each inoculation batch in date order. Points = Mean FHB score per accession, within an inoculation batch. Number of replicate plants per accession varied between batch depending on the number at correct developmental stage.	28
Figure 2-4 Mean FHB susceptibility (10 dpi) of Bd diverse accessions within inoculation batches of 2017 glasshouse experiment. Error bars = ± 1 SE	29
Figure 2-5 FHB AUDPC predicted mean score for 54 Bd natural accessions. Error bars= ± 1 SE FHB score = Back transformed BLUPs resulting from REML analysis of AUDPC data.	30
Figure 2-6 <i>Brachypodium distachyon</i> accessions vary in height, example photographs (Left = Adi-9, Right=BdTR13C)	31
Figure 2-7 Distribution of predicted mean height of <i>Brachypodium</i> accessions under glasshouse conditions. Error bars = ± 1 SE	32
Figure 2-8 Correlation between height at flowering and mean FHB score (AUDPC, BLUPs) for a panel of 54 Bd accessions characterised under glasshouse conditions. A, Trendline prepared using Loess method, grey area = 95 % confidence interval, B, Points coloured by inoculation batch, each with trend line prepared using Linear Model method. There may are >1 data point for accessions in multiple batches.	33
Figure 2-9 Distribution of flowering time (based on heading date) for 54 diverse accessions of <i>Brachypodium distachyon</i> under glasshouse conditions (16 hr daylength), with six weeks vernalisation. Date off first emergence of immature flower heads was recorded for eight replicate plants per accession. Error bars = ± 1 SE	35
Figure 2-10 Correlation between flowering time and FHB susceptibility for a panel of 54 Bd accessions characterised under glasshouse conditions. Flowering time is presented as the mean number of days post vernalisation that emergence of immature floral spikes were observed, per accession. Trendline prepared using Loess method, grey area = 95 % confidence interval	36
Figure 2-11 Correlation between mature height (of primary spike) and flowering time of a panel of 54 Bd accessions under glasshouse conditions (16hr day length, 6 weeks vernalisation). Trendline prepared using Loess method, grey area = 95% confidence interval	36

- Figure 2-12 Photographs of Bd floral heads differing in lemma trichome phenotype. A, Bd21, B, ABR6 Taken by Phil Robinson (JIC photography service) .. 37
- Figure 2-13 FHB susceptibility by lemma trichome phenotype of *Brachypodium distachyon* panel of diverse accessions. Means presented as bars, individual accession means presented as points within each lemma trichome phenotype. Data: A, raw arithmetic means of FHB. B, FHB AUDPC BLUP, adjusted by REML analysis..... 38
- Figure 2-14. Lemma trichome absence overlaid on phylogeny of *Brachypan* accessions. Adapted from *Brachypan*. Crossed through accessions (red) were not phenotyped due to being unobtainable. 39
- Figure 2-15 Percentage of infected florets for five Bd accessions after 11dpi with *F.culmorum* spray inoculation, ordered by relatedness. Error bars= ± 1 SE. Below: mapping populations available with parents, Bd1-1, Bd21, ABR6, Luc-1 and Foz-1 arranged to span dendrogram (arm size not representative of genetic distance)..... 42
- Figure 2-16. ABR6 and Bd21 differential FHB susceptibility under controlled conditions a, Photograph of ABR6 (left) and Bd21 (right) infected with FHB after 17 dpi, and disease scores at 11- and 17- dpi. Bd21 shows greater coverage of bleaching and lesions. b: 11 dpi and 17 dpi, GLM predicted means cabinet FHB, Error bars= ± 1 SE..... 43
- Figure 2-17 Foz-1 x Luc-1 differential FHB infection when characterised under controlled conditions, scored at 11- and 17- dpi..... 44
- Figure 3-1 Representative FHB phenotypes for ABR6 x Bd21 RIL population (replicate experiment 1). Upper; typical symptoms of resistant parent, ABR6, and susceptible parent, Bd21. Lower; example disease scale composed of images of progeny lines, ranging from no visible symptoms, through increasing numbers of necrotic florets, to bleaching spikelets above infection points..... 61
- Figure 3-2 Histogram, mean FHB susceptibility of ABR6 and Bd21 in four replicate experiments for the characterisation of ABR6 x Bd21 F8 RIL population. FHB susceptibility score = means of back-transformed BLUPs obtained from analysis of AUDPC data. Error bars= ± 1 SE..... 62
- Figure 3-3 FHB distribution of 104 ABR6 x Bd21 RILs of combined AUDPC data from three replicate experiments (1-3, 4 excluded). Mean score highlighted by dashed line..... 64

- Figure 3-4 Distribution of predicted mean (BLUP) FHB scores for ABR6 x Bd21 RIL population (F1-x, F9-1). Data shown= back-transformed BLUPs obtained from REML analysis of AUDPC FHB data. Error bars = ± 1 SE 65
- Figure 3-5 Mature height summary for ABR6 x Bd21 F9 RIL population. Above: Distribution of height (cm) BLUPs. Dashed line is height mean=25.16 (SE=3.00). Below: Correlation between BLUP mature height (cm) and BLUP FHB AUDPC data for ABR6 x Bd21 F9 RIL population. Fit of line by linear method, $R^2=0.0042$ ($y=0.0173x+24.738$), grey= 95% confidence interval. 66
- Figure 3-6 Summary of ABR6 x Bd21 F8 genetic map, genotype by Jan Bettgenhaeuser (Unpublished). A, Centimorgan based location of each of the 169 spread over five Bd chromosomes, B, Missing genotypes per marker, C, Matrix of size (tot.mar x tot.mar); the diagonal contains the number of typed meioses per marker, the lower triangle contains the estimated recombination fractions, and the upper triangle contains the LOD scores (testing rf = 0.5)..... 67
- Figure 3-7 FHB susceptibility QTL summary for ABR6 x Bd21 F9 population summary. A: QTL plot of FHB SIM from AUDPC back transformed BLUPs. B: QTL plot of FHB CIM from AUDPC back transformed BLUPs. C: GxP plot for FHB QTL peak marker Bd4_27278128, showing mean FHB AUDPC scores for AA (ABR6 allele), AB (heterozygous) and BB (Bd21 allele) for ABR6 x Bd21 F9 RIL population. 69
- Figure 3-8. Photographs of ABR6 and Bd21 seeds displaying difference in lemma trichome phenotype. A, ABR6, B, Bd21. Courtesy of Jan Bettgenhaeuser. 71
- Figure 3-9 Distribution of lemma trichome presence-absence in ABR6 x Bd21 F9 population (104 RILs) 71
- Figure 3-10 Lemma trichome QTL summary for ABR6 x Bd21 F9 RIL population. A: QTL plot, SIM, non-parametric model, B: Lemma trichome QTL by CIM, non-parametric model. C: Genotype x Phenotype plot for lemma trichome phenotype at QTL peak marker Bd4_27278128 for ABR6 x Bd21 F9 RIL population, for AA (ABR6 allele), AB (heterozygous) and BB (Bd21 allele) for ABR6 x Bd21 F9 RIL population..... 73
- Figure 3-11 Height (cm, BLUP) SIM QTL summary in ABR6 x Bd21 F9 RIL population. Above: QTL peaks in association with height, of 169 markers. Below: GxP

plots for peak markers Bd1_47377165 and Bd5_25818174, genotypes:
AA= ABR6, BB=Bd21, AB = heterozygous 74

Figure 4-1 Illustration to summarise status of fine-mapping of *B. distachyon* chromosome four undertaken previously by collaborators, Jan Bettgenhaeuser, Matthew Moscou and Daniel Woods (Unpublished).... 84

Figure 4-2 Approximate locations of KASP markers to delineate the location of unresolved recombination events in ABR6 x Bd21 F4 RILs. A, Genotype data from Bettgenhaeuser et al. (2017) for markers surrounding the candidate region . B, loci of new markers designed within the region 87

Figure 4-3. Brachypodium floral meristem; A: Image showing example floral meristem dissected from ABR6 of typical developmental stage harvested for expression analysis. B: Electron micrograph showing awn initiation stage in wild type Bd21 with floral organ growth in the terminal spikelet more advanced in basal florets compared with apical florets (Derbyshire and Byrne, 2013)..... 90

Figure 4-4 Loci of sgRNA designed for the disruption of Bradi4g22650 as a candidate for lemma trichome related factor. A; Illustration of sgRNA loci (pink) on Bradi4g22650. B; Genomic sequence of Bradi4g22650.1 (Bd21 v3.1 reference) exon 2 with highlighted protospacer adjacent motifs (PAMs, grey), guide (teal) and target cleavage site (grey)..... 96

Figure 4-5 Schematic of binary vector (Level 2) delivered to Bd21. Transcriptional units were assembled into backbone x using Golden Gate Cloning. A hygromycin resistance cassette (hygromycin phosphotransferase II, hptII) was driven by ZmUbi promoter and terminated by ZmNosT. Cas9=ProUbi-WheatCas9-Porcine2A-Histone2A-GFP-NosT. Endlinker=pELE-4 Addgene #48019 from Icon Genetics. Guide 1 & 2 refer to sgRNA1 and sgRNA2..... 99

Figure 4-6 Refinement of lemma trichome candidate region using F4-5 lines unresolved in F8 map. A, Approximate locations of KASP markers to delineate the location of unresolved recombination events in ABR6 x Bd21 RILs. B, Summary of genotype and phenotype allocations for ABR6 x Bd21 F4-5 RILs for six lines with previously unresolved recombination events between F4 and F8 genetic maps. Only RIL F1-97 (F5 progeny) were genotyped with marker Bradi4g22653, following identification of recombination event between Bradi4g22651 and Bradi4g22656. 104

- Figure 4-7 Bd21v3.1 gene content for refined lemma trichome candidate interval by resolution of F5 heterozygous RIL 94, relative to the region fine-mapped through collaboration between Jan Bettgenhaeuser and Daniel Woods. Arrows indicate annotated genes. 105
- Figure 4-8 Relative expression of five genes within a refined lemma trichome candidate region on Bd chromosome 4, of leaf and floral meristem tissues from qPCR. Values are relative to housekeeping gene BdUBC18. Error bars = ± 1 SE 107
- Figure 4-9 Tissue specific expression data for genes in lemma trichome candidate interval on Bd chromosome 4, adapted from EMBL Expression Browser, data from (Davidson et al., 2012). Expression values in transcript per million (TPM) overlaid. Bradi4g22641 and Bradi4g22645 were absent from (Davidson et al., 2012) data set, so are not presented..... 108
- Figure 4-10. Dotplot Collinearity between Bd21 reference (Illumina, v3.1) and ABR6 nanopore Flye assembly for trichome candidate region..... 112
- Figure 4-11 Alignment of protein sequences annotated in Bradi4g22650 Bd21v3.1 with orthologous peptide sequences obtained from ABR6 nanopore assembly and Bd1-1 (v1.1) PacBio assembly, with peptide sequence predicted using FGENESH tool. Domain 1, highlighted green= Double CLP-N Motif (protease domain), domains two and three, highlighted red = P-loop containing nucleoside triphosphate hydrolase domains..... 116
- Figure 4-12 Loci of homozygous sodium azide mutations in Bradi4g22650 equivalent gene, BdiBd21-3.4G0316600 in Bd21-3. Derived from phytozome (V12) JBrowse function. 117
- Figure 4-13 Image of gel electrophoresis analysis on amplified products of hygromycin resistance for seven T1 Bd plants. Sample 1-7= T1 lines 1-7, left to right. Well 8 = vector pICSL11099 containing HYG resistance cassette as positive control. 100bp ladder (New England Biosciences). 118
- Figure 4-14 Sequencing results file for Bradi4g22650 CRISPR T2 lines, highlighting target edit site in red and polymorphisms in yellow. Top row for each clip is Bd21v3.1 reference sequence..... 119
- Figure 5-1 Setup of root assays in 1.2 mL tubes, a) Bd21 at 4 days LHS four seedlings in media contains 10 μ M DON, RHS four seedlings in control media

- (ethanol amended only agar), b) Bd21 seedlings removed from tubes at 6 days, suitable for root length measurement 133
- Figure 5-2 Variation in root length of Bd accessions when grown in agar supplemented with DON (10 μ M), after 5 days. SE = \pm 5.58 to 23.90. Accessions highlighted in grey, Bd2-3 and Bd21 that vary in phenotype, are parents of a biparental mapping population 141
- Figure 5-3 Photographs showing the differential responsiveness to growing in agar supplemented with 10 μ M DON between Bd21 and Bd2-3 accessions of *Brachypodium distachyon*..... 142
- Figure 5-4 Bd2-3 and Bd21 DON sensitivity in floral tissues. A, Representative images of Bd2-3 and Bd21 typical browning symptoms in response to application of DON. Point of treatment (DON or mock) application indicated by white triangle marker. Scale = 1 cm. B, Plots of predicted mean (derived from GLM analysis) spread of DON associated browning symptoms as number of florets above point of application for Bd21 and Bd2-3 for seven and ten days post treatment. Error bars = \pm 1SE..... 143
- Figure 5-5 Phenotypes of roots grown in supplemented 0.4% agar for five days. TIBA=triiodobenzoic acid, an auxin-transport inhibitor. Anisomycin and cycloheximide are protein-synthesis inhibitors, the latter described as most closely sharing cellular mechanism with DON. 145
- Figure 5-6. Differential phenotypes of roots of two accessions, Bd21 and Bd2-3 when grown in 10 μ M DON supplemented agar for 6 days, compared to no-treatment controls. Below: Roots grown in agar supplemented in 10 μ M DON for six days, demonstrating the three typical phenotypes observed, in comparison to control treated roots. 147
- Figure 5-7 Proportional distribution of Bd2-3-like and Bd21-like roots for each of 154 Bd2-3 x Bd21 F7 RILs when grown in agar supplemented with 10 μ M DON. Overlaid lines represent assignment of RILs as Bd2-3-like (to the right of dashed vertical line), Bd21-like (to the left of the vertical dotted line), or intermediate (between the two vertical lines) Four replicate roots per RIL. Dead roots excluded, resulting in >4 possible Bd2-3:Bd21 ratios 148
- Figure 5-8 Proportional distribution of Bd2-3-like and Bd21-like roots for each of 154 Bd2-3 x Bd21 F7 RILs when grown in agar supplemented with 20 μ M DON. Overlaid lines represent assignment of RILs as Bd2-3-like (to the right of dashed vertical line), Bd21-like (to the left of the vertical dotted line), or

intermediate (between the two vertical lines). Eight replicate roots per RIL. Dead roots excluded, resulting in >8 possible Bd2-3:Bd21 ratios 149

Figure 5-9 Illustration of KASP markers and single marker association results for association with DON sensitivity at for Bd2-3xBd21 population characterised in media supplemented with 10 μ M DON. P-values for associated are presented with marker names, for 10 μ M DON upper, 20 μ M DON red, italicised and below. Greyed out, unlabelled markers were unsuccessful and omitted from analyses. 150

Figure 5-10 Physical map of Bd1L overlaid with region of significantly associated KASP markers with DON sensitivity in root development in Bd2-3xBd21 RIL F6 populatio. For 10 μ M DON, area highlighted in green, for 20 μ M DON, area highlighted in purple = p-values<0.05. Total map size = 60.07 cM 152

Figure 5-11 Quality scores for BSA variants for Bd2-3xBd21 F7 RIL DON sensitivity, A, prior to filtering of variants, B, with filtering to remove all variants with quality <1500 score. 154

Figure 5-12 Bulked segregant analysis for DON sensitivity in Bd2-3 x Bd21 F7 high-confidence RILs. Thirty RILs per extreme phenotype pool. B, Physical map showing previous KASP mapping of DON sensitivity on Bd1L (Figure 5-12), overlaid with BSA Bd1L peak (purple), variants with bulk frequency ratio >7. 155

Figure 5-13 Multi-Dimensional Scaling (MDS) plot, describing the variance between DON treated root Bd21vsBd2-3 RNAseq samples. Generated using Degust (v4.1.1)..... 161

Figure 5-14 Venn diagrams assigning commonality of up- and down- regulation of genes between Bd21 and Bd2-3 in roots, responsive to DON at 5 μ M & 20 μ M, from RNAseq data. 163

Figure 5-15 Venn diagram containing gene expression in comparison between Bd2-3 relative to Bd21, at 5 μ M and 20 μ M DON RNAseq data. 164

Figure 5-16 Genotypes of Bd2-3xBd21 high-confidence DON sensitivity RILs for fine-mapping of Bd1L BSA peak.Marker names are derived from Bd21v2.1 reference genome differentiating SNP locus. Purple=Bd21 genotype, green=Bd2-3 genotype, grey=not genotyped Faded markers are within the Bd1L single-marker analysis significant region. 167

Figure 5-17 Variation in Bradi1g71460 between Bd2-3 and Bd21 (A and C), and Bd2-3-like and Bd21-like RIL pools. A, RNAseq coverage (SNPs indicated by colours), B, BSA coverage aligned to Bradi1g71460 reference, C, peptide alignment, sequences obtained from gene annotations from Bd21v2.1 (lower track) and Bd2-3v1 (upper track) (Phytozome)..... 171

Chapter 1 - General Introduction

1.1 Cereal Crops

Cereals form the staple for much of the global population's diet, contributing approximately 60 % of calories and 20 % of protein consumed (Cassman et al., 2003). Wheat (*Triticum aestivum*) is the third most produced cereal crop yet in 2013 occupied more land than any other, has the greatest world trade index and is therefore of huge economic and social importance (Food and Agricultural Organisation, 2014). Global population growth, predicted to reach 9.7 billion by 2050, and changing dietary habits will create pressure on food production capabilities, equating to a required increase in food production of 50 percent by 2050 (Gregory and George, 2011, Alexandratos and Bruinsma, 2012). Furthermore, globally arable land is under threat as a result of soil degradation, economic development, climate change, as well as from change of crop use, with grasses becoming increasingly important as lignocellulosic biomass for biofuels, furthering the demands for increasing yields by occupying high-quality land previously designated for food production (Prävälje et al., 2021). Disease related crop losses account for one of the greatest challenges to achieving maximal sustainable food production. Pathogens are estimated to cause losses of up to 20 % of potential yield for the three major cereals (wheat, rice and maize) at a huge loss economically (Oerke, 2005). There is therefore a need to increase the control of such pathogens, with genetic resistance considered the most appropriate and sustainable approach.

1.2 *Fusarium* Head Blight and other *Fusarium* diseases of cereals

Fusarium head blight (FHB) is an economically devastating fungal disease of temperate small-grain cereals such as wheat (*Triticum* spp.) and barley (*Hordeum vulgare*). Causal agents are predominantly *Fusarium* species, most significantly

Fusarium graminearum and *Fusarium culmorum*. Head blight can also occur on oats (*Avena sativa*), rye (*Secale cereale*) and rice (*Oryza* spp.), and as stalk and ear rot in maize (*Zea mays*) (Goswami and Kistler, 2004).

1.3 Economic Cost

FHB is considered a relatively modern disease, having re-emerged in the USA in the 1990's after being first described by Smith (1884). It is becoming an increasing problem in the UK. Losses of \$2.7 billion worth of wheat were recorded to be associated with FHB in the USA between 1998-2000 (Bai and Shaner, 2004). Wilson et al. (2018), using data for 2015/2016 harvests calculated the total annual cost to US wheat and barley through loss of yield to be \$1.47 billion, with a further \$211 million incurred in cost of fungicides. Along with limiting yields by typically between 10-50 % due to reduced kernel set and kernel weight, and cost of fungicide application, the fungus produces mycotoxins that accumulate in the kernels rendering them unsuitable for sale or consumption (Snijders, 2004). Disease pressure is described to be a function of natural inoculum supply, genetic resistance level of the host and climatic conditions; of these three factors, only genetic resistance is a plausible candidate for manipulation for the control of FHB.

1.4 Infection, symptoms, and tissues affected

FHB is present in all major cereal growing regions of the world, with contaminated crop residue remaining in the soil post-harvest and surviving saprophytically over winter to serve as inoculum for the crop in following years (Figure 1-1) (Leslie and Logrieco, 2014, Trail, 2009, Bai and Shaner, 2004).

An extensive taxonomic split of *F. graminearum* within the previous decade means that *F. graminearum* is now considered as a complex of species (O'Donnell et al.,

2004, Starkey et al., 2007). *F. culmorum* is not known to produce ascospores and therefore spreads only through the production and dispersal of asexual conidia (Wagacha and Muthomi, 2007) whereas *F. graminearum* can spread through wind dispersal of sexually produced ascospores (Figure 1-1). *F. culmorum* conidia are produced more readily under laboratory conditions than *F. graminearum* making the former a more amenable model.

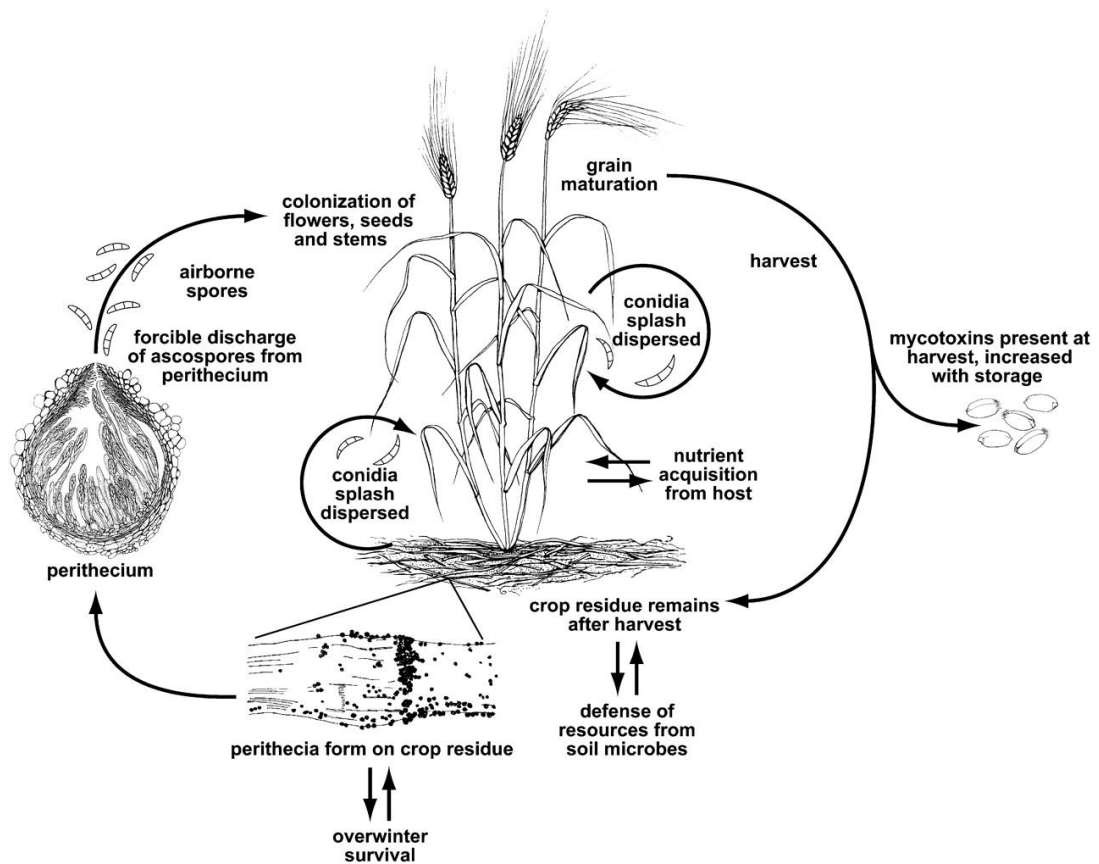


Figure 1-1 Life-cycle summary of *F. graminearum* (sexual stage, *Gibberella zeae*). *F. culmorum* is limited to asexual reproduction only Taken from publication: (Trail, 2009)

FHB infection occurs during grain development, spreading through the kernels causing necrosis and toxin accumulation. Moisture content is the most vital factor for successful infection, followed by temperature, host resistance level and chemical treatment (such as fertilisation and fungicide application). Susceptibility to infection

by conidia peaks during the short period of mid-anthesis (Wagacha and Muthomi, 2007). Host penetration occurs through a combination of degradation and pressure through secretion of cell wall degrading enzymes and formation of a penetration peg. Typically, natural recesses high in humidity are targeted as weak areas of tissue; for example, where the palea of one kernel meets the lemma of the next, particularly at floret base, and stomata. In a compatible interaction, hyphae spread intercellularly followed by intracellular growth once host cells have been compromised by pathogen colonisation (Beccari et al., 2011). Transition from biotrophic to necrotrophic phase is associated with increased biosynthesis of trichothecene mycotoxins and cell-wall degradation enzymes (Kang and Buchenauer, 2000). Symptoms typically appear as discolouration and subsequent premature bleaching of infected kernels, which are often underdeveloped and degraded in starch content (Brown et al., 2010). Symptoms of infection of barley in the field are often less readily apparent than in wheat (Goswami and Kistler, 2004).

Other diseases associated with the same *Fusarium* causal agents include root and stem rots (Figure 1-2). Although considered less devastating than FHB, these diseases are still damaging, leading to restricted vasculature, reduced vigour, and limited yields. When infection occurs early in seedling development death of the plant is likely as coleoptiles and immature roots are rapidly colonised. The infection mechanisms vary from that of FHB; fundamentally the inoculum is mycelium as opposed to germinating spores. Symptoms appear as browning associated with necrosis in roots, whilst also manifesting in general reduced vigour and grain development (Beccari et al., 2011).

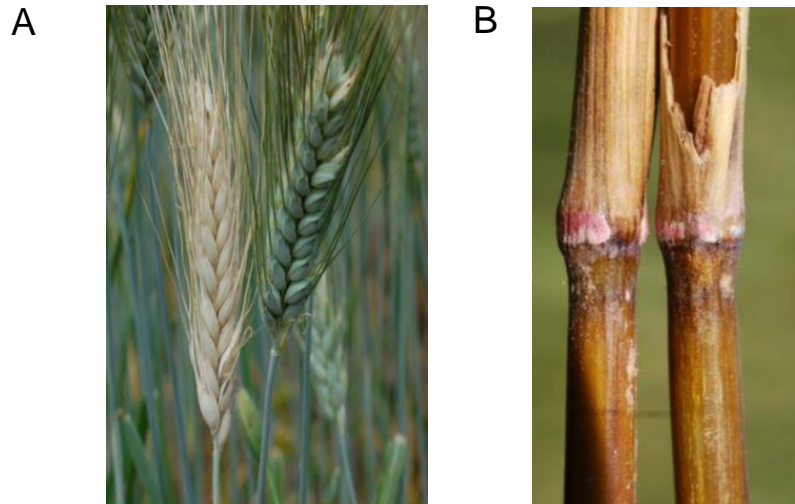


Figure 1-2 Symptoms of *Fusarium* infection; A, bleached heads resulting from vasculature damage by root or stem rot; B, pink discoloration of basal nodes in stem infection, taken from publication (Scherer et al., 2013)

1.5 Causal species & mycotoxins

Several species are known to cause FHB, from the *Fusarium* and *Microdochium* genera. Predominate species varies between geographical locations, determined mostly by temperature and humidity. Multiple *Fusarium* species can be present in a single environment, forming an FHB disease complex; symptoms of FHB infection are highly similar between causative species (Nicholson, 2009). Formerly recognised within the *Fusarium* genus, *Microdochium nivale* and *M. majus* are known to cause FHB but do not produce mycotoxins and are therefore of lesser overall significance (Nielsen et al., 2013). Of the *Fusarium* spp., *F. graminearum* and *F. culmorum* are the most significant; *F. graminearum*, associated with warmer and more humid conditions, is the major global pathogenic species (Xu et al., 2005).

The major challenge that FHB presents in cereals is the production and accumulation of mycotoxins, secondary metabolites produced by the fungus during host colonisation. As with the range of causative agents of FHB, there are many diverse mycotoxins produced, with each species producing a signature combination.

Trichothecenes are the most significant of these mycotoxins in terms of economic and industrial damage. There are approximately 170 trichothecenes identified the most significant of which is deoxynivalenol (DON), a type B trichothecene, also known as vomitoxin (Bai & Shaner, 2008). They all share a common tetracyclic sesquiterpenoid 12,13-epoxytrichothec-9-ene ring system and are grouped into four types (A-D) with types A and B found in cereals. Type A trichothecenes are typically produced by *F. sporotrichioides*, *F. langsethiae*, *F. acuminatum*, and *F. poae* and are represented by T-2 and HT-2; they are generally of higher toxicity but less widespread and produced in smaller quantities than DON. Type B, most important to this project and most widely found in wheat, are represented by DON, acetyl-DON (ADON) and nivalenol (NIV) (Marin et al., 2013, Kulik et al., 2017). *F. graminearum* and *F. culmorum*, the two species on which this project focusses, produce DON and its acetylated forms, or nivalenol (NIV), the latter of which is also produced by *F. poae* (Nazari et al., 2018). DON acts as a virulence factor in wheat, rendering these species more aggressive in infection than competitors (Ilgen et al., 2008). Secretion of these toxins is characterised as aiding fungal colonisation through inhibition of host protein synthesis leading to membrane degradation (Cundliffe et al., 1974, Cundliffe and Davies, 1977). This enhances host susceptibility and infection success, but is not fundamental to infection or strictly correlated with visual symptoms (Kimura et al., 2006). During colonisation of wheat, DON elicits the production of reactive-oxygen species (ROS), manipulating the host defence system and inducing cell death allowing spread of the pathogen within the host (Desmond et al., 2008, Bai et al., 2002). The role of mycotoxins during early infection of wheat is not known (Boenisch and Schafer, 2011). DON accumulation in the grain is intimately related to disease development and therefore strategies for DON management focus on control of FHB (Yuen and Schoneweis, 2007). Trichothecenes are highly stable compounds, with storage, milling, cooking and high temperatures resulting in little degradation (Marin et al., 2013). As well as directly decreasing yields through mediating infection severity,

ingestion of toxins can lead to toxicosis in both humans and livestock (Escriva et al., 2015). Therefore, DON concentration for grain entering the food chain is controlled, restricted to 1ppm for humans in the USA, higher for livestock (up to 30 ppm for beef cattle) (FDA, 2011). The European Community limits DON levels to 1.5 mg kg⁻¹ for wheat grain except for durum wheat and oats where it is 1.75 mg kg⁻¹ (Trail, 2009). However, a survey of exposure levels of DON by Mishra et al. (2020) concluded that current DON levels in the food chains of many regions pose a risk to human health, especially in children. It is not uncommon for harvest batches to exceed these levels, leading to the destruction of grain at the loss to both the grower and the chain of demand.

There are many other classes of mycotoxins produced by *Fusarium* species, not all relevant to FHB or cereal diseases (Marin et al., 2013). Particularly notable are the oestrogenic compounds zearalenones; these are known to be produced by *Fusarium graminearum*, *F. culmorum*, *F. cerealis*, *F. equiseti*, *F. verticillioides*, and *F. incarnatum*. In animals, these compounds bind to oestrogen receptors and elicit aberrant responses with implications during pregnancy, presenting a major issue upon contamination of grain for human or livestock consumption (Hueza et al., 2014).

1.6 Control measures for FHB

1.6.1 Chemical controls

It is widely accepted that the application of chemical fungicides is a vital part of FHB control, however they cannot be relied upon for complete control. A typical reduction of 40-50 % in FHB index for the best performing fungicides when applied within a limited efficacy window during anthesis, still only achieves relatively poor FHB control, particularly in high disease pressure situations where mycotoxin levels remain above the legislative thresholds (Madden et al., 2014). Of the fungicides most widely tested,

triazole-based compounds appear to be the most effective and consistent across studies (Paul et al., 2008).

The diversity of inoculum species present within the field means that upon treatment with fungicides that are only partially effective species balances are typically disrupted (Xu and Nicholson, 2009). More aggressive species will therefore become predominant, potentially increasing the proportion of DON producing pathogen such as *F. graminearum* and *F. culmorum*. Treatment with fungicides therefore, notably strobilurin, can fail to reduce DON contamination to acceptable levels and can even increase DON contamination (Scarpino et al., 2015, Madden et al., 2014).

1.6.2 Alternative controls

The ubiquitous nature of *Fusarium* spp. renders pathogen exclusion futile; the pathogen is already resident in all major cereal growing regions of the world and inoculum can be aurally disseminated between fields (Yuen and Schoneweis, 2007). Other control strategies, such as those based on targeting the pathogen in the soil, crop rotation, burial and burning of residues all present greater challenges than the one they aim to solve; coupled with limited successes at controlling the fungus they are inefficient and uneconomical (Yuen and Schoneweis, 2007). Extensive research has also been conducted into the use of biological control agents, but these require high inputs and are less sustainable in the long term than engineering durable resistance (Tian et al., 2016). Reduced tillage, a soil conservation practice in which soil is not turned over between crops, increases severity of FHB in comparison to ploughed soil during which inoculum carrying wheat residues are buried (Dill-Macky and Jones, 2000). The sequence of crop rotation can also have a significant effect on the incidence and severity of FHB and affects the balance of causal species; specifically, the inclusion of maize or sugar beet preceding winter wheat can increase

the risk of FHB, to an even greater extent than wheat following wheat (Tillmann et al., 2017).

1.6.3 Genetic resistance

Genes for stable control of FHB in wheat are rare, with most studies identifying polygenic FHB resistance with a large influence of environment on efficacy. Resistance to *F. graminearum* and *F. culmorum* has been shown to be closely correlated (Leslie and Logrieco, 2014). There is no evidence for race structure of either *F. graminearum* or *F. culmorum* adapted to different wheat genotypes, unlike in powdery mildew species for example, simplifying resistance breeding by rendering resistance to one species also conferring resistance to all others (Snijders, 2004). Resistance types can be classified into those that limit occurrence of initial infection, Type I, and those that limit the spread of fungus through tissues following infection, Type II (Schroeder and Christensen, 1963). Barley has inherent high levels of Type II resistance that prevents infection from spreading along the rachis, from spikelet to spikelet (McMullen and Stack, 2011). Other modes of resistance that do not fit within these classifications often involve interruption of mycotoxin accumulation in infection. The main driver for genetic resistance is to reduce contamination of mycotoxins to limit the amount entering the food chain (Kimura et al., 2006). Type V resistance is described as resistance to toxin accumulation; and is further separated into class I, which includes mechanisms for the degradation or detoxification of trichothecenes, and class II which mechanisms to inhibit trichothecene biosynthesis (Boutigny et al., 2008). Lemmens et al (2005) described the co-localisation of a QTL for type II FHB resistance in wheat with an ability to detoxify DON.

Stability of resistance in wheat depends largely on the level of resistance; the higher the level of resistance, the more stable it appears in trials across different years,

environments and disease pressures (Mesterhazy, 1995, Buerstmayr et al., 2008). Lower levels of resistance are typically therefore generally less stable. Resistances are often negatively associated with agronomic phenotypes including early flowering time, height and yield (Buerstmayr et al., 2008). Susceptibility to FHB at initial infection is associated with the *Rht-B1b* and *Rht-D1b* semi-dwarfing alleles in wheat (Srinivasachary et al., 2008a). Such trade-offs between resistance and crop performance often limit applications within a breeding program for crop improvement due to costs that would result from reduced marketability (Brown, 2002).

Fhb1 is a major quantitative trait locus (QTL) associated with Type II FHB resistance originating from Chinese spring wheat cultivar Sumai 3, a variety commonly used in breeding programs to provide FHB resistance, and was fine mapped to a region of 3BS (Cuthbert et al., 2006). Additional sources of resistance from Sumai 3, *Fhb2* and *Fhb3*, have been localised to chromosomes 6BS and 7AL respectively (Cuthbert et al., 2007). Attempts to clone the gene behind the *Fhb1* QTL have been complex and controversial but focus on a histidine-rich calcium binding protein (*TaHRC*) and conversely a separate report of the cloning of a pore forming toxin-like gene (Rawat et al., 2016, Su et al., 2019). Both loss-of-function and gain-of-function of *TaHRC* have been reported to be responsible for resistance (Su et al., 2019, Li et al., 2019, Lagudah and Krattinger, 2019, Su et al., 2018b).

1.7 Brachypodium distachyon as a model

The genetics of many crops, especially cereals, are notoriously difficult to study with wheat arguably being the most complex. This is due to their large genome sizes, 17 Gb in wheat, multiple highly similar genomes in polyploid species, large expanses of repetitive regions along with practical considerations such as long lifecycles and relatively large physical size. All of these factors can be theoretically overcome by

using a laboratory model species (Flavell, 2009). Historically *Arabidopsis thaliana* or rice (*Oryza* spp.) have been used for this purpose, however both present significant disadvantages. Although *Arabidopsis* is arguably the most convenient laboratory model for many applications, any information obtained has little practical relevance to cereal genetics and pathology and therefore doesn't satisfy the remit of a model for wheat (Draper et al., 2001). Rice in contrast is more relevant to the Pooideae and Triticeae yet is not as convenient to work with, having demanding growth requirements and relatively large size. Both *Arabidopsis* and rice are more distantly related to wheat than *Brachypodium distachyon* (Bd), a small temperate monocotyledonous species in the Poaceae family, subfamily Pooideae. With a short stature, a rapid life cycle as short as 10 weeks and morphology comparable with wheat it appears a more feasible experimental species than alternatives (Peraldi et al., 2011). Most importantly in terms of genetic relevance it shows high homology with wheat and barley and has a fully sequenced, gold-standard, diploid genome of approximately 272 Mb in size, with the genome for reference accession Bd21 available in its third, improved, version (Huo et al., 2009, International Brachypodium, 2010). Having diverged just prior to the core pooid clade in which most modern cereal crops are classified, strong synteny qualifies Bd as a useful tool for preliminary functional genomics with an aim of application in wheat, barley or maize (Figure 1-3) (Huo et al., 2009, Vain, 2011). Increasingly the value held within a model species is the ease and availability for the applications of the '-omics' age. (Draper et al., 2001).

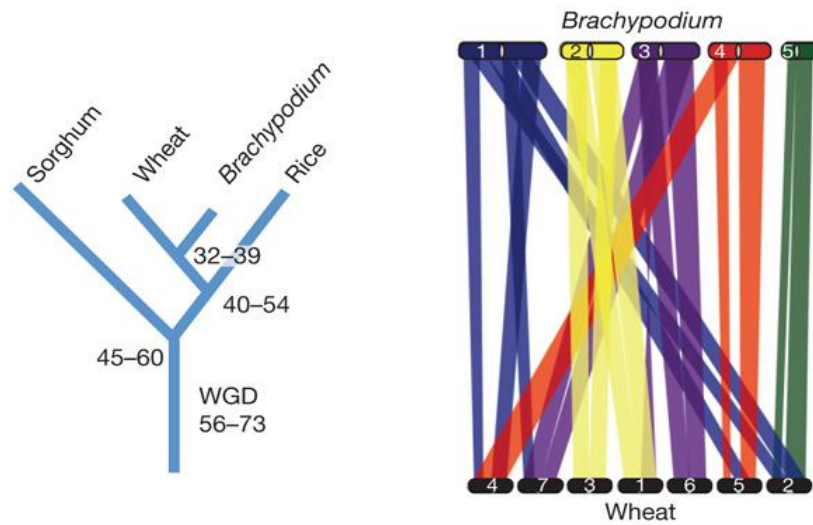


Figure 1-3 LHS, divergence times of cereal crop species sorghum, wheat rice and model genus *Brachypodium*. WGD, whole-genome duplication. The numbers refer to the predicted divergence times measured as Myr ago; RHS, Orthologous gene relationships between *Brachypodium* and hexaploid bread wheat defined by 5,003 ESTs mapped to wheat deletion bins. Each set of orthologous relationships is represented by a band that is evenly spread across each deletion interval on the wheat chromosomes. Figure adapted from publication: International *Brachypodium* Initiative (2010)

Bd has been used as an intermediate between fundamental research in *Arabidopsis* to practical relevance in wheat (Girin et al., 2014). Emphasis of the *Brachypodium* research community initially focussed on the investigation of cell wall and lignin biosynthesis, as a model for the development of sustainable and renewable biofuels of other grasses. It has previously been used to characterise and model grain development, and most importantly for this project, host-pathogen interactions (Fitzgerald et al., 2015). The root system morphology is highly similar between wheat and *Brachypodium* compared to *Arabidopsis*, making it a much more relevant tool for root-based assays (Figure 1-4). There are several species within the *Brachypodium* genus with a variety of specialist applications.

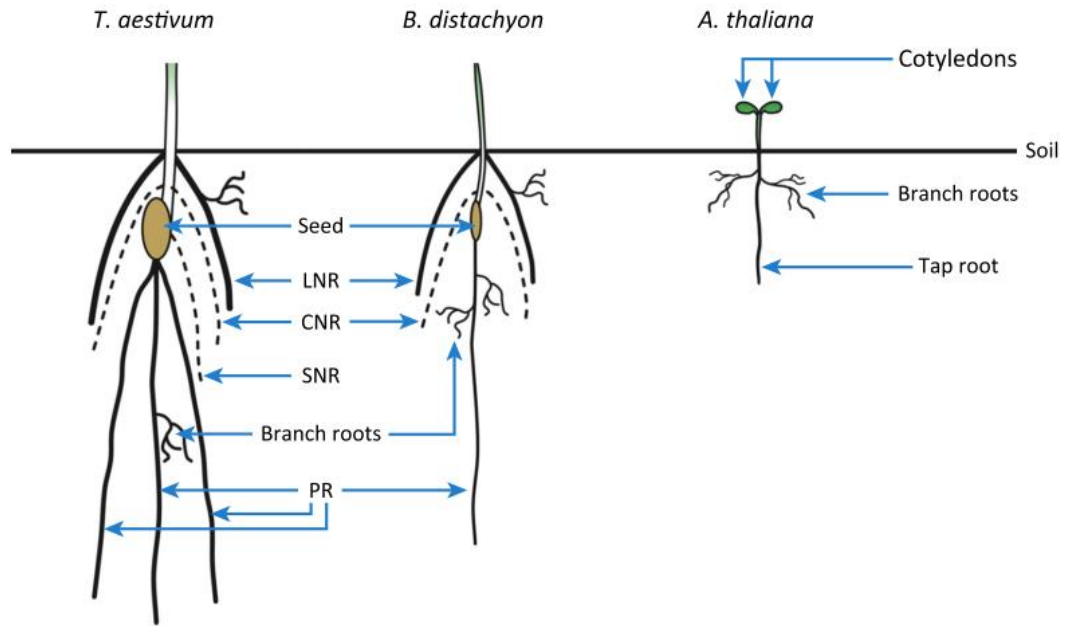


Figure 1-4. Comparison of wheat, *Brachypodium distachyon* and *Arabidopsis thaliana* root systems. Horizontal line represents soil level. Abbreviations: CNR, coleoptile node axile root; LNR, leaf node axile root; PR, primary axile root; SNR, scutella node axile root. (Catalan et al., 2014).

1.7.1 *Brachypodium* as a pathosystem

Bd has been used to study a variety of fungal, bacterial and viral pathogens. These fungal pathogens include compatible interactions with, for example, *Fusarium*, *Blumeria*, *Puccinia* and *Magnaporthe* species (Fitzgerald et al., 2015, Bettgenhaeuser et al., 2018, Della Coletta et al., 2019, Su et al., 2018a). Work by Peraldi colleagues (2011) demonstrated the successful infection of *Bd* with *F. graminearum* and *F. culmorum* across floral, leaf and root tissues, representative of the range of *Fusarium* diseases on cereals. Figure 1-5 shows the development of disease symptoms upon inoculation with *Fusarium* conidia and the visual similarity that is shared with wheat FHB. Since this introduction of *Bd* as a model pathosystem for *Fusarium* diseases, additional studies have continued to characterise *Bd-Fusarium* interactions, including the effect of phytohormones on *F. graminearum* in *Bd* heads and roots, demonstration of reduced FHB susceptibility of *Bd* when primed with DON, host-induced gene silencing of *F. graminearum* genes to enhance

resistance and characterisation of *Fusarium* species on different Bd natural genotypes (Haidoulis and Nicholson, 2020, Dinolfo et al., 2020, He et al., 2019, Blümke et al., 2015). The complexity of host-pathogen interactions necessitates the use of large-scale studies to account for inherent variability; the use of *Brachypodium* as a small, amenable pathosystem is therefore particularly useful to overcome these hindrances.

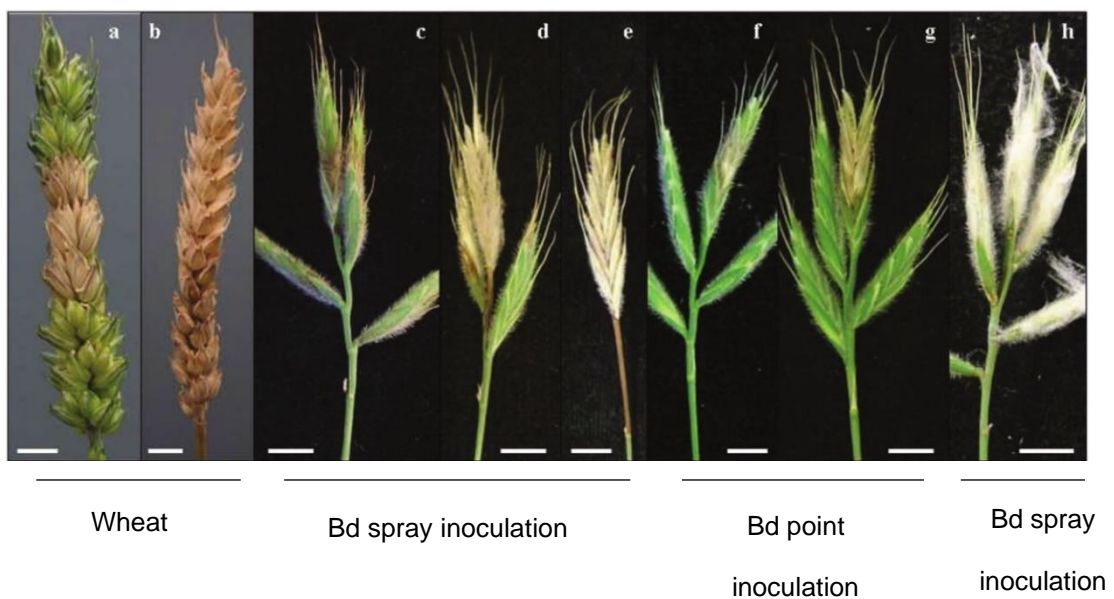


Figure 1-5. Visual comparison of *Fusarium* head blight symptoms between wheat and *Brachypodium distachyon*. (Peraldi et al., 2011)

1.7.2 *Brachypodium* resources

The most useful model organisms are built upon extensive, openly accessible resources, and Bd is no exception to this. These resources aim to capture and generate extensive genetic variation in the form of germplasm collections and mutant populations, the latter playing a vital role in the functional characterisation of genes, facilitating diverse research strategies and approaches (Girin et al., 2014). Several collections have been made of diverse, wild germplasm across the native range of Bd, surrounding the Mediterranean (Figure 1-6), composing multiple separate collections each characterised separately (Filiz et al., 2009, Gordon et al., 2014, Tyler

et al., 2016). Complete, high quality genome sequences and associated data are currently available for fifty-two accessions under the Brachypan-genome project (Gordon et al., 2017). Sequencing, de novo assembly and analysis is currently in progress to achieve a total of 90 sequenced accessions (Gordon et al., 2014). The publication of the pan-genome in late 2017 provides a powerful tool for exploring genetic variation between accessions which can be employed in the use of map-based cloning for in-depth comparison of candidate loci (Gordon et al., 2017).

Inbred lines and mapping populations have been generated from these germplasm collections, mainly in the form of recombinant inbred line populations (RILs) but more recently include collections of accessions for Genome Wide Association Studies (GWAS) (Garvin et al., 2008, Tyler et al., 2016, Dell'Acqua et al., 2014). GWAS was first demonstrated as a key tool for the identification of loci associated with agronomic traits using leaf architecture in maize; however it is most appropriate for traits of simple inheritance and genetics (Tian et al., 2011). The ABR6 x Bd21 RIL population has been utilised for the mapping of quantitative trait loci associated with vernalisation and flowering time (Bettgenhaeuser et al., 2017). Della Coletta et al. (2019) used the Bd2-3 x Bd21 RIL population to elucidate loci associated with non-host resistance to wheat steam rust (*Puccinia graminis* f. sp. *Tritici*) using bulked segregant analysis (BSA).



Figure 1-6 Geographical distribution of *Brachypodium* germplasm collection sites, from a representation of the native range. Colour of marker described clade of origin (Gordon, Contreras-Moreira et al. 2017)

Several extensive mutant populations have been generated for both forward and reverse genetic approaches. The BRACHYTAG collection generated at and held by the John Innes Centre is a resource of approximately 5000 T-DNA insertion lines (Bd21 source material) (Thole et al., 2012). A recent report on the status of another T-DNA tagged collection describes a total of 21,165 T-DNA insertion lines (containing 21,078 unique insertion sites, 9,754 within genes), with flanking regions sequenced, generated from accession Bd21-3 (Hsia et al., 2017, Bragg et al., 2012).

A TILLING platform for Bd, BRACHYTIL has been developed by Dalmais et al. (2013a). TILLING is a non-transgenic reverse genetics approach requiring a reference genome sequence for the detection and location of induced mutations (Barkley and Wang, 2008). It is possible to obtain a variety of mutant phenotypes, from modification of- to loss-of-function, within a single locus, potentially allowing a more detailed examination of gene function (Stephenson et al., 2010). The BRACHYTIL resource of 5,731 families was generated through sodium azide mutagenesis of accession Bd21-3 by Institut National de la Recherche Agronomique (INRA, Versailles, France), with a mutations rate predicted to be one per 396 kb, with an average of 680 mutations per line (Dalmais et al., 2013b). Phenotypes along with sequence data are freely available to the community via an online phenotypic tree and a database (UTILLdb) searchable through a BLAST tool and mutations listed as a track on Bd21-3 and Bd21 JBrowse (Phytozome). The utility of the platform was originally validated by the investigation of seven genes belonging to a multi-gene family of the lignin biosynthesis pathway (Dalmais et al., 2013b). An additional, non-redundant sodium azide mutagenized resource has evolved with the advancements in sequencing technology, with all mutations on Bd21-3 being fully characterised by whole genome sequencing, and therefore is no longer designated as TILLING, instead designated 'sequenced lines' (INRA).

EcoTILLING populations were also generated to exploit natural variation within *B. distachyon*. EcoTILLING has been described as a beneficial tool for species with large, complex genomes or long generation times (Banik et al., 2008) and therefore it is likely that alternative methods such as genotyping by sequencing may be more efficient and cost effective for a model such as *Brachypodium* for which these factors are not an issue. These mutant populations, suitable for a reverse genetics approach, provide the opportunity for the investigation of genes playing a putative role in *Fusarium* – *Brachypodium* interactions.

1.8 Research objectives

The overarching aim of this project is to better understand the interaction between *F. graminearum* and *F. culmorum* with wheat during infection of floral tissues, FHB, through the utilisation of Bd as a laboratory model. Primarily, this will focus on the identification of possible sources of genetic resistance to FHB in Bd. The specific objectives being:

- i) To characterise natural diversity in Bd, focussing on FHB. Agronomic traits including height, flowering time, and lemma trichome presence will be assessed in relation to FHB. Existing mapping populations from the Bd research community will be used to map genetic loci associated with variation in resistance to FHB between natural Bd accessions. This work is described in Chapters 2, 3 & 4.
- ii) To investigate the function and mechanism of DON *in planta* by characterising natural variation in the DON sensitivity of Bd accessions. This follows previous work by colleagues that identified a concentration dependent response of Bd root development. Again, mapping populations

will be used to delineate, and fine-map loci associated with DON responsive root development. This work is described in Chapter 5, in which bulked segregant analysis and RNAseq are applied to delineate loci associated with DON sensitivity.

Chapter 2 - Assessing natural variation in Fusarium head blight susceptibility of *Brachypodium distachyon*

2.1 Introduction

Many of the complexities of studying FHB in wheat, be they physical, genetic, or practical may be overcome by use of a model plant system. *Arabidopsis thaliana* is not a natural host of FHB causing *Fusarium* species, with incomparable floral anatomy to wheat, and displays different symptoms when infected (Urban et al., 2002). *Brachypodium distachyon* (Bd) was first introduced as a model pathosystem for FHB amongst other fungal pathogens by characterisation of accessions Bd21 and Bd3-1 (Peraldi et al., 2011, Peraldi, 2012). Studies by Blümke et al. (2015) and Pasquet et al. (2014) have reported corroboration of *F. graminearum* infection symptoms in Bd that are comparable to wheat. The application of Bd as a model pathosystem has since expanded to include studying of *Puccinia striiformis*, *Cochliobolus sativus*, *Rhizoctonia solani* causing root rot and *Claviceps purpurea* (Bettgenhaeuser et al., 2018, Gilbert et al., 2018, Schneebeli et al., 2015, Zhong et al., 2015, Kind et al., 2018). Variation of FHB-Bd interactions within the species has not yet been evaluated.

The publication of a Bd pan-genome, Brachypan, which includes the genome sequence of 54 accessions provides a powerful foundation for investigating the genetic diversity underlying FHB susceptibility within the species that had previously been characterised in only a handful of accessions (Gordon et al., 2017, Peraldi et al., 2011). The work undertaken in this chapter was done so in the anticipation of the publication of Brachypan genomic sequences. A high rate of recombination is one of the major benefits of using Bd as a genetic model, along with rapid cycling time, self-

fertility, short stature and a small genome sequenced to a high reference standard in Bd21, rapidly expanding to more accessions (Draper et al., 2001). Especially for genetic studies, the availability of high-quality genomic data combined with the simple, diploid genetics of Bd means that this model can be a powerful tool.

A panel of 54 Bd accessions was obtained for characterisation under glasshouse conditions. Accessions were selected from a wider pool of more than 100 lines, on the basis that; 48 accessions selected were undergoing sequencing for the Brachypan genome sequencing project, whilst the remaining accessions were described to have beneficial characteristics that would make them ideal candidates for laboratory based experiments (Filiz et al., 2009). It was not possible to include all Brachypan project accessions due to limited availability of seed. This diverse panel of inbred lines derived from diverse Bd germplasm was assessed for susceptibility to FHB (by spray inoculation of *F. culmorum*) and other key traits typically implicated with susceptibility of cereal crops in the field, namely height, flowering time, and trichome presence-absence. It was hypothesised that susceptibility to FHB varied within the Bd species and this variation would be reflected within the Brachypan collection of diverse accessions.

2.1.1 Chapter aims

In this chapter, Bd accessions are characterised across two experiments, undertaken under glasshouse and CER conditions in Winter-Spring 2017. Susceptibility to FHB is characterised in 54 Bd accessions and the correlations between FHB, height, flowering time, and lemma trichome phenotype are investigated. Five accessions that are parents of known existing bi-parental mapping populations in the research community are characterised in greater detail with the aim of identifying populations that could be later used in identification of genetic loci associated with these traits through mapping.

2.2 Methods

2.2.1 Characterisation of Bd accessions under glasshouse conditions

2.2.1.1 Plant lines and growth conditions

Brachypodium accessions used were originally collected by (Filiz et al., 2009) (all BdTR prefixed accessions) and (Vogel et al., 2009). The Nicholson group obtained the seed from The Sainsbury Laboratory Collection, supplied by Matt Moscou, after which they were bulked for use in pathology experiments. The list of the 54 accessions prepared for characterisation is given in Supplementary Table 1.

Following the removal of glumes, seeds were stratified in the dark at 4 °C for 5 days between filter paper discs on Petri dishes with 3 mL sterile distilled H₂O, before a 24 hr incubation at 22 °C with light excluded. Germinated seeds were planted one to a cell (224 cell tray) in a soil mix of 1:1, cereal mix: peat and sand (Supplementary Table 2).

Seedlings were grown for 8 days under winter glasshouse conditions at 16 hr day-length before being transferred to controlled environment for 6 weeks vernalisation at 4°C, 16hr daylength (Norwich, UK, winter-spring 2017). Following vernalisation plants were grown for a further 9 days under glasshouse conditions, and then transferred to FP8 square pots (8x8x8 cm), two individuals of the same accession per pot. The same soil mix was used. A total of eight plants per accession (across four pots) were used for characterisation, with the exception of accessions ABR6 and Uni2 which had only six and four replicate plants respectively. Plants were staked and tied as appropriate. Pots were arranged in a randomised incomplete block design, twelve blocks (trays) of nineteen pots, generated by Design Computing Gendex DOE Toolkit 8.0 (Module IBD, <http://designcomputing.net/>) and randomised within blocks using Microsoft Excel RANDBETWEEN list sorting function Supplementary Figure 1.

2.2.1.2 Pathology – inoculum preparation, inoculation, incubation, and assessment

Conidia of *F. culmorum* isolates Fc2037 and Fc2076 combined were grown on sterile barley kernels and harvested by Andrew Steed to a stock concentration of 2.5×10^6 conidia per mL in water. Aliquots of 1.5 mL were stored at $-20\text{ }^{\circ}\text{C}$ until use. On the day of inoculation defrosted stocks were diluted 1:20, conidia: sterile distilled water, to a final concentration of approximately 1.25×10^5 conidia per mL and amended with Tween 20 (0.05%).

Individual pots were selected for inoculation once three heads on each plant had reached mid-anthesis stage. Three dominant heads per plant were tagged and numbered for identification and tracking. Each plant was spray inoculated with c. 2 mL of conidia solution using a 50 mL atomiser, focussed on dominant tillers. Inoculated plants were incubated in a raised humidity chamber for three days, and the inoculation/humidity treatment was repeated. Plants were then returned to a glasshouse bench, under standard 16hr conditions.



Figure 2-1 Brachypodium tiller spray inoculated with F. culmorum conidial suspension. To illustrate the saturation of floral tissues during inoculation.

Six inoculation batches were used to span the developmental range of flowering within the diverse accessions (Table 2.1). Batches were colour coded by tagging for ease of scoring (Table 2.1). Accessions BdTR7a and ABR8 did not flower in time for inoculation. The initial inoculation of the first two batches appeared to have failed, with no disease symptoms observed after 10 days; an additional inoculation was applied.

*Table 2.1 Details of inoculation batches for glasshouse characterisation trial of diverse Brachypodium accessions, in chronological order. *Inoculations failed, an extra inoculation was applied*

Order	Batch identifier	Number of accessions	Inoculation date		
			First	Second	Third
1	A	19	07 Feb*	10 Feb	21 Feb
2	B	25	10 Feb*	13 Feb	21 Feb
3	C	27	14 Feb	17 Feb	-
4	D	9	21 Feb	24 Feb	-
5	E	5	24 Feb	28 Feb	-
6	F	6	28 Feb	03 Mar	-

Three infected heads for each plant, tagged with a number for tracking, were scored for percentage of infected florets/floral tissue at three time intervals (4, 6 and 10 days post inoculation (dpi) for batches A and B; 6-, 10- and 14- dpi for batches C-F).

2.2.1.3 Phenotyping of developmental and morphological traits

Heading date was scored as the emergence date of the immature primary tiller from the leaf sheath per plant, recorded daily. Height at flowering, excluding awns, of the primary, secondary and tertiary tillers was measured from soil level ten days post mid-anthesis, and once senesced, for all experiments. Presence and absence of lemma trichomes on source seed was recorded by eye and confirmed at flowering.

2.2.1.4 Data analysis and statistics

Genstat (19th edition) was used to carry out statistical analyses on all glasshouse experimental data. Visual analysis of residues was undertaken for all analyses to assess normality of data. FHB percentage 10 dpi data were log₁₀ transformed then analysed using linear mixed model (REML) with inoculation batch as a fixed effect, and tray, pot and rep nested within the random effects model together with accession. Best linear unbiased predicted (BLUP) means were generated from the model for accessions overall and within inoculation batches. Additionally, area under disease progress curve (AUDPC) was calculated across three time points for each head scored. REML analysis was carried out as for 10 dpi FHB, using the same statistical model. For presentation, predicted means were back transformed to the original scales.

Height and flowering time data were analysed using generalised linear modelling (GLM), with replicate, tray and accession included within the statistical model. Residuals were visualised to assess normality, and predicted means were calculated for each accession.

2.2.2 Further characterisation of a subset of Bd accessions under controlled conditions

2.2.2.1 Plant lines and growth conditions

A subset of accessions was selected for further characterisation under controlled environment conditions; Bd21, Bd21-3, Bd3-1, Bd2-3, Koz-3, ABR6, Bd1-1, Bd18-1, Foz-1, Luc-1. Plants were prepared as described above (Chapter 2.2.1.1) until after vernalisation, whereby they were maintained at 22 °C, 70 % relative humidity and 16hr/8hr light/dark cycle in a controlled environment cabinet. Preparation of plants was staggered to synchronise mid-anthesis based on flowering time of accessions

under 16hr glasshouse conditions (Winter-Spring 2017); two germination batches were prepared, separated by one week. Batch one contained ABR6, Bd21, Foz-1, Bd1-1, Luc-1. Batch two, containing all other lines (Bd21-3, Bd3-1, Bd2-3, Koz-3, Bd1-1, Bd18-1) failed due to loss of plants caused by root rot, therefore no data is available for accessions that were exclusively in batch two.

2.2.2.2 Pathology – inoculum preparation, inoculation, incubation, and assessment

Spray inoculation was performed at approximately mid-anthesis with *F. culmorum* conidia at a concentration of 1×10^5 conidia per mL amended to 0.05 % Tween 20 prepared as described above. Trays were sprayed at a rate of c. 2 mL per plant and whole trays bagged for 3 days to raise humidity to promote infection. FHB was scored for three tagged predominant tillers after 11- and 17- dpi; total number of infected (brown discolouration or bleached) and uninfected florets were counted, and the percentage of infected florets calculated per head scored.

2.2.2.3 Data analysis

Genstat (19th edition) was used for statistical analyses of CER data. Visual analysis of residues was undertaken to assess normality of data. Score dates (11- and 17- dpi) were analysed separately using GLM following log₁₀ transformation. Predicted means and standard errors were generated for accessions along with t-probability of pairwise differences using Bonferroni method. For presentation, predicted means were back transformed to the original scale.

2.3 Results

2.3.1 Characterisation of Bd accessions under glasshouse conditions

2.3.1.1 *Fusarium* head blight susceptibility

Variation in FHB was characterised within a panel of Bd accessions using a spray inoculation experiment under glasshouse conditions (Winter 2016-Spring 2017, JIC). Sprayed heads were scored for FHB symptoms at 4-, 6-, 10- and 14- dpi on a modified percentage scale.

Browning of floral tissues was the predominant symptom of infection with FHB, first visible on lemma tissues from 4 dpi and demonstrated by sample Bd spike images in Figure 2-2. In some spikes, symptoms were limited to within a single floret and did not spread over time, whilst most plants displayed spread of browning symptoms but only above the point of infection. Bleaching symptoms occurred in the minority of infected heads. Figure 2-2b shows browning and bleaching of individual florets within a spikelet; it was common for browning symptoms to progress to bleaching locally between 6-10 dpi score dates. Spread of FHB symptoms was always restricted to individual spikelets, therefore a single infecting spore could not lead to infection of a whole spike, as Bd morphology is more similar to rice and oats than to wheat in this sense. Notably, the accession Jer-1 developed small brown circular lesions generally restricted to lower florets that did not spread over time (Figure 2-2d). There were no evident symptoms of infection in any other tissues, namely leaves and roots.

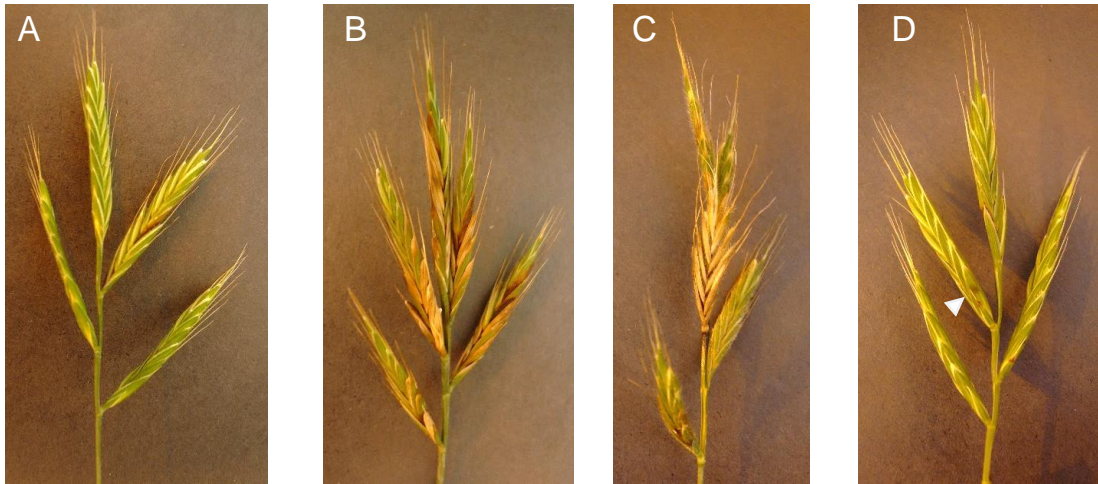


Figure 2-2 Example *Fusarium* infection phenotypes from accessions characterised under glasshouse conditions. Accessions left-right: ABR6, ABR7, BdTR12C and Jer-1. D, arrow highlights non-spreading browning lesion.

FHB susceptibility was scored on an adaptive percentage scale for the number of florets with browning or bleaching symptoms. Symptoms were scored across multiple days post inoculation (dpi) and initially analysed separately for each inoculation batch. Results presented subsequently are simplified and presented either as the single score date 10 dpi, or as AUDPC as a measure for spread of FBH symptoms over time. Mean FHB susceptibility was shown to vary significantly between the six inoculation batches ($F(5,179.8)=80.07$, $p\text{-value}<0.001$). Figure 2-3 presents the mean percentage FHB susceptibility for each inoculation batch at 10 dpi, together with the mean FHB scores for accessions within the batch. Each sequential inoculation batch had a lower mean susceptibility score than the previous (in sequential order, 46.51, 23.35, 11.34, 5.17, 3.29 & 2.51). There are more data points overall than accessions due to some accessions being present across multiple inoculation batches; for example, Koz-5 spans batches A, B and C, with mean scores of 26.01, 18.28 and 3.37 % respectively.

There was evidence that FHB susceptibility of accessions varied significantly at a 95% significance level within inoculation batches ($F(53,243.0)=4.40$, $p\text{-value}<0.001$; Figure 2-3, Figure 2-4). There was greatest range in FHB scores within the inoculation

batch C, which contained the largest number of accessions. Variation of mean FHB scores within batches is greatest in earlier inoculated batches; a small proportion of extreme early flowering accessions (Bd21-3, Bd3-1, Bd21, Bis1 and Bd2-3) have a mean score greater than 60 % in batch A, perhaps contributing the greatly inflated mean FHB for batch A. Most accessions were present only in a single inoculation batch and therefore inoculation batch could not be suitably applied as a blocking factor to account for these differences for statistical analysis.

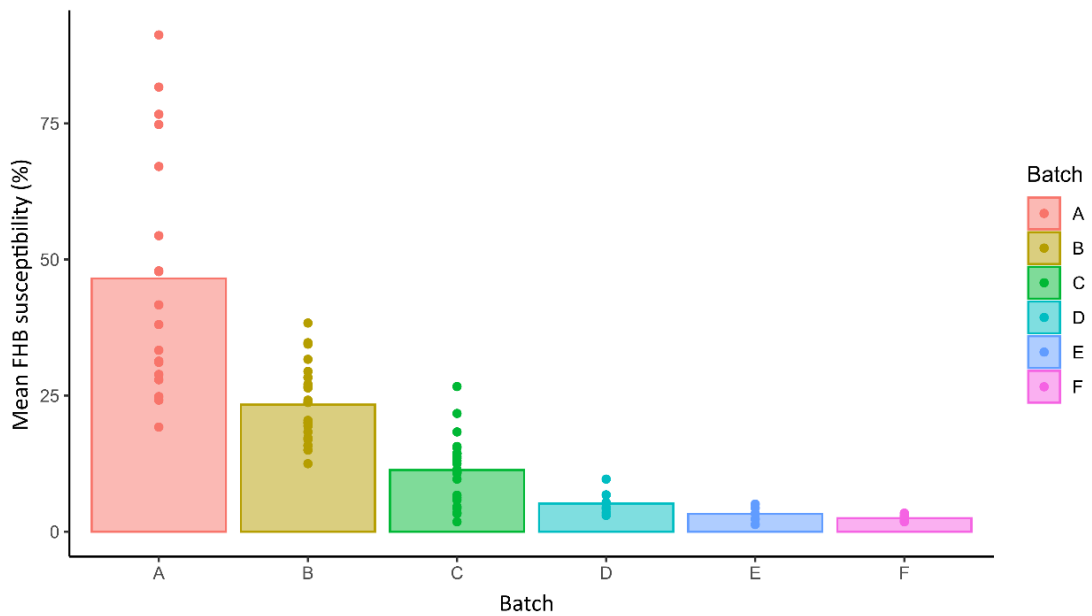


Figure 2-3 Variation in mean FHB susceptibility between inoculation batches for 2017 glasshouse spray experiment. Bars = Mean FHB percentage score at 10 dpi for each inoculation batch in date order. Points = Mean FHB score per accession, within an inoculation batch. Number of replicate plants per accession varied between batch depending on the number at correct developmental stage.

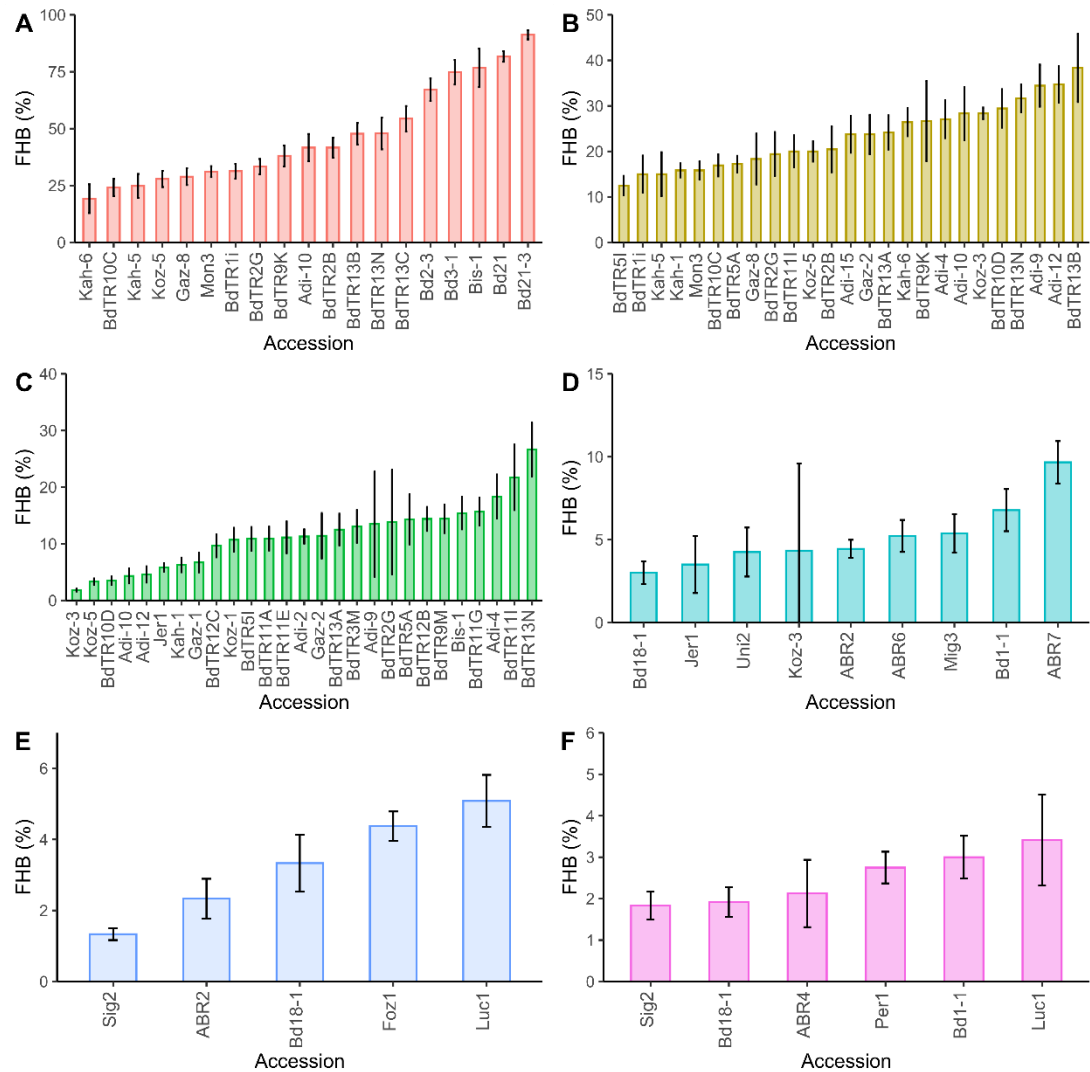


Figure 2-4 Mean FHB susceptibility (10 dpi) of *Bd* diverse accessions within inoculation batches of 2017 glasshouse experiment. Error bars = ± 1 SE

Statistical analysis using linear mixed models was undertaken on LOGIT transformed AUDPC FHB data to obtain adjusted mean FHB scores for each *Bd* accession characterised (Figure 2-5). Statistically adjusted FHB susceptibility scores ranged from 4.23 % (SE= +0.74, -0.65) for the line Jer-1 to 18.50 % (SE=+3.08,-2.66) for Bd21-3 (Figure 2-5), whereas raw mean FHB scores for these lines were 3.50 % (± 1.74) and 91.25 % (± 2.02) respectively. These values demonstrate a typical contraction in scale described for the output of linear mixed model analyses. Accessions Bd21 and Bd21-3 are significantly more susceptible than the majority of others; both of these lines are parents of mapping populations.

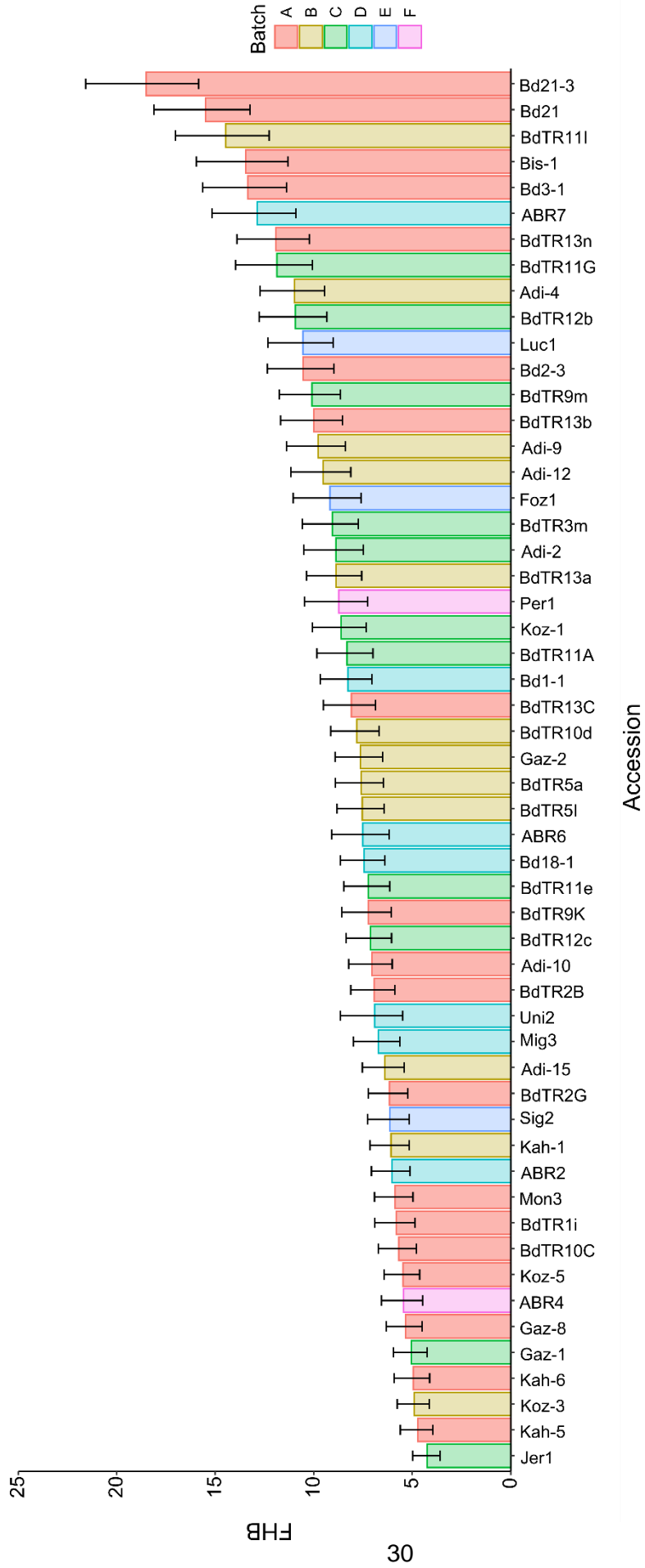


Figure 2-5 FHB AUDPC predicted mean score for 54 *Bd* natural accessions. Error bars = ± 1 SE FHB score = Back transformed BLUPs resulting from REML analysis of AUDPC data.

2.3.1.2 Is height correlated with FHB susceptibility in Bd?

In wheat, typically there is a negative association in the field between height and susceptibility to FHB. Therefore, the relationship between height and susceptibility to FHB was examined in the panel of diverse Bd accessions. Within the glasshouse experiment previously described, height of each plant was measured at the point of FHB scoring and later following senescence at mature height (Figure 2-6). No evidence for significant difference between these two heights was found (p-value= 0.68), therefore for the purposes of analysis are considered equivalent, and only mature height data is shown.

There was extensive variation in mature height of Bd accessions (Figure 2-7), with lines shown to differ significantly (p-value<0.001). Heights of primary spike at maturity ranged from 34.88 cm (SE=2.04) for Bd21-3 to 59.50 cm (SE=2.04) for Mig3, a difference of 24.62 cm.



Figure 2-6 *Brachypodium distachyon* accessions vary in height, example photographs (Left = Adi-9, Right=BdTR13C)

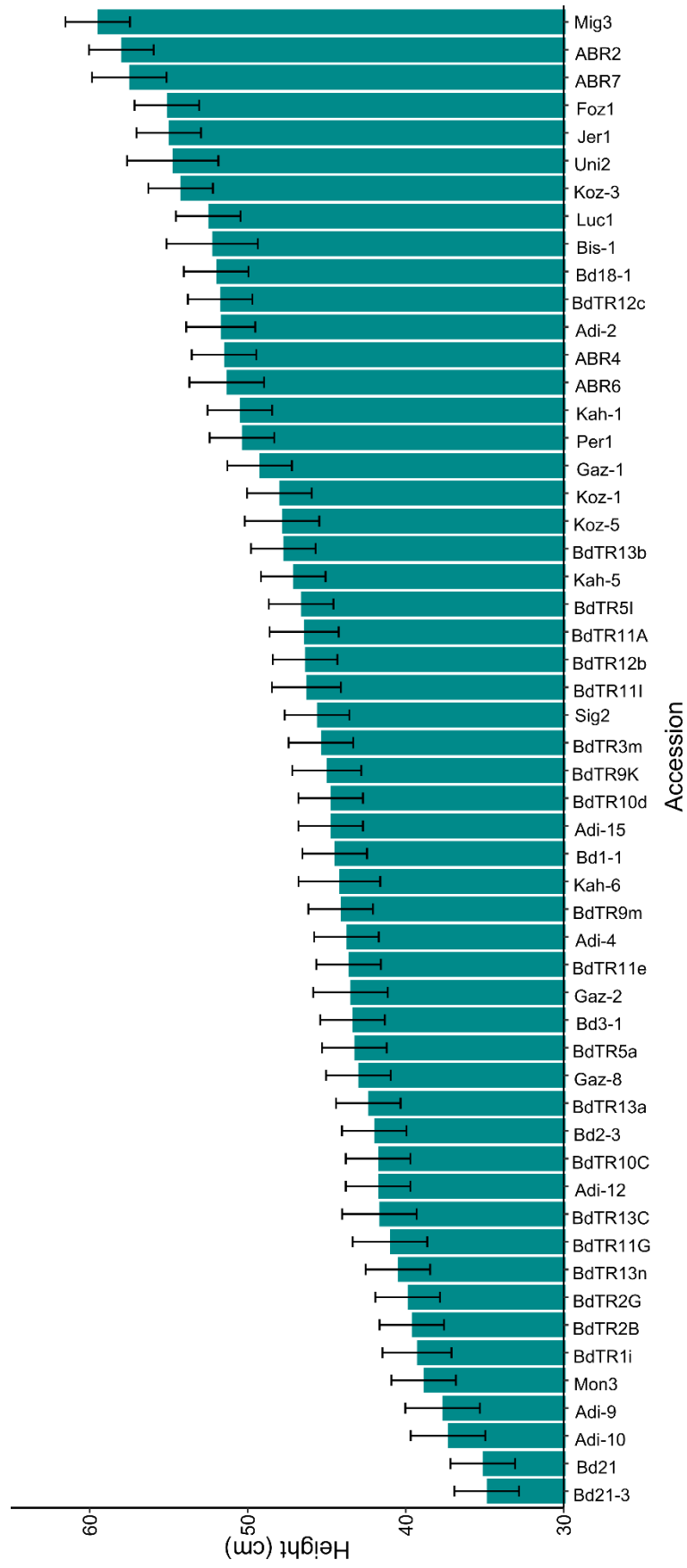


Figure 2-7 Distribution of predicted mean height of *Brachypodium* accessions under glasshouse conditions. Error bars = ± 1 SE

A negative correlation was identified between height at flowering and mean FHB score (AUDPC) within the natural Bd accessions characterised (Figure 2-8); the taller the plant the less susceptible to FHB upon inoculation. Six accessions (BdTR9K, BdTR13B, BdTR13C, Bd2-3, Bd3-1, and Bis-1) showed a greater susceptibility than predicted under this statistical trend (Figure 2-8a). No correlations were identified between mature height and FHB susceptibility within any individual inoculation batch (Figure 2-8b).

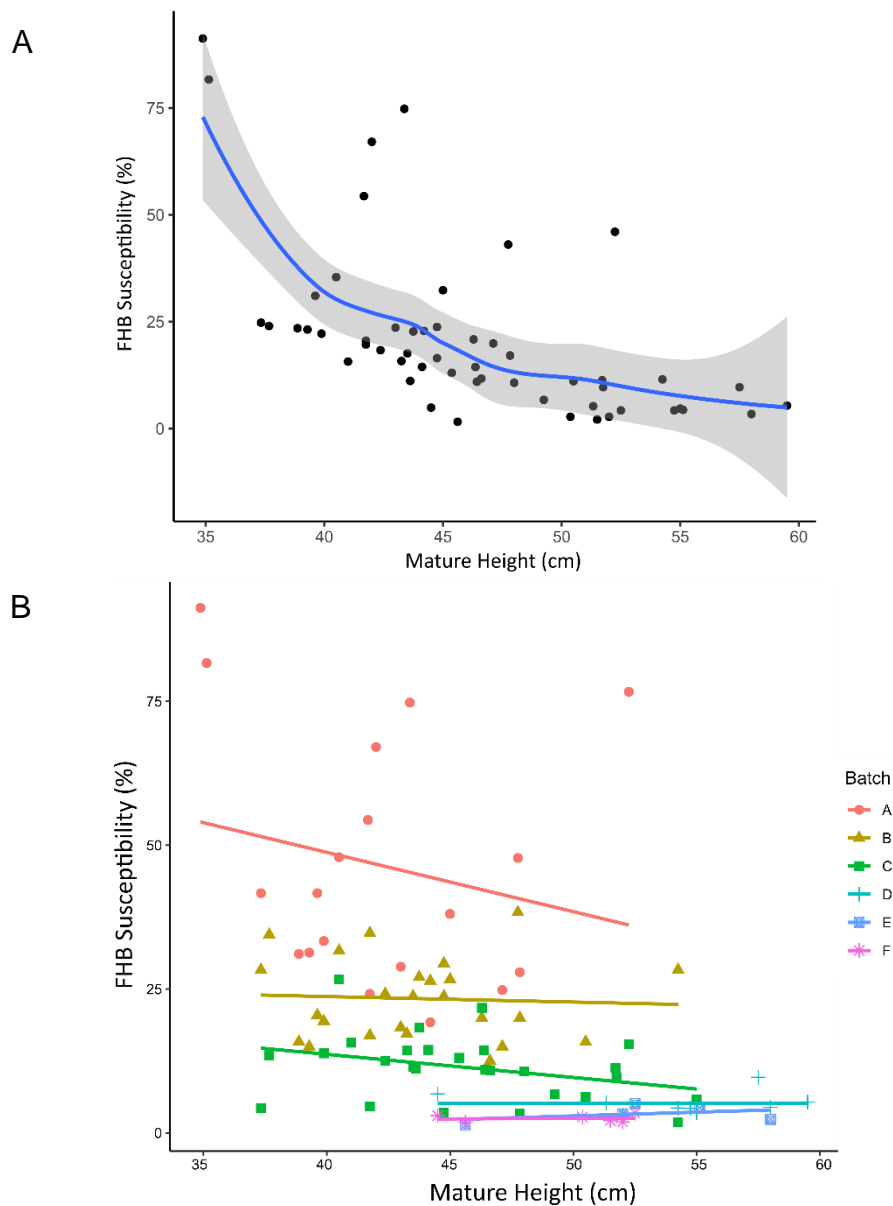


Figure 2-8 Correlation between height at flowering and mean FHB score (AUDPC, BLUPs) for a panel of 54 Bd accessions characterised under glasshouse conditions. A, Trendline prepared using Loess method, grey area = 95 % confidence interval, B, Points coloured by inoculation batch, each with trend line prepared using Linear Model method. There are >1 data point for accessions in multiple batches.

2.3.1.3 Flowering time vs FHB

To allow the examination of flowering time-FHB relationship, the panel of Bd accessions was characterised for flowering time following a six-week period of vernalisation, under glasshouse conditions (16-hour daylength). The date of emergence of the first immature floral spike was recorded for each replicate plant (Figure 2-9).

Flowering time was shown to be significantly different between accessions ($p < 0.001$). The earliest flowering accessions were Bd21-3 and Bd21, with mean emergence of 19.62 and 20.5 days respectively ($SE = 0.59$). Conversely, the accession flowering latest was ARB4 with a mean emergence time of 41.43 days post vernalisation ($SE = 0.63$). This difference of just under 22 days, represents a differential of 211 % between the early- and late- flowering extremes of Bd21-3 and ABR4.

Within the glasshouse experiment, the earlier the flowering time of an accession, the higher the susceptibility to FHB; susceptibility declined exponentially with later flowering (Figure 2-10). Spread of the heading date – FHB relationship curve observed within the central flowering-time period is a result of the greater representation within the population scored; there are a limited number of accessions showing extreme flowering times, either early or late (Figure 2-10). Mature height and flowering time of the Bd accessions were also found to be positively correlated (Figure 2-11).

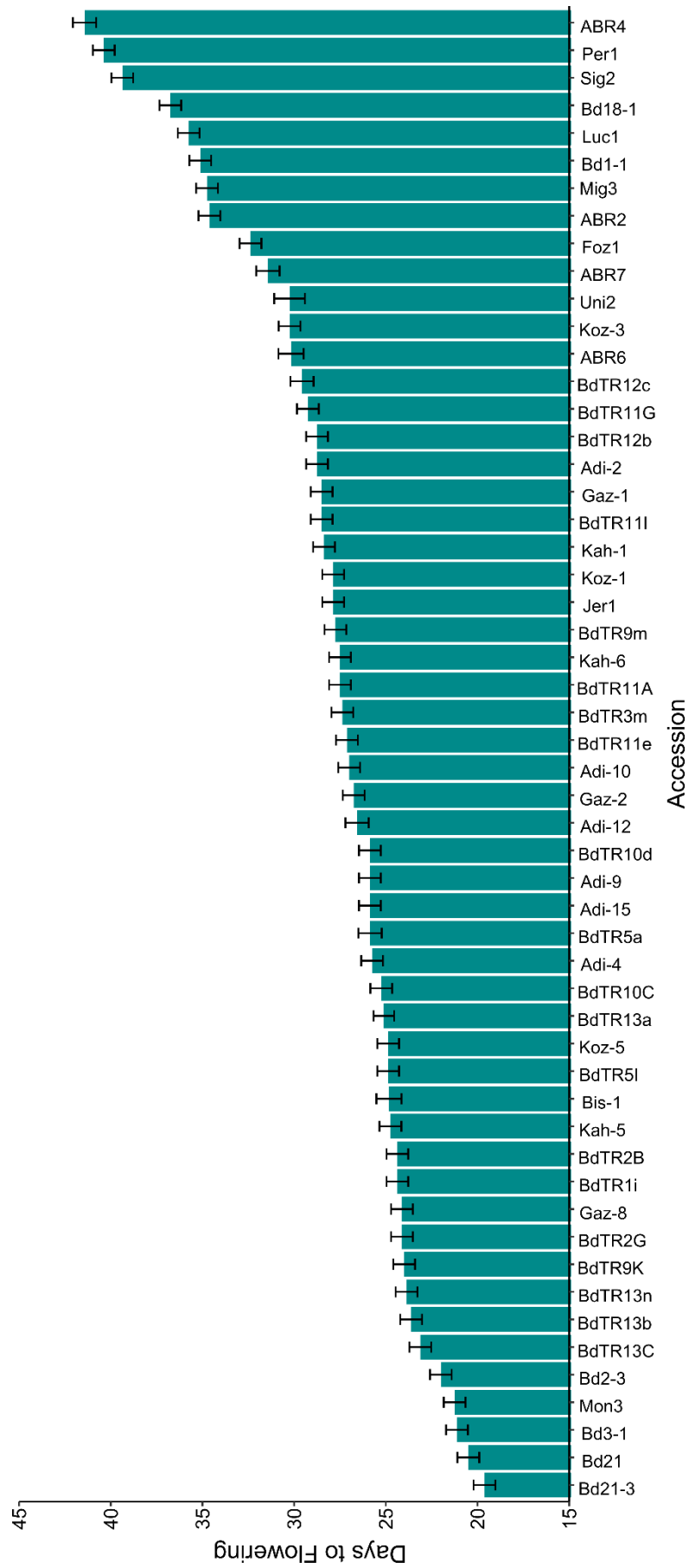


Figure 2-9 Distribution of flowering time (based on heading date) for 54 diverse accessions of *Brachypodium distachyon* under glasshouse conditions (16 hr daylength), with six weeks vernalisation. Date of first emergence of immature flower heads was recorded for eight replicate plants per accession. Error bars = ± 1 SE

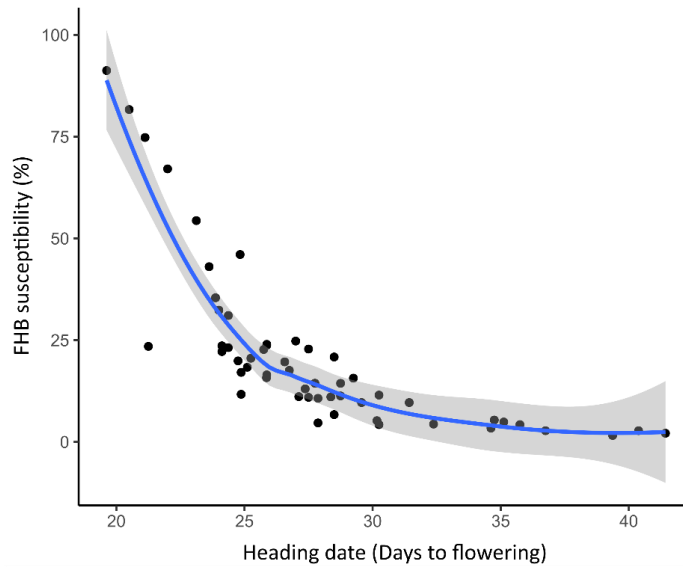


Figure 2-10 Correlation between flowering time and FHB susceptibility for a panel of 54 *Bd* accessions characterised under glasshouse conditions. Flowering time is presented as the mean number of days post vernalisation that emergence of immature floral spikes was observed, per accession. Trendline prepared using Loess method, grey area = 95 % confidence interval

The flowering time-FHB correlation is similar to the height-FHB correlation; it is not clear the causative extent of influence each of these factors may be having on susceptibility to FHB. This similarity is demonstrated by visualising the correlation between flowering time – height, presented in Figure 2-11.

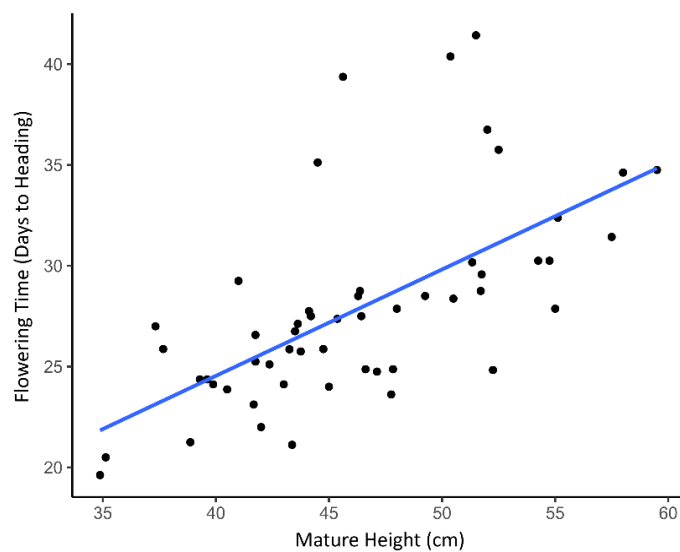


Figure 2-11 Correlation between mature height (of primary spike) and flowering time of a panel of 54 *Bd* accessions under glasshouse conditions (16hr day length, 6 weeks vernalisation). Trendline prepared using Loess method, grey area = 95% confidence interval.

2.3.1.4 FHB and trichomes

Previous studies have highlighted trichomes microscopically as potential points of infection for *F. graminearum* in Bd, maize and barley (Peraldi et al., 2011, Imboden et al., 2018, Nguyen et al., 2016b). Under this hypothesis, susceptibility of Brachypodium accessions lacking lemma trichomes would possess type I resistance to initial infection relative to trichomed lines.

Lemma trichome presence/absence was recorded for the panel of 54 Bd accessions. A clear trichome presence/absence variation was observed on the lemmas between Bd accessions (Figure 2-12).

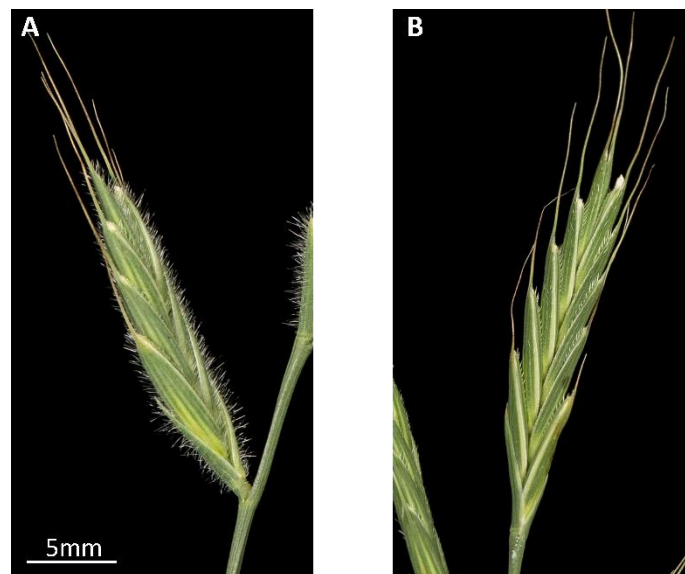


Figure 2-12 Photographs of Bd floral heads differing in lemma trichome phenotype. A, Bd21, B, ABR6 Taken by Phil Robinson (JIC photography service).

FHB susceptibility was shown to be associated with trichome presence; accessions lacking lemma trichomes were shown on average to be more resistant to FHB than accessions with lemma trichomes present (means=6.02 and 26.95 respectively, p-value<0.001). This difference observed based upon raw arithmetic mean FHB susceptibility scores was diminished following application of mixed modelling

statistical analysis that adjusted predicted means (Figure 2-13). The mean FHB difference observed between trichomed and non-trichomed accessions may reflect flowering time, as lemma trichome phenotype is confounded by this factor; the mean difference between trichome phenotypes is greatly reduced in FHB susceptibility values that account for flowering time Figure 2-13b.

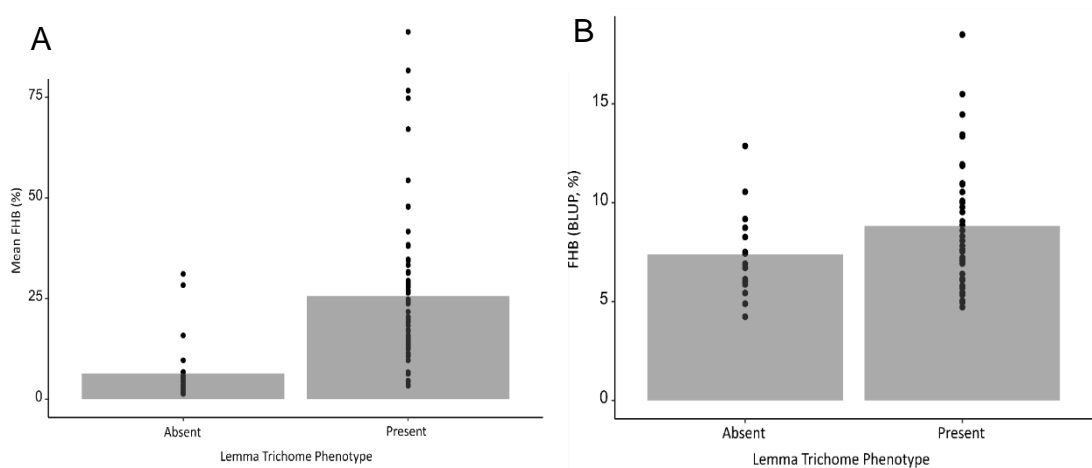


Figure 2-13 FHB susceptibility by lemma trichome phenotype of *Brachypodium distachyon* panel of diverse accessions. Means presented as bars, individual accession means presented as points within each lemma trichome phenotype. Data: A, raw arithmetic means of FHB. B, FHB AUDPC BLUP, adjusted by REML analysis.

For *Brachypodium* accessions only (48 of the 54 tested), phenotype is highlighted according to phylogeny (Figure 2-14). Trichome phenotype was largely associated with population structure, the patterns of which were suggestive of three separate/independent evolution events resulting in the disruption of functional trichome development spatially limited to lemma tissue. These events, highlighted in Figure 2-14, are thought to be located at the divergence of the 'extreme-delayed flowering' clade, the divergence of the clade of accessions of Spanish origin (plus Bd18-1), and divergence of the single accession Koz-3, of Turkish origin.

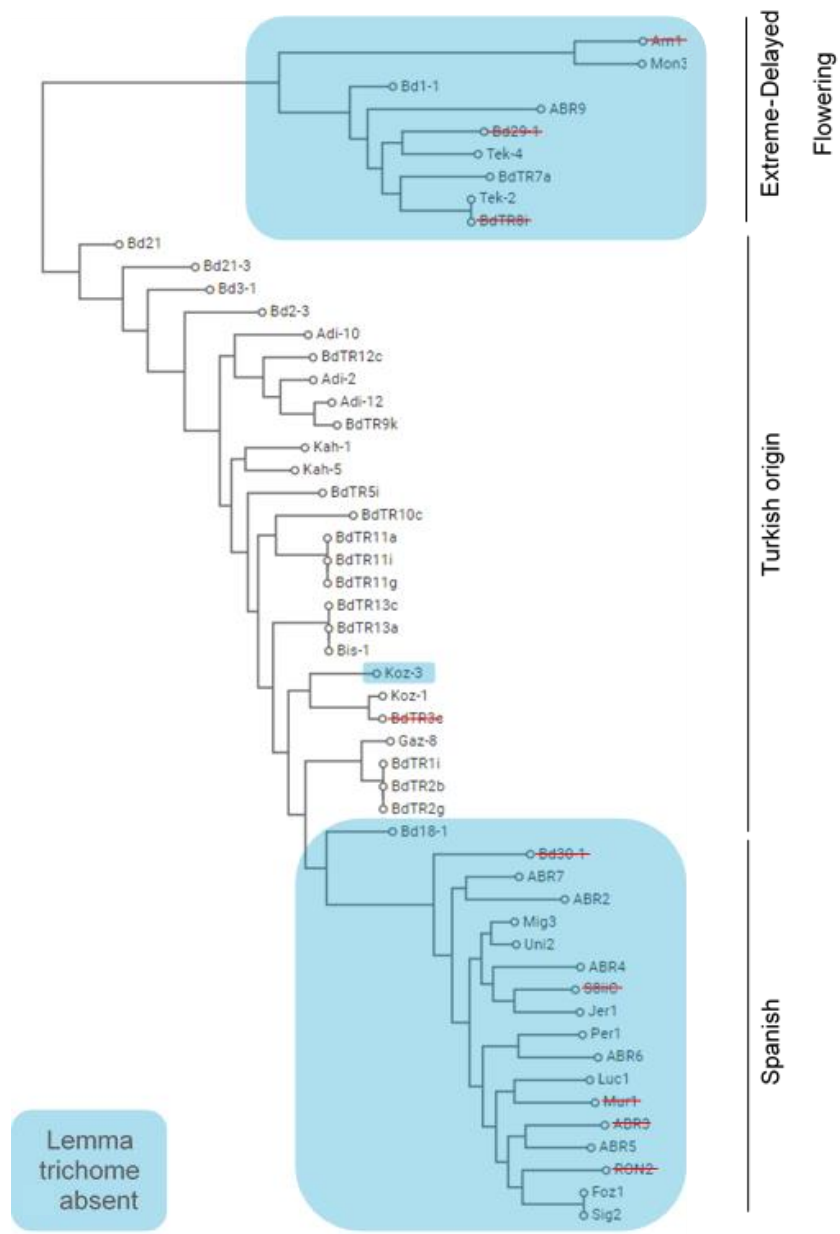


Figure 2-14. Lemma trichome absence overlaid on phylogeny of *Brachypan* accessions. Adapted from *Brachypan*. Crossed through accessions (red) were not phenotyped due to being unobtainable.

2.3.2 Further characterisation of a subset of Bd accessions under controlled conditions

For the validation of the glasshouse experiment, and more detailed comparison of a subset of Bd accessions, characterisation under controlled environment room conditions was undertaken. The aim of this experiment was to identify differential FHB susceptibility between accessions that were parental lines in a panel of available Bd mapping populations (Bd21 x Bd1-1, ABR6 x Bd21 and Foz-1 x Luc-1).

Germination of accessions was staggered according to glasshouse flowering time data (Figure 2-9), aiming to synchronise occurrence of mid-anthesis between the subset of accessions. Bd21, an accession shown to be hyper-susceptible, was sown across a range of dates as an internal control. This was successful overall, however differences in photoperiod and light levels of the CER (compared to the glasshouse) led to further variation in flowering time manifesting in non-concurrent mid-anthesis; five accessions flowered in synchronisation and were inoculated together in a single inoculation batch. Accessions that flowered more than one week later were excluded from the experiment. All plants from some lines (Bd21-3, Bd2-3, Bd3-1, Jer-1, Bd18-1) were heavily affected by root rot and therefore could not be scored for FHB and included in the data presented. Correlations between height, flowering time and FHB were not calculated due to too few accessions being characterised. Symptoms of FHB infection were scored by the counting of symptomatic vs asymptomatic florets, reported as a percentage of total florets.

Infection levels for the CER experiment were high; the most susceptible accession was Bd21, with 46.0 % of florets infected at 11 dpi (Figure 2-15). Accessions Bd1-1 (mean= 30.7 %, $p=0.018$), ABR6 (mean= 14.7 %, $p<0.001$) and Foz-1 (mean= 19.5 %, $p\text{-value}<0.001$) were significantly less susceptible than Bd21 at 11 dpi. Luc-1 (mean=39.5 %, $p\text{-value}=0.334$) was not significantly different in FHB susceptibility to Bd21.

Three mapping populations exist with parental lines included among the five accessions shown in Figure 2-15, Bd21 x Bd1-1, ABR6 x Bd21 and Foz-1 x Luc-1. FHB susceptibility varied significantly after 11 dpi for all three populations: Bd21 x Bd1-1 (means=46.0 and 30.7 % respectively, p-value=0.018), ABR6 x Bd21 (means=14.7 and 46.0 % respectively, p-value<0.001) and Foz-1 x Luc-1 (19.5 and 39.5 % respectively, p-value<0.001).

Of the Bd RIL populations available for characterisation, ABR6 x Bd21 showed the greatest parental differential in FHB susceptibility across both time points scored Figure 2-16. Bd21 showed a greater percentage (46 %) of necrotic lesions and bleaching than ABR6 (14.7 %, p-value<0.001). ABR6 and Bd21 also vary in lemma trichome phenotype. The difference in FHB susceptibility between ABR6 and Bd21 was maintained at 17 dpi (Figure 2-16). FHB symptoms in Bd21 did not progress between 11- and 17- dpi (means =46.0 and 45.3 % respectively, p-value=0.911). FHB disease symptoms ABR6 progressed between 11- and 17- dpi but this increase was not statistically significant (means=14.7 and 21.1 % respectively, p-value=0.032). This significant differential in FHB is the first known to be identified between Bd RIL parental lines and provided a promising opportunity to characterise any contributing resistance or susceptibility factors.

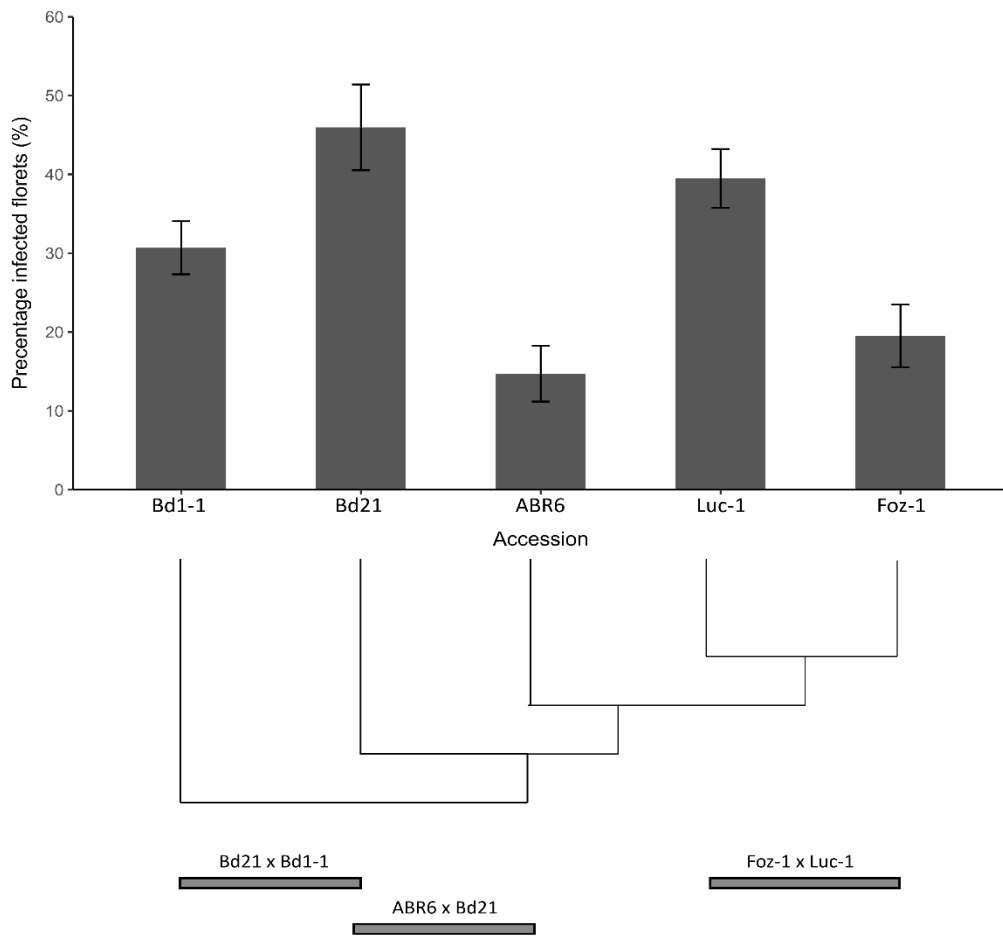


Figure 2-15 Percentage of infected florets for five *Bd* accessions after 11dpi with *F.culmorum* spray inoculation, ordered by relatedness. Error bars= ± 1 SE. Below: mapping populations available with parents, Bd1-1, Bd21, ABR6, Luc-1 and Foz-1 arranged to span dendrogram (arm size not representative of genetic distance).

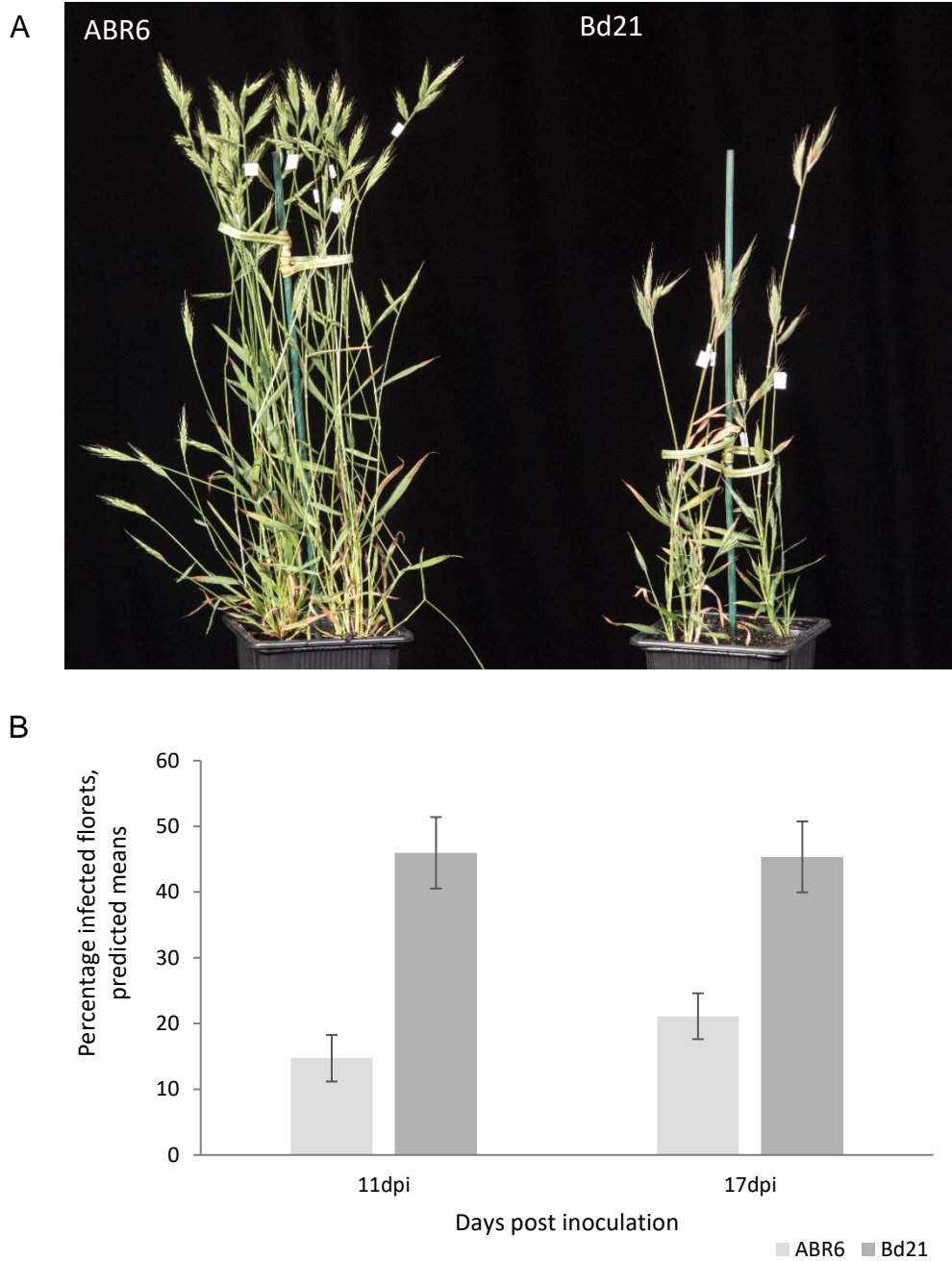


Figure 2-16. ABR6 and Bd21 differential FHB susceptibility under controlled conditions a, Photograph of ABR6 (left) and Bd21 (right) infected with FHB after 17 dpi, and disease scores at 11- and 17- dpi. Bd21 shows greater coverage of bleaching and lesions. b: 11 dpi and 17 dpi, GLM predicted means cabinet FHB, Error bars= ± 1 SE.

Foz-1 and Luc-1 also differed significantly in FHB susceptibility at both 11- and 17-dpi (Figure 2-17). Luc-1 had significantly higher FHB symptom coverage than Foz-1 at both 11- (18.24 and 39.35 %, p-value <0.001) and 17- dpi (29.77 and 56.4 %, p-value <0.001) The difference in susceptibility between Foz-1 and Luc-1 increased slightly over time from 21.11 % at 11 dpi to 26.63 % 17 dpi. Both accessions lack trichomes, so the difference in susceptibility must be independent from trichome phenotype.

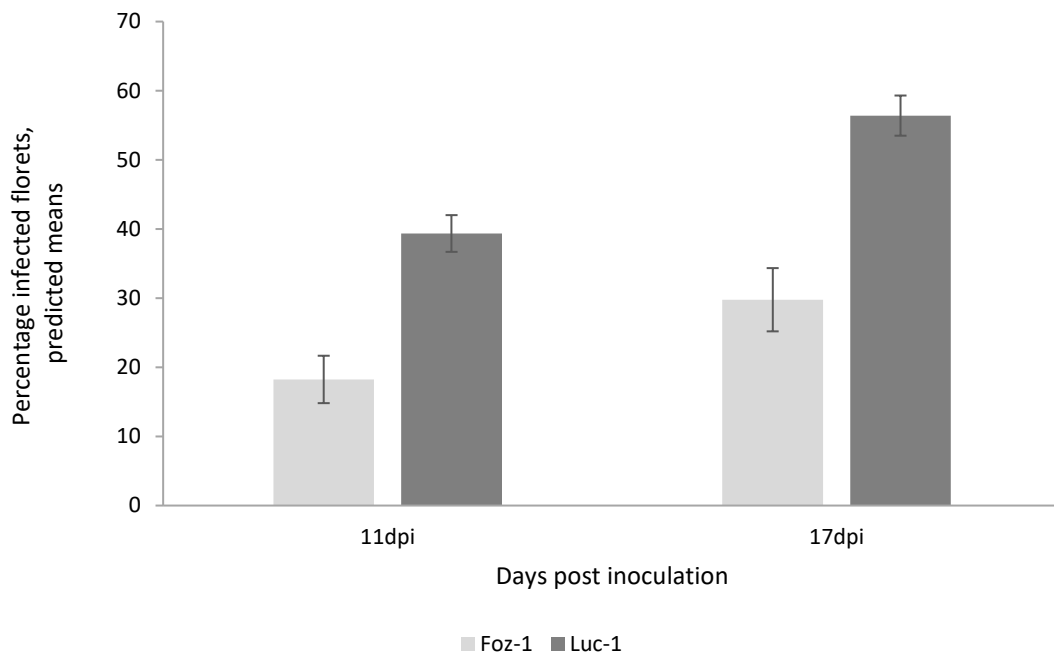


Figure 2-17 Foz-1 x Luc-1 differential FHB infection when characterised under controlled conditions, scored at 11- and 17- dpi. Error bars = ± 1 SE.

2.4 Discussion

A panel of 54 diverse Bd accessions was characterised under glasshouse conditions for susceptibility to FHB, height, flowering time, and lemma trichome phenotype. Variation was found within all traits assessed, and negative correlations between FHB and both height and flowering time were observed. Confounding variation in flowering time meant that conclusions that could be made from the glasshouse experiment alone were extremely limited. Most accessions characterised in the glasshouse experiment were sequenced as part of the Brachypan project (Gordon et al., 2017), the data available from which could mediate fine-scale genotype by phenotype relationships to be determined and compared in later work.

The main driver behind the selection of accessions for more detailed characterisation was the availability of mapping populations from the Bd research community; the direction and the aim of the overall project, once differential susceptibility was identified, was to exploit these phenotypic differences for the identification of linked genetic loci. Therefore, subsequent characterisation of a subset of lines was undertaken under controlled conditions. The ABR6 x Bd21 population was identified to be the best candidate population for the fulfilment of these requirements. These parental accessions differed significantly in FHB susceptibility in both the glasshouse and CER experiments.

2.4.1 Natural variation of FHB susceptibility in Bd

Peraldi et al. (2011) compared and characterised variation between Bd21 and Bd3-1 compatible interactions with FHB. More extensive variation was anticipated across a wider panel of accessions. Symptoms of infection observed within the glasshouse experiment, browning and bleaching spreading above infection points, were comparable to those described by (Peraldi et al., 2011), who highlighted the

similarities that are shared with symptoms of infection in wheat (Parry et al., 1995). Overall, other than in the quantitative extent, symptoms did not differ extensively across the accessions. Jer-1 was the predominant exception; extremely localised, small brown spots of infected lemma tissue, developed soon after inoculation with no development over time, with the complete absence of bleaching (Figure 2-2). These lesions looked typical of a hypersensitive, extreme resistance response of plant defence (Morel and Dangl, 1997). This is suggestive of a strong resistance response resulting in the extreme limitation of spread before infection even reaches the rachilla and spreads to adjacent florets within a spikelet.

Su et al. (2018a) published an FHB characterisation study using a similar germplasm resource after the completion of the experiments presented in this chapter, but before the submission of thesis. Only a few accessions overlap between the work of Su et al. (2018a), and the experiments described in this chapter, and the data is not comparable as widescale quantitative susceptibility scoring was not included for any lines; only example images are included for a subset of lines, three of which are present in my set of accessions. The focus of their study was on type II resistance, so plants were maintained at low humidity, whereas I wanted to gain insight into overall resistance levels and identify potent sources of resistance through achieving the maximum infection levels possible.

2.4.2 FHB and Flowering time

Flowering time varied extremely widely in the set of diverse accessions; accessions Tek-2 and Tek-4 had to be excluded from the experiment as they had not flowered even 10 weeks after vernalisation, with the earliest flowering within three weeks. All Bd accessions received six weeks of vernalisation which may not have been sufficient for Tek-2 and Tek-4. Flowering time is a highly complex trait, with vernalisation and

photoperiod mainly controlling development prior to anthesis, in response to environmental stimuli (Kamran et al., 2014). Orthologues of key wheat and barley *VERNALIZATION* (*VRN*) and *FLOWERING LOCUS T* (*FT*) genes have conserved roles in Bd (Ream et al., 2014). Woods et al. (2017b) further characterised vernalisation requirement in Bd, identifying an additional factor upstream of *VRN1*, *REPRESSOR OF VERNALIZATION 1* (*RVR1*). Natural variation in flowering time and vernalisation response has previously been characterised, on many of the same accessions that I used in this chapter (Schwartz et al., 2010, Ream et al., 2014). Two biparental Bd populations, Bd21 x Bd1-1, and ABR6 x Bd21, have been used to identify genetic loci associated with flowering time, both confirming conserved control of *VRN* genes, and identifying additional quantitative trait loci suggesting additional complexity (Woods et al., 2017a, Bettgenhaeuser et al., 2017).

FHB infection of floral tissues is highly dependent on floral development stage in wheat, with susceptibility to infection peaking at mid anthesis following the extrusion of anthers, but rapidly declining thereafter (Goswami and Kistler, 2004, Sutton, 1982, Parry et al., 1995). The relationship with FHB and flowering time is typically highly complex and relates to how conducive the environmental conditions are to infection at varying times of mid-anthesis, most importantly humidity and temperature. Due to extensive variation in flowering time between the Bd accessions, it was necessary to separate inoculations of accessions across batches (labelled A to F, A being the first and F being the last), depending on which plants had reached mid-anthesis on a given inoculation day, and therefore introducing additional variation. This resulted in some accessions being split across multiple inoculation batches. The first inoculation of batch A (earliest) failed due to low humidity and was repeated, therefore the flowering stage of these plants was advanced relative to other inoculation batches. It is unavoidable under glasshouse conditions that other factors, particularly humidity and temperature, are not constant between the batches. However, such a continuous

decreasing trend, reflected in the negative correlation between flowering time and FHB, is unlikely to be explained by random variation of these factors. Some accessions are present in two or more inoculation batches and provide evidence that the association between inoculation batch and FHB susceptibility may instead be an artefact of the experiment, rather than a genuine reflection of the effect of flowering time. It is possible that inoculum viability decreased over time, and over batches, resulting in the lower disease levels of the later inoculation batches. Within the three inoculation batches containing the largest number of accessions (A, B and C), large differences in FHB susceptibility were observed; the flowering time effect is therefore most probably an artefact of the experiment. Mean FHB scores for Koz-5 decreased across three sequential inoculation batches, which suggests a decline in mean FHB score due to experimental conditions independent of flowering time of an accession (Figure 2-4). This is highly suggestive that the correlation between susceptibility and flowering time is at least in part an artefact of the experimental conditions. Flowering time data obtained from this experiment can be used to synchronise flowering in later experiments, to account for and avoid these limiting problems.

Flowering time alone is linked with population structure, with accessions in the clades of Spanish origin and 'extreme-delayed flowering' taking longer to flower, and requiring vernalisation, compared to most accessions of Turkish origin including Bd21, the reference accession. Higher confidence FHB scores for individual accessions would be required before investigating whether population structure is associated with susceptibility to FHB. Under glasshouse conditions, with 6 weeks of vernalisation, Mon3 was amongst the most rapid flowering accessions. However, within the Brachypan project, Mon3 is classified with the extreme-delayed flowering clade. Other accessions classified into this clade, Bd1-1, ABR7, Tek-2 and Tek-4 were some of the latest flowering in my experiment, and Bd1-1 in both the glasshouse and CER 20-hour conditions. It is possible that the Mon3 seed held at JIC and used

for our experiment was genetically distinct from that sequenced for the Brachypan-genome project, and therefore the reference sequence cannot safely be assumed to be relevant for further work.

Overall, there are some conclusions that can be made from the glasshouse experiment (Winter-Spring 2017). There is evidence for variation in susceptibility to FHB within the 54 Bd accessions within the diversity panel. Many confounding factors in the glasshouse experimental setup limit the power of any conclusions, specifically for the direct comparisons between individual accessions that cannot be determined outside of the confounds of an individual inoculation batch. Therefore, these glasshouse data are insufficient alone for the assignment of relative FHB susceptibility of accessions, and by extension the identification of Bd mapping populations for the purpose of elucidating genetic factors influencing susceptibility to FHB. Replication of characterisation of the whole set of accessions, staggering germination and potting to standardise flowering time to best attempt to remove flowering time as a confounding factor, was setup as a glasshouse experiment but unfortunately this failed most likely due to the extreme heat of the summer glasshouse (2017) resulting in failure of *Fusarium* infection.

2.4.3 FHB and Height

Accessions varied dramatically in height, with the tallest accession, Mig3, almost double the height of the shortest, Bd21 and Bd21-3. Extensive variation in height is not unexpected given the highly diverse nature of the germplasm collection, and Bd being a non-cultivated species, not subject to breeder selection.

Plant height in modern wheat varieties is much more limited, with semi-dwarf varieties dramatically reduced in height compared to the genetic diversity existing in landraces. The inclusion of reduced height (*Rht*) genes in hexaploid wheat formed the basis of

the Green Revolution, breaking a historic positive correlation of plant height with grain yields, and allowing for increased fertiliser application with reduced risk of lodging, for an overall rapid increase of grain yields.

Both height and flowering-time traits are reported to be associated with FHB in wheat in the field, so the evidence provided within this experiment furthers work by (Peraldi et al., 2011) examining the suitability of *Bd* as a model pathosystem for the wheat-FHB interaction. Height was negatively correlated with FHB susceptibility in the accessions characterised under glasshouse conditions. It is often assumed that the effect of height is due to differences in microclimate with humidity levels around heads being greater in shorter plants. However, as the experiments used the artificial conditions of inoculation and incubation in humidity chambers, height should not have had a direct effect on FHB; it is much more likely a consequence of the height-flowering time correlation, and interaction with population structure. This is supported by the evidence provided by Figure 2-8b, which shows no correlation between height and FHB score within inoculation batches, therefore does not support a direct pleiotropic effect of height on FHB independent of environment.

Alternatively, pleiotropic effects of genes controlling height, such as phytohormone related genes, could influence the *Bd*-Fusarium interaction. Susceptibility to FHB at initial infection is associated with the *Rht*-B1b and *Rht*-D1b semi-dwarfing alleles in wheat (Srinivasachary et al., 2008a). For example, Saville et al. (2012) characterised the effects of *Rht* DELLA gain- and loss-of function in barley in relation to susceptibility to FHB and obligate biotrophic pathogens. The genetic nature of height differences within the *Bd* diversity panel is unknown, but if it is related to gibberellic acid signalling and metabolism, as may be expected, then this could account for the negative correlation between height and FHB. Saville et al. (2012) also discuss the effect that DELLA proteins have on cell death, and as FHB is a hemi-biotrophic pathogen with a necrotrophic stage that derives nutrients from dead cells, this could also plausibly

affect *Fusarium*-host interactions. Such trade-offs between resistance and crop performance often limit applications within a breeding program for crop improvement due to costs that would result from reduced marketability (Brown, 2002).

2.4.4 FHB and Trichomes

Presence – absence variation in lemma trichomes was widespread in the accessions characterised and shown to be closely linked to population structure. Lemma trichome absence is associated with accessions in clades of Spanish origin and ‘extreme-delayed flowering’, with the exception of Koz-3, as classified by (Gordon et al., 2017). It is possible from this population structure – phenotype overlay that three independent loss-of-function events occurred to result in the loss of trichomes in these three distinct population groups. Accessions that lacked lemma trichomes were on average more resistant to FHB than those with lemma trichomes present. Relationship between FHB and trichome could not be examined within inoculation batches due to confounding of trichomes and flowering time, for example all accessions in the earliest flowering inoculation batch possess trichomes and all accessions in the final inoculation batch lack trichomes. Reports of physical association of infecting *Fusarium* hyphae with trichomes have been made across *Brachypodium* and cereal species (Peraldi et al., 2011, Imboden et al., 2018, Jansen et al., 2005, Liu and Liu, 2016, Wang et al., 2015, Nguyen et al., 2016a). Accessions that vary in both lemma trichome phenotype, and FHB susceptibility provide an opportunity to explore genetic factors that may link the two traits. However, the glasshouse data alone is not of sufficient quality to assign FHB phenotypes of individual lines, especially as trichome phenotype is confounded within inoculation batches due to population structure.

2.4.5 Further characterisation of a subset of Bd accessions under controlled conditions

Following the uncertainty of results from the confounding factors in the glasshouse experiments, a subset of accessions was selected to be characterised under controlled conditions. These accessions were selected due to being parents of publicly available mapping populations. Therefore, characterisation under controlled conditions could serve two purposes, firstly to assess the quality of glasshouse experiment data, and secondly to identify mapping populations that could be used to identify genetic loci associated with FHB, and other traits.

Characterisation under controlled conditions showed maintenance of high susceptibility in Bd21, in line with the glasshouse assay, whereas late flowering accessions Luc-1 and Bd1-1, showed dramatically higher susceptibility compared to the glasshouse experiment whilst being significantly reduced compared to Bd21. This suggests that issues with reduced disease levels over time were overcome in this experiment compared to the glasshouse experiment.

Glasshouse flowering time data was used to stagger preparation of plant material, which was generally successful in synchronising flowering and mid anthesis therefore allowing fewer inoculation batches. Deviation from predicted flowering time, likely resulting from the daylength and light intensity differing between the experiments, resulted in the grouping of accessions into two batches. Variation in plant age presented a complication in scoring of FHB symptoms with senescence in rapid flowering lines masking both browning and bleaching symptoms at later score dates. Data could not be presented for all lines as some had to be excluded due to root rot infection or flowering earlier than expected. A different scoring method was developed, compared to the glasshouse experiment, that accounted for variation in floret and spikelet number between the accessions. It worked well for this experiment,

but was significantly more time-consuming, restricting its use to small trials with few lines.

Two populations stood out with parents differing significantly in FHB susceptibility, ABR6 x Bd21 and Foz-1 x Luc-1. Bettgenhaeuser et al. (2018) have since published the utilisation of Foz-1 x Luc-1 and ABR6 x Bd21 to investigate resistance to *Puccinia striiformis*, stripe rust.

Foz-1 and Luc-1, maternal and paternal parents of the mapping population respectively, were shown to differ significantly in FHB susceptibility at both 11- and 17- dpi. The FHB difference increases marginally over time, but it remains unclear as to whether a Type I or Type II resistance or susceptibility is responsible for the differential FHB scores from this data. No significant difference in FHB susceptibility between Foz-1 and Luc-1 was detected in the glasshouse experiment, even when both accessions were present in the same inoculation batch. Perhaps the resistance or susceptibility is more environmentally sensitive and unstable. Both Foz-1 and Luc-1 lack lemma trichomes, so any difference in susceptibility must be independent of this trait. Foz-1 and Luc-1 are very closely related relative to other accessions in the species, especially compared with the genetic distance between Bd21 x ABR6. At the time of lab work, Foz-1 x Luc-1 was in early stage of development and had not been sufficiently stabilised through single seed descent to utilise for mapping. At the time of writing, the population has been advanced to a stage that could be effectively utilised in future work. Characterisation of FHB in the Foz-1 x Luc-1 RIL population would likely explore a different source of resistance or susceptibility than the ABR6 x Bd21 population.

Parental accessions for the ABR6 x Bd21 population had an FHB difference at 11- and 17- dpi. The difference between ABR6 and Bd21 at 17 dpi was less than at 11 dpi; this suggests the primary factor is likely to be a Type I resistance, as over time the difference in susceptibility does not increase. ABR6 was also significantly more

resistant to FHB than Bd21 in the glasshouse experiment, showing that the difference is stable across environments. ABR6 and Bd21 also differ extensively in height and flowering time, and whilst ABR6 lacks lemma trichomes Bd21 has high trichome density on lemmas. Therefore, this population provides the perfect opportunity to investigate the genetic architecture of not only FHB, but the possible interactions of these loci with those of height and trichome.

Chapter 3 - Identification of QTL associated with FHB, height, and lemma trichome in ABR6 x Bd21

3.1 Introduction

Identification of quantitative trait loci (QTL) is the predominant course of research into genetic components of FHB in wheat due to the quantitative nature and environmental sensitivity of host responses (Steiner et al., 2017, Buerstmayr et al., 2009). Extensive independent studies have been undertaken in wheat, cumulatively resulting in the detection of more than 52 QTL, varying in repeatability and stability (Buerstmayr et al., 2009).

Chapter 2 described the identification of three Bd RIL bi-parental populations with parents that differ in susceptibility to FHB. The population with the greatest differential in susceptibility between the parents was between Bd accessions Bd21, susceptible, and ABR6, resistant. These accessions were also shown to vary in a lemma trichome presence/absence phenotype, and height. A study by Bettgenhaeuser et al. (2017) utilised the ABR6 x Bd21 population to identify QTL associated with vernalisation and flowering time in Bd; an additional F8 genetic map was provided by the authors for use in this chapter.

Method of inoculation typically determines resistance type under investigation; spray inoculation is used to analyse Type I, resistance to initial infection, and point inoculation is used to assess Type II, resistance to spread of infection within the head (Gosman et al., 2005, Draeger et al., 2007, Saville et al., 2012). To allow the investigation of the hypothesis that lemma trichomes provide a point of infection, spray inoculation is here applied for the analysis of Type I resistances in ABR6 x Bd21.

The aim of this chapter was to explore the following questions that were raised from the results of Chapter 2: firstly, could resistance or susceptibility factors be identified and localised in the ABR6 x Bd21 population, after which the relationships of FHB with height and lemma trichome phenotype (a possible mechanism of Type I resistance) could be examined. This chapter therefore describes the characterisation of the ABR6 x Bd21 F9 RIL population for Type I FHB susceptibility by spray inoculation, lemma trichome presence/absence and height, and the subsequent genetic mapping to identify associated genetic loci.

3.2 Methods

3.2.1 Plant materials

Seed of 104 lines from the ABR6 x Bd21 RIL population (F9) was obtained from Matt Moscou (TSL, Norwich). Plants were prepared as described in Chapter 2, grown within a CER maintained at 22 °C, 20/4 hr day/night length and 70 % relative humidity and planted two replicate RILs within a 7x7x7 cm pot. To synchronise flowering and mid-anthesis, progeny lines were grouped into staggered germination batches according to flowering time data obtained from Bettgenhaeuser *et al.* 2017, allowing for a single inoculation date to be applied to each replicate experiment. All preparation of plant material, for each germination batch, was carried out one day later than the previous germination batch.

RILs were spatially arranged in an Alpha lattice design in order to best account for uncontrollable variation in conditions between trays and replicate experiments Supplementary Figure 2. Four replicate experiments were carried out between September 2017 and March 2018, each containing two replicate plants per line. Two replicate plants of each parent, ABR6 and Bd21, were included per tray. Replicate experiment four was excluded from analysis due to low infection levels.

3.2.2 *Fusarium* inoculation

F. culmorum conidial inoculum was prepared from the same batch as described in Chapter 2. Following the tagging of the predominant three tillers, plants were spray inoculated at mid-anthesis with *F. culmorum* conidia at an approximate concentration of 1×10^5 conidia per mL amended to 0.05 % Tween 20. Trays were sprayed at a rate of c. 2 mL per plant. Humidity chambers were placed over the inoculated plants, each covering two trays, and the benches flooded with water to maintain maximal humidity.

A repeat inoculation was carried out three days later, for all reps, and the humid chamber removed at the time of the first score date.

3.2.3 Phenotyping

FHB symptoms were scored as macroscopic browning of florets, partial or complete, or bleaching. Each tagged tiller was scored for FHB susceptibility on a modified percentage scale; heads were scored 1 for signs only of initial infection, 2 for spreading of browning symptoms within but not covering a floret, and 5 for a floret completely browned by infection. For heads with two or more browned or bleached florets, percentage cover of symptoms was approximately calculated to the nearest 5%. Area under disease progress curve (AUDPC) was calculated using the formula described by (Jeger and Viljanen-Rollinson, 2001).

Height at flowering, excluding awns, of primary, secondary and tertiary tillers was measured from soil level ten days post mid-anthesis and following senescence, for all experiments. Presence and absence of lemma trichomes was recorded by eye at flowering for experiment plants and source seed.

3.2.4 Data analysis, statistics, and QTL mapping

ABR6 x Bd21 characterisation data was analysed using linear mixed modelling (REML) to obtain Best linear unbiased predictions (BLUP) across three replicate experiments (Genstat 21st edition). RIL (line) was included in the model as an effect in the fixed model along with germination batch and replicate experiment; rep, tray, pot, and plant were nested in the random model. Residuals were visually assessed for normality of the data, and independence from fitted values. FHB AUDPC values were transformed using the Logit+ formula:

$$\text{Logit + transformation;} = \ln \frac{x + 0.5}{(\text{MaxAUDPC} + 0.5) - x}$$

Multiple comparisons between lines were made using Fisher's unprotected LSD test. Predicted means (BLUP) obtained from analyses were back transformed (using Expit+ formula specific to AUDPC) to obtain predictors on the AUDPC scale for further analysis. All plots were generated using the ggplot2 package of R (3.5.2), in Rstudio (version 1.2.1335).

$$\text{Backtransformation;} x = \text{MaxAUDPC} \left(\frac{e^x}{1 + e^x} \right) - 0.5$$

Additionally, FHB data was analysed within replicate experiment using GLM (Genstat 19th edition), and predicted means obtained for a score time point (data not shown).

Height data was analysed using GLM using Genstat, with replicate experiment, tray and line included in the model. Predicted means were calculated and pairwise comparisons were performed using the RPAIR function, with parameters combinations=estimable, and adjustment=equal.

QTL mapping was carried out using the R/QTL package (Broman et al., 2003) on R version 3.5.2 and Rstudio (version 1.2.1335), using an F8 genetic map and genotype files for 169 markers obtained from Bettgenhaeuser (Unpublished). Functions 'plotMap', 'plotRF' and 'plotMissing' were used to interrogate the map. Interval mapping was performed using the 'scanone' function (SIM) and multiple imputation method (Sen and Churchill, 2001); FHB and height used parametric model, binary lemma trichome trait used non-parametric model, 'np'. Conditional genotype probabilities were calculated using the Kosambi mapping function and genotypes simulated with fixed-step distance of 2 cM, error probability of 0.001% and 128 simulation replicates. A permutation test was used to determine statistical significance of QTL, using 1000 permutations and $\alpha=0.05$ (Churchill and Doerge,

1994). Composite interval mapping (CIM) was performed for FHB and trichome traits, using the 'cim' function using the imputation method, Kosambi map function and number of marker covariates = 5. A 95 % Bayes credible interval (BCI) was calculated for each QTL using the 'bayesint' function expanded to the closest flanking markers. Percentage variance explained (PVE) was calculated for all statistically significant QTL peaks, dependent on the number of lines in the map (n):

$$PVE = \left(1 - 10^{\frac{-2 \times LOD}{n}}\right) \times 100, \quad n = 117.$$

3.3 Results

3.3.1 Characterisation of ABR6 x Bd21 F9 for FHB susceptibility

A genetic mapping approach was undertaken to identify quantitative trait loci (QTL) associated with FHB (by spray inoculation), height and lemma trichome phenotype. Characterisation of the Bd ABR6 x Bd21 F9 RIL population was undertaken under controlled environment room (CER) conditions. Severity of FHB symptoms were scored on a modified percentage scale across a time course (6, 9, 13 and 17 dpi) for three spikes per plant and two plants per RIL, as described in Chapter 2. Susceptible symptoms were observed as macroscopic necrotic brown lesions that developed within a floret and subsequently spread to and within adjacent florets (Figure 3-1). Bleaching symptoms were observed in florets terminal to necrosis within a spikelet (Figure 3-1). Some spikes showed no symptoms of infection after 17 dpi.

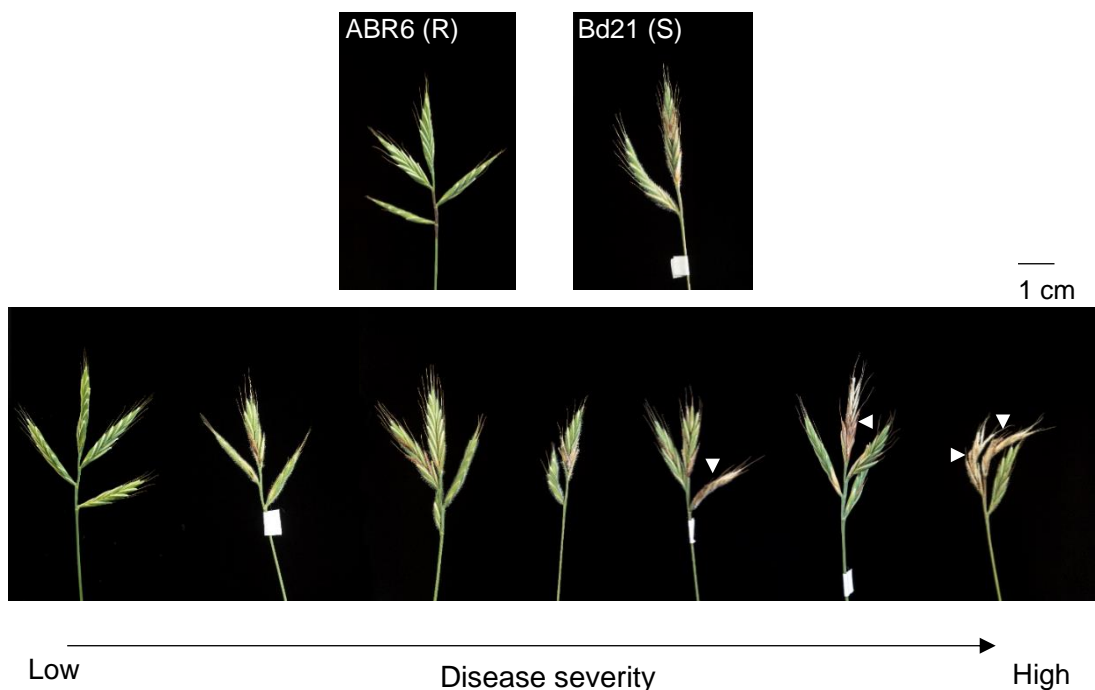


Figure 3-1 Representative FHB phenotypes for ABR6 x Bd21 RIL population (replicate experiment 1). Upper; typical symptoms of resistant parent, ABR6, and susceptible parent, Bd21. Lower; example disease scale composed of images of progeny lines, ranging from no visible symptoms, through increasing numbers of necrotic florets, to bleaching spikelets above infection points.

When analysed using REML there was evidence for differences in FHB susceptibility between the parental accessions at a 95 % significance level ($F(104,699.4)=3.33$, p -value <0.001). The scale obtained for FHB susceptibility is derived from back-transformation of predicted means based upon AUDPC FHB data. The parental difference in FHB susceptibility was maintained when screening the ABR6 x Bd21 F9 population across all four replicate experiments; ABR6 (means = 8.04, 29.47, 45.25 and 5.23) showed consistently significantly lower percentage FHB score than the hypersusceptible accession Bd21 (means = 16.56, 57.19, 85.25, 11.02) (Figure 3-2). Under the same model, there was evidence for substantial differences between replicate experiments ($F(3,19.2)=10.40$, p -value <0.001), suggesting a large effect of environmental variation. To account for this, replicate experiment was maintained in the statistical model as a nuisance blocking factor. Experiment 4 was excluded from the dataset for further analysis due to a lower infection rate and high proportion of missing values (Figure 3-2).

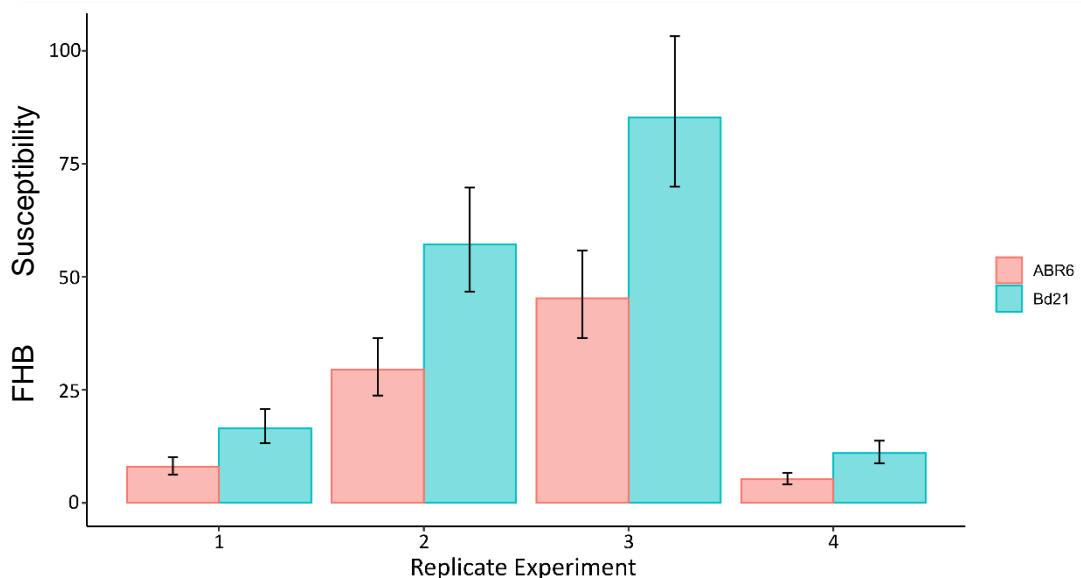


Figure 3-2 Histogram, mean FHB susceptibility of ABR6 and Bd21 in four replicate experiments for the characterisation of ABR6 x Bd21 F8 RIL population. FHB susceptibility score = means of back-transformed BLUPs obtained from analysis of AUDPC data. Error bars= ± 1 SE.

Combined analysis of the three replicate experiments was undertaken to produce a single predicted mean FHB susceptibility score for each RIL, and the parent accessions ABR6 and Bd21 (Figure 3-3, Figure 3-4). Using REML analysis there was evidence for differences between RILs across the three replicate experiments, at a 95 % significance threshold ($F(104,699.4)=3.33$, $p\text{-value}<0.001$). Bd21 was significantly more susceptible than ABR6 (FHB scores, 31.60 and 15.78 respectively, $p\text{-value}<0.001$) across the three experiments average (Figure 3-4).

Twenty-nine out of 104 accessions (proportionally 28 %) were more resistant than the resistant parent ABR6. Of these, two lines, 24 and 100 were significantly more resistant than ABR6, with scores of 4.95 and 5.52 respectively ($p\text{-values} = 0.0245$ and 0.0369 respectively). Thirty out of 104 accessions (proportion 29 %) had greater susceptibility than the susceptible parent, Bd21, with three accessions, 5, 88 and 51 significantly more susceptible than Bd21 ($p\text{-values} = 0.439$, 0.0371 and 0.435). RIL 51 showed the greatest susceptibility with a score of 58.61 ($p\text{-value}=0.435$). The remaining 45 lines showed susceptibility intermediate between the parents (43 %). The distribution in the range of FHB susceptibility of the population RILs is typical of a trait under transgressive segregation with multiple genes contributing to the phenotype.

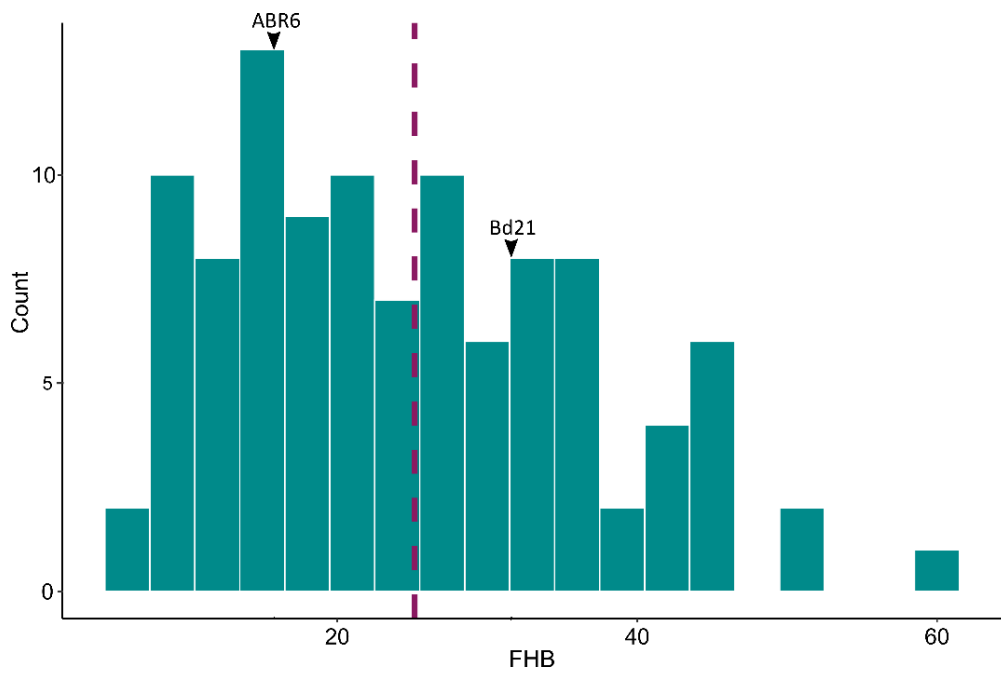


Figure 3-3 FHB distribution of 104 ABR6 x Bd21 RILs of combined AUDPC data from three replicate experiments (1-3, 4 excluded). Mean score highlighted by dashed line.

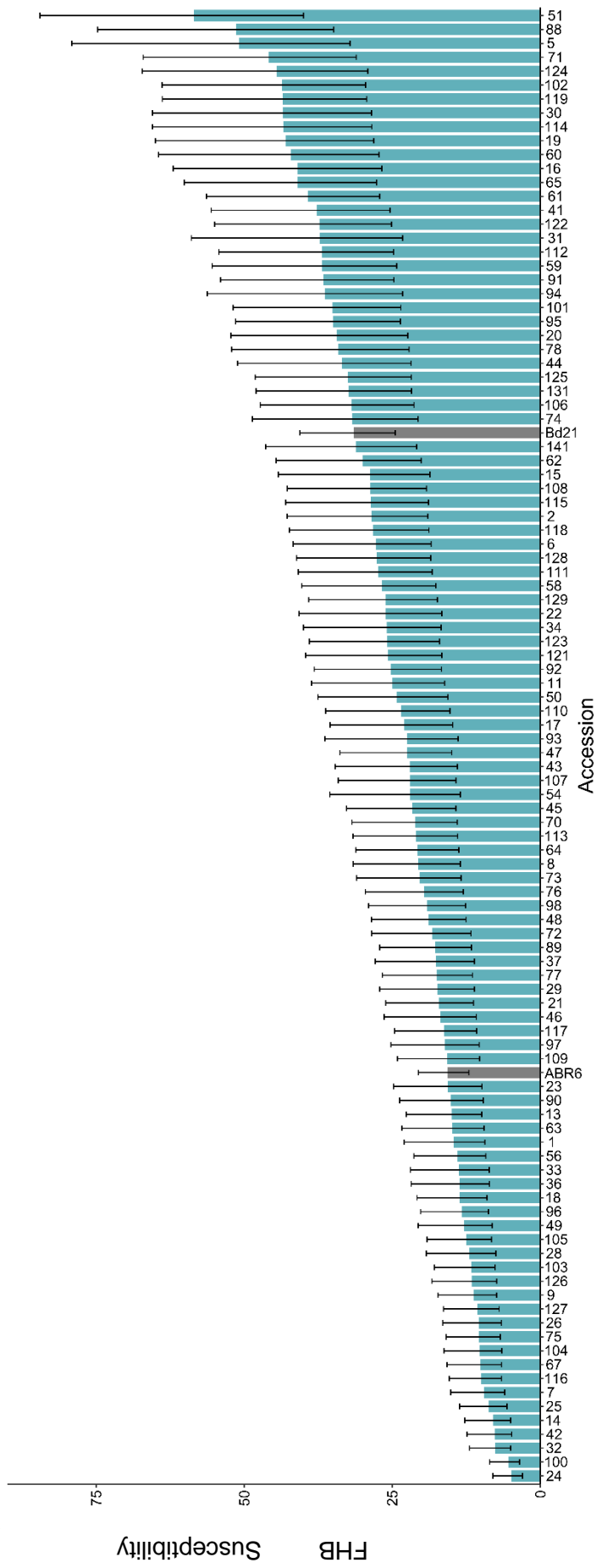


Figure 3-4 Distribution of predicted mean (BLUP) FHB scores for ABR6 x Bd21 RIL population (F1-x, F9-1). Data shown= back-transformed BLUPs obtained from REML analysis of AUDPC FHB data. Error bars = ± 1 SE

3.3.2 Height distribution, and correlation with FHB

Height was measured at maturity for the RILs in the ABR6 x Bd21 population; height ranged from 14.23 cm for RIL 126 to 32.45 cm for RIL 141 (Figure 3-5). Mean height in the population was 25.16 cm (SE=3.00). Height of the parents differed significantly but marginally compared to the variation identified in Chapter 2 (Bd21 mean=25.42, ABR6 mean=27.78, p-value=0.005). No significant correlation was found between height and FHB susceptibility for the ABR6 x Bd21 F9 RILs ($R^2=0.0042$, Figure 3-5b).

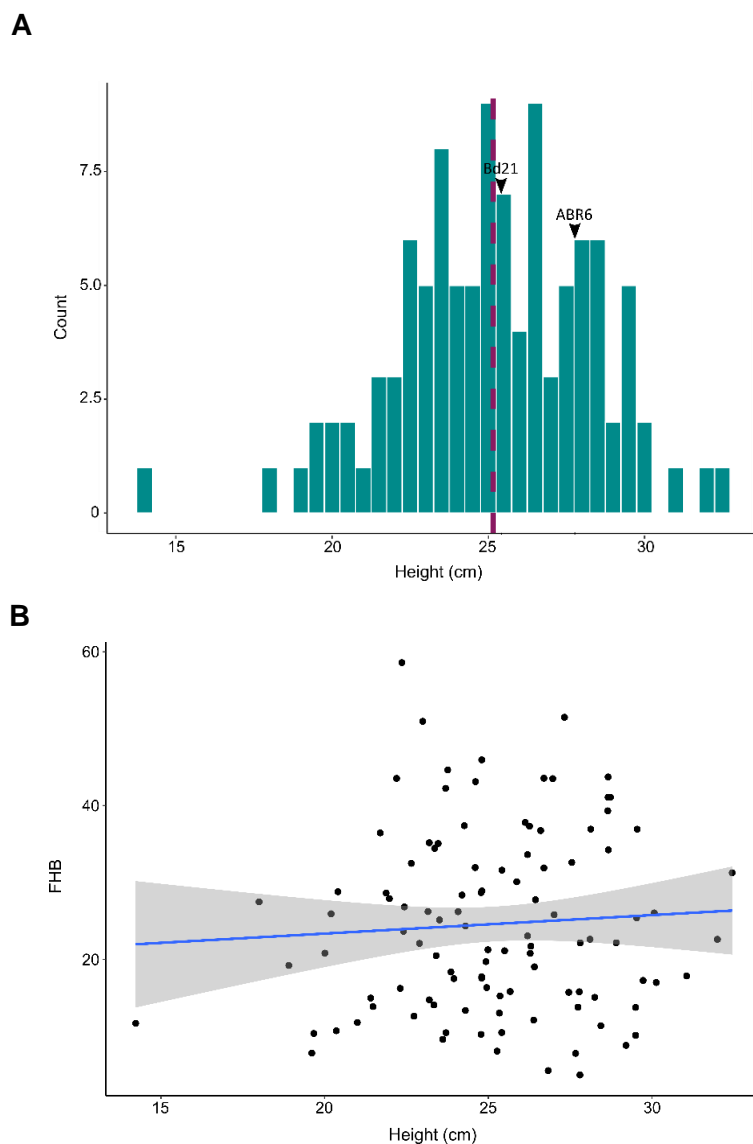


Figure 3-5 Mature height summary for ABR6 x Bd21 F9 RIL population. Above: Distribution of height (cm) BLUPs. Dashed line is height mean=25.16 (SE=3.00). Below: Correlation between BLUP mature height (cm) and BLUP FHB AUDPC data for ABR6 x Bd21 F9 RIL population. Fit of line by linear method, $R^2=0.0042$ ($y=0.0173x+24.738$), grey= 95% confidence interval.

3.3.3 QTL mapping of ABR6 x Bd21 population

Variation within the ABR6 x Bd21 population was demonstrated to be of sufficient magnitude and significance, with minimal error, that QTL mapping could be applied with confidence. A genetic map consisting of SNP marker genotype data for the 104 lines of the ABR6 x Bd21 (from F8 generation) was obtained from Jan Bettgenhaeuser (unpublished). A summary of the genetic map and genotype dataset are presented in Figure 3-6. The set of 169 markers are spread evenly across the five Bd chromosomes in centimorgan (cM) distances providing even, genome-wide representation.

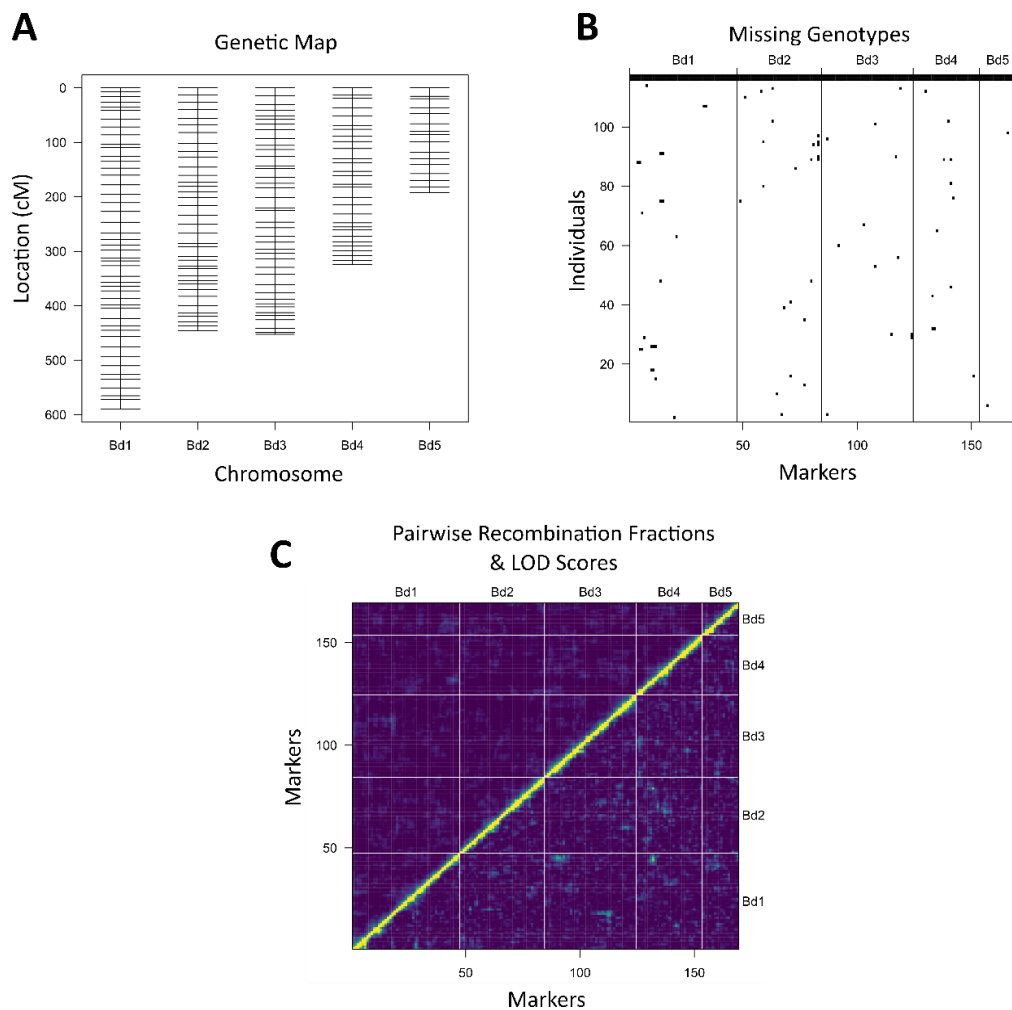


Figure 3-6 Summary of ABR6 x Bd21 F8 genetic map, genotype by Jan Bettgenhaeuser (Unpublished). A, Centimorgan based location of each of the 169 spread over five Bd chromosomes, B, Missing genotypes per marker, C, Matrix of size (tot.mar x tot.mar); the diagonal contains the number of typed meioses per marker, the lower triangle contains the estimated recombination fractions, and the upper triangle contains the LOD scores (testing $r_f = 0.5$)

Missing genotypes are also well spread, with no individual markers or RILs lacking sufficient data for exclusion in the mapping set, therefore all were retained for analysis. There are no prominent regions of extreme recombination fractions between pairwise markers (Figure 3-6c).

3.3.3.1 Identifying genetic loci associated with FHB in ABR6 x Bd21

Genome scan (SIM) and composite interval mapping (CIM) were carried out using the FHB susceptibility data obtained for the population (Figure 3-7a&b). Specifically, AUDPC predicted means (BLUPs) obtained by applying linear mixed models to LOGIT+ transformed AUDPC data, described above in Figure 3-4, were used as input data for the mapping analysis.

A single highly significant QTL was observed on chromosome 4 with a log of the odds (base 10, LOD) score of 8.98. There were no other peaks, or markers, associated with FHB susceptibility at a 95 % significance level (above a LOD permutation threshold of 3.31). Two small peaks on chromosome three did not breach this significance threshold under the conditions of this experiment (Figure 3-7b). The FHB AUDPC QTL is located in the centromeric region on the long arm of chromosome four. For the peak marker, Bd4_27278128, increased susceptibility is contributed by the B allele, Bd21; as expected considering Bd21 is the susceptible parent in the population under analysis. Percentage variation explained (PVE) is 29.77 %; there is still a lot of variation within the FHB scores for AA and BB genotypes of this peak marker (Figure 3-7c). This suggests that there may be other genes involved in controlling this trait and corroborates the transgressive segregation of FHB susceptibility observed in the population (Figure 3-4). A single RIL had a heterozygous genotype for the FHB QTL peak marker Bd4_27278128 (Figure 3-7c).

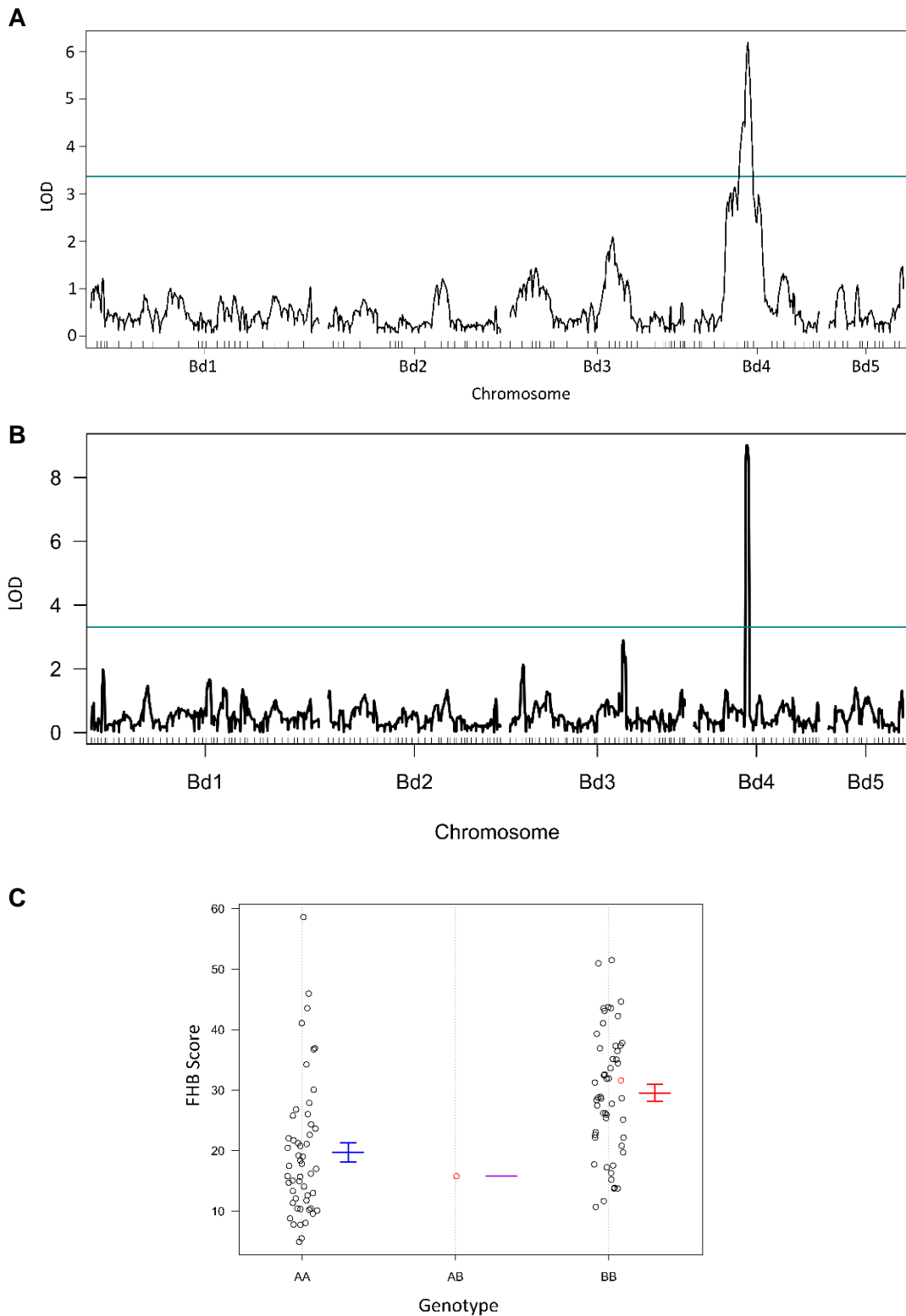


Figure 3-7 FHB susceptibility QTL summary for ABR6 x Bd21 F9 population summary. A: QTL plot of FHB SIM from AUDPC back transformed BLUPs. B: QTL plot of FHB CIM from AUDPC back transformed BLUPs. C: GxP plot for FHB QTL peak marker Bd4_27278128, showing mean FHB AUDPC scores for AA (ABR6 allele), AB (heterozygous) and BB (Bd21 allele) for ABR6 x Bd21 F9 RIL population.

A Bayes credible interval (BCI) was calculated for the Bd4 FHB QTL as a 22.9 cM region defined by markers Bd4_24653785 and Bd_29530471 (names derived from bp loci according to Bd21 reference sequence v2), a physical distance of 4.88 Mb. The Bd21 v3.1 reference sequence equivalent loci for the SNPs that these markers are designed around are Bd4_24523423 and Bd4_29421905 respectively. Each marker sits intergenic, within Bradi4g21277 and Bradi4g24390 respectively. There are 404 annotated genes within the confidence interval in Bd21 v3.1 (98 of these genes were novel annotations in Bd21 v3.1 compared to Bd21 v2.1 reference annotation).

3.3.3.2 Identifying genetic loci associated with lemma trichome presence-absence

Under the hypothesis that the presence of lemma trichomes acts as a susceptibility factor for FHB, I also characterised lemma trichome phenotype within the population. Bd21 possesses a dense, hairy coat of trichomes on the lemma, with no evident macroscopic differences on other tissues of the plant; a small number of trichomes are present at the tip of the palea tissue, with leaves appearing evenly trichomed as expected for this wild grass species (Figure 3-8b). Conversely, ABR6 lacks all visible trichomes to the naked eye exclusively on lemma tissue, with all other tissues appearing equivalent to Bd21 and other trichomed accessions (Figure 3-8a). As described in Chapter 2, this phenotypic difference is strongly tied to population structure, with accessions of Spanish origin, and those categorised as 'Extreme delayed flowering' lacking lemma trichomes (Figure 2-14).

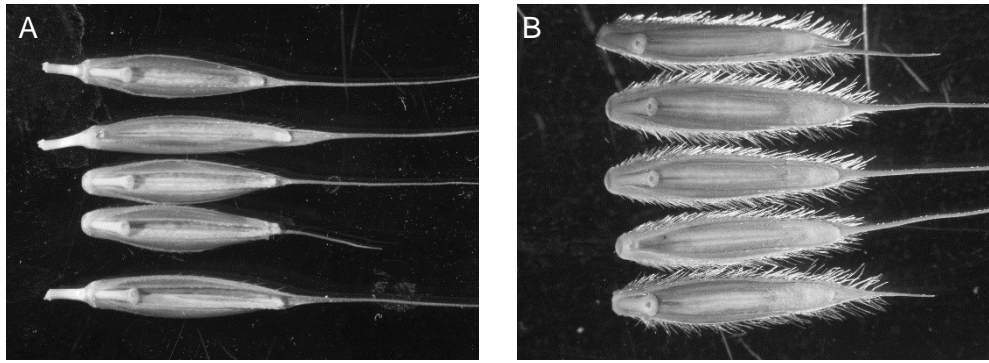


Figure 3-8. Photographs of ABR6 and Bd21 seeds displaying difference in lemma trichome phenotype. A, ABR6, B, Bd21. Courtesy of Jan Bettgenhaeuser.

The ABR6 x Bd21 population was characterised for lemma trichome phenotype, being assigned macroscopically as either lacking or possessing lemma trichomes. Distribution of the phenotype in the population was 51:53, lemma trichomes absent: present (Figure 3-9). The bimodal distribution is suggestive of a single major gene controlling a simple Mendelian trait.

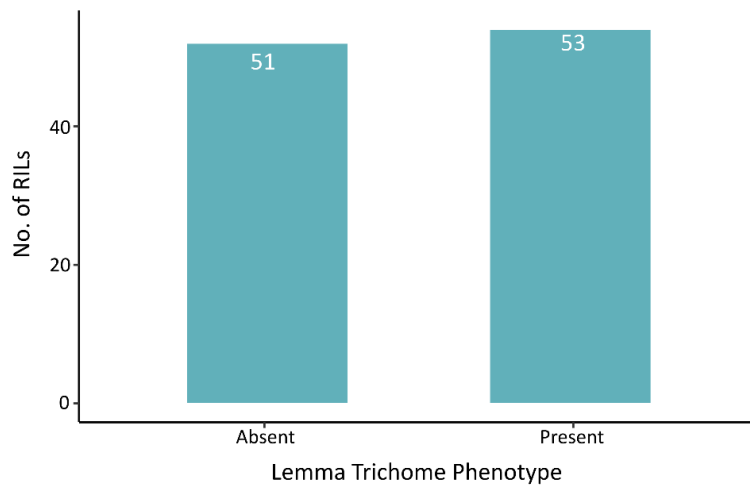


Figure 3-9 Distribution of lemma trichome presence-absence in ABR6 x Bd21 F9 population (104 RILs)

A conservative, non-parametric QTL mapping algorithm was applied to trichome data for the 104 lines to account for bimodal distribution of trichome phenotype. A single, highly significant QTL, with LOD score of 35.43, was associated with lemma trichome presence-absence, which is well over the permutation threshold of 3.31. The peak marker associated with lemma trichome presence-absence is Bd4_27278128, the same peak marker for the QTL associated with FHB (Figure 3-7). The Bayes credible interval for the trichome QTL was calculated to be a 7.6 cM region (130.2 to 137.8 cM) between markers Bd_24653785 and Bd_27278128 on Bd chromosome four. Bd21 contributes the allele conferring presence of lemma trichomes (Figure 3-10a). A single heterozygous RIL has trichome phenotype of 0 (lacking lemma trichomes) suggestive that it is not a dominant trait (Figure 3-10c). Relatively few homozygous genotypes, for both AA and BB individuals, on the genotype x phenotype plot do not align with the phenotype (Figure 3-10c). This indicates that the gene underlying the trait is linked to, but located away from, the peak marker; recombination events in these lines could be used to define a smaller peak interval.

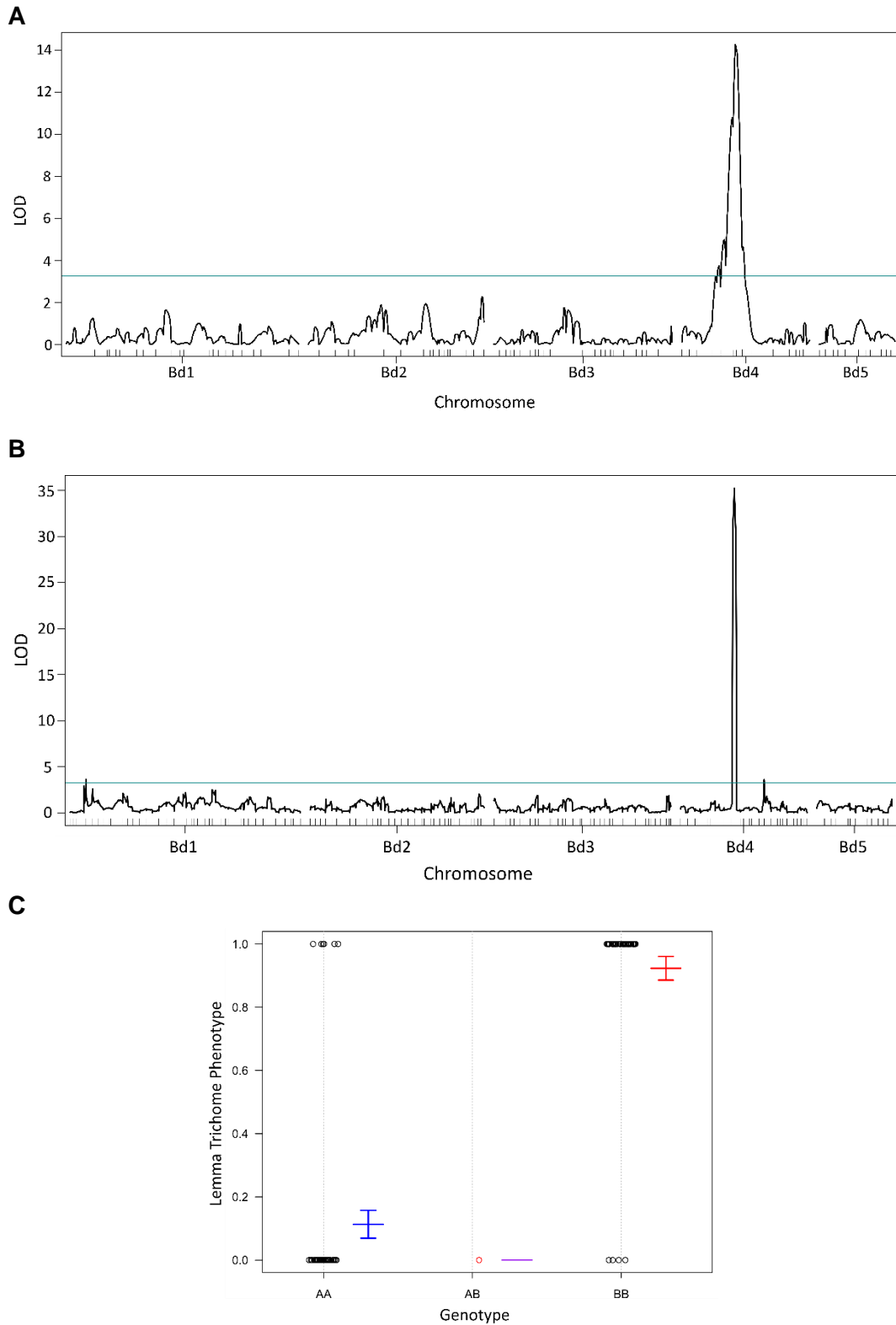


Figure 3-10 Lemma trichome QTL summary for ABR6 x Bd21 F9 RIL population. A: QTL plot, SIM, non-parametric model, B: Lemma trichome QTL by CIM, non-parametric model. C: Genotype x Phenotype plot for lemma trichome phenotype at QTL peak marker Bd4_27278128 for ABR6 x Bd21 F9 RIL population, for AA (ABR6 allele), AB (heterozygous) and BB (Bd21 allele) for ABR6 x Bd21 F9 RIL population.

There are two QTL for height in the ABR6 x Bd21 population over the LOD significance threshold of 3.29 (Figure 3-11a); a QTL peak on marker Bd1_47377165 with a LOD score of 3.92, and on marker Bd5_25818174 with a LOD score of 3.60. PVE for the QTL on Bd1 and Bd5 are 14.3 and 12.975 respectively. GxP plots for both markers show lower mean height for Bd21 marker allele than for ABR6, but with a relatively small effect for each allele (Figure 3-11b&c).

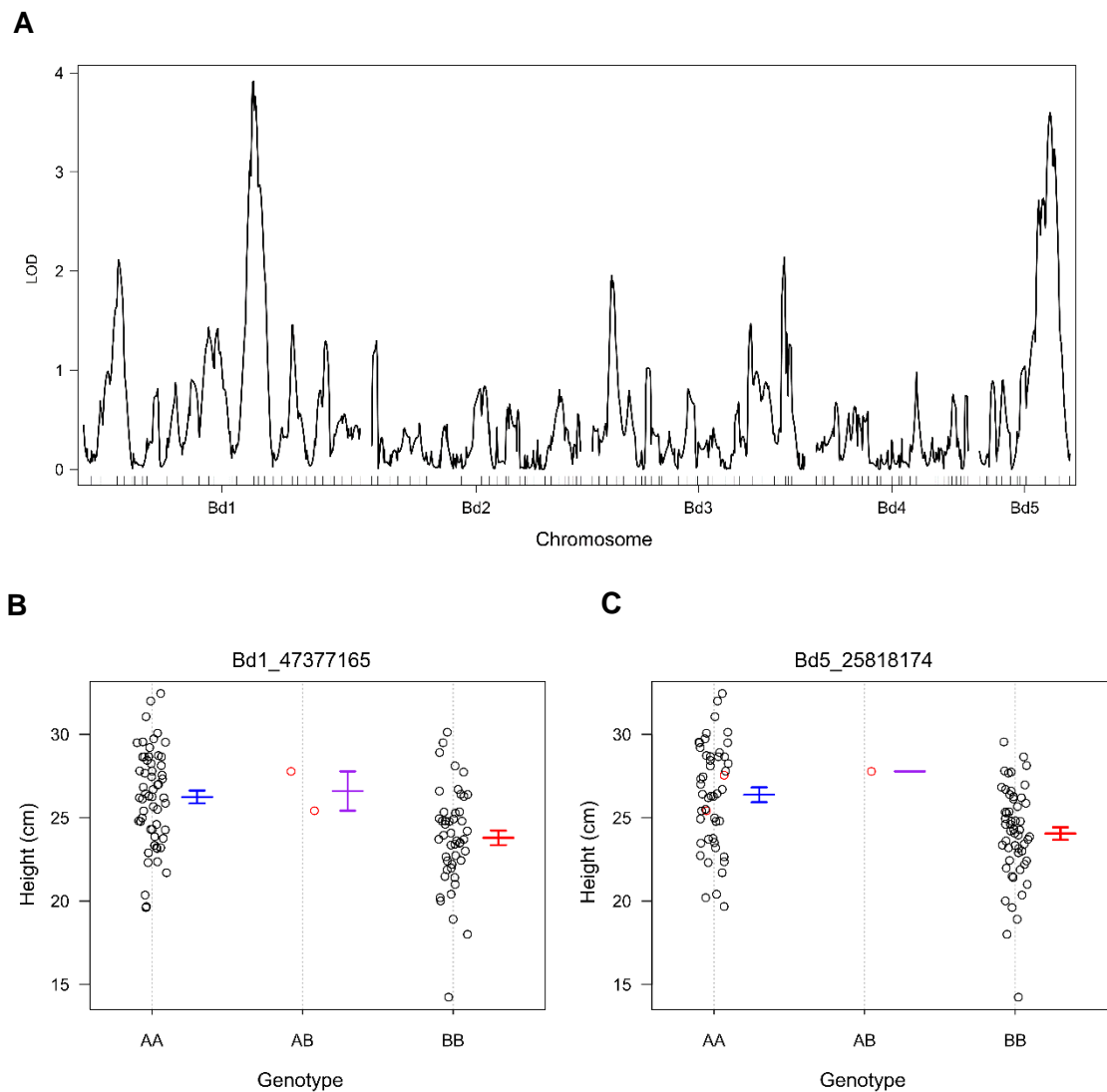


Figure 3-11 Height (cm, BLUP) SIM QTL summary in ABR6 x Bd21 F9 RIL population. Above: QTL peaks in association with height, of 169 markers. Below: GxP plots for peak markers Bd1_47377165 and Bd5_25818174, genotypes: AA= ABR6, BB=Bd21, AB = heterozygous.

A summary of the QTL identified to be associated with FHB, lemma trichome and height within the ABR6 x Bd21 population is presented in Table 3-1.

*Table 3-1 Summary of QTL identified through the characterisation of ABR6 x Bd21 population (F9) using composite interval mapping. *PT= permutation threshold, BCI= Bayes credible interval*

Trait	Chromosome: Locus, bp (cM)	High value allele	LOD	PT*	PVE (%)	p-value	BCI*
FHB	Bd4:27278128 (138cM)	Bd21	8.98	3.31	29.77	<0.004	Bd4_24653785.. Bd4_29530471 (130.2 .. 153.1 cM)
Lemma trichome	Bd4:27278128 (136cM)	Bd21	35.43	3.33	75.21	<0.004	Bd4_24653785.. Bd4_27278128 (130.2 .. 137.8 cM)
Height	Bd1:47377165 (362 cM)	ABR6	3.92	3.29	14.30	0.014	Bd1_49940174.. Bd_55510069 (71.6..386.0 cM)
Height	Bd5:25818174 (150 cM)	ABR6	3.60	3.29	12.97	0.023	Bd5_26472136.. Bd5_22654106 (118.6..170.2 cM)

3.4 Discussion

The ABR6 x Bd21 Bd F9 RIL population was characterised for FHB susceptibility to identify associated genetic loci through QTL mapping. A single QTL was identified centromeric on the long arm of chromosome four. A coincident QTL was identified in the same population, associated with the presence/absence of lemma trichomes. Coincidence of these QTL loci is suggestive that trichome phenotype on the floral tissues contributes to resistance/ susceptibility to FHB. This is consistent with the evidence that trichome structures provide points of infection to *Fusarium*. The findings allow the hypothesis to be tested through fine mapping to establish whether the relationship is causal (pleiotropic) or due to linkage.

3.4.1 Is there a genetic link between lemma trichomes and FHB?

A number of studies have identified and highlighted trichome structures playing a role in *Fusarium* infection of grasses. Peraldi et al. (2011) demonstrated accumulation of *F. graminearum* hyphae on trichome structures, and apparent penetration of trichome basal cells in *B. distachyon*. No further cytological studies have been reported for Brachypodium-*Fusarium* infection. A similar interaction was characterised in barley (Imboden et al., 2018), initially highlighted by (Jansen et al., 2005). This study observed deposition of lignin and cellulose at trichome cells in response to infection and described a difference in susceptibility between two- and six-row barley, which also differ in trichome morphology. Also in barley, Liu and Liu (2016) identified a positive correlation between trichome length and density with biomass of *Fusarium pseudograminearum* during crown rot infection. Studies of maize have described *F. graminearum* successfully penetrating three distinct trichome morphologies of maize leaves, bicellular, prickle cells and macro-hairs (Nguyen et al., 2016b, Nguyen et al., 2016a). A study of wheat by Wang et al. (2015) described leaf colonization (variety Florence-Aurore) by *F. graminearum* hyphae exploiting trichome structures and

localised within and beneath trichome cells. Furthermore, *F. graminearum* has been demonstrated to penetrate and invade host tissues through prickle cells on detached wheat glumes (Rittenour and Harris, 2010). Silica rich cells, such as trichome basal cells, have been described as sites of hyphal differentiation, penetration and mycotoxin producing infection structures (Rittenour and Harris, 2010, Imboden et al., 2018). Boenisch and Schafer (2011) observed that preferred sites of penetration of *Tri5*-GFP tagged *F. graminearum* colocalised with silica cells in wheat.

It is hypothesised that trichome structures provide sites for attachment, anchorage and penetration leading to infection by vasculature access. It is possible that the chemistry or structure of trichome basal cells is particularly amenable to infection penetration of *Fusarium* species.

The concurrence of FHB and lemma trichome QTL in the ABR6 x Bd21 population adds weight to these hypotheses and provides a method by which the genetics behind the traits can be compared. ABR6 x Bd21 is the perfect population to question the hypothesised interaction between trichome and FHB, as the parental lines differs in both FHB susceptibility and trichome presence /absence.

3.4.2 Characterisation of ABR6 x Bd21

When characterising the population, differential susceptibility of parents ABR6 and Bd21 was stable across all four replicate experiments, even the fourth in which infection levels were very low. Confounds of the experimental design, resulting in limited number of replicate plants within replicate experiments, meant that genetic analyses were also limited. When I did QTL mapping within replicate experiments, from individual reps, no significant QTL were identified. This is normal for wheat genetic analyses where it is accepted that there has to be replicated multivariate trials to see QTL.

There is evidence that lines in the F9 ABR6 x Bd21 population vary in susceptibility to FHB, independently of infection pressure. This variation was sufficient to be used for genetic analysis by QTL mapping.

Bd21 and ABR6 do not lie at the extremes of the population distribution for FHB susceptibility; this was the case for all three replicate experiments included in the analysis. It was most extreme for replicate experiment two, which had the highest disease pressure in which the parents ranked 19th and 45th (ABR6 and Bd21 respectively) in the order of FHB score for the population; 22 of 104 RILs were significantly more susceptible than Bd21 (data not shown).

The distribution of susceptibility of the 104 RILs is suggestive of a trait exhibiting transgressive segregation. Conventionally, transgressive phenotypes are controlled by the combinations of multiple genetic factors and mechanisms; these include additive alleles conferring positive or negative effects, epistatic interactions of parental genetic factors or the resolution of parental heterozygosity resulting in functional recessive alleles (de los Reyes, 2019). However, the apparent transgressive segregation distribution may instead reflect the large errors in FHB score for RILs resulting from complexity and difficulty in phenotyping; only two RILs (24 and 100) were significantly more resistant than ABR6 and only three RILs (5, 88 and 51) were significantly more susceptible than Bd21, out of a total of 104 lines.

Although only a single FHB QTL was identified, it is highly likely that other FHB-influencing factors segregated within the ABR6 x Bd21 population, if the distribution of FHB score in the population was reflective of transgressive segregation and not phenotyping complexities and errors. The substantial statistical power required to identify such minor effects means that they often go unaccounted for, especially using the conventional bi-parental mapping approach used in this chapter. PVE for the FHB QTL was 29 %, which although high compared to many published FHB QTL in cereals also supports the idea that a remaining 71 % of variance in FHB may be unaccounted

for elsewhere in the genome. This likely has the effect of quantitatively complicating the accurate assessment of FHB phenotype when it comes to fine mapping the FHB trait; the RILs do not have uniform, equivalent background genomes in terms of overall FHB susceptibility.

3.4.3 Height

Height varied extensively within the ABR6 x Bd21 population, varying from 14.23 cm for RIL 126 to 32.45 cm for RIL 141 (Figure 3-5), and to a much greater extent than the parents (Bd21= 25.42 cm, ABR6= 27.78 cm). This is a much more plausible case of transgressive segregation within the population than for FHB as discussed.

Most importantly for the focus of the thesis, characterisation of the FHB factor, no evidence was found for a correlation between height and susceptibility or resistance to FHB (Figure 3-5). This supports the rationale that the height-FHB relationship identified in Chapter 2 was in fact a confounded manifestation of the height-flowering time correlation. Two QTL were identified in associating with height, only marginally significant, with low PVE values, each independent of FHB QTL. These two pieces of evidence eliminate focus on Bd height in this thesis.

3.4.4 FHB QTL

Genetic mechanisms of Fusarium resistance in wheat are largely unknown due to the highly complex, quantitative, polygenic, and environmentally sensitive nature of the trait. Consequently, very few large effect QTL have been identified against FHB. Therefore, a single, highly significant FHB QTL in Bd, which explains a high proportion of variation, provides a potential source to identify novel genetic factors associated with FHB resistance.

At this point in the mapping process, a broad QTL peak (defined by the BCI) of 4.88 Mb physical distance has an extensive list of candidate genes, 404 in total (based on Bd21v3.1 annotation). This is far too great a number to warrant investigation into individual genes without further refinement of the physical interval. However, the most notable gene annotated within the FHB QTL region is Bradi4g22656, the orthologue of *TaFROG*. This orphan gene, restricted to within the *Pooideae* subfamily of grasses, has been reported to enhance resistance to FHB causing species, especially those producing deoxynivalenol mycotoxin (Perochon et al., 2015).

Bd21 contributed the high value (susceptible) allele in the population (Figure 3-7). A single RIL with AB genotype for the peak marker (Bd4_27278128) has an FHB score that sits closer to the mean of the AA genotype RILs, suggesting dominance of the resistant A allele on the basis of this one event; however the range of susceptibility of the BB genotype RILs extends to below the score of the AB RIL, so the dominance of the QTL cannot be confidently concluded.

The significant peak in association with FHB on chromosome four is close to, but not co-incident with, a region of segregation distortion on Bd4 identified by (Bettgenhaeuser et al., 2017). The region of segregation distortion is centromeric on the short arm of chromosome four while the FHB QTL is centromeric on the long arm, so the two are physically distinct. This is a plausible reason behind the upstream shoulder on the FHB QTL peak.

The FHB QTL Bd region is approximately syntenic with regions on group 4 chromosomes of wheat; corresponding orthologues in Chinese Spring wheat identified by BLASTP of the flanking genes Bradi4g21277 and Bradi4g24378, and a range of genes within the QTL interval were used to define syntenic regions. Non-contiguous regions were identified as follows: a 42 Mb region on 4A(L):492527576..534546838, a 26 Mb region on 4B(S):89518545..116209591 and a 23 Mb region on 4D(S):62465720..85588218 (IWGSCv2 loci). The most notable

characterised FHB related factor of chromosome 4BS is *Rht-B1*, shown to confer Type 1 susceptibility to FHB, which lies as the designated gene within an extensive list of FHB QTL identified on 4BS (Steiner et al., 2019, Chu et al., 2011, Liu et al., 2013, Lu et al., 2013, He et al., 2016, Buerstmayr et al., 2012, Prat et al., 2017); however, *Rht-B1* lies outside of the syntenic region of my QTL. The Bd Chr4 FHB QTL orthologous region does overlap with a region of 4D in wheat to which an FHB susceptibility factor has recently been mapped in the reported factor affects Type 2 resistance rather than Type 1 as observed in this Bd population (Hales et al., 2020b, Hales et al., 2020a).

3.4.5 Trichome QTL

Lemma trichome phenotype is a binomially segregated macroscopic trait in the ABR6 x Bd21 population; it is characteristic of such a trait with, as one would expect, no or very little environmental influence on this development trait. This is reflected in the LOD association score of 35.43, and PVE of 75 %. Consequently, a much smaller BCI was calculated for lemma trichome than for FHB, of 2.62 Mb (compared to 4.88 Mb for FHB), due to the simplicity of the trait leading to cleaner genotype by phenotype association. This physical interval contains 163 genes in Bd21v2, from Bradi4g21257 to Bradi4g22690.

A high number of aberrant RILs from the GxP plot (Figure 3-10) provide opportunities to define the candidate region and fine-map the gene controlling trichome development based on location of recombination events in the population. A single heterozygous RIL has trichome phenotype of 0 (lacking lemma trichomes), suggestive that the presence of trichomes is a recessive trait; as only a single individual, it is possible that this is a result of genotyping error and additional lines need assessing before concluding that this is so. Assessment of ABR6 x Bd21 F4

heterozygous RILs, presented in Chapter 4, confirmed that trichome presence is indeed a dominant trait.

Arabidopsis has been the primary model of trichome research, an extensive field, which can largely be divided into trichome patterning and trichome differentiation. Bd orthologues of *Arabidopsis* genes described in the literature as controlling trichome development are located away from the QTL in Bd (Vadde et al., 2019, Cox and Smith, 2019) (Table 3-2). A chromosome four gene, Bradi4g23967 is orthologous to both trichomeless TCL1 and TCL2 genes, at Bd21 v2 locus of Bd4_28860348 which lies outside of the right boundary of the trichome QTL BCI of Bd4_27278128.

Table 3-2 *Brachypodium distachyon* genes orthologous to key trichome development in *Arabidopsis*

<i>Arabidopsis</i> Trichome Related Gene	Bd orthologue (Bd21v2)	
	Top BLAST hit(s) (Ensembl Plants)	Locus
TRICHOMELESS 1 & 2 (TCL1 & TCL2)	Bradi1g60106	Bd1: 59599498-59601441
	Bradi4g23967	Bd4: 29038530-29039517
	Bradi2g47367	Bd2: 47762586-47763462
GLABRA1 (GL1)	Bradi3g51820	Bd3: 52883784-52884839
GLABRA2 (GL2)	Bradi3g15327	Bd3: 13621558-13625805
GLABRA3 (GL3)	Bradi1g54070	Bd1: 52719687-52724721
TCP4	Bradi2g06890	Bd2: 5303550-5304989

Gramene lists 19 Bd genes annotated with GO:0010090 biological process term, named for 'trichome morphogenesis'. None of them are anywhere near the fine-mapped candidate interval. The closest is Bradi4g29250, a gene annotated with phosphopyruvate hydratase activity (Phytozome v12, Bd21 v3.1), does not sit within the BCI for either trichome or FHB QTL.

Therefore, as no genes contained have been annotated as being involved with trichome morphogenesis, and there are no orthologous of known *Arabidopsis*

trichome genes within the region, the lemma trichome QTL on Bd chromosome four is thought to be a novel locus.

3.4.6 Concluding remarks

In conclusion, this chapter identified a single significant QTL co-localised for FHB susceptibility and lemma trichome phenotype in the ABR6 x Bd21 population. Collaborators have also twice independently identified the lemma trichome QTL. The lemma trichome phenotype is a clear major gene effect. These findings will be used to fine-map the causative factor(s) within the lemma trichome QTL as a proxy for FHB, under the assumption of a causative relationship; this will be detailed in Chapter 4.

Chapter 4 - Fine mapping of lemma trichome as a potential FHB susceptibility trait

4.1 Introduction

Chapter 3 described the localisation of QTL for FHB susceptibility and lemma specific trichome absence to a coincident marker on chromosome four of *Brachypodium distachyon* in the ABR6 x Bd21 RIL population.

Preliminary work towards the fine mapping of lemma trichome phenotype was previously undertaken under a collaboration between Jan Bettgenhaeuser (Matt Moscou group, TSL) and Daniel Woods (University of Wisconsin, Madison) using the ABR6 (trichomeless) x Bd21 (trichomed) and Bd21 (trichomed) x Bd1-1 (trichomeless) populations respectively (Bettgenhaeuser et al., Unpublished). Figure 4-1 illustrates the overlapping candidate regions from these two mapping populations, resulting in a consensus candidate region approximately 125 Mb in size and containing 13 genes, the right border being defined by recombinants within ABR6 x Bd21 and the left border being defined by recombinants within Bd21 x Bd1-1.

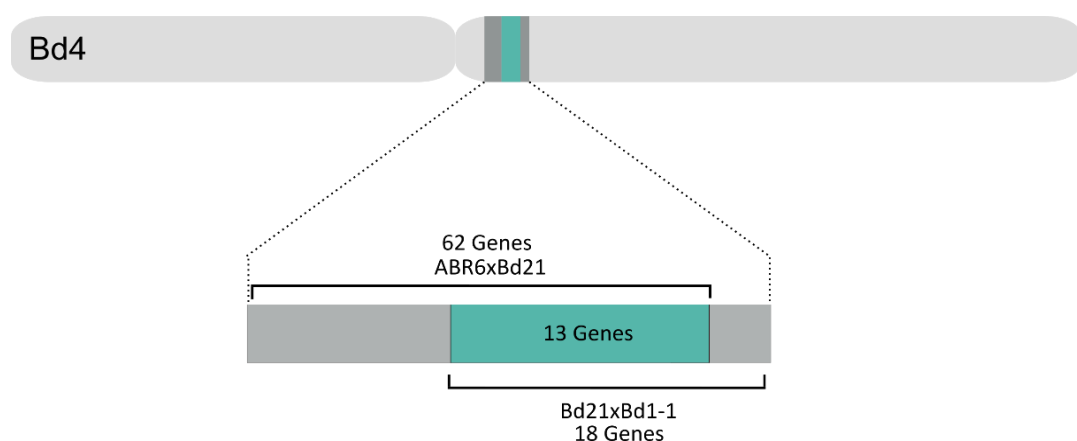


Figure 4-1 Illustration to summarise status of fine-mapping of *B. distachyon* chromosome four undertaken previously by collaborators, Jan Bettgenhaeuser, Matthew Moscou and Daniel Woods (Unpublished)

Most studies concerning trichome development focus on *Arabidopsis* as a model, and therefore also dominate trichome literature; hugely elaborate gene regulatory networks have been delineated controlling trichome development in *Arabidopsis* (Pattanaik et al., 2014). Three major classes of transcription factors typically control trichome development: R2R3 MYB, basic helix-loop-helix (bHLH), and WD40 repeat (WDR) proteins (Pattanaik et al., 2014). Phytohormones, particularly gibberellic acid, jasmonates and cytokinins, also play significant roles through modulating the expression of many regulatory genes (Qi et al., 2011, Maes et al., 2008). In *Bd* leaves, Peraldi et al. (2011) described voluminous unicellular macro-hair and prickle cells localised to rib structures overlaying vascular bundles.

As described in Chapter 3, multiple studies in *Bd*, barley, wheat and maize have highlighted trichome structures and cells as potential points of infection for *Fusarium* species (Peraldi et al., 2011, Imboden et al., 2018, Jansen et al., 2005, Liu and Liu, 2016, Nguyen et al., 2016a, Nguyen et al., 2016b, Wang et al., 2015, Rittenour and Harris, 2010). It is therefore hypothesised that the trichome projection and basal cell are exploited by pathogenic *Fusarium* species as a point of entry during infection. Under the assumption of a causative relationship between lemma trichome presence and susceptibility to *Fusarium culmorum*, this Chapter describes the continuation of fine mapping the lemma trichome phenotype as a proxy for the more complex, quantitative FHB trait.

4.2 Methods

4.2.1 Plant material and growth conditions

Brachypodium distachyon seeds were stratified for 5 days following the removal of glumes, between filter paper discs on Petri dishes saturated with three mL H₂O. Primed seeds were transferred into a mix of 50 % cereal mix, 50 % peat and sand (Supplementary Table 2), pot size depending on experiment. If vernalisation was required, seven-day old seedlings underwent six-weeks incubation at 4 °C and 16hr/8hr light/dark cycle. Seedlings were transferred to conditions of 22 °C, 20/4 hr day/night length and 70 % relative humidity in a controlled environment room or glasshouse at 16hr/8hr light/dark cycle.

4.2.2 Refinement of interval – exploiting F4-5 heterozygous families

Five F4 seed from six RILs identified as being heterozygous within the interval at F4, but unresolved at F8 (F1-x, F4-1, x=14, 47, 94, 97, 102, 117, Figure 4-2a, genotype data from Bettgenhaeuser et al. (2017)), were grown under conditions as previously described in Chapter 2. Lemma trichome phenotype was recorded for F4-5 Bd lines generated. Kompetitive Allele Specific PCR (KASP) markers were designed around intergenic SNPs identified by alignment of ABR6 and Bd21 for genes selected across the candidate interval using EMBL-EBI CLUSTAL OMEGA online multiple alignment tool (Madeira et al., 2019). Approximate locations of markers are illustrated in Figure 4-2, noting gene names. Bradi4g22630 was selected as containing the closest high-confidence SNP upstream of Bradi4g22651 and the left interval border.

A

RIL ID	Bd4_14177814	Bd4_17676468	Bd4_24719893	Bd4_27350359	Bd4_27798776	Bd4_29088128	Bd4_29307262
14	ABR6	Bd21	ABR6	Not genotyped	Het	ABR6	ABR6
47	Het	Het	Het	Bd21	Bd21	Het	Het
94	ABR6	Bd21	Bd21	Not genotyped	Het	Het	Het
97	Bd21	Bd21	Het	ABR6	ABR6	ABR6	ABR6
102	ABR6	Het	Het	Not genotyped	Bd21	Bd21	Bd21
117	ABR6	ABR6	Het	Bd21	Bd21	ABR6	ABR6

■ ABR6
■ Bd21
■ Het
■ Not genotyped

B

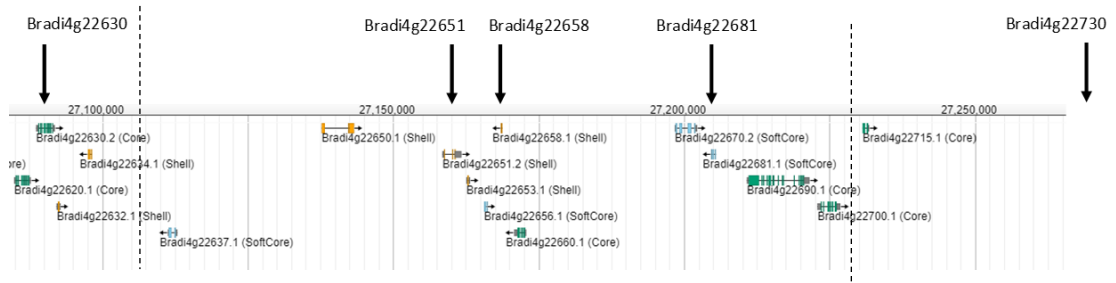


Figure 4-2 Approximate locations of KASP markers to delineate the location of unresolved recombination events in ABR6 x Bd21 F4 RILs. A, Genotype data from Bettgenhaeuser et al. (2017) for markers surrounding the candidate region. B, loci of new markers designed within the region.

Leaf material was harvested from F4-5 plants and DNA extracted in deep 96 well plates (1.2 mL) using a protocol adapted from (Pallotta et al., 2003). Samples were ground to a fine powder using the Spex GenoGrinder 2000 at 160 strokes (20 Hz) for 2 min, one tungsten bead per well. Following 5 min centrifugation at 2232 x g, 500 μ L extraction buffer (0.1 M Tris-HCl (pH 7.5), 0.05 M EDTA (pH 8.0), 1.25 % SDS, in dH₂O) was added to each well, shaken and incubated at 65 °C for 60 min, with occasional shaking. After cooling, 250 μ L ammonium acetate (6 M) was added to each well, the plate centrifuged at 2916 x g for 15 mins and 600 μ L of the supernatant transferred to ice-cold 360 μ L propan-2-ol in a new plate and mixed. Following incubation at 4 °C overnight and centrifugation at 2916 x g for 15 min, the supernatant was disposed and 500 μ L ethanol (70 %) was added to each sample. After mixing,

further centrifugation at 2916 x g for 15 min and disposal of supernatant, remaining pellets were dried prior to resuspension in 100 μ L dH₂O. DNA samples were diluted to 5-40 ng/ μ L for KASP assays.

Sequences for allele-specific and common primers are listed in Table 4-1. Following resuspension of oligonucleotides (Sigma) in dH₂O to 100 μ M, for each marker a primer master mix was made containing 12 μ L of each allele-specific primer (F1 and F2), 30 μ L of common primer and 46 μ L dH₂O. A reaction master mix was made for each marker assay allowing for 2 μ L of KASP master mix (v4.0, LGC Genomics) and 0.07 μ L primer mix per reaction, plus 20 % excess. Assays were assembled in 384 well plates, each reaction containing 2 μ L DNA and 2 μ L reaction master mix; no-template control reactions were setup with 2 μ L dH₂O instead of DNA, and plates sealed with an optically clear adhesive film. PCR reactions were performed on Eppendorf MasterCycler Pro 384 machine using the following PCR conditions: 15 min at 94 °C; 10 cycles of 20 s at 94 °C, 60 s at 65–57 °C (decreasing 0.8 °C per cycle); and 26–35 cycles of 20 s at 94 °C, 60 s at 57 °C (Burt et al., 2015). Fluorescence readings were read after forty amplification cycles using a PHERAstar microplate reader (BMG LABTECH). Relative VIC and FAM values were visualised and analysed using KlusterCaller software (LGC Biosearch®). Parental controls included in each reaction plate were used to assign the genotype of each sample based on the pooling of samples relative VIC and FAM fluorescence intensity.

Table 4-1 KASP primers used for the genotyping of ABR6 x Bd21 F4-5 RILs. Polymorphism listed in lower case. 5' tags are F1 = VIC, F2 = FAM

Marker Gene	Identifier	Primer Sequence 5'-3'	T _m
Bradi4g22630	Bradi4g22630F1	GAAGGTCGGAGTCAACGGATTGGAGCATCAAGGATTATTGGC	64.8
	Bradi4g22630F2	GAAGGTGACCAAGTTCATGCTGGAGCATCAAGGATTATTGGT	62.1
	Bradi4g22630R	CGAATCTACTGGCATTTCAGG	62.6
Bradi4g22651	Bradi4g22651F1	GAAGGTCGGAGTCAACGGATTCTGCAGAATGGCCCTCAA	65.6
	Bradi4g22651F2	GAAGGTGACCAAGTTCATGCTCTGCAGAATGGCCCTCAC	65.1
	Bradi4g22651R	GACTGCTGAAAATGATATCCG	61.5
Bradi4g22658	Bradi4g22658F1	GAAGGTCGGAGTCAACGGATTAACCAATTAATGGCATCCAAC	62.7
	Bradi4g22658F2	GAAGGTGACCAAGTTCATGCTAACCAATTAATGGCATCCAAT	62.1
	Bradi4g22658R	TAAAGCGACGGCCATGTACT	64.8
Bradi4g22681	Bradi4g22681-1F1	GAAGGTCGGAGTCAACGGATTTTCATGGAGGCTAATCGTGAA	64.7
	Bradi4g22681-1F2	GAAGGTGACCAAGTTCATGCTTTCATGGAGGCTAATCGTGAC	64.3
	Bradi4g22681-1R	TGGATGGAGCTACTCGCAA	65
Bradi4g22730	Bradi4g22730F1	GAAGGTCGGAGTCAACGGATTCTGCTGGAGTAGGCAAGAGC	64.6
	Bradi4g22730F2	GAAGGTGACCAAGTTCATGCTGCTGCTGGAGTAGGCAAGAGT	65.2
	Bradi4g22730R	TCGTAGCTTCTGTACCTGGG	62.3
Bradi4g22653	Bradi4g22653F1	GAAGGTCGGAGTCAACGGATTTCCAAGAAGAGGCATCGG	64.5
	Bradi4g22653F2	GAAGGTGACCAAGTTCATGCTTCCAAGAAGAGGCATCGA	62.7
	Bradi4g22653R	CCACTCTTCTTCCCCTCCTC	64.5
Bradi4g22656	Bradi4g22656F1	GAAGGTCGGAGTCAACGGATTATCAATTCCCCTTCCATGA	62.2
	Bradi4g22656F2	GAAGGTGACCAAGTTCATGCTATCAATTCCCCTTCCATGC	64
	Bradi4g22656R	TCTTCAGCAGAATCAGCCGT	65.4

4.2.3 Expression analysis of candidate genes

Transcription of the five genes within the refined fine-mapped trichome interval was quantified in leaf and floral meristem tissue for Bd21, ABR6 and Bd1-1 accessions using quantitative reverse transcription PCR (qRT-PCR).

At weekly intervals, a total of six plant batches were prepared for the dissection of floral meristem material; ten seed of Bd21, ABR6 and Bd1-1 were prepared using standard *Brachypodium* protocol described previously, including a vernalisation period of 5 weeks. Using a dissecting microscope, floral meristem at approximate awn initiation stage according to electron micrograph images from Derbyshire and Byrne (2013) were dissected at a stage before which trichome primordia were visible in Bd21, and the equivalent stage in the two trichome-less accessions.

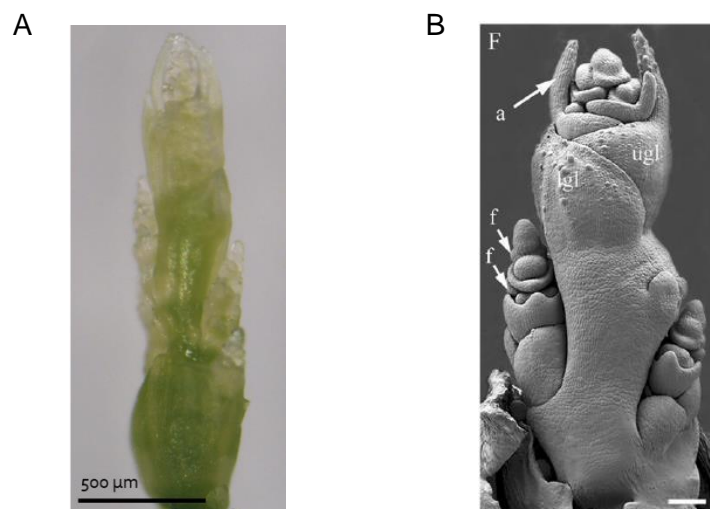


Figure 4-3. Brachypodium floral meristem; A: Image showing example floral meristem dissected from ABR6 of typical developmental stage harvested for expression analysis. B: Electron micrograph showing awn initiation stage in wild type Bd21 with floral organ growth in the terminal spikelet more advanced in basal florets compared with apical florets (Derbyshire and Byrne, 2013).

Immediately following detachment, material was flash frozen in liquid nitrogen and stored at -80°C . Leaf material was collected equivalently. Samples were pooled into three replicates per tissue, per accession. RNA extraction was carried out using the

Qiagen RNeasy Mini Kit following manufacturers protocol (eluting in 30 μ L water). Following DNase treatment using Ambion® TURBO DNA-free™ kit, RNA content was quantified using Nanodrop (v2). The Invitrogen™ SuperScript™ III First-Strand Synthesis System was used to convert 1.2 μ g per sample of RNA to cDNA, using the reaction components described in Table 4-2.

Table 4-2 Reaction components for cDNA synthesis

Component	Amount	Final Concentration
RNA	to 1.2 μ g	60 ng/ μ L
50 μ M oligo(dT) ₂₀ primers	0.5 μ L	1.25 μ M
50 ng/ μ L random hexamer primers	0.5 μ L	1.25 ng/ μ L
10 mM dNTP mix	1 μ L	0.5 mM
10X RT buffer	2 μ L	1X
25 mM MgCl ₂	4 μ L	5 mM
0.1 M DTT	2 μ L	10 mM
RNaseOUT™(40 U/ μ L)	1 μ L	2 U
Superscript® III RT (200 u/ μ L)	1 μ L	10 U
DEPC-treated water	To 20 μ L	

qRT-PCR half-volume reactions (10 μ L) were assembled in '4titude Framestar480' 384 well plates, containing 2 μ L cDNA diluted 1:4, 0.25 μ L forward and reverse primer, 5 μ L Luna ® Universal qPCR Master Mix (5X, New England Biolabs® Inc.) and 2.5 μ L nuclease-free H₂O. A Roche LightCycler480 instrument was used to carry out reactions in 384 well plates with optically clear seals. All samples had minimum two technical repetitions, most having three. qRT-PCR cycle conditions are described in Table 4-3, fluorescence for each well was read immediately following each cycle.

Table 4-3 Reaction conditions for qPCR expression quantification of lemma trichome candidate genes

Step	Sub-step	Temp (°C)	Time
	Pre-incubation	95	5 min
45 cycles of:	Denaturation	95	10 s
	Annealing	60	10 s
	Extension	72	10 s
	Fluorescence acquisition, single	75	2 s
Melting curve	Denaturation	95	5 s
	Cooling	65	1 min
	Incremental heating Fluorescence acquisition, continuous	To 97 (0.11 °C/s)	
Cooling	-	40	30 s

Primers were designed to span exons where possible, to avoid the effect of DNA contamination on transcript quantification. This was not possible for single exon genes (Table 4-4). Specificity to targets was confirmed *in silico* based on sequence alignments across accessions in case of variation disrupting efficiency and quantification.

A concentration curve for each gene primer pair was generated from pooled cDNA at a range of dilutions to confirm primer specificity through melt-curve analysis; a suitable cDNA dilution factor was determined for each gene. Three technical replicate qPCR reactions were prepared for quantification of target transcripts in each sample.

Table 4-4 qPCR primers used for the specific amplification of lemma trichome candidate genes

Gene target/ primer name	Primer sequence (5' to 3')	Length of amplicon (bp)	Exons spanned	Tm (°C)
Bradi4g22637_qF3	ATATGCTGACGCCAAACCC	210	1 only	65.2
Bradi4g22637_qR3	TCGGACGAATTCAGCTCATC			65.7
Bradi4g22641_qF1	GCACGTAGGAGAGGAACAGG	49	1 only	63.8
Bradi4g22641_qR1	AGACGGCTCTTTATGCTGGA			63.8
Bradi4g22645_qF1	TGATTTGGTGGCTGATCTTG	41	1 & 2	63.7
Bradi4g22645_qR1	CTCCCACTTGC GGATAGTTC			63.5
Bradi4g22650_qF1	GAAGCTCGGCCATAACAAAC	99	3 & 4	63.4
Bradi4g22650_qR1	GTGAGCTCCGTGAATTTTGG			64.5
Bradi4g22651_qF1	ACGCGGAAATAACGAGATTG	87	1 & 2	63.8
Bradi4g22651_qR1	CTTCATTGATGTGCTTCTCCA			62.8
UBC18_F	GGAGGCACCTCAGGTCATTT	73	1 only	65.3
UBC18_R	ATAGCGGTCATTGTCTTGCG			65.0

Arithmetic means of Cq are equivalent to the mean concentration of cDNA transcript in a sample (Orton et al., 2017). LinRegPCR software was used to calculate amplification efficiency of individual samples (Ruijter et al., 2009); mean efficiency per primer pair was used for relative expression quantification calculations. Target transcript quantity within each sample was calculated relative to UBC18 (Hong et al., 2008), using the following formula.

$$Relative\ Expression = \frac{Eff_{Gene}^{-Cq_{Gene}}}{Eff_{UBC18}^{-Cq_{UBC18}}}$$

Expression data was then analysed using GLM modelling (Genstat 19th edition) for individual gene-tissue combinations to obtain predicted means, standard errors, and significance values.

4.2.4 Comparison of candidate regions *in silico*

Annotated functions of candidate genes were obtained from Phytozome (v12) for Bd21v3.1. The closest orthologous genes in *Arabidopsis thaliana* and *Hordeum vulgare* were identified using the BLAST tool from Ensembl Plants.

4.2.4.1 Nanopore sequencing of ABR6

ABR6 plants were prepared as described in Chapter 2. Approximately 3 g (fresh weight) leaf material was harvested and ground using liquid nitrogen in a pestle and mortar prior to DNA extraction using Cytiva Nucleon™ Phytopure™ Genomic DNA Extraction kit (1 g). Genomic DNA underwent size-selection using a BluePippin (Sage Science) electrophoresis unit to remove fragments ≤ 15 kb. A sequencing library was prepared, from the fraction containing fragments >15 kb, using the Genomic DNA by Ligation Kit (SQK-LSK109, Oxford Nanopore Technologies, protocol version GDE_9063_v109_revQ_14Aug2019) using KAPA Pure Beads (Roche Sequencing Solutions) in substitution for AMPure XP. The library (756 ng) was sequenced on a single MinION flow cell using a GridION.

4.2.4.2 Tissue-specific expression (eFP)

The EMBL-EBI Expression Atlas resource (Papatheodorou et al., 2019) used to access tissue-specific expression data for *Brachypodium distachyon* Bd21 originating from a study by Davidson et al. (2012), including transcript per million (TPM) values.

4.2.4.3 Sequence comparison between parental accessions

The BLAST tool from brachypan.jgi.doe.gov (Phytozome) was used to identify equivalent ABR6 and Bd1-1 (both v1) loci for the five genes within the trichome candidate interval in Bd21 (v3.1). Alignments of Bd21 v3.1 mRNA annotated

sequences and BLAST targets were made using EMBL-EBI CLUSTAL-OMEGA and viewed using Jalview. Additionally, our ABR6 nanopore scaffold (see above, Chapter 0 & 4.3.3.3) covering the candidate region was searched as the target sequence using NCBI BLASTN using default parameters, along with Bd1-1 (v1.1) PACBIO based assembly, for comparison of gene sequences (Zhang et al., 2000). FGENESH was used to annotate exons in ABR6 nanopore and Bd1-1 (V1.1), and to predict peptide sequences (Solovyev et al., 2006).

4.2.5 Community Bd mutant materials

Seed from a Bd21-3 mutant collection containing NaN₃, EMS and fast neutron radiation treated lines described to contain mutations in the genes within the candidate trichome interval, Bradi4g22637-Bradi4g22651 were identified within the Jbrowse feature of Phytozome v12 on the Bd21-3 v1.1 reference genome. Glumes of seed were visually assessed by Richard Sibout (Institut National de la Recherche Agronomique) for lemma trichome presence/absence phenotype.

4.2.6 Disruption of candidate gene Bradi4g22650 using CRISPR in Bd21

For disruption using CRISPR-Cas9, a pair of guide RNAs were designed targeting within exon 2 of Bradi4g22650, positions illustrated in Figure 4-4. Off target effects of sgRNAs were assessed using BLAST to the Bd21 v3.1 reference genome using a local database (Born Again database, Martin Trick) with short sequence settings. Targets with off-target hits with greater than 80 % match within the seed region (3' terminal) were excluded.



B

ATCGAGCTAG**CCATACGAGTACCCTAGCTTAG**CCATAGCTAACATGCAGCTCACAGCAGCAGCTG
 GTCCGGAGGAGGAAGCCGCGGGCGGGTTCGTTGGTGGCGCAGGCGAGGAACCTGGCGTCGCGGGC
 AGGCCACGCGCATGTCACCCCGCTCCACATCGCCAGCGCCATCCTCTCCGCTTCGCCCCGCTCCT**CC**
TACGCTCCTCAAACAGCATTACAACAACGACAACATCGACGCGCTGGCGCTCCTCCCTGGGCGCCGC
 GCTCGACGGCCTCCCCGTCTGACGACGACGTCCCCGTCCCCGGCCCCGGCCCCGGCGGCAGCGCC
 TTCGAACGCGTTCCTGGCAGCGCTGAAGCGGGCGGGAAGAAGCGCCGGCGTCTGATCAGCAGGG
 CAGCAGCGGGCAGCAGCGAGGTCGAGCGGCTCGTGGCCTCCGTCTCCTCGACCCAGCGTGGACC
 GCGCCCTGCGCTCCGCCAGCTTATTACTACGACCGTCTGATCCTGATCCTGTTCTGATCGT
 GGGACGAAGCAGCTGGCACGTCGGCACCAACGACCAGCTGCAGTCGTCCCAATGGAAG

Figure 4-4 Loci of sgRNA designed for the disruption of Bradi4g22650 as a candidate for lemma trichome related factor. A; Illustration of sgRNA loci (pink) on Bradi4g22650. B; Genomic sequence of Bradi4g22650.1 (Bd21 v3.1 reference) exon 2 with highlighted protospacer adjacent motifs (PAMs, grey), guide (teal) and target cleavage site (grey).

Each target sequence was introduced into a sgRNA scaffold (pICSL70001, Addgene #46966) by PCR in separate reactions using the primers detailed in (Figure 4-6), Q5 High-Fidelity DNA Polymerase (New England Biolabs) reaction components (Table 4-6) and reaction conditions listed in Table 4-7.

Table 4-5 Primers for CRISPR Level 0 sgRNA plasmid construction. sgRNA1 and sgRNA2 relate to the two target sites.

Identifier	Sequence
sgRNA1	tgtggctcacttgGTAAGCTAGGGGTACTCGTAgttttagagctagaaatagcaag
sgRNA2	tgtggctcacttgGAATGCTGTTTGAGGAGCGTgttttagagctagaaatagcaag
sgREV	TGTGGTCTCAAGCGTAATGCCAACTTTGTAC

Table 4-6 Reaction components for Level 0 assembly. A separate reaction was prepared for each guide/target. Final reaction volumes = 25 μ L

Component	Final concentration
5X Q5 Reaction Buffer	1 X
10 mM dNTPs	200 μ M
10 μ M Forward primer	0.5 μ M
10 μ M Reverse primer (SgREV)	0.5 μ M
Template DNA (pICSL70001)	10 ng
Q5 High-Fidelity DNA Polymerase	0.02 U/ μ L
Nuclease free water	N/A (to 25 μ L)

Table 4-7 Level 0 construction cycle conditions for Bradi4g22650 CRISPR plasmid construction using Q5 High-Fidelity DNA Polymerase

Step	Temperature ($^{\circ}$ C)	Duration
Initial denaturation	98	30 s
	98	10 s
35 cycles	60	15 s
	72	20 s
Final extension	72	2 min

The PCR product (with the addition of 125 μ L buffer PB) was purified using a Qiagen PCR Purification Kit according to manufacturer's protocol and 5 μ L of each product was confirmed to contain a single product of the correct approximate size using gel electrophoresis (50 mL TE buffer, 0.8 % agarose, 2 μ L EtBr).

NanodropTM 2000 microvolume spectrophotometer (Thermo Fisher Scientific) was used to quantify sgRNA1 and sgRNA2 Level 0 products, as 42.8 ng/ μ L and 32.9 ng/ μ L respectively.

Golden Gate Digestion-Ligation (DigLig, long protocol) 15 μ L reactions were setup to combine a BdU6 promoter and each guide (Level 0) within an acceptor plasmid (Level 1). Guide 1 was inserted into pICH47751 and guide 2 into pICH47761. The BdU6 promoter was synthesised from the sequence obtained from (van der Schuren et al., 2018). A 2:1 parts promoter:acceptor ratio of components was used, specifically 100 ng acceptor, 7 ng guide Level 0, 125 ng BdU6, based on plasmid sizes. Reactions

were composed as described in Table 4-8 and carried out under the conditions described in Table 4-9.

Table 4-8 Digestion-Ligation reaction components for assembly of Level 1 plasmids for Bradi4g22650 CRISPR

Component	Volume per reaction
Acceptor plasmid (100 ng/μL)	1 μL
Level 0 sgRNA (7ng/μL)	1 μL
BdU6 (125 ng/μL)	1 μL
T4 Ligase buffer	1.5 μL
T4 Ligase (400 U/μL)	0.5 μL
Bovine Serum Albumin (10x)	1.5 μL
<i>Bsa</i> 1 20 U/μL	0.25 μL
Nuclease free water	N/A (to 15 μL)

Table 4-9 Digestion-Ligation reaction conditions for assembly of Level 1 plasmids for Bradi4g22650 CRISPR

No. of cycles	Temperature (°C)	Duration
1	37	20 s
26	37	3 min
	16	4 min
1	50	5 min
1	80	5 min
1	16	5 min

Guide Level 1 plasmids were transformed into Top10 competent *E. coli* cells (Oneshot Top10, Invitrogen). On ice, 5 μL of Level 1 DigLig reaction was added to 25 μL competent cells and incubated on ice for 30 mins. A 1 min heat-shock treatment at 42 °C was applied followed by a further 2 mins on ice. A 250 μL volume of SOC medium (super optimal broth with catabolite repression, Sigma S1797) was added to each sample and incubated at 37 °C for 1 hour with shaking; aliquots of 75 μL and

150 μ L were spread onto two Petri dishes of LB agar supplemented with ampicillin, X-gal and IPTG for blue/white selection.

A single white (transformed) colony was selected for guide 1, and three were selected for guide 2. Each colony was removed using a sterile toothpick into 5 mL volume of LB broth (+ ampicillin, 200 mg/mL) and incubated at 37 °C overnight with shaking. Samples were centrifuged and 2 mL used to extract Level 1 constructs using QIAprep® Spin Miniprep kit (Qiagen), eluting in 30 μ L water.

To confirm the sequence of Level 1 constructs, constructs were digested with 1 μ L *Bpi*I, 1 μ L Buffer G and 6 μ L water (for 2 μ L construct) with incubation at 37 °C for two hours. Digestion of samples was confirmed using gel electrophoresis (50 mL TE buffer, 0.8 % agarose, 2 μ L EtBr). Purified Level 1 constructs were sequenced using standard primers described in Table 4-10.

Table 4-10 Primers used for sequencing Level 1 and Level 2 construct vectors for disruption of *Bradi4g22650* by CRISPR/Cas9

Primer Name	Sequence (5' - 3')
Level 1 Forward F(0229)	GAACCCTGTGGTTGGCATGCACATAC
Level 1 Reverse R(0230)	CTGGTGGCAGGATATATTGTGGTG
Level 2 Forward F(0231)	GTGGTGTAACAAATTGACGC
Level 2 Reverse R(0232)	GGATAAACCTTTTCACGCC

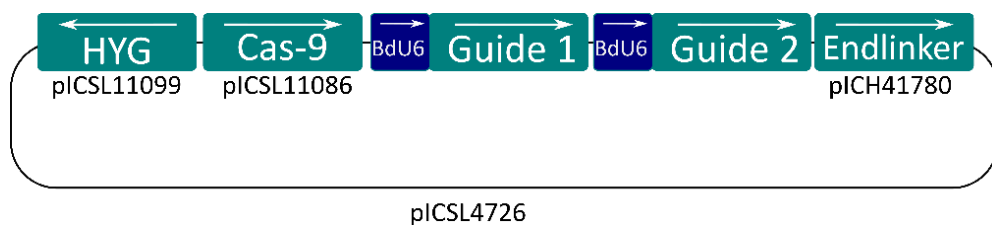


Figure 4-5 Schematic of binary vector (Level 2) delivered to *Bd21*. Transcriptional units were assembled into backbone *x* using Golden Gate Cloning. A hygromycin resistance cassette (hygromycin phosphotransferase II, *hptII*) was driven by *ZmUbi* promoter and terminated by *ZmNosT*. Cas9=ProUbi-WheatCas9-Porcine2A-Histone2A-GFP-NosT. Endlinker=pELE-4 Addgene #48019 from Icon Genetics. Guide 1 & 2 refer to *sgRNA1* and *sgRNA2*.

For the construction of Level 2 binary vectors into an acceptor with reporter system included (Figure 4-5), a digestion-ligation reaction was used with the components listed in Table 4-11, under the conditions described in Table 4-9. The reaction product was transformed into Top10 competent cells as described above and grown on LB agar (supplemented with kanamycin 100 µg/µL) at 37 °C overnight. No red/orange colonies were present therefore it was concluded that all colonies were transformed. A white colony was selected, amplified in LB broth supplemented with kanamycin overnight with shaking at 37 °C. The Level 2 construct was extracted from culture using QIAprep® Spin Miniprep kit (Qiagen), eluting in 30 µL water. The construct was sequenced (Eurofins, Sanger) using the primers listed in Table 4-10 and analysed to confirm correct position and sequence of each component.

Table 4-11 Digestion-Ligation reaction components for assembly of Level 2 plasmids for Bradi4g22650 CRISPR

Component	Volume per reaction
Acceptor plasmid pICSL4723 (100 ng/uL)	1 µL
HYG donor pICSL11099 (125 ng/uL)	1 µL
Cas9 donor pICSL11086 (194 ng/uL)	1 µL
Endlinker pICH41780 (51 ng/uL)	1 µL
T4 Ligase buffer	1.5 µL
T4 Ligase (400 U/uL)	0.5 µL
Bovine Serum Albumin (10x)	1.5 µL
<i>Bpi</i> 1 10U/uL	0.5 µL
Level 1 sgRNA1 (82 ng/uL)	1.11 µL
Level 1 sgRNA2 (82 ng/uL)	1.33 µL
Nuclease free water	N/A (to 15 µL)

Transformation into *Agrobacterium* and plant transformation was carried out by Inmaculada Hernandez-Pinzon of The Sainsbury Laboratory (TSL) and Matthew Smoker (TSL Tissue Culture and Transformation), respectively. Seven T₁ plants were

recovered, and twenty-seven seed from each of these were planted to generate T₂ lines for phenotyping and mutation analysis.

4.2.7 Assessment of CRISPR lines to identify transformants (HYG) and target-site edits

DNA was extracted from freeze dried leaf material of seven T₂ lines (27 plants per line) using the plate extraction method previously described in Chapter 0. PCR was used to detect the presence of hygromycin (HYG) resistance gene for a single T₂ per T₁ line, using the following primers: F= GGATTTCGGCTCCAACAATG, R= TATTGGGAATCCCCGAACA. The HYG donating construct (pICSL11099) containing HYG was used as a positive control. Amplified products were analysed by gel electrophoresis (1.5 % agarose, 1 µL EtBr, 50 mL).

CRISPR target sites within Bradi4g22650 for 27 T₂ lines per T₁ plant, were amplified and sequenced using primers ACTGCTAGCTCCTCCGATCC and CTGCCCTGCTGCTACGAC (5' to 3', forward and reverse respectively). A touchdown PCR protocol was applied to increase specificity of amplification; GoTaq® Green Master Mix (Promega®) standard 15 µL reactions were prepared and amplification performed on an Eppendorf MasterCycler Pro according to the conditions described in Figure 4-11.

Table 4-12 PCR conditions for the amplification of *Bradi4g22650* CRISPR target-edit sites in T_2 transformed lines. *annealing temperature decreasing 0.5 °C per cycle for 16 cycles.

Step	Sub-step	Temp (°C)	Time
Pre-incubation		95	4 min
45 cycles	Denaturation	95	45 s
	Annealing	66-58*	1 min
	Extension	72	45 s
20 cycles	Denaturation	95	45 s
	Annealing	61	1 min
	Extension	72	45 s
Final Extension		72	5 min

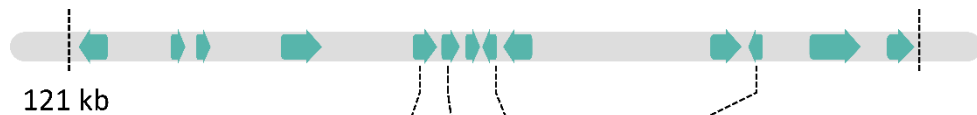
Four T_2 lines per T_1 family were analysed to confirm a single PCR product by gel electrophoresis. Three of these lines per T_1 family were sequenced using the amplification primers (Eurofins) and assessed for edits by aligning to the Bd21 v3 reference sequence for *Bradi4g22650*.

4.3 Results

4.3.1 Exploiting F4-5 heterozygous families to refine candidate region

Previous work, described in Chapter 3, identified a QTL for lemma trichome phenotype on Bd4L using the ABR6 x Bd21 F8 RIL population, peaking at Bd4L_27278128. A collaboration between Jan Bettgenhaeuser and Daniel Woods, prior to my work, defined a candidate interval of thirteen genes. I undertook further fine mapping of the candidate interval. For this purpose, six heterozygous F4 RILs with unresolved recombination events were identified by comparison of genotype data from F4 and F8 maps ((Bettgenhaeuser et al., 2017). Seeds were obtained for these lines (F1-x, F4-1, x=14, 47, 94, 97, 102 and 117) and five F4-5 lines were generated for each. Phenotypic assessment of lemma trichome was undertaken on these F4-5 lines. For genotyping, intragenic KASP markers were designed using SNPs identified by alignment of gene sequences from ABR6 and Bd21 and were used to characterise the F4-5 lines (Figure 4-6).

Parental lines, Bd21 and ABR6, genotypes and phenotypes match as expected for all markers tested. No evidence was identified for recombination events in four RILs (F1-x F4-5, x=14, 47, 97, 102 and 117), with phenotype and genotype as expected; ABR6 genotype associated with trichome absence and Bd21 genotype with trichome presence. Heterozygous lines always possessed trichomes. Evidence of an unresolved recombination event within RIL 94 was identified in four (of five) F4-5 lines, initially localised between markers Bradi4g22651 and Bradi4g22656; all five individuals had lemma trichomes present. The only marker consistently matching genotype and phenotype was Bradi4g22651. Therefore, all regions downstream of Bradi4g22658, where the genotype is no longer associated with the phenotype, were excluded from the candidate interval.



RIL F4-5	Bradi4g22651	Bradi4g22653	Bradi4g22658	Bradi4g22730	Trichome Phenotype
14 - 1	+		-	+	+
14 - 2	-		-	-	-
14 - 3	+		+	+	+
14 - 4	+		+	+	+
14 - 5	+		+	+	+
102 - 1	+		+	+	+
102 - 2	+		+	+	+
102 - 3	+		+	+	+
102 - 4	-		-	-	-
102 - 5	+		+	+	+
117 - 1	+		+	+	+
117 - 2	+		+	+	+
117 - 3	+		+	+	+
117 - 4	+		+	+	+
117 - 5	+		+	+	+
47 - 1	-		+	+	+
47 - 2	+		+	+	+
47 - 3	+		+	-	+
47 - 4	+		+	+	+
47 - 5	+		+	+	+
94 - 1	+	-	-	-	+
94 - 2	+	-	-	-	+
94 - 3	+	-	-	-	+
94 - 4	+	-	-	-	+
94 - 5	+	+	+	+	+
97 - 1	+		-	+	+
97 - 2	-		-	-	-
97 - 3	-		-	-	-
97 - 4	+		+	+	+
97 - 5	+		+	+	+
ABR6	-	-	-	-	-
Bd21	+	+	+	+	+

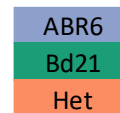


Figure 4-6 Refinement of lemma trichome candidate region using F4-5 lines unresolved in F8 map. A, Approximate locations of KASP markers to delineate the location of unresolved recombination events in ABR6 x Bd21 RILs. B, Summary of genotype and phenotype allocations for ABR6 x Bd21 F4-5 RILs for six lines with previously unresolved recombination events between F4 and F8 genetic maps. Only RIL F1-97 (F5 progeny) were genotyped with marker Bradi4g22653, following identification of recombination event between Bradi4g22651 and Bradi4g22656.

An additional KASP marker was designed within Bradi4g22653 to further delineate the new right-border of the new candidate region; only RIL F1-94, F4-5 progeny were genotyped with marker Bradi4g22653. This redefined the right border of the interval to the marker within Bradi4g22651, in total excluding eight genes downstream from the candidate interval (Figure 4-7). The left border of the candidate region remained defined by the Bd21 x Bd1-1 population (Bettgenhaeuser et al., Unpublished).

The refined candidate region of 53.4 kb contained five genes annotated in Bd21v3.1; Bradi4g22637, Bradi4g22641, Bradi4g22645, Bradi4g22650 and Bradi4g22651 (Figure 4-7).

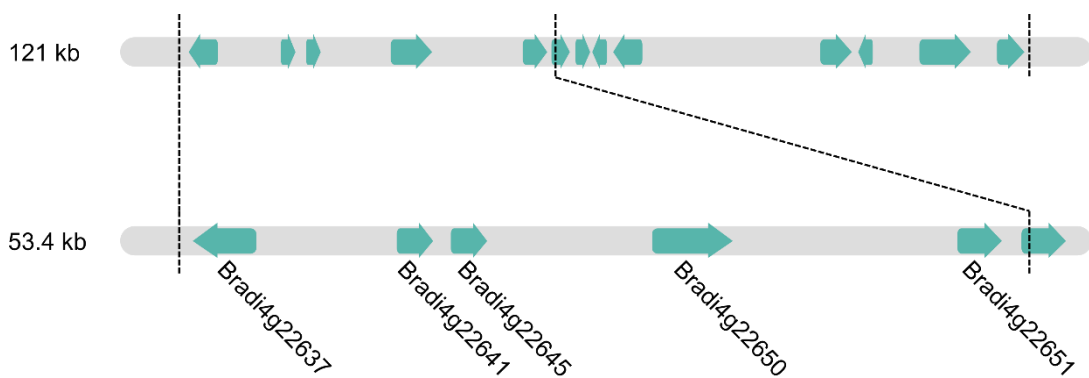


Figure 4-7 Bd21v3.1 gene content for refined lemma trichome candidate interval by resolution of F5 heterozygous RIL 94, relative to the region fine-mapped through collaboration between Jan Bettgenhaeuser and Daniel Woods. Arrows indicate annotated genes.

4.3.2 Expression analysis of candidate genes

A causal gene for lemma trichome development would likely vary in expression between trichomed and non-trichomed accessions. A qRT-PCR experiment was undertaken to compare expression of the five candidate genes between trichomed (Bd21) and trichomeless (ABR6 and Bd1-1) parental accessions in developing floral tissue. Expression of the causal gene would be expected to occur during development of the floral tissues, in the floral meristem, at a stage before trichomes are visible (in

trichomed genotypes). Therefore, RNA samples were obtained from flash-frozen floral meristem dissected from Bd21 (trichomed), ABR6 and Bd1-1 (both non-trichomed) just prior to the awn initiation stage (Figure 4-3). As the phenotype is tissue specific (leaf trichomes are unaffected), leaf material was sampled as a control for each line. qRT-PCR was used to quantify mRNA transcripts (converted to cDNA) and expression was quantified relative to BdUBC18, a constitutively expressed ubiquitin gene described to be stable across development and a range of environmental variables (Hong et al., 2008).

Graphic representations of expression of the five candidate genes in floral meristem and leaf tissue are presented in Figure 4-8. Overall expression for all candidate genes was low compared to the housekeeping gene. Bradi4g22637, Bradi4g22641 and Bradi4g22651 showed no evidence of significantly different expression between accessions in either leaf or floral meristem tissues (F-values presented in full, Supplementary Table 3). Bradi4g22645 was significantly more highly expressed in floral tissues of Bd21 (trichomed) than in ABR6 and Bd1-1 (non-trichomed). Bd1-1 appears to be more highly expressed than other accessions in leaf samples, but this is due to a single high value replicate (outlier). Bradi4g22650 was not expressed in foliar tissue of any of the three accessions. Bradi4g22650 was not expressed in floral tissue of ABR6 or Bd1-1 and was only expressed in Bd21. This pattern of expression makes Bradi4g22650 an excellent candidate for the gene controlling trichome development in Bd21.

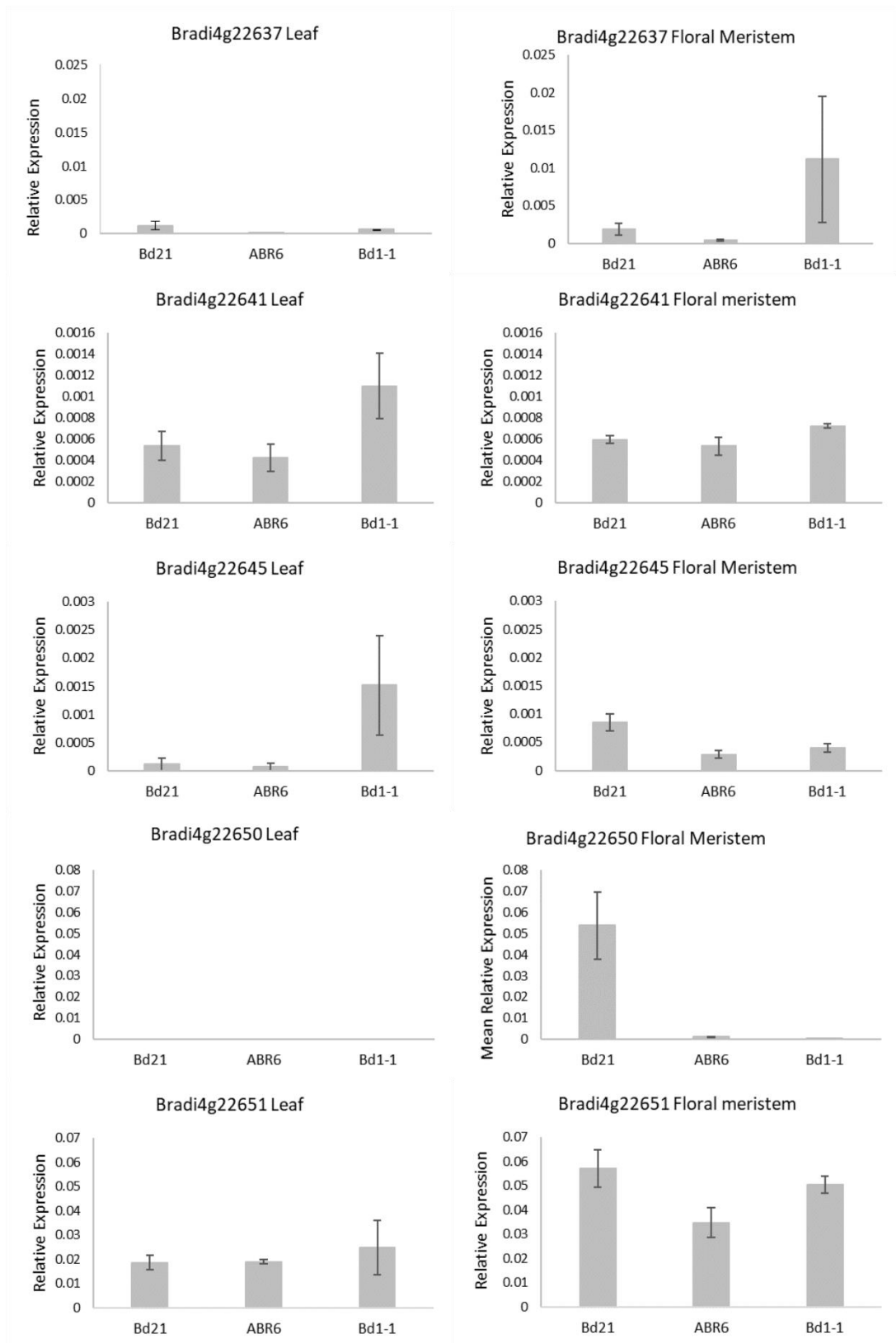


Figure 4-8 Relative expression of five genes within a refined lemma trichome candidate region on *Bd* chromosome 4, of leaf and floral meristem tissues from qPCR. Values are relative to housekeeping gene *BdUBC18*. Error bars = ± 1 SE.

4.3.3 Comparison of Bd21, ABR6 and Bd1-1 candidate region *in silico*

The availability of Brachypan genomic data allowed for the comparison of the candidate region between the parents, Bd21 and ABR6. These data were explored for differences in gene content, sequence identity, and tissue specific expression.

4.3.3.1 Expression browser data for candidate genes

Due to the tissue specificity of the trichome trait, the EMBL-EBI expression browser was used to search published RNAseq datasets for expression specific to floral tissues (Sibout et al., 2017, Davidson et al., 2012). Bradi4g22651 is expressed across many tissues to a varying degree (Figure 4-9). Both Bradi4g22637 and Bradi4g22650 are expressed in early and emerging inflorescences with low expression of Bradi4g22637 also reported in the plant embryo (Figure 4-9). No expression data were available for Bradi4g22641 and Bradi4g22645 as they were not annotated in the reference version (Bd21v2.1) used for the contributing RNAseq experiment. Based on the published eFP expression data, Bradi4g22650 tissue specific expression profile best fits that expected of the lemma-specific trichome phenotype.

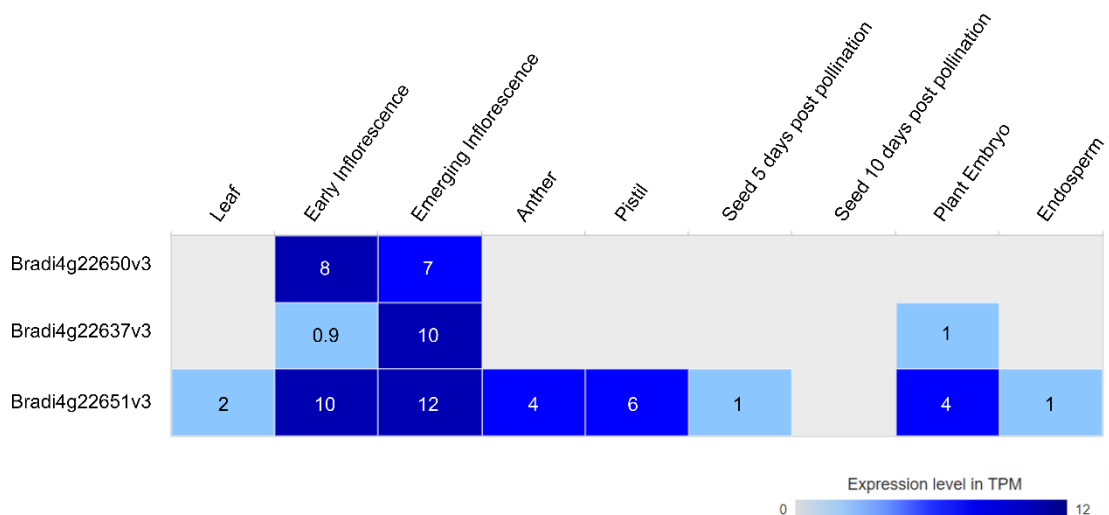


Figure 4-9 Tissue specific expression data for genes in lemma trichome candidate interval on *Bd* chromosome 4, adapted from EMBL Expression Browser, data from (Davidson et al., 2012). Expression values in transcript per million (TPM) overlaid. Bradi4g22641 and Bradi4g22645 were absent from (Davidson et al., 2012) data set, so are not presented.

4.3.3.2 Annotation of candidate genes

The predicted function of the five annotated genes, and that of an *Arabidopsis thaliana* (*At*) and barley (*Hordeum vulgare*, *Hv*) orthologue were identified from Phytozome12 (Goodstein et al., 2012) based on v3.1 of genome assembly and annotation for Bd, or Ensembl Genomes (Plants) for orthologues (Kersey et al., 2017)(Table 4-13).

Three genes were annotated only as hypothetical protein in Bd, Bradi4g22641, Bradi4g22645 and Bradi4g22651 (Table 4-13). Bradi4g22641 is orthologous to a lipoxygenase gene in barley but has no orthologues in Arabidopsis. Bradi4g22645, has no orthologues in either barley or Arabidopsis, fitting the profile of an orphan gene. Bradi4g22651, has orthologues in Arabidopsis and barley as AtAUR2, a serine/threonine kinase and a PRA1 family protein respectively. Bradi4g22637 is annotated in Bd21v3.1 as a MYB transcription factor, supported by similarly annotated orthologues in both Arabidopsis and barley. Bradi4g22650 is annotated as an ATP-dependent CLP protease in Bd21v3.1; its closest orthologues in Arabidopsis are SMXL3 and in barley HORVU3Hr1G093470, a gene with no annotated function.

Table 4-13 Annotated function of trichome candidate genes and orthologues in *Arabidopsis thaliana* and *Hordeum vulgare*. *Top hit BLASTP orthologue using EnsemblPlants, assembly TAIR10 for *At* and IBSC_v2 for *Hv*. “-“= no BLAST hits

Gene	<i>Brachypodium</i> annotation		<i>Arabidopsis</i> orthologue*		<i>Barley</i> orthologue*
<i>Bradi4g22637</i>	MYB factor	transcription	AtMYB96 (MYBCOV1)		HORVU4Hr1G023510 (HTH myb-type predicted protein)
<i>Bradi4g22641</i>	Hypothetical protein		-		HORVU7Hr1G050680 (Lipoxygenase)
<i>Bradi4g22645</i>	Hypothetical protein		-		-
<i>Bradi4g22650</i>	ATP-dependent protease	CLP	SMXL3 (Protein SMAX1-LIKE)		HORVU3Hr1G093470
<i>Bradi4g22651</i>	Hypothetical protein		AtAUR2 Kinase)	(Ser/Thr	HORVU3Hr1G088130 (PRA1 family protein)

Loci of BLAST results of candidate gene searches suggested a translocation of part of the candidate region in ABR6 to pseudomolecule 2, including *Bradi4g22637*, *Bradi4g22641* and *Bradi4g22645* (Table 4-14). Genes up- and down-stream of these genes BLAST onto ABR6 pseudomolecule 3 along with the orthologue for *Bradi4g22651*. No other sequenced *Bd* accessions shared the putative translocation event. An improved, PacBio based genomic assembly was available for *Bd1-1*, whereas no long-read based alternative genome assembly was available for ABR6.

Table 4-14 Loci of lemma trichome candidate genes in ABR6 and Bd1-1 *Brachypan-genomes*. Locus for non-annotated genes were identified using BLAST (*Phytozome*)

Bd21 Gene Name	Bd21 (v3.1) Gene Locus	ABR6 (v1) Gene Name and Locus	Bd1-1 (v1) Gene Locus and Locus
Bradi4g22637	Bd4:26932692..26934398	Brd1sv1ABR6_r1023025m pseudomolecule_2: 52633649..52635281	Brd1sv1Bd1-11041363m pseudomolecule_6:17006114..17007388
Bradi4g22641	Bd4:26945541..26946833	Brd1sv1ABR6_r1023024m pseudomolecule_2:52621099..52622858	Not annotated* pseudomolecule_4:13665662..13666902
Bradi4g22645	Bd4:26948081..26949191	Not annotated* pseudomolecule_2:52619600..52618490	Not annotated* pseudomolecule_6:17005859..17007572
Bradi4g22650	Bd4:26958903..26964917	Brd1sv1ABR6_r1023022m pseudomolecule_2:52596370..52597197	Brd1sv1Bd1-11032095m pseudomolecule_4:13679916..13685625
Bradi4g22651	Bd4:26980048..26983247	Brd1sv1ABR6_r1027243m pseudomolecule_3:23306626..23311919	Brd1sv1Bd1-11032097m pseudomolecule_4:13699325..13703398

4.3.3.3 Nanopore re-sequencing of ABR6

In order to obtain an accurate sequence for the physical candidate region in ABR6; therefore, long read nanopore sequencing of ABR6 was carried out in collaboration with Richard Leggett's group at Earlham Institute. Genomic assembly of sequencing data was carried out by Matt Moscou using Flye (Kolmogorov et al., 2019, Schmidt et al., 2017). The translocation reported in the ABR6 *Brachypan* genomic sequence (v1) was not identified; a 72 kb scaffold covering the Bd4L candidate region was assembled to confirm the physical structure of the region in ABR6; no translocation event is present between Bd21 and ABR6 in the candidate region. Significant differences between the ABR6 material that we are using and the JGI *Brachypan* Illumina ABR6 sequence (which was utilised for hybrid assembly) were observed. A sequence approximately 9-10 kb in length is present in the ABR6 scaffold, but absent in the equivalent region of Bd21 resulting in a 70 kb region in ABR6 compared with 60 kb in Bd21 (Figure 4-10). The insertion in ABR6 is upstream of *Bradi4g22650*. There is no evidence of gene content in the extra region based when using the Augustus gene predictor tool (Stanke and Morgenstern, 2005).

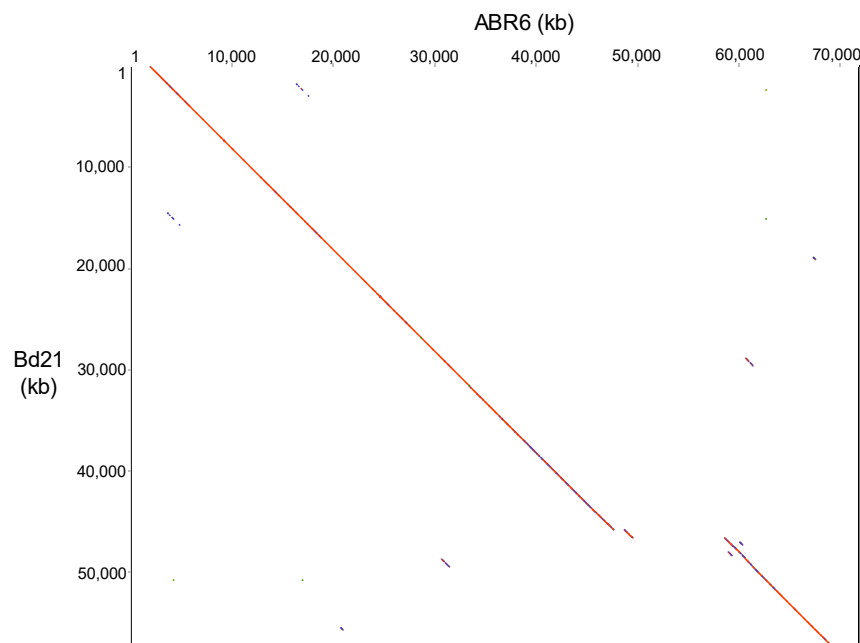


Figure 4-10. Dotplot Collinearity between *Bd21* reference (Illumina, v3.1) and ABR6 nanopore Flye assembly for trichome candidate region.

Comparison of the five gene region between ABR6 and Bd21 could now proceed under the knowledge that the overall architecture of the region is consistent between the parental accessions. Where possible, from here on in, ABR6 nanopore sequencing data was used for analysis in preference over the Brachypan Illumina references, including for comparison of gene sequences between accessions. Likewise, a PacBio based assembly of Bd1-1 (v1.1) is used in preference to the Brachypan Bd1-1 v1 pseudomolecule based genomic sequence.

4.3.3.4 Sequence variation of five candidate genes - Bd21, ABR6 and Bd1-1

Bradi4g22637

Alignment with Bd21 showed that Bd1-1 differed in two major ways: a six bp deletion 153 bp from the start of gene, and alignment, in the 5' untranslated region (UTR) and a 12 bp insertion 894 bp from gene start in the intron. A total of 16 SNPs were identified between Bd1-1 and Bd21, and a further single bp insertion in the intron; of these, one SNP was in the first exon, five were in the second exon, one in each of the 5' and 3' UTRs and the remaining 8 found in the only intron. ABR6 had two single bp deletions compared to Bd21, one in the 3' UTR and the other in the intron. Neither would be expected to affect the final transcript.

Bradi4g22641

Alignment with the ABR6 nanopore scaffold covering the region finds no evidence for disrupted sequence of the *Bradi4g22641* equivalent gene in ABR6; the sequences are highly similar, with 100 % identity in the coding sequence, and a single three bp deletion in the 3' UTR at position 645 from gene start. Alignment of *Bradi4g22641* with Bd1-1 (v1.1, PacBio) showed many polymorphisms with Bd21, including total gaps in Bd1-1 of 64/1273 bp, leaving 1207 identical compared with Bd21 and a large deletion in Bd1-1 (position 648-704) 56 bp in length. Additionally, a 3 bp insertion at

position 1219 is present in Bd1-1 and many SNPs are spread across the gene, with 7 in the coding sequence and 21 in the 3' UTR.

Bradi4g22645

For the 1111bp length mRNA sequence of Bd21 Bradi4g22645, 100 % identity was found with the equivalent sequence in our ABR6 Nanopore scaffold. Conversely, Bd1-1 has a large deletion relative to Bd21 73 bp in length within the intron, in alignments with both Brachypan (v1) and PacBio (v1.1) assemblies (for the latter, coverage of 93 % of query, 98.22 % identity). Most polymorphisms are within the intron, but four SNPs are located within the second exon.

Bradi4g22650

Alignment of DNA sequences shows that the promoter region and start of Bradi4g22650 are present in Bd21, ABR6 (nanopore scaffold) and Bd1-1 (v1.1). No variation was identified in the first 3 exons of Bradi4g22650, but 16 SNPs were present in exon 4 compared to Bd21. Alignment of the coding sequence with Bd1-1 shows a large 304 bp deletion within exon two of Bradi4g22650 at positions 358 to 662 from the annotated gene start, and an overall identity with Bd21 of 99 %. Alignment with ABR6 nanopore scaffold spanning the region, with an overall sequence identify of 91.18 %, shows a 29 bp deletion in ABR6, located in an intron between exons 2 and 3 of Bradi4g22650, with one SNP present in exon 3 and a further 16 SNPs present within exon 4; the remaining non-identity percentage between Bd21 and ABR6 is due to intronic SNPs.

Bradi4g22651

Three SNPs were identified in the first exon of Bradi4g22651 between ABR6 (nanopore) and Bd21, and a further one bp deletion in the second exon at position 1727 (Bd21 transcript). Alignment of Bd1-1 (v1.1) with Bradi4g22651 from Bd21 had 98.72 % identity, with one large deletion, 27 bp in length in the 3' UTR, but no variation in coding sequence between Bd21 and Bd1-1.

Summary of identify between Bd21 and the trichomeless lines Bd1-1 and ABR6 are presented in Table 4-15, along with summary of expression for the five candidate genes from both published datasets in developing floral tissues and my qPCR data.

Table 4-15 Summary of sequence comparison and expression analysis of five Bd21 v3.1 genes annotated in candidate region for lemma trichome phenotype, between Bd21, ABR6 and Bd1-1 accessions.

Gene name	Annotated function (Function of orthologue)	Expressed in early inflorescence? (eFP)	Differential expression between Bd21 and ABR6/Bd1-1?	Coding sequence variation between parents?	
				Bd21vs ABR6	Bd21 vs Bd1-1
Bradi4g22637	MYB transcription factor	Yes	No	No	Yes
Bradi4g22641	Hypothetical protein (Lipoxygenase)	-	No	No	Yes
Bradi4g22645	Hypothetical protein	-	Yes	No	No
Bradi4g22650	ATP-dependent CLP protease	Yes	Yes	Yes	Yes
Bradi4g22651	Hypothetical protein (AtAUR2, Ser/Thr kinase)	Yes	No	Yes	No

Based on the expression profiles, combined with *in silico* analysis of genomic and protein sequences, Bradi4g22650 is the best candidate causative gene for lemma trichome presence/ absence observed between Bd21, ABR6 and Bd1-1.

4.3.5 Other Bd mutant material

From a resource of sodium-azide (NaN₃) treated Bd21-3 sequenced lines, three homozygous mutant lines were identified that were reported to contain mutation events within Bradi4g22650 (BdiBd21-3.4G0316600); NaN235_Bd4_26999500_Hom, NaN1620_Bd4_26999637_Hom and NaN1977_Bd4_26999841_Hom (Figure 4-12). All mutations were in the final exon, which encodes a P-loop containing nucleoside triphosphate hydrolase domain (or even the segment of the protein 3' to this domain). The glumes of all three lines were phenotyped and found to possess visible trichomes. No lines were identified with mutations in the protease domain (Figure 4-12).

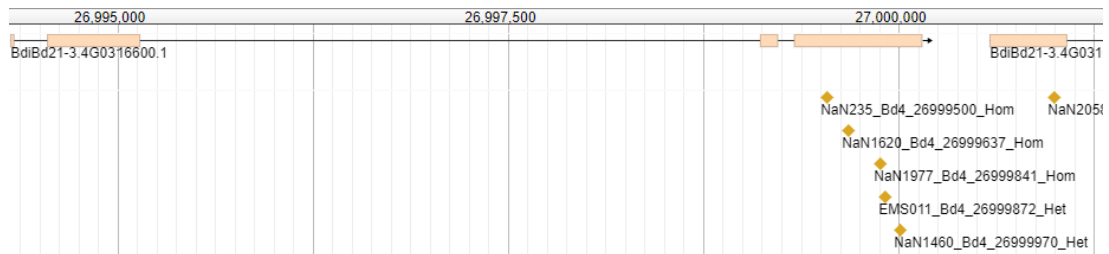


Figure 4-12 Loci of homozygous sodium azide mutations in Bradi4g22650 equivalent gene, BdiBd21-3.4G0316600 in Bd21-3. Derived from phytozome (V12) JBrowse function.

4.3.6 Disruption of Bradi4g22650 using CRISPR/Cas9

Bradi4g22650 was identified as the primary candidate gene. Expression was identified only in Bd21, and I showed it to be a dominant trait therefore disruption of Bradi4g22650 in Bd21 using CRISPR Cas9 was undertaken for functional analysis.

Two guide RNAs were designed to target editing within the first exon of Bradi4g22650. A construct containing both guides was generated using Golden Gate cloning and transformed into Bd21 inbred line. Transformation was confirmed by amplification of HYG resistance gene from all seven plants regenerated from transformed callus (Figure 4-13).

Twenty-seven T-2 lines were generated for each T-1 line, and the target edit site sequenced; no evidence of edits was identified from either of the target sites (Figure 4-14). All individuals were phenotyped and were found to possess lemma trichomes.



Figure 4-13 Image of gel electrophoresis analysis on amplified products of hygromycin resistance for seven T1 Bd plants. Sample 1-7= T1 lines 1-7, left to right. Well 8 = vector pICSL11099 containing HYG resistance cassette as positive control. 100bp ladder (New England Biosciences).

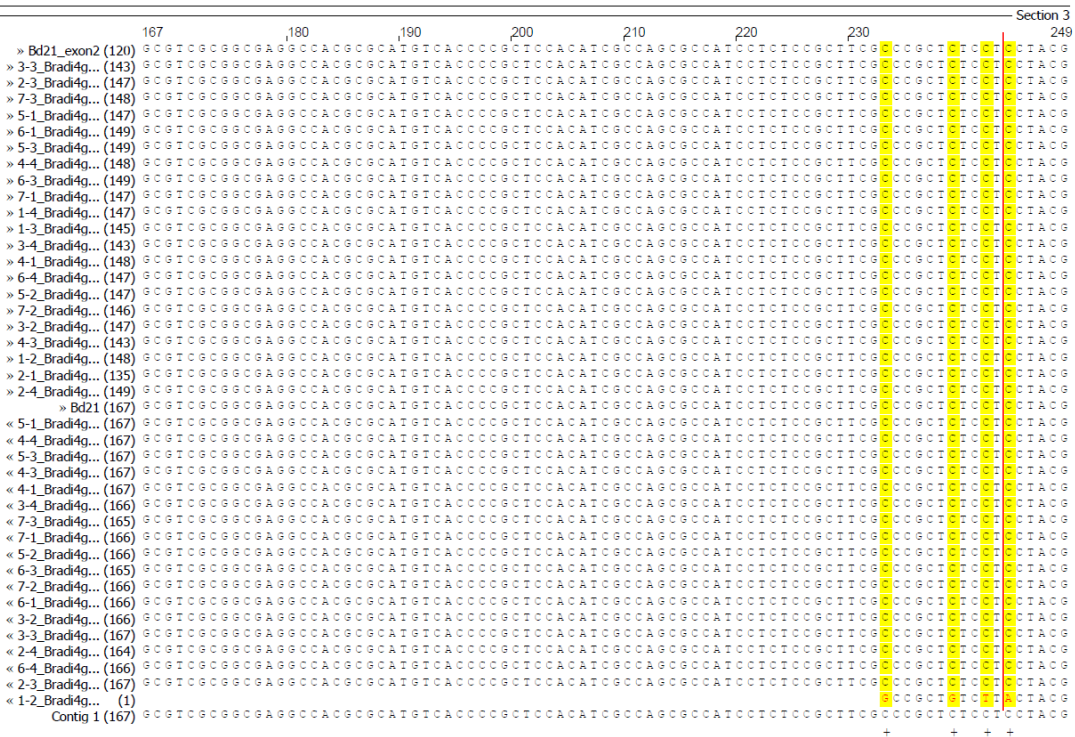
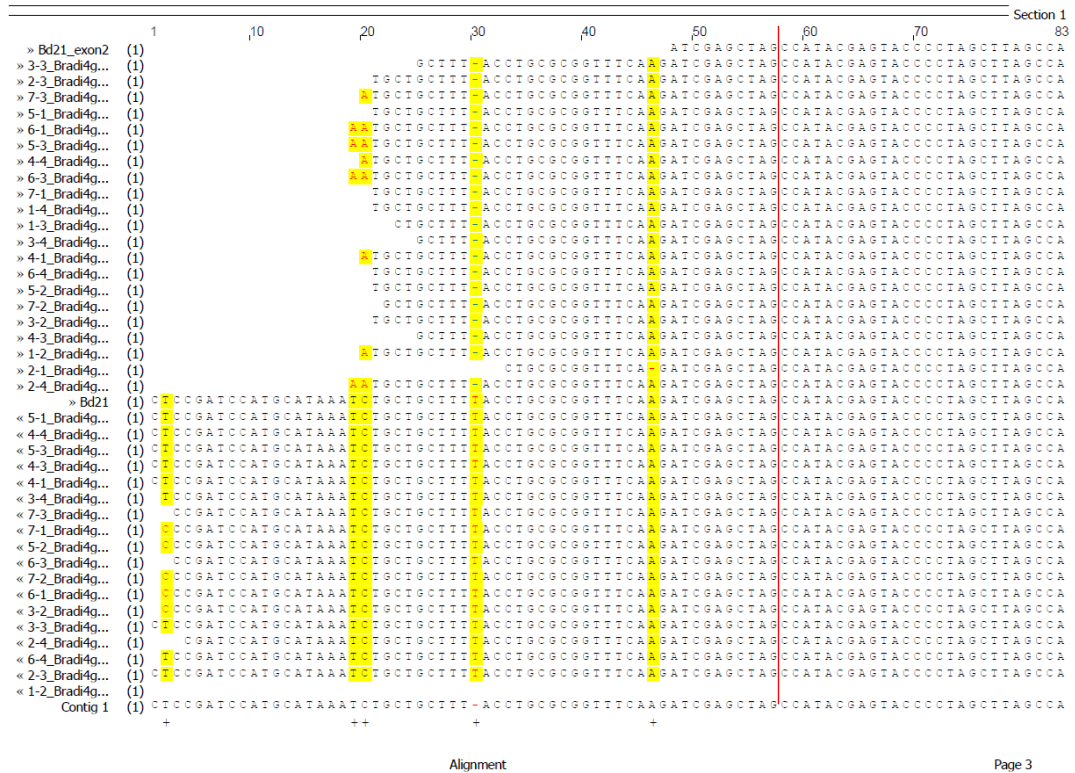


Figure 4-14 Sequencing results file for Bradi4g22650 CRISPR T2 lines, highlighting target edit site in red and polymorphisms in yellow. Top row for each clip is Bd21v3.1 reference sequence.

4.4 Discussion

4.4.1 Trichome candidate interval refined to five genes

Two independent studies of collaborators identified a region of Bd chromosome four associated with lemma trichome presence/absence (Bettgenhaeuser et al., Unpublished). The resultant consensus region, containing 13 genes, was confirmed in the ABR6 x Bd21 population, using KASP markers (data not shown).

Through chance during the development of the F8 population, it is inevitable that progeny selected for some lines did not contain the recombination events identified in earlier generations due to subsequent segregation and selection through single seed descent. This was exploited by identifying six RILs for which this was the case and, returning to the F4 families of these six RILs (14, 47, 94, 97, 102 and 117) before the locus had become fixed homozygous, and generating new progeny. This effectively increased the size of the population in a targeted way, focussing on lines that provided a high chance of containing an unresolved recombination event.

These segregating progenies were then genotyped to assess whether they were homozygous for either ABR6 or Bd21 parent, or heterozygous, for a number of new markers designed within the candidate region, allowing recombination events within the interval to be identified.

A single F4-5 RIL, 94, was found to have a recombination event within the candidate interval; in combination with lemma trichome phenotyping data for the new RIL94 F4-5 families, the region downstream of, and including, Bradi4g22658 was excluded from the candidate interval. This was further refined to exclude all genes downstream of Bradi4g22651 after an additional marker was designed. The candidate interval was therefore refined to a 53.4 kb physical region, containing five genes annotated in Bd21 (v3.1). It is possible that a non-gene sequence that sits within the region, such as a regulatory element for a gene outside of the physical interval, could be responsible for controlling the lemma trichome phenotype.

All F5 progeny that were heterozygous for markers across the candidate interval possessed lemma trichomes. It is therefore concluded that the causative gene is dominant in function, with Bd21 containing a dominant positive regulator of trichome development in lemma tissue.

Loci of recombination events from lines 14,102 and 97 were not identified. It is possible that the region could be further refined by advancing heterozygous F5 plants to a further generation and continuing the genotyping and lemma phenotyping. This was considered unnecessary following the identification of the RIL 94 recombinant, that reduced the candidate region from 13 to 5 genes but could provide validation for the current findings if carried out in future work.

The five genes annotated in Bd21 (v3.1) within the physical candidate region were assessed for tissue specific expression in Bd21, ABR6 and Bd1-1, and the sequences compared between accessions.

4.4.2 Bradi4g22651

The recombination event that defined the right border of the trichome candidate interval has been localised to between markers within Bradi4g22651 and Bradi4g22653; it is therefore possible that the recombination event actually lies within the Bradi4g22651, therefore if this gene appeared to be a promising candidate, further localisation of the recombination event would be required to confirm that the whole gene is contained within the interval.

The closest *Arabidopsis* orthologue to Bradi4g22651 is *AtAUR2*, an aurora kinase. These serine/threonine kinases have highly conserved functions in eukaryotes during mitotic cell division and maintenance of meristematic tissues; in *Arabidopsis* *AtAUR2* specifically plays a key role in vascular cell differentiation (Lee et al., 2018). Conversely the closest barley orthologue is described as *PRA1* (PHENYLATED RAB

ACCEPTOR PROTEIN 1), a small transmembrane protein involved in the regulation of vesicle mediated transport and intracellular trafficking. As Bradi4g22651 is simply annotated as a hypothetical protein with unknown function, it is unclear the role that this gene is playing in Bd without further functional characterisation.

Variation in coding sequence was identified between Bd21 with both ABR6 and Bd1-1; a single SNP between Bd21 and Bd1-1 was present in the final exon of Bradi4g22651, whereas ABR6 contained three SNPs in the first exon and a one bp deletion in exon two, which is likely to cause a frameshift in transcript relative to Bd21. Data from the Bd expression browser (EMBL-EBI) showed expression across all tissues sampled, with the highest expression values in early and emerging inflorescence tissues. From my qPCR experiments, expression was identified in both leaf and floral meristem tissues, with no significant differences between accessions in leaves. ABR6 had significantly less expression in floral meristem tissue compared to Bd21 but it is still clearly expressed. No difference was detected between the other trichomeless accession, Bd1-1, and trichomed Bd21. Therefore, it is concluded to be unlikely that Bradi4g22651 plays a role in trichome development.

4.4.3 Bradi4g22641

Bradi4g22641 is annotated as a hypothetical gene with unknown function. No orthologous genes in Arabidopsis were identified, with a single lipoygenase orthologous gene found in barley. Then again, based on BLASTP results Bradi4g22641 also appears to be an orphan gene, extremely taxonomically restricted, with no BLASTP hits in any grass species available (Ensembl Plants) with the exception of *Eragrostis curvula*, a warm season C4 grass, for which two BLAST hits to hypothetical proteins were identified (Arendsee et al., 2014). Along with the fact that Bradi4g22641 had not been annotated in any previous versions of the Bd21 genome, it was considered that Bradi4g22641 had been mis-annotated and is not a

functional gene. However, I confirmed the presence of expression by measuring the transcript by qPCR, so it is concluded to be a gene with a potentially important function. From my qPCR experiments, expression was identified in both leaf and floral meristem tissues, with no significant differences between trichomed and trichomeless accessions. Additionally, no variation between the coding sequence of ABR6 and Bd21 was identified in Bradi4g22641. Based on these data, Bradi4g22641 is an unlikely candidate for controlling lemma trichome development in Bd.

4.4.4 Bradi4g22645

Bradi4g22645 is annotated to be a hypothetical gene with unknown function and no orthologous genes were identified in either *Arabidopsis* or barley by either BLASTP or BLASTN searches. The taxonomic restriction of this gene is similar to that for Bradi4g22641, with no orthologous genes identified in related grass species, this time with the exception of *Saccharum spontaneum* in addition to *Eragrostis curvula*, all hypothetical proteins (Arendsee et al., 2014).

No variation in coding, or in fact genomic, sequence was identified between trichomeless ABR6 and trichomed Bd21. Conversely, four SNPs were present in trichomeless Bd1-1 in the second exon. Expression was identified, by qPCR, in both leaf and floral meristem tissues for all accessions tested. Both trichomeless accessions, ABR6 and Bd1-1, had significantly lower expression of Bradi4g22645 than Bd21 in floral meristem but this gene was evidently expressed in both accessions. Even with the lack of functional annotation, this warrants future characterisation of loss-of-function mutants, from publicly available collections as this expression pattern is suggestive that Bradi4g22645 may be playing a causative role in trichome development in Bd21.

4.4.5 Bradi4g22637

Bradi4g22637 is annotated as a MYB transcription factor in Bd (Phytozome). The closest orthologous MYB gene in Arabidopsis is *AtMYB96*, a transcription factor that influences abscisic acid (ABA) signalling via interactions with both negative and positive regulators of ABA (Lee and Seo, 2019). The closest orthologous gene in barley, HORVU4Hr1G023510, is a MYB-type predicted protein with gene ontology (GO) annotation predicting a role in response to auxin and cell differentiation (GO:0009733 & GO:0030154), both roles that could plausibly affect cellular and tissue patterning such as trichome development.

Transcription factors are often key regulators of developmental and metabolic processes and hormonal pathways. *TRANSPARENT TESTA GLABRA2 (TTG)* is a WRKY transcription factor in *Arabidopsis* that is a positive regulator of trichome development (Johnson et al., 2002). Many single repeat R3 MYB transcription factors have been identified in *Arabidopsis* that directly influence trichome initiation and development. *Arabidopsis* MYB transcription factors that are positive regulators of trichome initiation include *GL1*, an R2-R3 domain containing MYB, and *AtMYB23* (Machado et al., 2009). Additionally, acting in competition with *GL1* and therefore negatively regulating trichome initiation is *TRICHOMELESS2 (TCL2)*, an R3 MYB transcription factor (Gan et al., 2011). *ENHANCER OF TRY AND CPC1,2* and *3 (ETC1, ETC2* and *ETC3)*, *CAPRICE (CPC)* and *TRIPTYCHON (TRY)* are also MYBs that act as negative regulators of trichome development (Schnittger et al., 1999, Schellmann et al., 2002, Wester et al., 2009). MYBs with functions in trichome development have also been identified in other plant species, including *GhMYB25* in cotton, *SITRY* and *SIGL3* in tomato (Machado et al., 2009, Tominaga-Wada et al., 2013). Therefore, based purely on the annotation of Bradi4g22637 orthologues, this is a good candidate for controlling lemma trichome development.

Published tissue specific RNAseq data in Bd21 showed that Bradi4g22637 is exclusively expressed in the plant embryo and early and emerging inflorescence, with the latter two relevant to our lemma specific trichome phenotype. However, no variation was found between Bd21 and ABR6 coding sequence, or that of the 1000bp preceding the transcriptional start. The Bd1-1 coding sequence contained six SNPs compared to the Bd21 reference. Additionally, expression did not vary in floral meristem tissue between Bd21 and ABR6, with the higher expression observed in Bd1-1 considered to be due to a single outlier replicate (Figure 4-8).

The annotated MYB function, coupled with tissue specific expression in Bd21, would warrant future work to investigate the effect of induced mutation on trichome phenotype; this could be achieved by exploiting the sodium azide, EMS mutant or T-DNA collections of Bd21-3, an accession that also possesses lemma trichomes, so that loss of function could theoretically be observed.

4.4.6 Bradi4g22650

Bradi4g22650 is annotated to encode a protein that contains an ATP-dependent CLP protease domain in Bd21. The *SMAX-1-LIKE 3 (SMXL3)* orthologue (Uniprot) description indicates that this gene in *Arabidopsis* may function in a transcriptional corepressor complex and interact with TOPLESS/TOPLESS-RELATED (TPL/TPR) in an ethylene response factor (ERF)- associated amphiphilic repression (EAR)-motif dependent manner (Causier et al., 2012); however, sequence identity is low between Bd and *Arabidopsis*, with 45-65 % identity for the closest BLAST results.

Proteases, proteolytic enzymes, play a vital role in many aspects of plant physiology and development. These functions range from the general recycling of protein constituents to the highly specific post-translational modification of proteins required for enzyme maturation, subcellular localisation and specific activities (Schaller, 2004). An example of this highly-specific function in plants is the action by a subtilisin-like

protease (SLP1) that is required to cleave the pro-peptide form of REGULATOR OF AWN ELONGATION 2 (RAE2) to a mature peptide, in rice, a process that is required for awn elongation (Bessho-Uehara et al., 2016). Loss of RAE2 function leads to disrupted awn development in rice. RAE2 is a member of the EPIDERMAL PATTERNING FACTOR-LIKE (EPFL) family. Jin et al. (2016) presented another member of the EPFL family in rice, GRAIN NUMBER, GRAIN LENGTH AND AWN DEVELOPMENT1 (GAD1), to be a small secretory, highly mobile peptide that also requires cleavage by a specific protease for maturation to a functional protein. These examples provide evidence and biological relevance to the idea that the loss of the Bradi4g22650 protease function could lead to a loss of trichome phenotype, perhaps indirectly through a role in the maturation of a peptide vital to trichome development. Bradi4g22650 is the only gene within the five gene interval for which the tissue-specific expression is fully relevant to the lemma specific trichome phenotype. Expression data from Davidson et al. (2012) showed that Bradi4g22650 was exclusively expressed in early and emerging inflorescence. From my qPCR experiments of tissue specific expression, between trichomed and trichomeless accessions, Bradi4g22650 was also the only gene tested that was expressed exclusively in floral meristem tissue and was undetectable in leaf tissue. Furthermore, expression was significantly, and dramatically, higher in trichomed Bd21 compared with both trichomeless accessions, ABR6 and Bd1-1. This pattern of expression is highly suggestive that Bradi4g22650 may be playing a coordinating role in the observed lemma trichome phenotype.

Variation was detected between the genomic sequences of ABR6 and Bd1-1 relative to Bd21, in which the gene is assumed to be functional. A large 304 bp deletion was identified in exon 2 Bd1-1 (PacBio) compared to Bd21; this deletion is highly likely to result in loss of function, with the deletion of a large portion of the encoded protease functional domain in the final protein, and frameshift of downstream codons.

Alignment of peptide sequences, obtained from Bd21 annotation (v3.1) and predicted from my ABR6 nanopore and Bd1-1 (v1.1) genomic data, shows the absence of a large segment at the beginning of the protein, including the functional protease domain, in the trichomeless accessions compared to Bd21 (Figure 4-11). This cannot be due to loss of transcriptional start, as this has been shown to be present for all three accessions, from additional sources of sequencing data. Absence of the functional protease domain would be expected to result in loss-of-function. Coincidentally, annotated protein sequences derived from Brachypan-genomic project data, when aligned also show the absence of predicted peptide sequence including the protease domain, in both ABR6 and Bd1-1. This is further evidence for Bradi4g22650 being the strongest candidate gene within the fine-mapped interval.

4.4.6.1 Bradi4g22650 - CRISPR and other mutants

Public collections of mutants of Bd21-3, a different accession that possesses lemma trichomes, are available in the form of EMS, fast neutron sodium azide and T-DNA mutants. Four homozygous sodium azide mutations were identified within Bradi4g22650, all in the fourth exon encoding the hydrolase domain, that is conserved between the trichomed and trichomeless lines. All four homozygous mutants were reported to possess lemma trichomes. Sodium azide mutations are typically highly localised, with low incidence of clustering (Olsen et al., 1993). Mutation would not therefore be expected to have a direct effect on the protease domain function of the gene. As a result, this data does not exclude Bradi4g22650 as the predominant candidate gene for lemma trichome absence in ABR6.

Bradi4g22650 (intron) and Bradi4g22651 (exon) both have T-DNA insertion, single gene mutants available in Bd21-3 (Bragg et al., 2012, Hsia et al., 2017). We were unable to obtain seed for these lines during the timeframe of this project. For future

work, this material could provide rapid confirmation of Bradi4g22650 as the causal gene for lemma trichome difference in Bd21, ABR6 and Bd1-1.

Following the exhaustion of the publicly available mutant resources, I undertook gene-editing of Bradi4g22650 in Bd21 by CRISPR-Cas9. The first reported successful disruption of a gene in Bd using CRISPR-Cas9 gene editing was carried out by on the target of *BdAUX1* by van der Schuren et al. (2018); we used the Bd specific U6 promoter derived from this study. Two guide RNAs were designed within the second exon of Bradi4g22650, which encodes part of the protease domain. Depending on efficiency, it would be expected to obtain edits at either or both target sites, or more rarely deletion of the sequence between the two target sites. Bd21 was transformed with the CRISPR-Cas9 construct containing the two guide RNAs. Twenty-seven T₂ families for each of the seven T₁ plants regenerated from transformed callus were confirmed to contain the hygromycin resistance selection gene, indicating that all T₁ plants were successfully transformed. All plants possessed lemma trichomes. However, upon sequencing, it was found that no plants contained any modifications in sequences at either of the edit sites to which the sgRNAs were designed to target, within the second exon of Bradi4g22650. The attempt to obtain a loss-of-function mutation, through genome editing, was therefore unsuccessful. A comprehensive guide to performing CRISPR/Cas9 mutagenesis in Bd has been published since the completion of lab work for this thesis providing a potential avenue for successful disruption of Bradi4g22650 in the future (Hus et al., 2020).

Without obtaining a loss-of-function mutant, it was not possible to assess whether the relationship between lemma trichome phenotype and FHB susceptibility was due to linkage, or whether trichomes on the floral tissue provide a causative Type I mechanism of infection for FHB causing *Fusarium* species.

4.4.7 Concluding remarks and future work

To summarise, building upon results from earlier chapters and the work of collaborators, who had begun fine-mapping of the lemma trichome trait, a candidate interval was reduced to a region encoding five annotated genes in Bd21 by exploiting unresolved recombination events in the ABR6 x Bd21 population. The five candidate genes were compared for tissue specific expression, including between accessions, and sequence variation assessed between Bd21, ABR6 and Bd1-1. For this purpose, whole genome re-sequencing of ABR6 was completed using long-read nanopore sequencing. Bradi4g22650, an ATP-dependent CLP protease appears to be the most promising candidate gene; expression is specific to developing floral tissue and only identified in trichomed accession Bd21, whilst variation was identified between ABR6 and Bd1-1 compared to Bd21, including the predicted absence of protease domain in ABR6 and Bd1-1, expected to result in loss of function. After mutant resources for the gene proved to be inconclusive, disruption of Bradi4g22650 by CRISPR-Cas9 gene editing was initiated, but recovery of edited mutants was not successful. Without loss of function mutations, it is not possible to fully examine the genetic relationship between lemma trichomes and susceptibility to FHB. Therefore, future work should be focussed on repeat of the generation of loss of function mutation, ideally using CRISPR.

Chapter 5 - Characterisation and mapping of DON responsive root development in *Brachypodium distachyon*

5.1 Introduction

Deoxynivalenol (DON) is produced only by FHB causing species *F. graminearum* and *F. culmorum*, and is globally one of the most common grain contaminants reducing food and feed quality, rendering these species the most economically damaging (Foroud et al., 2012). DON acts as a virulence factor in wheat, mediating the spread of infection throughout host tissues, but the mechanism of virulence is unclear; loss of function of DON biosynthetic pathway genes (*Tri* genes) results in reduced ability to infect, and successfully spread within, the wheat host (Langevin et al., 2004, Desjardins et al., 1996, Kazan et al., 2012). Symptoms of DON in floral tissues during FHB infection of wheat are typically bleaching above the point of infection, followed by necrosis extending below the point of infection as the fungus colonises down through the rachis. Peraldi et al. (2011) observed similar bleaching symptoms in Bd when inoculated with *F. graminearum* and *F. culmorum*, and I confirmed this in the characterisation of diverse Bd accessions in Chapter 2 and in ABR6 x Bd21 RILs in Chapter 3. The primary toxicity of DON across eukaryotes is facilitated by protein synthesis inhibitor action, but DON also inhibits RNA and DNA synthesis, damages cell membranes and organelles particularly mitochondria, inhibits mitosis and can induce rapid apoptosis (Rocha et al., 2005). Kang and Buchenauer (1999) characterised subcellular localisation of DON *In Planta* describing that DON was found on ribosomes but by no means exclusively, suggesting that DON might be influencing additional aspects of host metabolism beyond protein synthesis, especially during early stages of infection.

5.1.1 Previous work

Previous unpublished work by Steed and Nicholson (Unpublished), described by Peraldi (2012), identified differential phenotypes of *Arabidopsis* roots when grown on the surface of DON containing low, and high, concentrations of DON; at low concentration the roots were not significantly different in length to controls, whereas at higher concentration roots were significantly shorter than controls and exhibited an altered gravitropic, waving growth pattern of roots. Peraldi (2012) further identified a concentration dependent response of Bd root development in Bd21 to DON, with elongation of primary roots at low concentrations and reduced root primary length at high concentrations of DON, and universally reduced root hair length. These DON induced phenotypes are not attributed to inhibition of protein synthesis suggesting that DON is playing an additional role within the plant host cell during the establishment of infection.

5.1.2 Chapter Aims

This chapter describes a genetic based approach to identify factors associated with response to DON, utilising the effects of DON on Bd root development as a rapid, low cost, non-destructive and high-throughput tool to investigate natural variation in Bd continuing upon the previous work by Peraldi and Steed to explore DON sensitivity in Bd roots.

The Brachy-pan-genome natural accessions were characterised for DON responsive root development, and a novel phenotype identified. The Bd2-3 x Bd21 population was obtained and characterised for DON sensitivity, and genetic loci identified through association with genetic markers and bulked segregant analysis by next generation sequencing. DON responsive gene expression analysis in Bd2-3 and Bd21 accessions was undertaken using RNAseq.

5.2 Methods

5.2.1 Plant materials

Seed of 48 diverse Bd accessions was obtained as described in Chapter 2. Seed of a Bd2-3xBd21 recombinant inbred line (RIL) population (F6) was obtained from David Garvin (USDA ARS). In preparation for all experiments described seeds from 153 RILs, and/or parental lines Bd21 and Bd2-3, were stratified for five days and germinated at 22 °C in the dark for 24 hrs as described in Chapter 2.

5.2.2 Characterisation of Bd accessions; DON responsive root development

Seeds from forty-eight Bd accessions (previously described in Chapter 2) were stratified at 4 °C in the dark for four days, following the removal of glumes, in Petri dishes containing 3 mL sterile distilled water between filter paper discs. Seeds were incubated at 22 °C (dark) for 24 hrs to initiate root growth before being placed in Qiagen 1.2 mL collection tubes containing 1 mL of 0.4 % agar, either control or supplemented with 10 µM DON, both containing 0.03 % ethanol. Four seedlings were used per treatment per accession. Assays were maintained in a growth cabinet as described above. Photographs were taken at 24 hr intervals and following removal of roots from medium after 6 days. Root lengths were measured using the semi-automated SMARTROOT plugin for ImageJ (FIJI)(Lobet et al., 2011). Statistically adjusted predicted means were obtained for root length (5 day) data using GLM in Genstat (18th ed.), with block, replicate treatment and accession included in the statistical model. Percentage of predicted mean DON treated roots was calculated compared to controls, per accession.

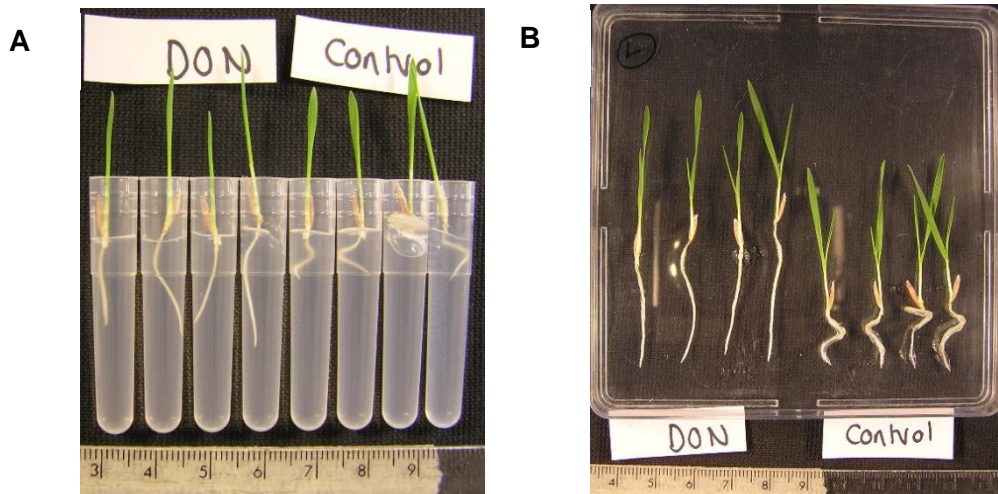


Figure 5-1 Setup of root assays in 1.2 mL tubes, a) *Bd21* at 4 days LHS four seedlings in media contains 10 μM DON, RHS four seedlings in control media (ethanol amended only agar), b) *Bd21* seedlings removed from tubes at 6 days, suitable for root length measurement

5.2.3 DON head assay

Twenty-five *Bd2-3* and *Bd21* plants were grown to heading, as described in Chapter 3. At mid-anthesis, a single floret per head (three per plant) was cut to remove the top half and filled with 3 μL of 10 μM DON supplemented with Tween20 (0.05 %). Control florets were filled with water supplemented with Tween20 (0.05 %). Symptoms of DON toxicity were scored by counting the number of affected florets at 7- and 10- days post-treatment and photographed 12 days post-treatment. Statistical analysis was undertaken using REML in R, as described in Chapter 3 (fixed effects model= Rep+Pot.Tray, random effects model = Line) to obtain BLUP predicted means and standard errors for each line.

5.2.4 Induction of *Bd2-3* root branching phenotype by other compounds?

Bd accession *Bd2-3* was stratified and germinated as previously described; after 24 hrs at 22 $^{\circ}\text{C}$, seeds were transferred to individual Qiagen collection tubes containing 1 mL of supplemented 0.4 % agar, prepared to concentrations described in Table 5-1.

Seedlings were maintained at 22 °C, photographed daily and at experiment completion (7 days) when they were removed from tubes.

Table 5-1 Chemical treatments and concentrations to assess stress responses of Bd2-3 root development

Treatment	Final concentration (µM)	Final [EtOH] (%)
Control	n/a	0.033
DON	10	0.033
IAA	0.5	0.033
TIBA	0.01	0.033
Anisomycin	0.5	0.033
Cycloheximide	0.5	0.033

5.2.5 Characterisation of Bd2-3 x Bd21 population for DON sensitivity in roots

Seeds of the Bd2-3 x Bd21 RIL population (ten seeds per line at F6) were obtained from David Garvin (USDA ARS, St. Paul Minnesota). Eight seeds from 153 progeny lines, and parental lines, were stratified for six days and germinated at 22 °C in the dark for 24 hrs. Germinated seeds were transferred to individual, racked 1.2 mL Qiagen collection tubes containing 1 mL of 0.4 % agar (Foremedium, Cas No. 009002-18-0) amended with DON. For phenotyping at 10 µM DON, four seedlings were used per treatment; control (ethanol amended to 0.03 %) and DON (10 µM). Placed in a propagator tray with clear lid containing water to maintain humidity, seedlings were incubated in a growth cabinet at 22 °C under 16hr/8hr light/dark cycle. Roots were photographed after six days for the visual scoring of DON response type. A subset of roots showing typical phenotypes were removed from tubes and photographed after a further four days.

Two seedlings grown under control treatment were further used for bulking seed, potted two per 8x8x8 cm pot and grown under winter glasshouse conditions; resultant seed was used for screening root development response at a higher DON concentration. The experiment was constructed equivalent to above with the following

exceptions: 20 μ M DON supplemented media was used, eight seedlings were prepared for DON treatment, and control treatments (ethanol amended to 0.03 %) were included for parental lines only, not RILs.

For characterisation at 10- and 20- μ M, individual roots were assigned a phenotype of like-Bd21, like-Bd2-3 or intermediate (showing both elongation and branching) from photographs; intermediate roots were excluded from analysis. The proportion of Bd21-like and Bd2-3-like roots was calculated and plotted for each concentration of DON, 10- and 20- μ M.

5.2.6 KASP mapping of DON root sensitivity

Leaf material from Bd2-3 x Bd21 F6 RIL population was harvested, freeze dried and DNA extracted using the plate extraction method described in Chapter 4. Martin Trick (Computational Biology, JIC) prepared a high-confidence SNP file for Bd2-3 vs Bd21(v2) using sequencing read data from Phytozome (v12), from which two KASP markers were designed to each Bd chromosome arm. KASP markers were run on the Bd2-3 x Bd21 population using the protocol described in Chapter 4; the sequences of successful markers are listed in Supplementary Table 4. Single marker association analysis was undertaken (Genstat, GLM) to identify markers significantly associated with the DON root phenotyping data from experiments Chapter 5.2.5. For fine-mapping, iterative rounds of additional KASP markers were designed (from the same SNP resource) and run on the Bd2-3 x Bd21 F7 population and aligned with phenotype data; (Supplementary Table 5). Using these fine-mapping marker data, MapDisto was used to generate a physical map (loci specific to Bd21v2).

5.2.7 Bulk Segregant Analysis by Next-Generation Sequencing

Thirty RILs showing consensus phenotypes, elongatory like Bd21 or inhibitory like Bd2-3, were selected for analysis by bulk segregant analysis (BSA) by next

generation sequencing (NGS). Three pools of ten individual RILs (Table 5-2), a total of 30 per phenotype, were grown for leaf material as previously described. Leaves were pooled prior to DNA extraction; equal representation of leaf material from individuals within each pool was ensured by measuring 50 mg of freeze-dried material, approximately equivalent to two leaves per RIL per pool.

Table 5-2 Pools of Bd21xBd2-3 RILs F1-x, F7-1 used for bulked segregant analysis of DON sensitivity in Brachypodium distachyon roots.

Bd21-like	Bd21-like	Bd21-like	Bd2-3-like	Bd2-3-like	Bd2-3-like
Pool1	Pool2	Pool3	Pool1	Pool2	Pool3
22	26	51	7	21	32
23	27	79	18	30	36
107	41	100	42	31	37
108	109	124	47	50	76
127	116	125	92	71	82
128	117	126	93	73	85
129	130	132	94	96	105
149	131	134	122	102	115
155	158	146	138	154	120
156	162	173	147	157	159

DNA was extracted from pooled leaves, ground under liquid nitrogen, using a CTAB method: CTAB buffer (0.8 % cetyl-trimethylammonium bromide, 1 % polyvinyl pyrrolidone, 34 mM sarkosyl, 137 mM sorbitol, 0.8 M NaCl, 27 mM EDTA in water) was heated to 65 °C and 4 mL added to 50 mg per sample leaf material, then incubated at 65 °C for 2 hours. One volume chloroform: isoamyl alcohol (24:1) was added, vortexed and centrifuged at 4226 x g for 10 mins. The upper aqueous phase was removed to a fresh tube, 100 U of RNaseA added and incubated at 37 °C for 45 mins. One volume of isopropanol (-20 °C) was added, gently mixed and incubated overnight at -20 °C to precipitate DNA, then centrifuged at 4226 x g for 10 mins. The resultant DNA pellet was washed with 70 % ethanol, allowed to dry and dissolved in TE buffer. Analysis by gel electrophoresis confirmed absence of RNA in samples. DNA was quantified using Qubit™ dsDNA HS kit (Thermo Fisher Scientific), read on

a Qubit™ 2.0 Fluorometer, and 1500 ng of each sample prepared for submission to Novogene (HK) Company Ltd. for quality control, library preparation and DNA sequencing by Illumina HiSeq to generate c. 40X coverage (12 Gb data per sample) 150 bp paired-end (PE) reads.

The three replicate pools were grouped by phenotype for final analysis. Quality control of samples was executed using fastQC (version 0.11.8, Andrews (2010)). Trimmomatic (version 0.33) was used to clip reads of any remaining Illumina Truseq2adapter sequences, and to clean reads using a sliding window (size 10, quality 20) and to a minimum read length of 50 base-pairs (Bolger et al., 2014). Reads were aligned, per merged sample, to the Bd21 v3.1 reference sequence using BWA (v.0.7.5) then sorted and indexed using Samtools (v1.9)(Li et al., 2009). Freebayes (v.1.3.1) was used to call variants in parallel for the Bd21-like and Bd2-3-like samples using the following parameters: quality >20, coverage >20 and mapping quality >42. VCFtools was used to remove variants with mean depth below 60 and quality score below 1500 (Danecek et al., 2011); the resultant .vcf file was converted to .txt using the 'query' command from BCFtools.

Calculations for bulk frequency ratio of variants (BFR) were undertaken using R, and Rstudio, following the principals described by Trick et al. (2012). The ratio of frequencies between the bulks of the alternative, informative allele (AO) was calculated for each variant, Bd2-3-like/Bd21-like, and plotted by Bd21 v3.1 genomic position using R (Rstudio, ggplot2 package (Wickham, 2016)).

5.2.8 Fine mapping of Bd1L BSA interval

DNA material previously described in Chapter 5.2.5 was used for KASP analysis for fine mapping of Bd1L BSA peak, for high-confidence RILs only (Table 5-2). Primers used are listed in Supplementary Table 6. KASP reactions analysis was carried out

as previously described. Relationships between KASP genotypes, and DON induced phenotypes at 10- and 20- μ M were assessed.

5.2.9 RNAseq analysis of Bd2-3 and Bd21 in response to DON

Germinated seeds of Bd21 and Bd2-3 were transferred to open Petri dishes containing a filter paper disc moistened with water (seven seedlings per plate). Four replicate Petri dishes were prepared for each treatment (Mock control, 5 μ M DON and 20 μ M DON), per accession (Bd2-3 and Bd21), arranged in a propagator tray with clear lid to maintain humidity. Seedlings were incubated at 22 °C, 16 hr daylength for five days until roots were c. 4-5 cm in length.

Treatments, prepared as described in Chapter 5.2.2 to 0-, 5- and 20- μ M DON, were applied to roots in 10 mL volumes, incubated for 6 hrs then root tissue was harvested and flash frozen in liquid nitrogen. Four replicate samples were prepared per treatment. Samples were ground using a pestle and mortar under liquid nitrogen and total RNA extracted using RNeasy® Plant Mini Kit (Qiagen) following manufacturers protocol (eluting in 30 μ L water). Following DNase treatment by TURBO DNA-free™ kit (Ambion®), RNA content was quantified using Nanodrop (v2). All samples had an RNA-integrity number >6. At least 500 ng of RNA for 18 samples (three out of four replicates per treatment) was submitted to Genewiz (UK) for quality control, library preparation and RNA sequencing by Illumina HiSeq to generate 15-20 million 150 bp paired-end reads per sample.

Quality control of samples was executed using fastQC (version 0.11.8). Trimmomatic (version 0.33,) was used to clip reads of remaining Illumina adapter sequences and clean to the same parameters described in Chapter 5.2.7 (Bolger et al., 2014). Resultant reads were mapped to the *Brachypodium distachyon* v3.1 reference, sequence available from Phytozome (12th edition (International Brachypodium,

2010)) using HISAT2 (version 2.1.0) (Kim et al., 2015) and sorted using Samtools (version 1.9). A python script obtained from Burkhard Steuernagel (Computational Biology, JIC) was used to calculate non-normalised read counts for each sample (gene count matrix). Differential expression values, and plots (MA, Multi-Dimensional Scaling (MDS) and volcano plots) were generated using Degust (v4.1.1), an interactive online tool (Powell et al., 2019). Venn diagrams were produced using the webtool Venny v2.1, and used to obtain lists of shared up- and down-regulated genes with a false-discovery-rate cut off of 0.05 and a log fold-change >2 (Oliveros, 2007-2015).

5.3 Results

5.3.1 Brachypodium accessions vary in response/sensitivity to DON

A set of 48 diverse Bd accessions, previously described in Chapter 2 (and listed in Supplementary Table 1), was characterised for DON responsive root development; seedlings were grown in agar supplemented with 10 μ M DON a concentration that induces root elongation in Bd21. After five days root length was measured and calculated relative to control roots (Figure 5-2). The majority of accessions showed an elongatory response to DON; twenty-seven accessions had a significantly greater root length compared to controls (Adi-10 to BdTR13A, Figure 5-2). Three accessions had significantly reduced root length in response to DON: Bd2-3, Koz-1 and Luc-1 (means=59.6, 63.7 and 73.4 % respectively). Luc-1 roots were simply reduced in length whereas accession Bd2-3 and Koz-1 roots showed inhibition of the primary root meristem and induction of branching secondary roots immediately above the inhibited root tip. Assuming that elongation is a representation of lesser DON sensitivity, and inhibition is a manifestation of greater DON sensitivity, accessions could be selected that vary significantly in sensitivity to DON. Representative images of two accessions of interest are shown (Figure 5-3) and highlighted in Figure 5-2, Bd21 and Bd2-3; the former showed an elongatory effect typical in this experiment at 10 μ M DON, increased gravitropism, and reduced root hairs. In contrast Bd2-3 showed an extreme inhibition of primary root growth and the development of branching roots in response to a low concentration of DON; all four replicate roots showed the same phenotype and this novel phenotype in response to DON was reproducible over three replicate experiments. This varies from previously published accounts of DON-induced root inhibition that have typically reduced root hairs and are unbranched in wheat (Eudes et al., 2000).

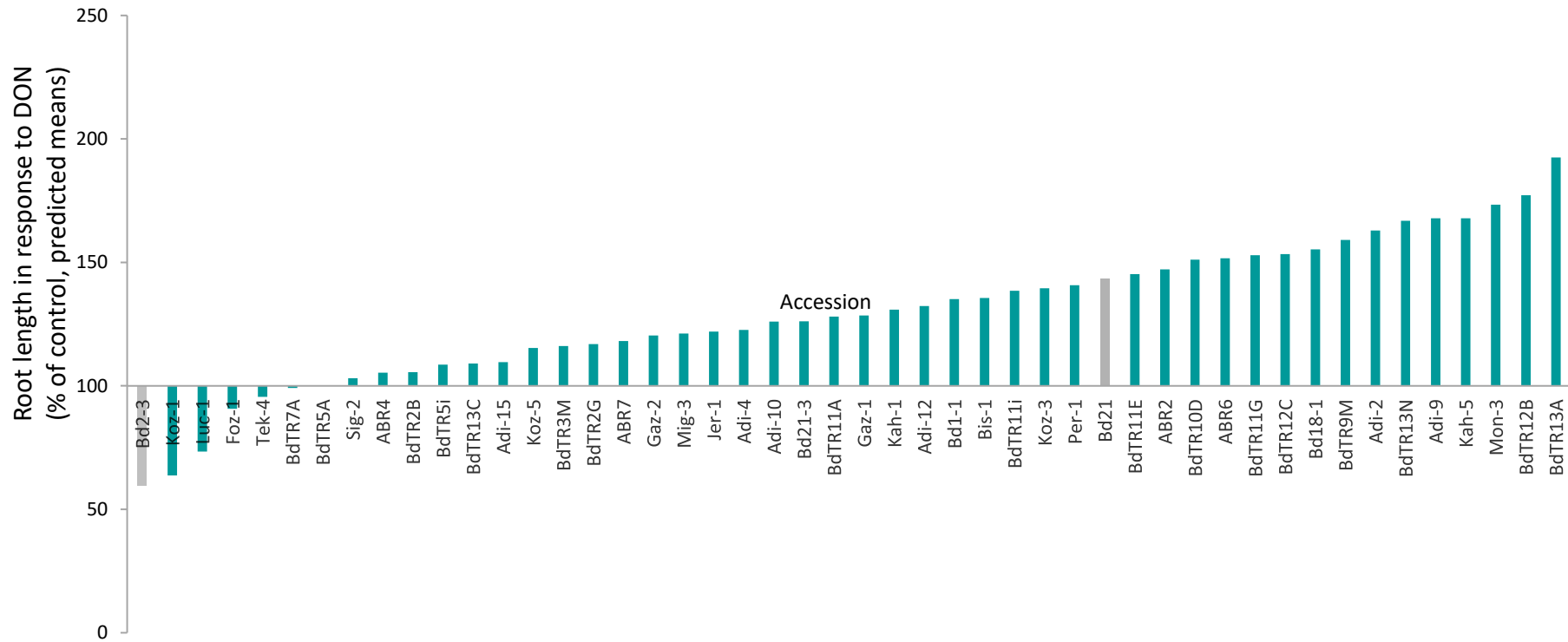


Figure 5-2 Variation in root length of *Bd* accessions when grown in agar supplemented with DON (10 μ M), after 5 days. SE = \pm 5.58 to 23.90. Accessions highlighted in grey, Bd2-3 and Bd21 that vary in phenotype, are parents of a biparental mapping population

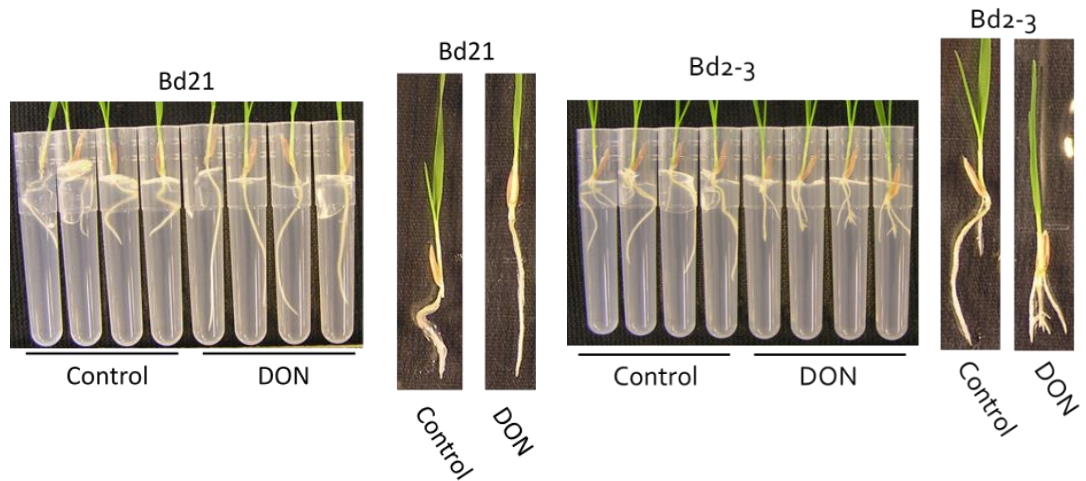


Figure 5-3 Photographs showing the differential responsiveness to growing in agar supplemented with 10 μ M DON between Bd21 and Bd2-3 accessions of *Brachypodium distachyon*.

5.3.2 DON sensitivity in floral tissues (Bd2-3 vs Bd21)

To assess whether the differential response to DON is root tissue specific, and relevance of the differential response in root DON sensitivity to *Fusarium* head blight, response to DON in the floral tissues was characterised for Bd2-3 and Bd21. A DON head-based point application experiment was carried out under controlled environment conditions, and the results shown in Figure 5-4. Symptoms appeared as browning of florets and spread only to tissues above the point of application. The production of symptoms above the point of DON application is also observed in wheat (Lemmens et al., 2005). Browning symptoms were observed to spread within the treated spikelet and to above spikelets, never below; this was a deviation from expected bleaching phenotype yet browning resulting from contamination is unlikely as the mock treated controls showed no browning symptoms. At both seven- and ten-days post application, DON resulted in symptoms spreading to a greater number of florets in Bd2-3 (means=1.98 and 2.48) compared with Bd21 (means=1.12 and 1.38, p -value<0.001). The greater DON sensitivity of Bd2-3 compared to Bd21 indicates

that the differential observed in root tissue may reflect greater DON sensitivity of Bd2-3 in both tissues (Chapter 5.3.1).

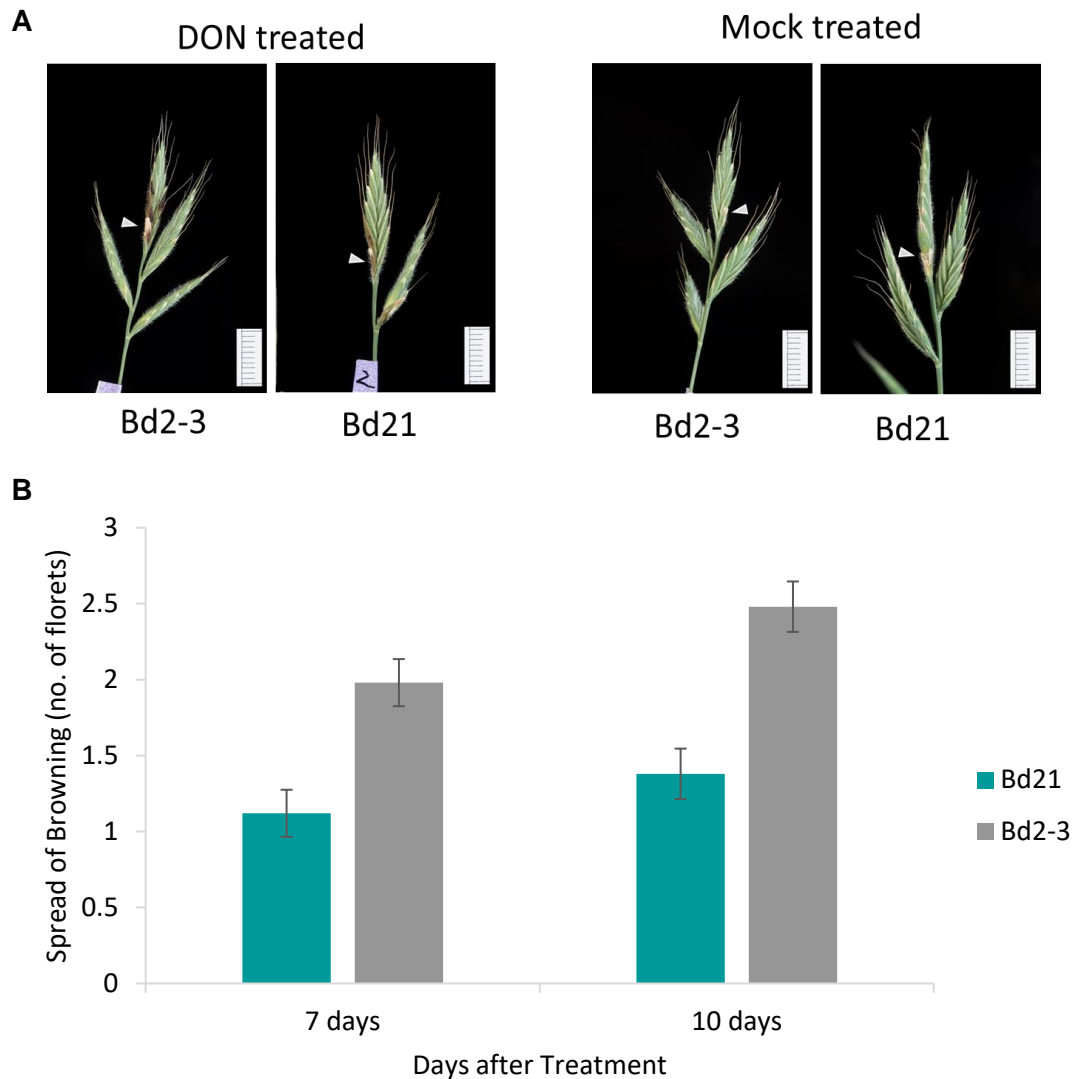


Figure 5-4 Bd2-3 and Bd21 DON sensitivity in floral tissues. A, Representative images of Bd2-3 and Bd21 typical browning symptoms in response to application of DON. Point of treatment (DON or mock) application indicated by white triangle marker. Scale = 1 cm. B, Plots of predicted mean (derived from GLM analysis) spread of DON associated browning symptoms as number of florets above point of application for Bd21 and Bd2-3 for seven and ten days post treatment. Error bars = $\pm 1SE$

5.3.3 Do other stress treatments induce root branching in Bd2-3?

Bd2-3 seedlings were grown on agar treated to simulate a variety of stress conditions to assess whether the inhibited, branched-root phenotype shown in response to DON was general, or specific to DON. Treatments included auxin, auxin transport inhibitor (triiodobenzoic acid, TIBA) and protein-synthesis inhibitors (anisomycin and cycloheximide). Images from stress treated roots at 7 days following removal from growth medium are shown in Figure 5-5. Roots grown in control and DON treated media were typical for Bd2-3; DON treated Bd2-3 roots were inhibited and produced lateral roots, as described above. Auxin (IAA) at 0.5 μ M had no major visible effect on root development (Figure 5-5). One (out of four) roots treated with TIBA (10 nM) and protein synthesis inhibitors anisomycin and cycloheximide (both 0.5 μ M) was branched at a point that is similar to that in which Bd2-3 roots are inhibited and branch with DON, and three roots appeared to be unaffected (Figure 5-5); the primary difference in these phenotypes is that for DON the primary root ceases to elongate while the other three treatments show the primary root continuing to extend (Figure 5-5).

5.3.4 Characterisation of Bd2-3x Bd21 population for DON sensitivity

An F6-7 Bd2-3 x Bd21 population of 154 recombinant inbred lines (RILs) was assessed for DON sensitivity manifesting as differential root development. The population was first phenotyped at a concentration of 10 μ M DON; parental phenotypes were typical to those previously observed, with Bd2-3 primary roots inhibited and emergence of lateral branching and Bd21 roots elongated and exhibited hyper-gravitropic growth (Figure 5-6a). Control treated roots varied between the accessions; Bd2-3 roots were longer in length and coiled less within the growth tubes than Bd21 (Figure 5-6a).

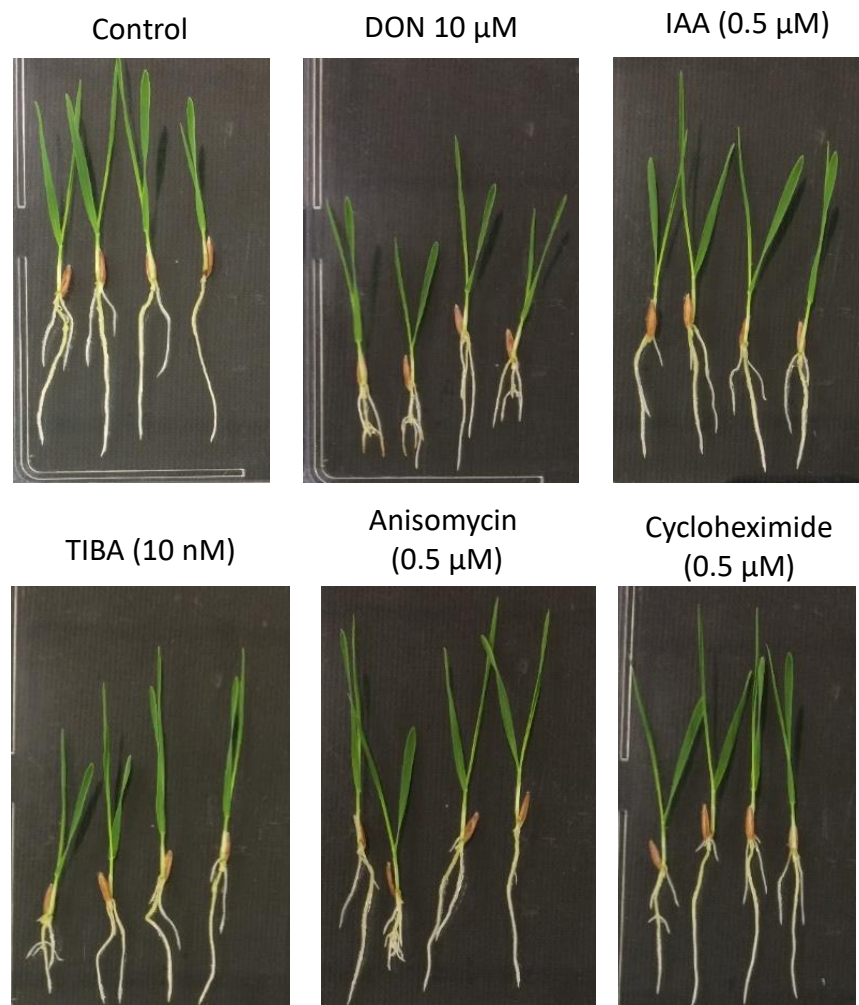


Figure 5-5 Phenotypes of roots grown in supplemented 0.4% agar for five days. TIBA=triiodobenzoic acid, an auxin-transport inhibitor. Anisomycin and cycloheximide are protein-synthesis inhibitors, the latter described as most closely sharing cellular mechanism with DON.

In response to growth in media supplemented with 10 μ M DON, progeny of the population segregated between the two phenotypes at approximately equal proportions Figure 5-7 Proportional distribution of Bd2-3-like and Bd21-like roots for each of 154 Bd2-3 x Bd21 F7 RILs when grown in agar supplemented with 10 μ M DON, Bd2-3-like:Bd21-like, with some lines showing an intermediate sensitivity phenotype in which lateral roots were produced but growth of the root tip was not inhibited, instead continuing to grow with hyper-gravitropism. Individual progeny roots were assigned a phenotype as Bd2-3-like, Bd21-like or intermediate, plotted in Figure 5-7 with intermediate roots excluded from subsequent analysis.

The experiment was repeated at the higher DON concentration of 20 μ M, under the expectation that a greater proportion of lines would exceed a DON sensitivity threshold and develop branching instead of elongation. The proportion of roots showing each parental phenotype for each RIL is shown in Figure 5-8. A greater proportion of RILs have a Bd2-3-like phenotype compared to the equivalent histogram for 10 μ M DON. From these data, RILs were designated as Bd2-3-like or Bd21-like in DON sensitivity. Sixty-five RILs had the same phenotype at both concentrations: 30 Bd21-like, 30 Bd2-3-like and 5 intermediate in both assays (Supplementary Table 7). Sixty-four RILs appeared more DON sensitive at 20 μ M, tending towards a Bd2-3-like phenotype: 21 were Bd21-like at 10 μ M and Bd2-3-like at 20 μ M, 25 RILs were Bd21-like at 10 μ M to intermediate at 20 μ M and 18 RILs were intermediate at 10 μ M and Bd2-3-like at 20 μ M (Supplementary Table 7). However, 23 lines appeared less sensitive at 20 μ M DON than 10 μ M: 16 were either Bd2-3-like to intermediate, or intermediate to Bd21-like with 7 RILs Bd2-3 like to Bd21 like.

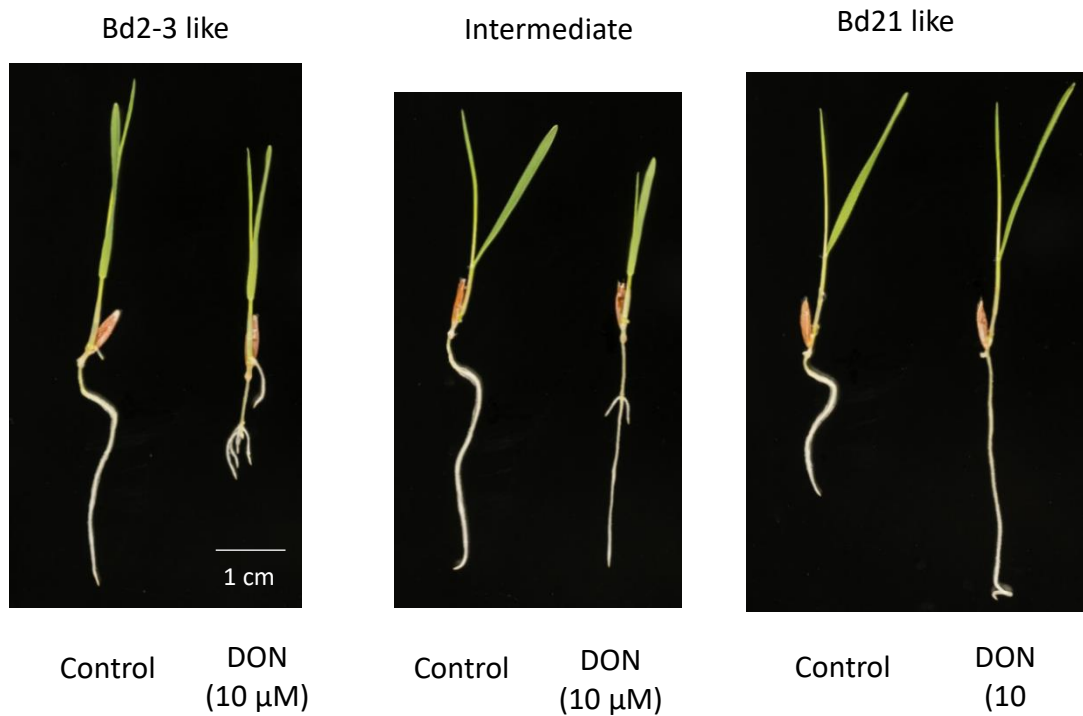
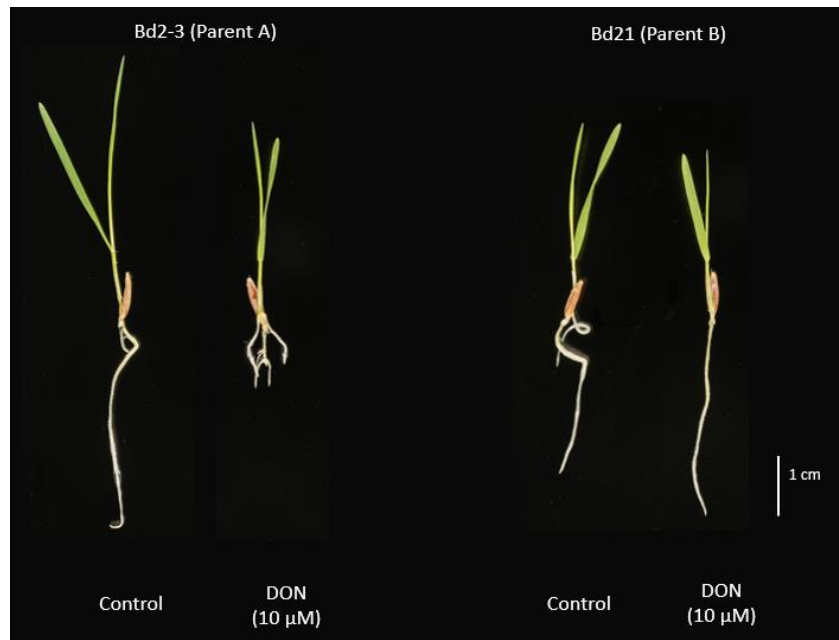


Figure 5-6. Differential phenotypes of roots of two accessions, *Bd21* and *Bd2-3* when grown in 10 μM DON supplemented agar for 6 days, compared to no-treatment controls. Below: Roots grown in agar supplemented in 10 μM DON for six days, demonstrating the three typical phenotypes observed, in comparison to control treated roots.

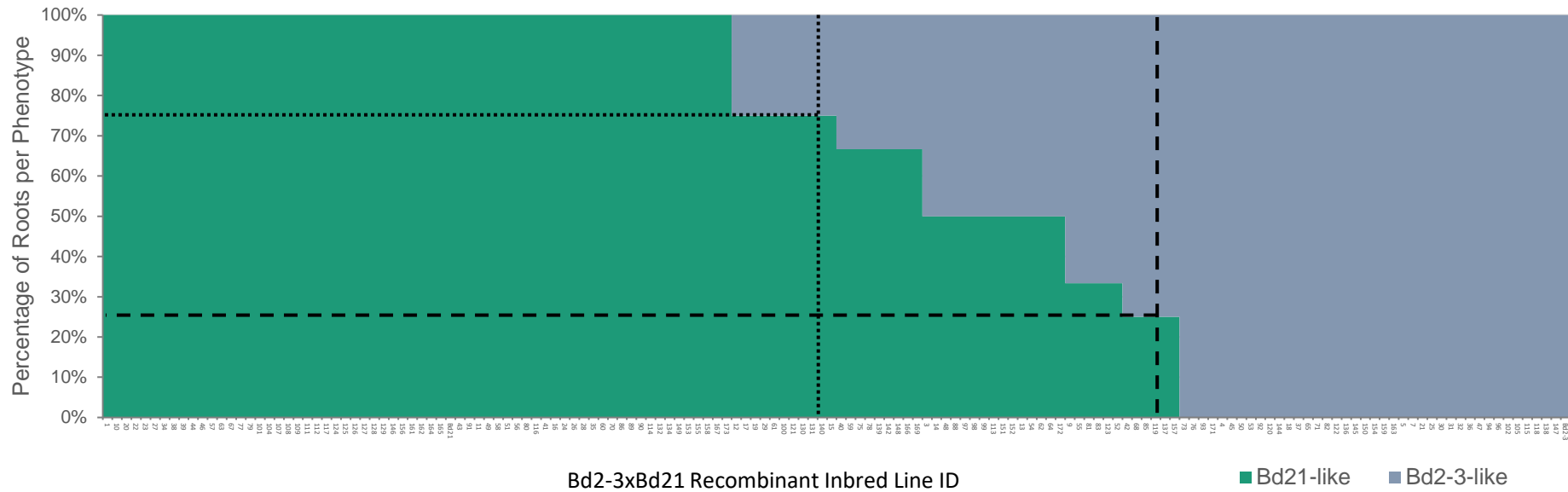


Figure 5-7 Proportional distribution of Bd2-3-like and Bd21-like roots for each of 154 Bd2-3 x Bd21 F7 RILs when grown in agar supplemented with 10 μ M DON. Overlaid lines represent assignment of RILs as Bd2-3-like (to the right of dashed vertical line), Bd21-like (to the left of the vertical dotted line), or intermediate (between the two vertical lines) Four replicate roots per RIL. Dead roots excluded, resulting in >4 possible Bd2-3:Bd21 ratios

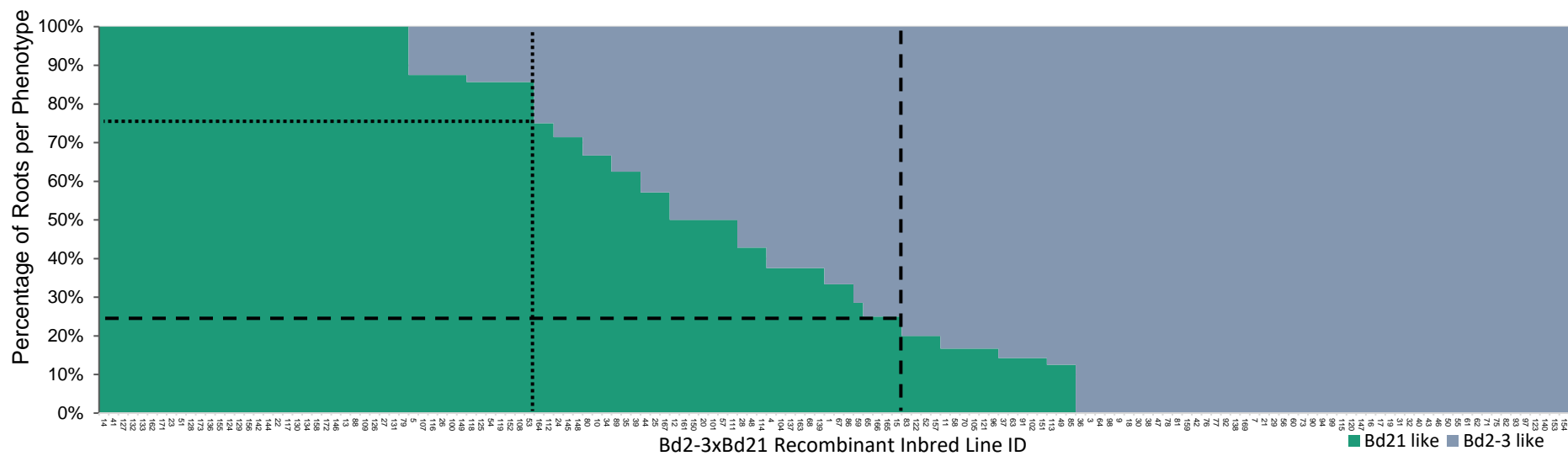


Figure 5-8 Proportional distribution of Bd2-3-like and Bd21-like roots for each of 154 Bd2-3 x Bd21 F7 RILs when grown in agar supplemented with 20 μ M DON. Overlaid lines represent assignment of RILs as Bd2-3-like (to the right of dashed vertical line), Bd21-like (to the left of the vertical dotted line), or intermediate (between the two vertical lines). Eight replicate roots per RIL. Dead roots excluded, resulting in >8 possible Bd2-3:Bd21 ratios

5.3.5 Identification of region associated with DON sensitivity

Once the Bd2-3 x Bd21 population had been characterised for DON sensitivity through assessment of root development, identification of associated genetic loci could be initiated. However, no genetic map, or any other genotypic data, was available for the Bd2-3 x Bd21 RIL population. Therefore, a set of KASP markers was designed, two to each chromosome arm, for single marker association analysis using the 10 μ M and 20 μ M DON sensitivity phenotype data. RILs were assigned a phenotype, as like parent A, B or intermediate according to Figure 5-7 & Figure 5-8. Figure 5-9 illustrates the approximate positions, and p-values for association with DON sensitivity, of each marker. Bd1LD was the only significantly associated marker with DON-sensitivity at 10 μ M ($p < 0.001$) (Figure 5-9). The Bd1L marker was not

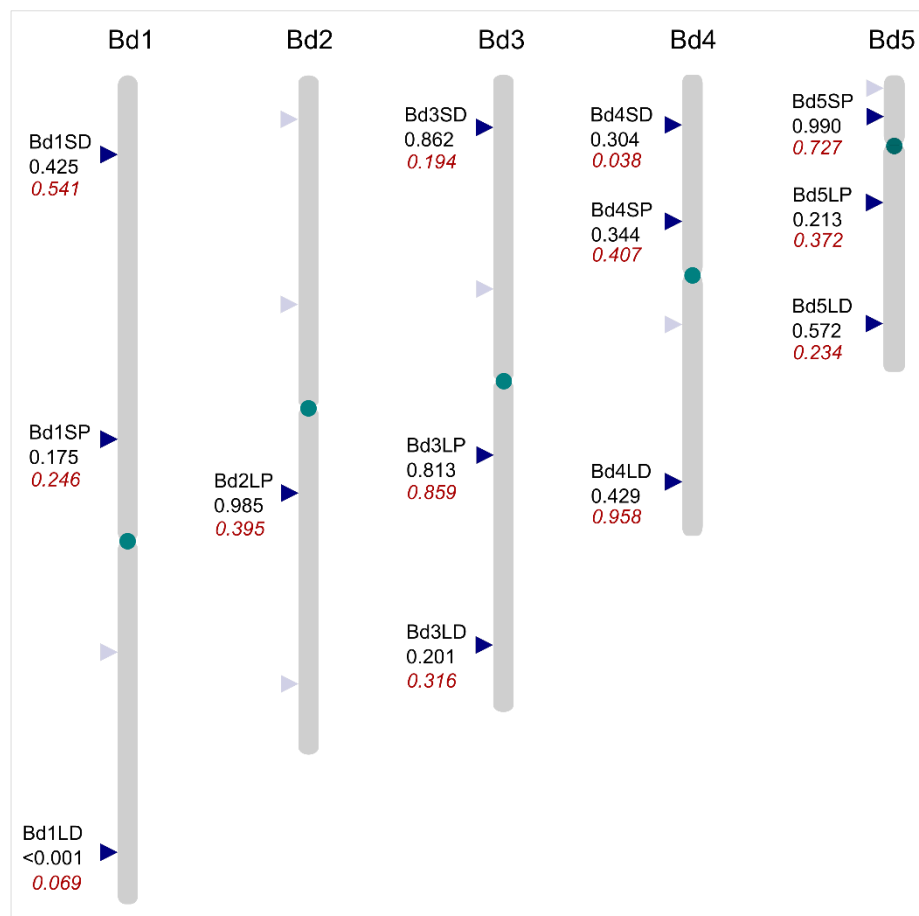


Figure 5-9 Illustration of KASP markers and single marker association results for association with DON sensitivity at for Bd2-3xBd21 population characterised in media supplemented with 10 μ M DON. P-values for associated are presented with marker names, for 10 μ M DON upper, 20 μ M DON red, italicised and below. Greyed out, unlabelled markers were unsuccessful and omitted from analyses.

significantly associated with DON sensitivity at 20 μ M by a small margin ($p=0.069$), whereas marker Bd4SD was ($p=0.038$).

Bd1LD was found to be the closest associated marker with DON sensitivity in Bd2-3 x Bd21 between 10 μ M and 20 μ M datasets, genotyping focus was refined to the long arm of chromosome Bd1. Iterative rounds of KASP markers were designed and applied to genotype the population for enrichment of the Bd1L chromosome arm and single marker analysis was again undertaken on a total of 23 markers on the Bd1L chromosome arm. Figure 5-10 highlights eleven markers that were significantly associated with DON sensitivity (p -values <0.05), covering a region of 2.4 Mb, and 8.7 cM) (or 3.3 Mb and 16.2 cM to the non-significant flanking markers). However, no complete segregations were clear when analysing the genotype and phenotype data; for all markers there were many lines where phenotype and genotype did not associate; the agreement was best for RILs with Bd2-3 phenotype suggesting there are roots escaping the sensitivity phenotype. Between the flanking markers of Bd1L_68688411 and Bd1L_72052958 are 487 genes annotated in Bd21v2, from Bradi1g69940 to Bradi1g74580. This remained much too large a region to warrant investigations into the plausibility of individual genes being involved in a DON sensitivity mechanism.

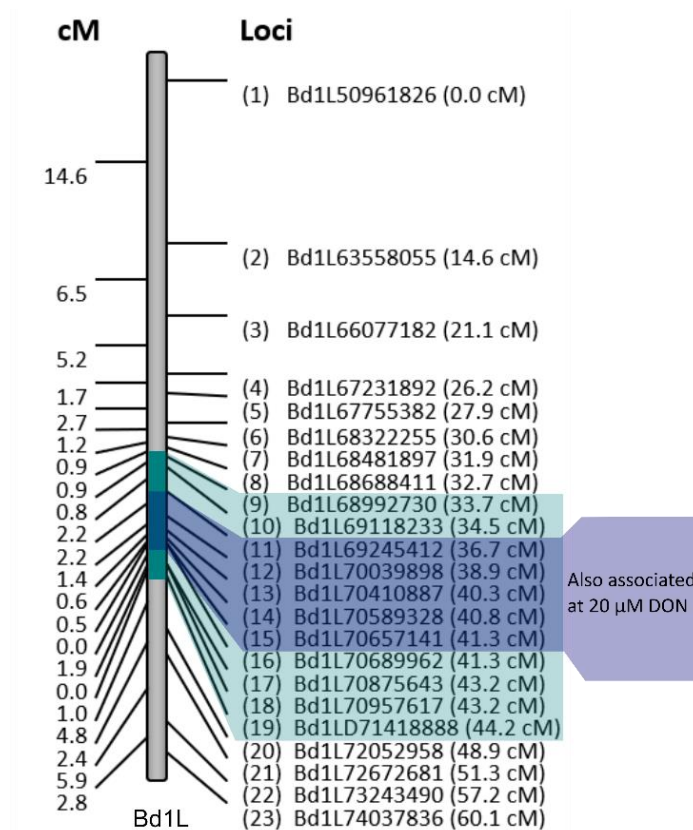


Figure 5-10 Physical map of Bd1L overlaid with region of significantly associated KASP markers with DON sensitivity in root development in Bd2-3xBd21 RIL F6 population. For 10 μM DON, area highlighted in green, for 20 μM DON, area highlighted in purple = p -values < 0.05. Total map size = 60.07 cM.

5.3.6 Bulk segregant analysis for extreme DON sensitivity RILs of Bd2-3 x Bd21

Bulk segregant analysis (BSA) by whole genome re-sequencing was carried out to identify genomic loci associated with DON sensitivity (Michelmore et al., 1991). Based on consensus phenotypes at 10- and 20- μM DON treatments (Supplementary Table 7), high-confidence subsets of RILs at the extremes of low- and high-sensitivity to DON, each containing 30 RILs, were pooled (Table 5-2). Illumina sequencing was carried out on pooled DNA from leaf material to obtain 65.7 and 81.1 million paired end 150 base pair reads for Bd21-like and Bd2-3-like pools once merged. Initially three replicate pools were prepared per extreme phenotype, each containing ten unique RILs, providing the possibility to remove anomalous replicates from analysis to insure against any mis-phenotyped RILs skewing differential allele frequencies

between Bd21- and Bd2-3- like pools. Sequencing read fastq-files for all replicate pools were merged after initial analysis did not reveal any evidence of mis-assignment. Following alignment to the Bd21v3.1 reference genome sequence 1.08 million short sequence variants, specifically single nucleotide polymorphisms (SNPs), insertions and deletions (INDELs) and other (marked 'complex'), were identified in parallel between the merged Bd21 and Bd2-3-like pools using Freebayes (Garrison and Marth, 2012). Following plotting of quality frequency score for the variants called for each Bd chromosome (Figure 5-11a), a filtering threshold was determined and applied to exclude the lowest quality variants likely resulting from mis-calling and low read depth, with 801,145 variants remaining (Figure 5-11b).

The frequency of variants between the pools was calculated and is presented as a bulk frequency ratio in Figure 5-12a (Trick et al., 2012). A major peak on Bd1L was identified, peaking at 69782472 bp with a maximum bulk frequency ratio of 21.1 (Figure 5-12a). The peak borders were defined to include the physical distance in which bulk frequency ratio was greater than seven; a total of 74 variants with a bulk frequency ratio >7 were identified between loci 69579665 to 69969275, of which 55 were intergenic and 19 were intragenic across eight annotated genes (Table 5-3). The physical distance contains 56 genes in Bd21v3.1 sequentially from Bradi1g71373 to Bradi1g71820, listed in Table 5-4 with Bd2-3 equivalent loci and At orthologues. The Bd1L BSA peak lies centrally within the previous KASP-mapped significance interval (Figure 5-12b).

A smaller, secondary well-defined peak was identified on chromosome 2, at 47356029 and 48094910 bp with a bulk frequency ratio maximum of 16.69 at Bd2_47356029; nine variants were present in the range with a bulk frequency ratio >7, of Bd chromosome 2 which contains 94 genes annotated in Bd21v3.1, from Bradi2g47240 to Bradi2g47960 (Figure 5-12a). Two, less well defined and structured peaks were also identified on the long arm chromosome 4.

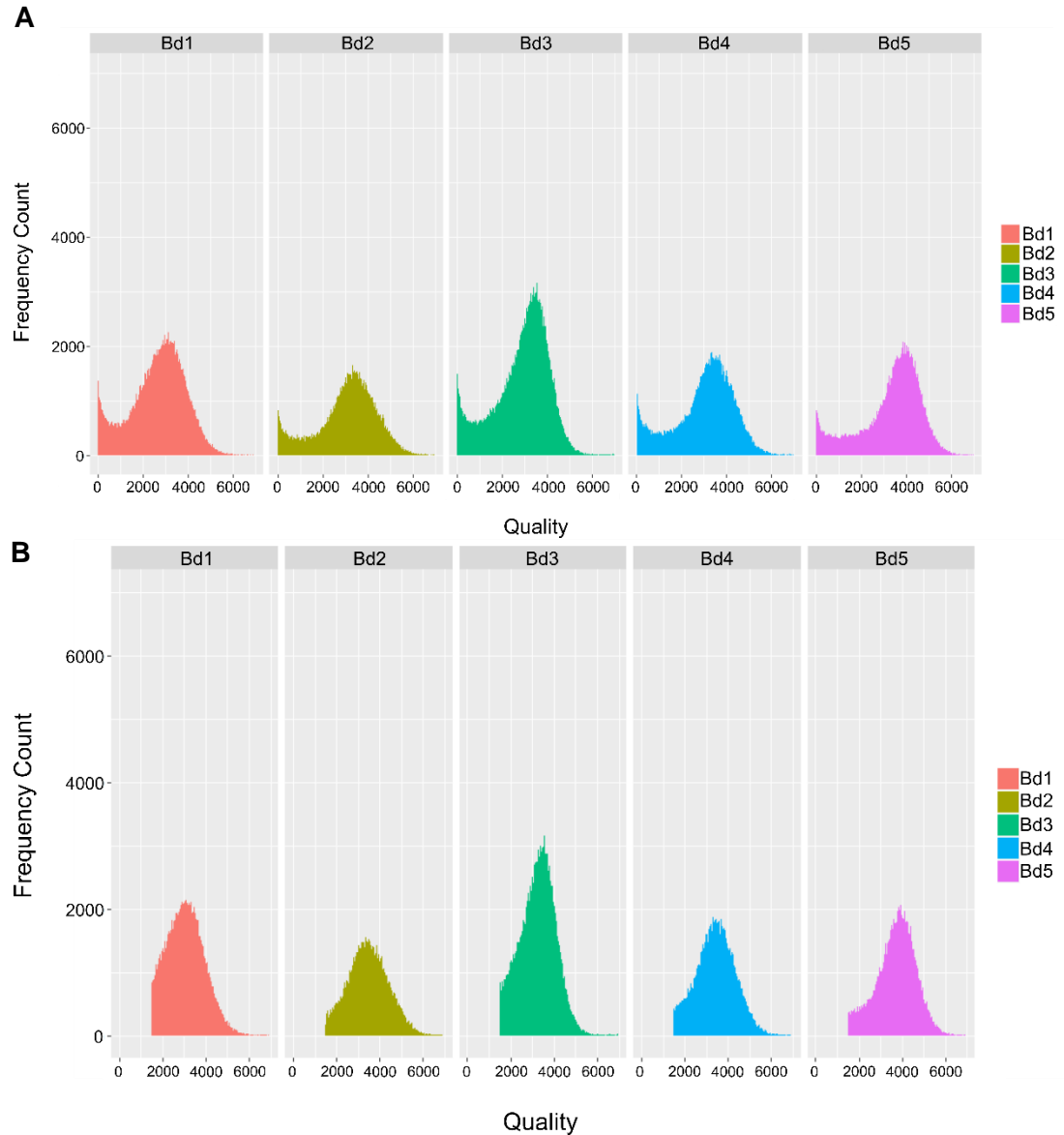


Figure 5-11 Quality scores for BSA variants for Bd2-3xBd21 F7 RIL DON sensitivity, A, prior to filtering of variants, B, with filtering to remove all variants with quality <1500 score.

Eleven genes out of the 56 within the Bd1L BSA interval are annotated to play roles in RNA binding and processing, five have links to plant hormone pathway regulation of response, with a final gene of note Bradi1g71465 related to a casparian strip regulatory gene (Table 5-4).

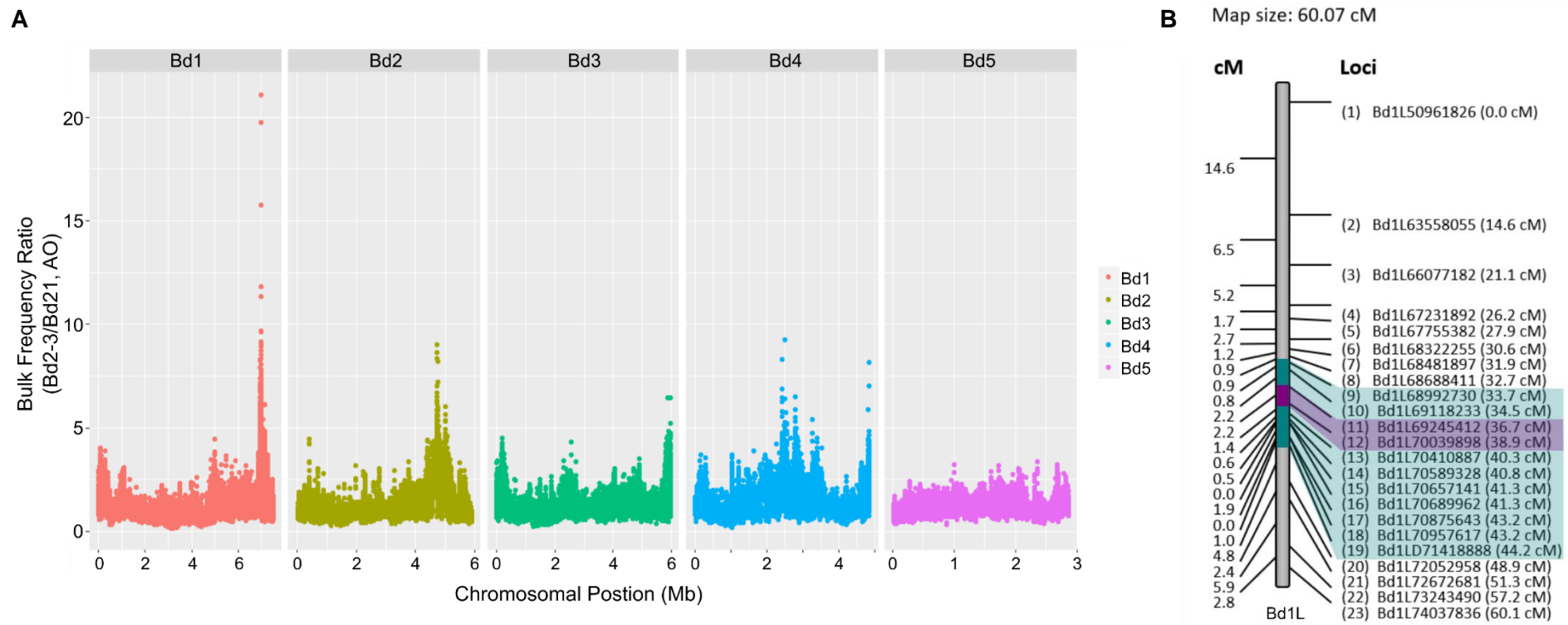


Figure 5-12 Bulk segregant analysis for DON sensitivity in Bd2-3 x Bd21 F7 high-confidence RILs. Thirty RILs per extreme phenotype pool. B, Physical map showing previous KASP mapping of DON sensitivity on Bd1L (Figure 5-10), overlaid with BSA Bd1L peak (purple), variants with bulk frequency ratio >7.

Table 5-3 Genes in BSA chromosome Bd1 peak and the variants within each with bulk frequency ratio (BFR) >7 for DON sensitivity in Bd2-3xBd21 F7 high-confidence Bd21-like and Bd2-3-like pools. Bd1 position applies to Bd21v3.1 bp locus on chromosome one.

Gene	BFR (AO, Bd2-3/Bd21)	Reference allele	Alternative allele	Bd1 position (bp)
Bradi1g71373	7.13	G	A	69616104
Bradi1g71390	9.90	TCAC	TTACTCAGACAG	69623640
	9.84	ACAC	CCAGCCACCCTCAAC	69623634
Bradi1g71420	7.16	TT	TAGG	69639005
	18.20	T	C	69736632
	11.84	G	C	69738506
	8.54	G	C	69736605
	8.38	GAA	AAG	69738525
	8.36	A	G	69736663
	7.39	C	T	69736957
	7.08	A	G	69738714
	7.019	TGGGGCGGT	TGGGGCGGT	69738542
Bradi1g71530	7.81	G	A	69746863
Bradi1g71611	7.83	G	A	69798745
	15.77	TGA	TGGA	69914641
	8.92	G	T	69914594
	8.75	T	A	69912656
	7.08	C	T	69914670
Bradi1g71820	8.92	GTTATTTTTATTTTGA	GTTATTTTTATTTTATTTTATTTTGA	69969275

Table 5-4 Genes annotated in Bd21 v3.1 within the 56 gene BSA candidate interval in association with DON sensitivity from high-confidence Bd2-3 x Bd21 RILs

Gene ID (Bd21 v3.1)	Bd2-3(v1) Gene	Bd annotation (Bd21v3.1)	At orthologue & (Annotation)
Bradi1g71373	Brdisv1Bd2-31010836m	NOGO-B receptor, Rer2p Z- prenyltransferase	AT1G11755.1 (LEW1 (Undecaprenyl pyrophosphate synthetase family protein))
Bradi1g71377	Brdisv1Bd2-31010839m	RNA recognition motif. (a.k.a. RRM, RBD, or RNP domain) (RRM_1)	AT2G21660.1 (AtGRP7,CCR2,GR-RBP7,GRP7 (cold, circadian rhythm, and RNA binding 2))
Bradi1g71383	Brdisv1Bd2-31010840m	n/a	n/a
Bradi1g71390	Brdisv1Bd2-31010841m	Hypothetical Protein	AT1G20460.1 (n/a)
Bradi1g71400	Brdisv1Bd2-31010842m	Transcription initiation factor IIB-related, zinc ion binding	AT4G36650.1 (n/a)
Bradi1g71410	Brdisv1Bd2-31010846m	Mitochondrial carrier protein	AT1G34065.1 (SAMC2, S-adenosylmethionine carrier 2)
Bradi1g71420	Brdisv1Bd2-31010847m	Alpha/beta-hydrolases superfamily protein	AT1G29840.1 (Alpha/beta-Hydrolases superfamily protein)
Bradi1g71425	Brdisv1Bd2-31010848m	37S ribosomal protein S10, mitochondrial	AT3G13120.1 (Ribosomal protein S10p/S20e family protein)
Bradi1g71430	Brdisv1Bd2-31010849m	Serine O-acetyltransferase	AT1G55920.1 (AtSERAT2;1, serine acetyltransferase 2;1)
Bradi1g71450	Brdisv1Bd2-31010853m	Hypothetical Protein	AT2G18910.1 (Hydroxyproline-rich glycoprotein family protein)
Bradi1g71460	Brdisv1Bd2-31010855m	F-Box	AT5G48170.1 (SLY2, F-box family protein)
Bradi1g71465	Brdisv1Bd2-31010856m	Nitrate, fromate, iron dehydrogenase // subfamily not named	AT2G35760.1 (CASPL2B1, CASP-LIKE PROTEIN 2B1)
Bradi1g71470	Brdisv1Bd2-31037589m	Ribosomal protein L2	ATCG00830.1 (Ribosomal protein L2)

Table 5-4 continued Genes annotated in Bd21 v3.1 within the 56 gene BSA candidate interval in association with DON sensitivity from high-confidence Bd2-3 x Bd21 RILs

Gene ID (Bd21 v3.1)	Bd2-3(v1) Gene	Bd annotation (Bd21v3.1)	At orthologue & (Annotation)
Bradi1g71475	Brd1sv1Bd2-31045608m	Small subunit ribosomal protein S19 (RP-S19, rpsS)	ATCG00820.1 (Ribosomal protein S19)
Bradi1g71480	Brd1sv1Bd2-31010857m	n/a	n/a
Bradi1g71490	Brd1sv1Bd2-31010858m	n/a	AT2G34250.1 (SecY protein transport family protein)
Bradi1g71495	Brd1sv1Bd2-31010859m	PPR repeat (PPR) // PPR repeat family (PPR_2)	AT5G65560.1 (Pentatricopeptide repeat (PPR) superfamily protein)
Bradi1g71500	Brd1sv1Bd2-31010860m	Sulfate transporter	AT1G22150.1 (SULTR1;3, sulfate transporter 1;3)
Bradi1g71510	Brd1sv1Bd2-31010863m	Sulfate transporter 2.1-related	AT5G10180.1 (AST68,SULTR2;1, sulfate transporter 2;1)
Bradi1g71513	n/a	n/a	n/a
Bradi1g71517	Brd1sv1Bd2-31010864m	Pre-rRNA-processing protein TSR3 (TSR3)	AT5G10070.2 (RNase L inhibitor protein-related)
Bradi1g71530	Brd1sv1Bd2-31010865m	LL-diaminopimelate aminotransferase (E2.6.1.83)	AT2G13810.1 (ALD1, AGD2-like defence response protein 1)
Bradi1g71540	Brd1sv1Bd2-31010866m	Eukaryotic cytochrome B561	AT3G25290.2 (Auxin-responsive family protein)
Bradi1g71560	Brd1sv1Bd2-31010867m	Protein of unknown function (DUF568) (DUF568)	AT3G59070.1 (Cytochrome b561/ferric reductase transmembrane with DOMON related domain)
Bradi1g71570	Brd1sv1Bd2-31010871m	Mitochondrial import inner membrane translocase subunit TIM22	AT4G26670.1 (Mitochondrial import inner membrane translocase subunit Tim17/Tim22/Tim23 family protein)
Bradi1g71575	Brd1sv1Bd2-31010872m	N-acetyltransferase 9	AT2G04845.1 (Acyl-CoA N-acyltransferases (NAT) superfamily protein)
Bradi1g71580	Brd1sv1Bd2-31010874m	Predicted membrane protein, contains DoH and Cytochrome b-561	AT2G04850.1 (Auxin-responsive family protein)
Bradi1g71590	Brd1sv1Bd2-31010877m	C2 domain	AT5G55530.3 (Calcium-dependent lipid-binding (CaLB domain) family protein)

Table 5-4 continued Genes annotated in Bd21 v3.1 within the 56 gene BSA candidate interval in association with DON sensitivity from high-confidence Bd2-3 x Bd21 RILs

Gene ID (Bd21 v3.1)	Bd2-3(v1) Gene	Bd annotation (Bd21v3.1)	At orthologue & (Annotation)
Bradi1g71600	Brd1sv1Bd2-31010880m	26S proteasome non-ATPase regulatory subunit 3/COP9 signalosome complex subunit 3	AT1G20200.1 (EMB2719,HAP15, PAM domain (PCI/PINT associated module) protein)
Bradi1g71611	Brd1sv1Bd2-31010881m	Polyamine oxidase (propane-1,3-diamine-forming) / MPAO	AT5G13700.1 (APAO,ATPAO1,PAO1, polyamine oxidase 1)
Bradi1g71620	Brd1sv1Bd2-31010882m	FRIGIDA-like protein	AT5G48385.1 (FRIGIDA-like protein)
Bradi1g71624	Brd1sv1Bd2-31010883m	RNA binding protein pumilio-related	AT2G29200.1 (APUM1,PUM1, pumilio 1)
Bradi1g71626	Brd1sv1Bd2-31010884m	n/a	n/a
Bradi1g71630	Brd1sv1Bd2-31010885m	RNA binding protein pumilio-related	AT4G25880.2 (APUM6,PUM6, pumilio 6)
Bradi1g71635	Brd1sv1Bd2-31010886m	n/a	n/a
Bradi1g71637	Brd1sv1Bd2-31010887m	n/a	AT2G29200.1 (APUM1,PUM1, pumilio 1)
Bradi1g71640	Brd1sv1Bd2-31010888m	Peptidyl-prolyl cis-trans isomerase	AT1G53720.1 (ATCYP59,CYP59, cyclophilin 59)
Bradi1g71650	Brd1sv1Bd2-31010890m	Small subunit ribosomal protein S17 (RP-S17, MRPS17, rpsQ)	AT3G18880.1 (Nucleic acid-binding, OB-fold-like protein)
Bradi1g71660	Brd1sv1Bd2-31010892m	Splicing factor 3B subunit 5 (SF3B5, SF3B10)	AT4G14342.1 (Splicing factor 3B subunit 5/RDS3 complex subunit 10)
Bradi1g71667	Brd1sv1Bd2-31010893m	Myo-inositol-1-phosphate synthase	AT2G22240.1 (MIPS2, myo-inositol-1-phosphate synthase 2)
Bradi1g71673	Brd1sv1Bd2-31010894m	n/a	n/a
Bradi1g71680	Brd1sv1Bd2-31010895m	Bifunctional inhibitor/lipid-transfer protein/seed storage 2S albumin superfamily protein-related	AT5G64080.2 (functional inhibitor/lipid-transfer protein/seed storage 2S albumin superfamily protein)
Bradi1g71690	Brd1sv1Bd2-31010896m	Protein phosphatase 2C	AT4G33500.1 (Protein phosphatase 2C family protein)
Bradi1g71700	Brd1sv1Bd2-31010897m	NADH dehydrogenase ubiquinone 1 alpha subcomplex subunit 13, GRIM-19 protein	AT2G33220.1 (GRIM-19 protein)

Table 5-4 continued Genes annotated in Bd21 v3.1 within the 56 gene BSA candidate interval in association with DON sensitivity from high-confidence Bd2-3 x Bd21 RILs

Gene ID (Bd21 v3.1)	Bd2-3(v1) Gene	Bd annotation (Bd21v3.1)	At orthologue & (Annotation)
Bradi1g71710	Brd1sv1Bd2-31010899m	PROTEIN UPSTREAM OF FLC	AT3G46110.1 (Domain of unknown function (DUF966))
Bradi1g71720	n/a	Serine carboxypeptidase	AT1G28110.1 (SCPL45, serine carboxypeptidase-like 45)
Bradi1g71730	Brd1sv1Bd2-31010900m	PHP domain protein	AT2G13840.1 (Polymerase/histidinol phosphatase-like)
Bradi1g71735	Brd1sv1Bd2-31010901m	F-box domain	AT3G49450.1 (F-box and associated interaction domains-containing protein)
Bradi1g71740	Brd1sv1Bd2-31010902m	EREBP-like factor, AP2 domain	AT4G39780.1 (Integrase-type DNA-binding superfamily protein)
Bradi1g71760	Brd1sv1Bd2-31010903m	Pumilio homolog 11-related	AT1G78160.1 (APUM7,PUM7, pumilio 7)
Bradi1g71770	Brd1sv1Bd2-31010904m	n/a	AT5G21130.1 (Late embryogenesis abundant (LEA) hydroxyproline-rich glycoprotein family)
Bradi1g71781	Brd1sv1Bd2-31010906m	RAS-related protein RABH1C-related	AT2G44610.1 (ATRAB6A,ATRABH1B, Ras-related small GTP-binding family protein)
Bradi1g71790	Brd1sv1Bd2-31041817m	BOMB/KIRA protein, E3 ubiquitin-protein ligase	AT1G78170.1 (E3 ubiquitin-protein ligase)
Bradi1g71800	Brd1sv1Bd2-31010908m	Mitochondrial carrier protein	AT5G64970.1 (Mitochondrial substrate carrier family protein)
Bradi1g71810	Brd1sv1Bd2-31010909m	Calmodulin-binding transcription activator CAMTA	AT5G09410.2 (CAMTA1,EICBP.B, ethylene induced calmodulin binding protein)
Bradi1g71820	Brd1sv1Bd2-31010910m	Uncharacterised transmembrane protein	AT1G34630.1 (n/a)

5.3.7 RNAseq - analysis of Bd2-3 and Bd21 response to DON

Developing roots of Bd2-3 and Bd21 were exposed to 5 μM and 20 μM of DON for six hours, RNA collected, sequenced, and mapped to reference genome Bd21 (v3.1) for analysis. Variance between the sample matrix of accessions and DON concentrations, was visualised using an MDS plot (Figure 5-13); clear separation between accessions was evident along the y-axis. Further proportional separation between concentrations of the DON treatments was also evident across the x-axis (Figure 5-13).

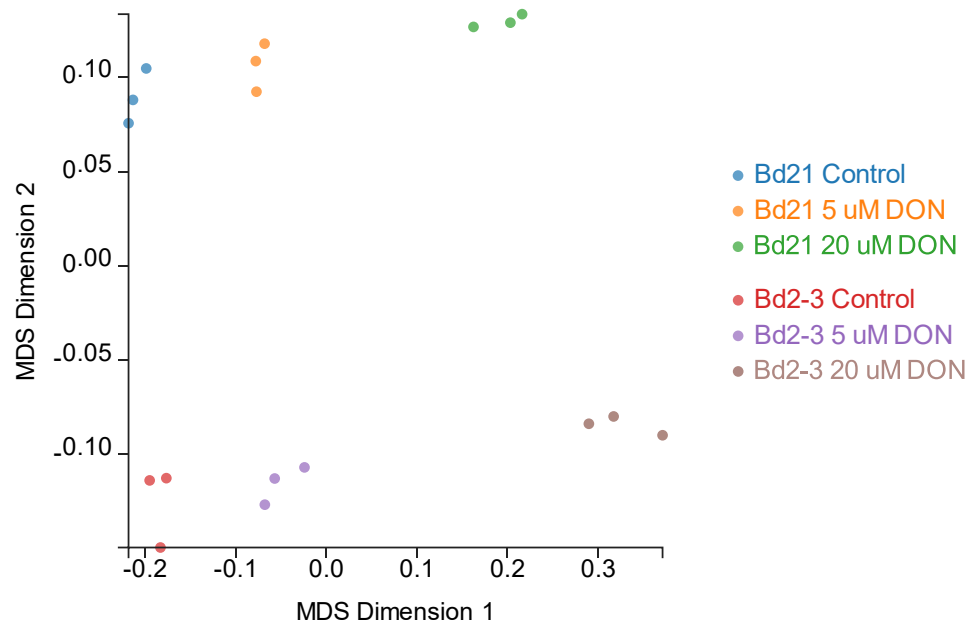


Figure 5-13 Multi-Dimensional Scaling (MDS) plot, describing the variance between DON treated root Bd21 vs Bd2-3 RNAseq samples. Generated using Degust (v4.1.1).

5.3.7.1 Genome wide RNAseq DON response

Degust was used to obtain genome wide lists of high confidence up- and down-regulated genes with a log fold-change greater than 2 in different combinations (between accessions and treatments), numbers of which are presented in Figure 5-14. A greater number of genes were up- or down-regulated at the higher

concentration of DON treatment (Figure 5-14a&b). Conservation of regulation is generally very high; only a single gene at 5 μ M DON, Bradi4g29939, was up-regulated in Bd21 and downregulated in Bd2-3 (Figure 5-14a). Conversely at 20 μ M DON a single gene, Bradi1g57885, was upregulated in Bd2-3 and down-regulated in Bd21 (Figure 5-14b).

A greater number of genes were differentially expressed in response to treatment with DON at 20 μ M than at 5 μ M; this is to be expected from the stronger chemical stimulus. Bd2-3, the more DON-sensitive accession, had a greater number of up- and down-regulated genes than Bd21 in response to DON indicating that Bd2-3 is experiencing greater perturbation at both 'stimulatory' and 'inhibitory' concentrations. Ratios between the two accessions varied at the two DON concentrations; at lower concentration c. 2:1 are down-: up-regulated. The difference is amplified at 20 μ M, to an approximate 5:1 ratio.

There were 85 genes upregulated in both accessions at 5 μ M DON, and 407 upregulated in both accessions at 20 μ M DON; 84 of these genes were upregulated in common between the accession at both concentrations, with 323 exclusively at 20 μ M and one gene exclusively at 5 μ M (Figure 5-14c).

Eight and 225 genes were downregulated in both accessions for 5 μ M and 20 μ M DON treatments respectively; of these genes, only 7 were downregulated at both concentrations, with 217 downregulated exclusively at 20 μ M and one gene exclusively at 5 μ M (Figure 5-14d).

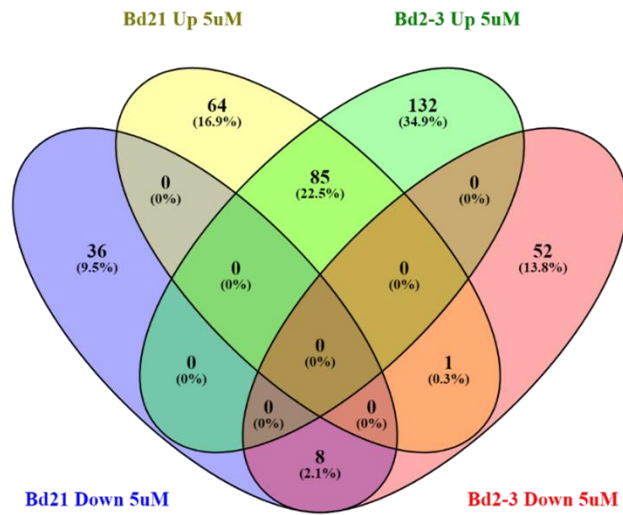
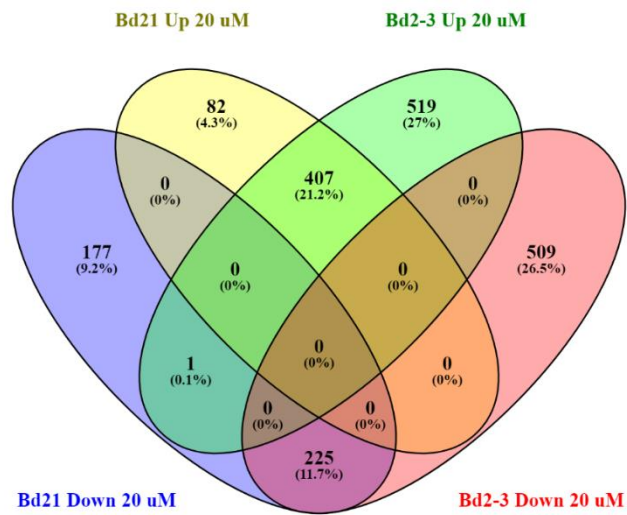
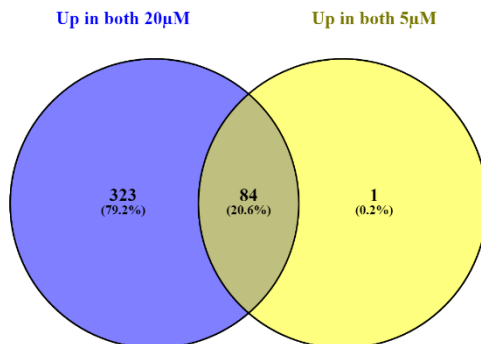
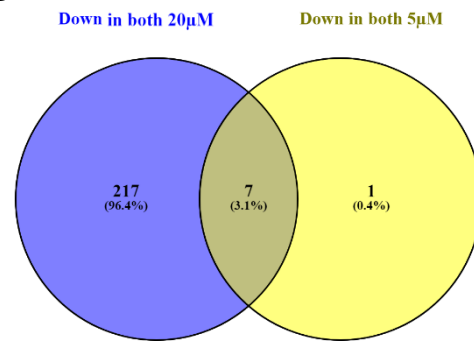
A**B****C****D**

Figure 5-14 Venn diagrams assigning commonality of up- and down- regulation of genes between Bd21 and Bd2-3 in roots, responsive to DON at 5 μM & 20 μM, from RNAseq data.

5.3.7.2 RNAseq DON response for Bd1L 56 gene DON interval

RNAseq gene expression data from the 56 genes in the candidate DON sensitivity interval were analysed; genes in the interval that were either up- or down-regulated in Bd2-3 relative to Bd21, at 5 μ M, 20 μ M, or both, are presented in Figure 5-15, with differential expression detailed in Table 5-5. Three genes, Bradi1g71465, Bradi1g71530 & Bradi1g71624 are upregulated in Bd2-3 relative to Bd21 at 5 μ M and 20 μ M DON, with only Bradi1g71410 downregulated in Bd2-3 at both concentrations. A further six genes were downregulated exclusively at a single concentration; Bradi1g71390, Bradi1g71630, Bradi1g71740 and Bradi1g71760 were exclusively downregulated at 5 μ M DON, with Bradi1g71510 and Bradi1g71710 exclusively downregulated at 20 μ M DON (Table 5-5) Finally, Bradi1g71640 and Bradi1g71790 were exclusively upregulated at 5 μ M DON, with Bradi1g71560 and Bradi1g71673 exclusively upregulated at 20 μ M DON (Table 5-5). Six genes within the 56 gene candidate interval were up- or down-regulated in Bd2-3 relative to Bd21 with >2 Log₂ fold change (Table 5-5).

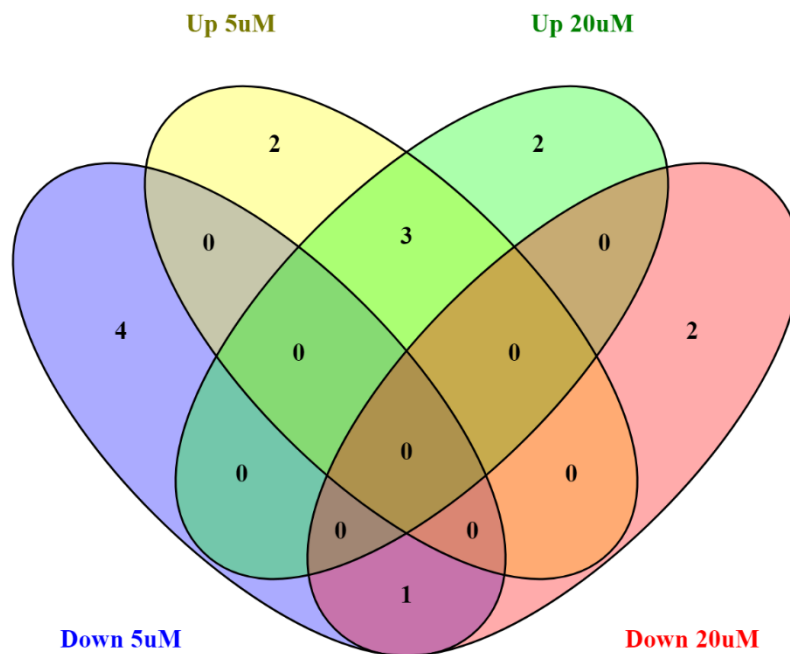


Figure 5-15 Venn diagram containing gene expression in comparison between Bd2-3 relative to Bd21, at 5 μ M and 20 μ M DON RNAseq data.

Table 5-5 RNAseq data for comparison of Bd2-3 relative to Bd21, genes included have a Log2 fold change >1, from within the 56 gene candidate DON interval on Bd1L. FDR = false discovery rate

Treatment(s)	Gene ID	Comparison (Bd21 vs Bd2-3)	RNAseq Fold Change (Log2)	FDR	p-value
Up in Bd2-3 relative to Bd21 at 5 μ M and 20 μ M	Bradi1g71465	5 μ M	1.34	0.028557	0.001881
		20 μ M	1.66	0.010676	0.000676
	Bradi1g71530	5 μ M	5.33	0.000694	1.78E-05
		20 μ M	3.40	0.007711	0.000443
	Bradi1g71624	5 μ M	2.24	0.095239	0.01015
		20 μ M	5.39	0.001286	4.51E-05
Down in Bd2-3 relative to Bd21 at 5 μ M and 20 μ M	Bradi1g71410	5 μ M	-1.44	0.000123	2.37E-06
		20 μ M	-1.42	0.000215	5.03E-06
Up exclusively at 5 μ M	Bradi1g71640	5 μ M	1.95	0.404362	0.111665
	Bradi1g71790	5 μ M	3.20	0.148767	0.020019
Up exclusively at 20 μ M	Bradi1g71560	20 μ M	5.01	0.046201	0.015724
	Bradi1g71673	20 μ M	3.07	0.064484	0.008018
Down exclusively at 5 μ M	Bradi1g71390	5 μ M	-1.07	0.00612	0.000255
	Bradi1g71630	5 μ M	-1.73	0.013495	0.000709
	Bradi1g71740	5 μ M	-1.05	0.534059	0.188127
	Bradi1g71760	5 μ M	-1.18	0.665602	0.296136
Down exclusively at 20 μ M	Bradi1g71510	20 μ M	-1.17	0.094712	0.013819
	Bradi1g71710	20 μ M	-2.96	0.199425	0.041135

5.3.7.3 Fine mapping of DON sensitivity on Bd1L

The closest existing flanking KASP markers to the Bd1L BSA peak were Bd1L_69245412 and Bd1L_70039898 (Bd21v2 locus nomenclature). Additional KASP markers were designed to further delineate the candidate region associated with DON sensitivity in the Bd2-3 x Bd21 population. The high-confidence set of 60 Bd2-3 x Bd21 F7 RILs used for BSA experiment was genotyped using new KASP markers. Figure 5-16 presents these genotypes and corresponding DON sensitivity phenotypes, spanned by markers previously used for single marker analysis on Bd1L (Figure 5-10).

As described in earlier mapping (Chapter 5.3.5), there were RILs where genotype and phenotype did not match as expected assuming association with DON sensitivity; RILs 51, 108, 126, 131, 134 and 158 have Bd21-like phenotype but Bd2-3 genotype and RILs 18, 42, 76 and 93 have B2-3-like phenotype but Bd21 genotype. These 10 RILs make up a high proportion, 17 % of the 60 high-confidence RILs. Therefore, the following further fine-mapping is presented under a cautious caveat considering these apparent aberrant lines.

A recombination event was identified in RIL 128, localised between markers Bd1L_69696725 and Bd1L69743518. RIL 128 is Bd21-like in phenotype so this recombinant could redefine, under caveat, the left border of the DON sensitivity candidate interval to Bd1L_69696725. Bd21-like RILs 41 and 117 also have recombination events supporting the refinement of the left border to at least Bd1L_69674361 (Figure 5-16). An additional recombination event was identified in Bd2-3-like RIL 120, localised between markers Bd1L_69718309 and Bd1L_69743518; this event could redefine the right-border of the DON sensitivity interval to Bd1L_69743518. Therefore, a proposed refined candidate interval for DON sensitivity under the caveat described above, between markers Bd1L_69696725 and Bd1L_69743518 contains six annotated genes in Bd21 v3.1 (Table 5-6). Two genes,

Bradi1g71470 and Bradi1g71475, have an annotated function involved with RNA synthesis, binding, or transport. Bradi1g71465 relates to CASP-like proteins involved in casparian strip development and certain family members in Arabidopsis are expressed at point of lateral root growth (Roppolo et al., 2014). Bradi1g71460 is annotated as an F-box gene, with Arabidopsis orthologue SNEEZY/SLEEPY2, a gene with a role in the regulation of the gibberellic acid pathway (Ariizumi et al., 2011).

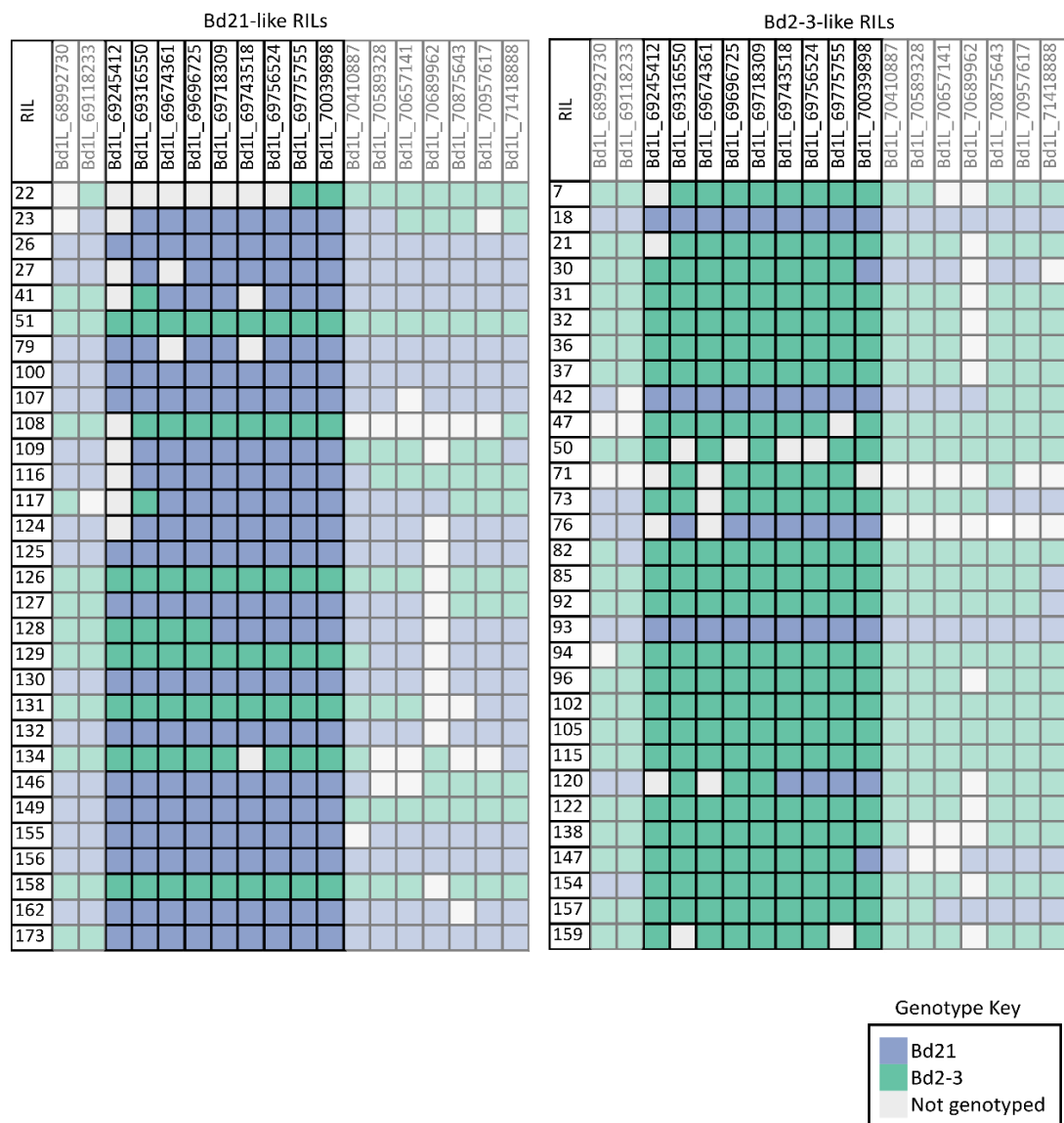


Figure 5-16 Genotypes of Bd2-3xBd21 high-confidence DON sensitivity RILs for fine-mapping of Bd1L BSA peak. Marker names are derived from Bd21v2.1 reference genome differentiating SNP locus. Purple=Bd21 genotype, green=Bd2-3 genotype, grey=not genotyped Faded markers are within the Bd1L single-marker analysis significant region.

Table 5-6 Genes annotated in Bd21 v3.1 in fine-mapped candidate region for DON sensitivity in Bd2-3xBd21 F7 RIL population, defined by fine-mapping markers Bd1L_69696725 and Bd1L_ (Bd21v2 bp nomenclature). At = *Arabidopsis thaliana*

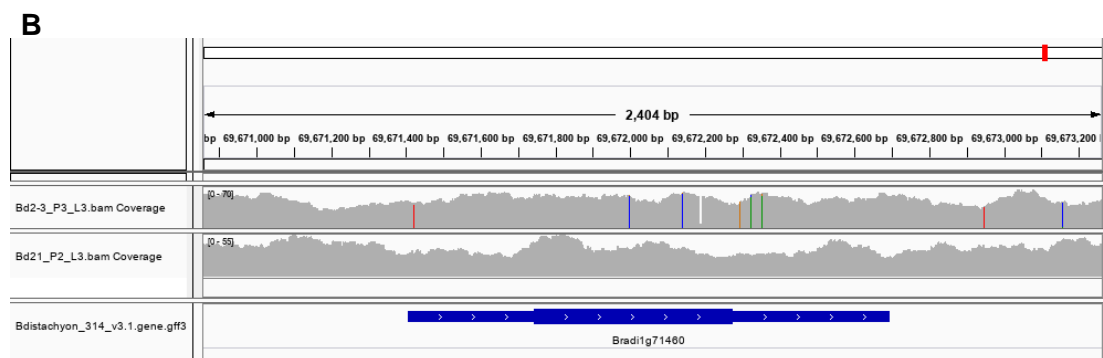
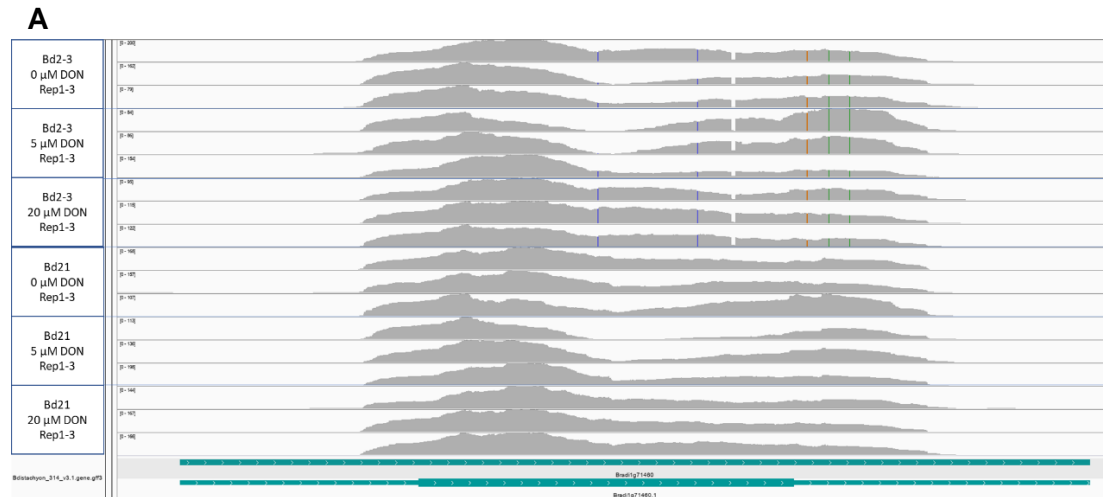
Gene ID (Bd21 v3.1)	Bd2-3 Gene	<i>Bd</i> annotation	<i>At</i> orthologue (type, % identity) & annotation
Bradi1g71450	Brd1sv1Bd2-31010853m	Unknown Protein	AT2G18910.1 (1-1, 13.3%) hydroxyproline-rich glycoprotein family protein
Bradi1g71460	Brd1sv1Bd2-31010855m	F-Box	AT5G48170.1 (1-1, 38.6%) F-box family protein (SNE/SLY2)
Bradi1g71465	Brd1sv1Bd2-31010856m	NITRATE, FROMATE, IRON DEHYDROGENASE	AT4G16442.1 (56.0%) CASP-LIKE PROTEIN 2B1 (UPF0497)
Bradi1g71470	Brd1sv1Bd2-31037589m	Large subunit ribosomal protein L2 (RP-L2, MRPL2, rplB)	ATCG01310.1 (81.8%) ribosomal protein L2
Bradi1g71475	Brd1sv1Bd2-31045608m	Small subunit ribosomal protein S19	ATCG00820.1 (M-1, 80.5%) ribosomal protein S19
Bradi1g71480	Brd1sv1Bd2-31010857m	Unknown Protein	n/a

The equivalent physical region in Bd2-3 contains an additional gene, Brdisv1Bd2-31010854m, that is not annotated in Bd21 v3.1, nor is identifiable through BLAST search, with only short fragment hits to hypothetical proteins. Brdisv1Bd2-31010854m has a coding sequence of 117 bp, with no annotated function. BLASTX resulted in no orthologues being identified in either *T. aestivum* or *H. vulgare* (Ensembl Plants). SNPs, INDELs and complex variants were identified between Bd21 and Bd2-3 from the RNAseq data, listed in Table 5-7.

Table 5-7 Intragenic variants within DON sensitivity candidate interval identified from RNAseq experiment comparing Bd21 and Bd2-3 response to DON at 6 hrs. Locus is bp position Bd21 v3.1 chromosome 1. Variant effect position applied to Bd21 v3.1 annotated protein

Gene	Type	Variant Detail	Locus	Exon	Variant Effect
Bradi1g71450	SNP	G to A	69652320	Exon 1	Synonymous
	SNP	C to T	69671423	5' UTR	Synonymous
	SNP	G to C	69671999	Exon 1	Synonymous
	SNP	G to C	69672140	Exon 1	Synonymous
Bradi1g71460	Deletion	6bp	69672188-69672193	Exon 1	Loss of Gly & Ala at pos. 123
	SNP	C to G	69672295	3' UTR	Synonymous
	SNP	C to A	69672326	3' UTR	Synonymous
	SNP	G to A	69672355	3' UTR	Synonymous
Bradi1g71465	SNP	T to C	69681692	5' UTR	Synonymous
	SNP	C to T	69681661	5' UTR	Synonymous
	SNP	A to G	69677453	3' UTR	Synonymous
Bradi1g71470		n/a			
Bradi1g71475		n/a			
Bradi1g71480	SNP	C to T	69693097	Exon 1	Synonymous
	SNP	A to G	69693237	Exon 1	Leu to Ser, pos. 61 (L61S)
	SNP	A to G	69693563	3' UTR	Synonymous

Visual inspection of RNAseq coverage data, and comparison between treatments in my Bd2-3 and Bd21 material illustrates SNPs and a 6bp-deletion in Bd2-3 relative to Bd21 in Bradi1g71460 (Figure 5-17a). Five out of the six SNPs in Bradi1g71460 are evident in both RNAseq and BSA data sets (Figure 5-17b). Visual analysis of coverage data between the treatments shows some samples decline in coverage in a central portion of the single exon of Bradi1g71460, mainly in response to DON (Figure 5-17b); however, this is variable between replicates within treatment. Alignment of Bradi1g71460 with Brachypan Bd2-3 homologue Brdisv1Bd2-31010855m DNA and protein (Figure 5-17c) sequences suggests that a central portion of the gene is missing in Bd2-3 relative to Bd21. This is not supported by the coverage observed in my RNAseq and BSA experiments (Figure 5-17a&b).



C

<i>B.distachyon</i> Bd 2-3/1-138	1	M G S R Q D R G K G G D E A E A V A P E P E E K R V Q L A G A A Y N I N D N	38
<i>B.distachyon</i> /1-177	1	M G S R Q D R E K G G D E A E A V A P E P E E K R V Q L A G A A Y N I N D N A D I L S	43
<i>B.distachyon</i> Bd 2-3/1-138	39 A L C L R H V G P T A	49
<i>B.distachyon</i> /1-177	44	E I L S R L D G R S L A A A A G V C R L W A A V S R R D A V W E A L C L R H V G P T A	86
<i>B.distachyon</i> Bd 2-3/1-138	50	R S G L G A T R A V V G A L G G Y R R L Y R L C L G P A P D R L G L A A P A P A P P R	92
<i>B.distachyon</i> /1-177	87	R S G L G A T R A V V G A L G G Y R R L Y R L C L G P A L D R L G L A A H A Q A R A R	129
<i>B.distachyon</i> Bd 2-3/1-138	93	L S L S L S L S L F S I D C Y E R L G G A G A - - G A G R P P P P P S S L L F L C K P	133
<i>B.distachyon</i> /1-177	130	L S L S L S L S L F S I D C Y E R L G G A G A G A G A G R P P P P P S S L L F L C K P	172
<i>B.distachyon</i> Bd 2-3/1-138	134	V D V S *	138
<i>B.distachyon</i> /1-177	173	V D V S *	177

Figure 5-17 Variation in Bradi1g71460 between Bd2-3 and Bd21 (A and C), and Bd2-3-like and Bd21-like RIL pools. A, RNAseq coverage (SNPs indicated by colours), B, BSA coverage aligned to Bradi1g71460 reference, C, peptide alignment, sequences obtained from gene annotations from Bd21v2.1 (lower track) and Bd2-3v1 (upper track) (Phytozome).

5.4 Discussion

5.4.1 Why map a DON induced root branching phenotype in a model grass species?

Whilst the primary toxicity of DON has long been explained by its role as a protein synthesis inhibitor (McLaughlin et al., 1977), the mechanism by which it functions as a virulence factor in the infection of wheat with DON producing *Fusarium* species, is unclear. The clear manifestation of difference in sensitivity response to DON between two parents of an existing Bd mapping population provided a new opportunity to investigate possible mechanistic functions of DON in the plant host.

5.4.2 There is natural variation in DON responsive root development in Bd

Contrary to the elongatory response I observed in Bd, Masuda et al. (2007) described inhibition of *Arabidopsis* and wheat roots when grown on the surface of media containing DON. Packa (1991) also reported reduction of mitotic index as a result of DON application to roots in wheat, amongst other plant species, concurrent with such inhibition. Additionally, work by Steed and Nicholson (Unpublished) identified root waving phenotype in *Arabidopsis* seedlings grown on the surface of DON-containing media. *Arabidopsis* root waving does not occur in *aux1* mutants with mutated auxin transporter function; this ties in with the Bd alteration in gravitropism. Bd does exhibit root growth inhibition, like *Arabidopsis*. *Arabidopsis* and *Brachypodium* auxin networks are fundamentally different, so if the DON response was auxin related this might explain why the phenotypes differ so much between the species (Pacheco-Villalobos et al., 2016; Pacheco-Villalobos et al., 2013). Peraldi (2012) identified concentration dependent root length in response to DON; it is possible that previous studies have focussed exclusively on characterisation of high-toxicity, high-concentration DON. Therefore, by using low DON concentrations I may be able to

identify the most sensitive elements in response to give insight into potential mechanisms. It is also possible that Bd is less sensitive to DON, and therefore the lower toxicity, elongatory response is more likely to occur. This possibility is supported by an experiment by Santos et al. (Unpublished) in which equivalent DON assays to mine were conducted on wheat, which was found to be much more sensitive to DON, with root inhibition occurring at lower concentrations in wheat.

DON induces a concentration dependent effect on Bd roots, causing elongation and enhanced gravitropism at low concentrations and root growth inhibition at high concentrations. Elongation of primary roots, observed in all accessions tested with exception of Bd2-3 and Koz-3, is thought to be a less sensitive manifestation in response to DON. Microscopic comparison of cells would be required to determine whether this is the result of an increase in cell division ergo cell number, or an increase in cell length, or a combination of factors. Relative to elongation, inhibition of the primary root and the induction of lateral root formation, observed in Bd2-3 and Koz-3 only, is thought to reflect greater sensitivity to DON. The accessions in the middle of the distribution showing very limited alteration in root growth may be either less sensitive to DON as they are not stimulated to elongate, or they may be more sensitive to DON with root growth beginning to be inhibited. All accessions would have to be tested with a range of DON concentrations in order to differentiate between these possibilities. Overall, the quantitative distribution suggests multiple factors influencing the trait. It is assumed that loss, or modification, of function in Bd2-3 is responsible for the altered phenotype compared to almost all other accessions.

5.4.3 Bd2-3 and Bd21 vary in response to DON in a non-tissue-specific way

The inhibition of primary root growth, and bifurcating formation of lateral roots seen in Bd2-3 and Koz-3 Bd accessions is a novel phenotype. A transition from proliferating to differentiating cells is required for the development of lateral root primordia

(Fernández-Marcos et al., 2017); division of primordia cells is dependent on strict auxin controls (Marhavý et al., 2016). It is unclear why, but highly interesting, that these accessions undergo complete inhibition of the root apical meristem, or primary root, at a conserved point, approximately one centimetre in root length in Bd2-3 and all Bd2-3-like accessions, across all experiments and DON treatments. Across multiple experiments, I observed development of green colouration in some individuals exclusively in Bd2-3-like, branching roots. The high light environment that the roots were maintained in is likely a key factor, but still curious that the roots of Bd21 like plants do not appear green. Auxin and cytokinin have been shown to regulate chlorophyll biosynthesis and chloroplast biogenesis in *Arabidopsis* roots (Kobayashi et al., 2012); perhaps this suggests that the difference between Bd2-3 and Bd21 might be auxin, or cytokinin, related. Koz-3, the only other accession to show the branching phenotype, could provide a useful opportunity to cross-compare variation in candidate genes in future work.

5.4.3.1 Bd2-3 branching response is specific to DON

Anisomycin and cycloheximide were included within the experiment to determine whether the branching phenotype is attributed to DON's well characterised molecular function as a protein-synthesis inhibitor; although there was some initiation of lateral roots, the phenotype of these treatments does not mimic that of DON and therefore it is concluded that a secondary function of DON may be in play.

Based on similarities in the concentration dependent inhibitory-elongatory relationship, hyper-gravitropic and reduced root hair DON induced phenotypes to those described in response to auxin (Overvoorde et al., 2010), the effect of auxin pathway disruption was investigated; an auxin-transport inhibitor, TIBA, was tested for effects on Bd root development. The phenotype of TIBA exposed roots are not equivalent to those of DON; it could be argued that combining the protein-synthesis

inhibitory and auxin-transport inhibitory phenotypes best mimics the DON-responsive root development. This could therefore be suggestive that DON is acting in both cellular roles.

Bd2-3 was found to be more sensitive than Bd21 to DON when applied to floral tissues. Symptoms of DON in floral tissues of wheat and barley are classically described as premature bleaching of spikelets above the point of infection with *Fusarium* (Parry et al., 1995, Lemmens et al., 2005). However, in my Bd DON head experiments, symptoms exclusively consisted of browning that spread from the point of application. The water-control treated Bd heads did not develop browning. This browning symptom could be due to cell death, or the accumulation of phenolic compounds; the latter have been associated with FHB resistance in wheat (Boutigny et al., 2008). Either way, the symptoms spread further over time in Bd2-3 than Bd21 indicating that as in roots, Bd2-3 is more sensitive to DON in floral tissues than Bd21. Concluding that the sensitivity is non-tissue-specific makes the findings of this chapter more likely to be relevant to FHB.

5.4.4 Characterisation of Bd2-3xBd21 population to DON sensitivity

The Bd2-3 x Bd21 population, obtained from David Garvin (USDA, St. Paul Minnesota), was characterised for DON sensitivity at two concentrations, initially at 10 μ M and later at 20 μ M. The F7 Bd2-3 x Bd21 progeny segregated largely in a 50:50 ratio for the parental DON phenotype; this would suggest that a single gene controls the branching trait in this population. However, there are intermediate phenotypes, which develop the branching production of lateral roots at the point typical of Bd2-3, but the root meristem persists in growth to become elongated like Bd21. This intermediate phenotype was not observed during the characterisation of natural accessions. This contradicts the likelihood of a single gene controlling the trait, instead suggesting that other factors are acting in addition to modify the phenotype.

For the purposes of analysis and mapping, RILs developing intermediate roots were considered to have a DON sensitivity between those of the robust classes of Bd21-like and Bd2-3-like RILs.

There were extensive differences in phenotypes between the two concentrations used to characterise the Bd2-3 x Bd21 population. Many RILs (42.2 %) had the same phenotype when grown at 10- and 20- μM DON, with a further 41.5 % of RILs displaying a higher-sensitivity phenotype at 20 μM DON than 10 μM . These lines are thought to be escapes at the lower concentration, not showing a true reflection of their DON sensitivity phenotype. This data supports a hypothesis that a threshold of DON sensitivity is required to induce the branching phenotype. Under this hypothesis, it would be expected that all lines would branch eventually on an increasing DON concentration treatment scale, once a DON sensitivity threshold has been reached before overall toxicity results in non-viability of root growth. It should be possible to test this experimentally but was not yet completed on a population wide level due to time constraints.

Most lines that differed between 10 and 20 μM went from intermediate to Bd2-3-like. However, 23 lines (8.38 %) appear less sensitive at the high DON concentrations, which is not concurrent with this hypothesis. It is unlikely that this switch in phenotype is due to the effects of additional modifier genes or loci, more likely that the identity of some RILs is incorrect. Could these be a result of under-exposure to DON due to variations in the tubes? This is a downside of growing the roots in individual tubes, as there is no way to account for tube-tube variation and exclude this possibility.

5.4.5 Identification of loci associated with DON sensitivity using mapping (KASPs)

Initial mapping, using the two datasets obtained by characterisation of the population at 10- and 20- μM DON, identified two large scale genomic loci associated with DON sensitivity, Bd1L and Bd4S; only the former was identified at both DON concentrations. The phenotype-genotype relationship was closest in association for the Bd2-3-like phenotype RILs.

Bd has an extremely high rate of recombination. This means that it is not unlikely that statistical association of a locus with any trait is lost through single marker analysis with such sparsely spread markers. It is possible therefore that there are other loci significantly associated with the trait that were missed by this approach if high recombination rate results in reduction of linkage disequilibrium, and would require a map of much greater density. As it was originally anticipated that a single major gene was responsible for the Bd21 versus Bd2-3 differential DON response, the skeleton map for the entire genome was not advanced. Even with the sparse map generated, a second locus was identified on Bd4 at 20 μM DON; this locus could account for variation in the genotype-phenotype association.

Additional markers were iteratively designed on Bd1L, and the relationship with DON sensitivity phenotype examined by association statistics and examination of recombination events. Markers between, and including, Bd1L68992730 and Bd1L71418888 were significantly associated with sensitivity to 10 μM DON, a region of 2.43 Mb. A smaller region of 1.42 Mb within this, between markers Bd1L69245412 and Bd1L70657141 was also significantly associated with sensitivity to 20 μM DON. There were no markers that allowed a clear separation of lines into Bd21 and Bd2-3 phenotype classes based on their genotype. For this reason, a genome wide approach was undertaken through BSA to identify potential additional loci.

5.4.6 Bulk segregant analysis for extreme DON sensitivity RILs of Bd2-3 x Bd21 population identifies 56-gene candidate region

Bulk segregant analysis by next generation sequencing is a powerful tool for the rapid identification of genome wide analysis to identify variation associated with a specific phenotype (Michelmore et al., 1991, Trick et al., 2012). The higher density of data obtained by BSA makes it much less likely that positive trait-variant associations would be missed due to breakdown of linkage disequilibrium (especially an issue in Bd due to high recombination frequency), compared with a marker-based map. A wide range of variants, from SNPs to insertions and deletions can be identified by this approach. Gilbert et al. (2018) used BSA for the rapid localisation of *Yrr1* in Bd using the Bd2-3xBd21 population that I have characterised in this chapter. Bd21 and Bd2-3 are very closely related, limiting the number of non-causative variants to complicate analysis and published reference genomic sequences were available for both parents, although of varying quality and completeness. Only RILs with equivalent phenotypes when tested at both 10 μ M and 20 μ M were included in pools for BSA analysis.

For my BSA analysis, statistical significance threshold for peaks could not be obtained due to the excessive computing time and power required for bootstrap analysis or permutation test (Watanabe et al., 2017). Peaks were therefore arbitrarily defined, based on a BFR at which a peak appeared clearly distinct from background noise.

The largest peak identified in association with DON sensitivity in the panel of 60 high-confidence RILs was located on the long arm of Bd chromosome one. There are 56 genes within this peak defined by flanking genes with a BFR >7. For the high-confidence RILs, within the 56 gene candidate interval there remained a number of lines with an aberrant genotype-phenotype relationship; several lines appear to have the 'wrong' genotype for their phenotype class. Careful reanalysis of the individual RILs revealed that a number of the lines had been incorrectly grouped. Given that

such a clear, well defined locus of association on Bd1 was still observed under the presence of mis-associated lines makes it even more convincing that it is significant and genuine.

Additional peaks are present on Bd2S and Bd chromosome four. Several KASP markers were designed within, and flanking, the Bd2S BSA peak and genotyping data used to see if the Bd2S status explained any of the apparently aberrant variation in the Bd1L phenotype by genotype relationship (data not shown), which it did not. The peaks on chromosome four were not investigated, mainly due to the relatively low BFR, presence of multiple less well-defined peaks with few variants breaching a BFR >7. The secondary peaks were close to regions that original single-marker association markers were located. If these were of major impact on the trait, we might expect some effect on the significance of association; this was the case at 20 μ M but not at 10 μ M. This may be evidence enough to warrant future investigation into the peaks on chromosome four.

5.4.7 Genes of most interest in the Bd1L candidate interval

Inhibition of protein synthesis is suggested to be the primary toxicity mechanism of trichothecenes in eukaryotes (McLaughlin et al., 1977). DON specifically, as a Type II trichothecene, inhibits the elongation-termination step of protein synthesis, by non-competitive inhibition of the active site of peptidyl transferase on ribosomes (Rocha et al., 2005). Eleven genes within the 56 gene interval have a functional annotation (Phytozome v.13) related to RNA; Bradi1g71924, Bradi1g71630, Bradi1g71760 and Bradi1g71495 are RNA binding proteins, whilst Bradi1g71425, Bradi1g71470, Bradi1g71475 and Bradi1g71650 encode components of ribosomal subunits, 37S, L2, S19 and S17 respectively (Table 5-5). Bradi1g71377 is annotated to have an RNA recognition motif, Bradi1g71517 is a pre-mRNA processing protein TSR3, and finally Bradi1g71660 encoding RNA splicing factor 3B subunit 5 (Table 5-4). Two of these

RNA processing-related genes, Bradi1g71470 and Bradi1g71475 are present after the proposed fine-mapping refinement of the candidate interval, but neither were found to differ in expression in response to DON for any treatment comparisons, and no variants were identified between Bd2-3 and Bd21 in the RNAseq data. Bradi1g71475 BLASTs to a region away from the other genes in the interval (Table 5-6); however, Bd2-3 has a lower quality genome assembled to pseudomolecule scale only, so it cannot be determined whether these genes are physically separated from the others in Bd2-3, compared to Bd21 without experimental assessment.

Five genes in the Bd1L BSA interval have annotated functions (Phytozome v.13) associated with plant hormones (Table 5-4). Bradi1g71740 is an ethylene responsive element binding protein (EREBP)-like factor with AP2 domain that in cotton play roles in stress response (Liu and Zhang, 2017). Bradi1g7140 was marginally downregulated only in response to 5 μ M DON, with a log₂ fold change of -1.05 (in Bd2-3 relative to Bd21).

Three cytochrome B561 genes Bradi1g71540, Bradi1g71560 and Bradi1g71480 are described to be auxin responsive in *Arabidopsis* orthologues (Preger et al., 2009). Auxin, known to play a role in plant growth almost universally, has particularly been implicated in a bimodal effect on primary root length, dose-dependent effect on lateral root primordia and gravitropic responses in *Arabidopsis* (Overvoorde et al., 2010, Marhavý et al., 2016); all of these phenotypes are affected by treatment with DON. It could therefore be plausible that DON responsive Bd root phenotypes may be a reflection of DON interacting with or manipulating auxin pathways. Brauer et al. (2019) characterised an association between auxin and susceptibility to FHB (*F. graminearum*) in wheat; furthermore, *TaTIR1*, that mediates Aux/IAA degradation and auxin-regulated transcription, has also been implicated in susceptibility to FHB (Su et al., 2021). A study by Pacheco-Villalobos et al. (2013) revealed that auxin cross-talk in Bd varies fundamentally from *Arabidopsis*, in which most auxin pathways have

been elucidated; moreover, loss of function in *TAA1-RELATED2-LIKE (BdTar)* genes result in root elongation and reduced root hair length, profoundly similar to the Bd21-like DON phenotypes I observed. BdTar proteins function in the seminal root elongation zone of cell differentiation and elongation, with mutants showing elevated levels of IAA leading to dramatic elongation of cells (Pacheco-Villalobos et al., 2016). Taken together with the previously observed *Arabidopsis* root waving, these independent pieces of evidence suggest a likely secondary role of DON as interacting with auxin pathways. Haidoulis and Nicholson (2020) described increased resistance to FHB as a result of application of exogenous auxin. *F. graminearum* has been shown to produce indole-3-acetic acid (IAA), which accumulates during early stages of infection in wheat (Luo et al., 2016). Neither Bradi1g71480 nor Bradi1g71540, however, were detected to have DON responsive expression in my RNAseq experiment. Bradi1g71480 contains three SNPs relative to Bd21, two silent whilst the final SNP exonic results in an amino acid change from leucine to serine at position 61. With no annotated domains, the effect of this substitution on protein function is unclear. Bradi1g71480 did not show any alteration in expression in the DON RNAseq experiment.

Bradi1g71460 is an F-box gene with the *Arabidopsis* orthologue SNEEZY/SLY2, described as a positive regulator of gibberellic acid (GA) signalling (Ariizumi and Steber, 2011, Strader et al., 2004). SNE/SLY2 does this by ubiquitination and subsequent degradation of DELLA proteins, which are negative regulators of GA signalling; SNE/ SLY2 interacts with CUL1, forming an essential part of the SCF (Skp1, Cullin, F-box) complex (Fu et al., 2004). Unlike SLY1, SNE/ SLY2 cannot interact directly with DELLA protein RGL2 (Ariizumi et al., 2011). Baluška et al. (1993) presented evidence for GAs affecting root growth and final cell size in maize, by directly controlling the arrangement of cortical microtubules. Furthermore, a family of *Gibberellic Acid Stimulated Transcript-like (GAST-like)* proteins have been described

in rice and maize with a suggested role in early lateral root formation, regulated by GA (Zimmermann et al., 2010). Both of these pieces of evidence suggest a plausible connection of Bradi1g71460 resulting in the DON-induced root phenotypes in Bd, potentially accounting for both the elongatory response common amongst Bd accessions and the branching response of Bd2-3.

The pattern of RNAseq coverage of Bradi1g71460 between treatments was interesting (Figure 5-17). For some samples treated with 5 μ M DON, no coverage was present in the central portion of the only exon, whereas for all samples at 0 μ M and 20 μ M DON the coverage did not reduce. Additionally, several SNPs and a 6 bp deletion were evident from both the RNAseq and BSA sequencing data; the deletion resulted in the loss of a G and A residue from the peptide sequence in Bd2-3 (visible in Figure 5-17c). No evidence was found for presence/absence variation of transcript expression in the RNAseq data. Alignment of Bd21 and Bd2-3 reference genomic and peptide sequences show a large deletion in the intron of Bd2-3 relative to Bd21 in Bradi1g71460. Targeted re-sequencing of Bradi1g71460 in our Bd2-3 and Bd21 material is required to confirm the deletion, especially as coverage from my RNAseq and BSA would suggest that it is not genuine. Additionally, there is a discrepancy in annotation between reference versions of Bd21, with version 2 reporting a c. 800 bp gene, and v3.1 reporting a c. 1200 bp gene.

Rht semi-dwarfing genes in wheat are homologous with *Arabidopsis GAI* (GA insensitive) and these are DELLA proteins that function as repressors of GA signalling (Hedden, 2003). *Rht* gain of function semi-dwarfing genes have been shown to be associated with both decreased Type I resistance to FHB and increased Type II resistance (*Rht-B1b* only) in wheat (Srinivasachary et al., 2009). Saville et al. (2012) further investigated the role of DELLA in pathogen interactions in barley and wheat and showed with gain-of-function mutants an increase in Type II resistance to FHB. This GA-FHB connection supports the hypothesis of a role for DON in GA signalling

manipulation during *Fusarium* infection, and hence Bradi1g71460 as a promising candidate gene.

Bradi1g71465, whose *Arabidopsis* orthologue At2G35760.1 is CASP-LIKE PROTEIN 2B1, described in regulation of casparian strip development and therefore plausibly involved in influencing root development and architecture (Roppolo et al., 2014). The casparian strip is essential for stress resistance and homeostasis. In *Gossypium arboreum* and *Arabidopsis*, loss of function mutants of the *GaCASP27* gene resulted in significant increase in lateral root number (Wang et al., 2020). This gene is retained in the proposed six gene candidate interval. Bradi1g71465 was also marginally upregulated in Bd2-3 relative to Bd21 at both 5 μ M and 20 μ M treated roots, with Log2 fold changes of 1.34 and 1.66 respectively (Table 5-6). Three variants in Bd2-3 detected by RNAseq were silent, with no effect on the peptide sequence. Differential DON sensitivity was also observed in floral tissues; no evidence of differential regulation of Bradi1g71465 in data from Pasquet et al. (2014), in which Bd heads were infected with a deoxynivalenol producing strain of *Fusarium graminearum*. Therefore, based on current evidence, Bradi1g71465 does not fit the DON sensitivity phenotype profile.

A final gene of note in the Bd1L BSA interval is Bradi1g71530, the *Arabidopsis* orthologue of which, an *ALD1* (*AGD2-LIKE DEFENCE RESPONSE PROTEIN*) has been described in *Lotus japonicus* to influence plant development and nodulation and a role in plant-pathogen interactions all by regulating the salicylic acid pathway (Chen et al., 2014). Haidoulis and Nicholson (2020) described increased susceptibility to initial infection of Bd roots with *F. graminearum* in response to exogenous application of salicylic acid. Song et al. (2004) described an antagonistic role of *ALD1* and *Arabidopsis thaliana aberrant growth and death2* (*AGD2*), in which mutation of *ALD1* leads to increased susceptibility to bacterial pathogen infection, concluding that *ALD1* is important in the activation of defence signalling in *Arabidopsis*. Bradi1g71530 was

the most upregulated gene in Bd2-3 compared with Bd21, with Log2 fold changes of 5.33 at 5 μ M and 3.40 at 20 μ M (Table 5-6).

5.4.8 RNAseq for comparison of DON responsive genes in Bd21 and Bd2-3

An RNAseq experiment was undertaken to identify DON responsive genes in Bd21 and Bd2-3, with a particular focus on the Bd1L region. The RNAseq data is compatible with the proposal that the Bd2-3 phenotype is a result of increased sensitivity than Bd21, as a greater proportion of genes were either up- or down-regulated in Bd2-3 compared with Bd21, in both 5 μ M and 20 μ M treatments. For future work, the RNAseq data provides the perfect material for the assessment of sequence variation between Bd2-3 and Bd21, without the uncertainty resulting from the relatively poor-quality sequence of the current published Bd2-3 reference genomic data.

There are six genes within the 56 gene candidate interval with a Log2 fold change >2: Bradi1g71530, Bradi1g71560, Bradi1g71624, Bradi1g71673, Bradi1g71710 and Bradi1g71790. For three of these, Bradi1g71673, Bradi1g71710 and Bradi1g71790, the coverage was very low (< 10 transcripts per position). Of the remainder, Bradi1g71530 is annotated to be an LL-diaminopimelate aminotransferase, an orthologue of *AtALD1* discussed above in connection with defence response, and contains three exonic SNPs. Bradi1g71560 is annotated as a cytochrome b561 described above to have auxin responsive orthologues, contains five SNPs within exons and finally Bradi1g71624 is a pumilio gene, previously discussed, that contains two SNPs in the coding sequence in Bd2-3 relative to Bd21. My expression analysis was done in root tissue only; none of these genes, or the CASP related gene Bradi1g71465 and the F-box gene Bradi1g71460, were found to be differentially regulated in an RNAseq study of *F. graminearum* infection in Bd heads by Pasquet et al. (2014).

5.4.9 Fine mapping of Bd1L candidate interval

The following work is discussed with extreme caution based on the high proportion, even of high-confidence RILs (17 %), for which phenotype and genotype are not in agreement for the markers within the candidate interval. Additional genotype data from new markers within the 56 gene interval identified several recombination events in the region in Bd2-3 x Bd21 RILs. If used exclusively to define the candidate region, it could be refined to contain six candidate genes. Two of these genes are of unknown function (Bradi1g71450 and Bradi1g71480) and two encode ribosomal subunits (Bradi1g71470, L2, and Bradi1g71475, S19) discussed previously. The final two genes, Bradi1g71460, an F-box gene related to GA regulation, and Bradi1g71465, a CASPL protein, both offer credible candidates for causation of the DON induced root development phenotypes. The only gene within the 6 gene interval found to be DON responsive, Bradi1g71465, was up-regulated in Bd2-3 compared to Bd21 at both 5- and 20- μ M DON. From RNAseq data, only Bradi1g71460 and Bradi1g71480 contains variants that affect peptide sequence in Bd2-3 relative to Bd21. Bd2-3 contains an additional annotated gene, with no known function or orthologues; however, it is expected that the Bd2-3 phenotype is due to the loss of-, not gain of-function compared to Bd21. I must reiterate and highlight caution due to the lines that have an 'incorrect' genotype across all markers within the interval. Future work to confirm the genotype and phenotype of these aberrant RILs should be able to either dismiss, or add confidence to, the refinement of the candidate interval by fine mapping.

5.4.10 Concluding Remarks

In this chapter, natural variation of DON sensitivity in Bd, reflected in differential elongatory and inhibitory root development, was identified. The Bd2-3 x Bd21 population was utilised to map the genetic basis of the extreme branching and inhibition of primary root seen in Bd2-3. A region on Bd1L was identified using two

independent methods, KASP based mapping and BSA to result in a 56 gene candidate region for DON sensitivity in Bd21. Several genes that offer plausible mechanisms for interaction with DON, across a wide range of functional classification, are included in the 56 gene candidate interval, including Bradi1g71530 (ALD1 orthologue) and Bradi1g71624, an RNA binding protein pumilio-related gene. Cautious fine mapping with a caveat on quality of phenotype or genotype data identified a potential refinement of the candidate region to six genes, of which only Bradi1g71465 was differentially expressed between Bd2-3 and Bd21 in response to DON. These candidates merit further investigation.

Chapter 6 - General Discussion

FHB in cereal crops presents a global challenge as an economically damaging disease caused predominantly by hemibiotrophic *Fusarium* species. Mycotoxins, particularly trichothecenes such as DON, are responsible for increased virulence in wheat and directly causing loss of quality and quantity of grain upon infection. Even given extensive protocols for the management of DON within food and feed processing and manufacturing industries, contamination remains a global threat to human health (Mishra et al., 2020). Control methods aimed at reducing the impact of FHB, including application of triazole fungicides and cultural practices including crop rotation are only moderately effective at controlling the disease and limiting crop losses. The improvement of genetic resistance in commercial wheat varieties is considered the most sustainable method by which to reduce the impact of FHB (Marburger et al., 2015).

Wheat based research concerning the genetic improvement of resistance to FHB is extremely complex. The use of model a pathosystem can alleviate some of these complexities as first demonstrated in Bd by Peraldi et al. (2011). Early in the PhD project, Brachypan was published and the genomes of 52 accessions made available providing a fantastic resource for exploring intra-species genetic variation in Bd. This material was the foundation of the thesis, with characterisation of natural variation being the starting points for both avenues of research explored, variation in FHB susceptibility and DON sensitivity. Bd diversity being a previously untapped resource in terms of FHB, the overarching aim focussed on identifying factors associated with FHB susceptibility in Bd, exploiting Bd's simple genetics and expansive genetic resources, looking towards translation into cereal crops to be of agronomic benefit.

Quantitative variation in susceptibility to FHB was identified across the 52 accessions characterised in Chapter 2. The wide diversity in Bd, reflected in extreme variation in flowering time amongst other traits, rendered flowering-time dependent pathology challenging. Therefore, the direction of work was dictated by FHB susceptibility data obtained under controlled conditions for a much smaller subset of accessions selected as parents of mapping populations. Two populations, ABR6 x Bd21 and Foz-1 x Luc-1, were identified with parents varying in FHB susceptibility. The aim of this thesis was to identify the genetic architecture underlying such variation in susceptibility or resistance to FHB in Bd that was initially described in Chapter 2.

6.1 Extensive FHB resistance variability in Bd

Extensive variation in FHB resistance was observed across Bd accessions, mainly quantitative but with a single accession, Jer-1 showing a typical hypersensitive response phenotype with highly restricted browning lesions that did not spread over time (Morel and Dangl, 1997). No such extreme, qualitative, hypersensitive response has been characterised in association with FHB, and therefore this warrants further investigation in the future. This would require the development of a population, by crossing with a susceptible accessions such as Bd21, because such a rare phenotype will not be detected using association genetics approaches such as GWAS (Li et al., 2013).

Whilst it is hard to compare this observed wide variation in Bd with that of domesticated wheat, where population structure is vastly different as a result of breeding practises, it is clear that most major, stable sources of resistance in wheat are limited in provenance to landraces, particularly Asian spring wheat including 'Sumai-3', 'Wangshuibai' and 'Nyu Bai' (Buerstmayr et al., 2020). With this relatively narrow pool of resistance, there is plausible benefit to exploring external variation

existing in related species and translating back into elite wheat varieties via induced mutagenesis platforms such as TILLING, or targeted CRISPR generated mutations where regulations allow. Although there are as of yet no examples of direct translation from Bd to wheat or barley, Goddard et al. (2014) described conservation of the effect of mutation of the gene *brassinosteroid insensitive-1 (BRI1)* on disease response between wheat and Bd.

6.2 No association of height with FHB

The effects of *Rht* genes in wheat are widely reported with *Rht-B1b* and *Rht-D1b* alleles, conferring insensitivity to GA, associated with increased susceptibility to FHB (Srinivasachary et al., 2008b, He et al., 2016). Little evidence for FHB-height relationship in Bd was observed; an association between height of Bd accessions and FHB susceptibility was the results of confounding flowering-time relationship, and no major height QTL were found to associate with the QTL for FHB on chromosome four. A similar finding was recently reported in wheat, in which none of the major height QTL were identified associated with FHB QTL in two wheat populations (Goddard et al., 2021). The reasons behind this lack of associations, observed in Bd and some wheat varieties is unclear, however Goddard et al. (2021) highlighted that the large increase in FHB susceptibility attributed to *Rht-D1b* in wheat is not directly the result of differential plant height, instead being caused by linkage with deleterious genes (Buerstmayr and Buerstmayr, 2016, Srinivasachary et al., 2008b). Additionally, wheat lines carrying *Rht-B1b* and *Rht-D1b* have shorter anther filaments, whilst such resultant incomplete extrusion of anthers is associated with increased susceptibility to FHB (Buerstmayr and Buerstmayr, 2016). As the floral architecture of Bd is more closed, anthers are typically not extruded at all, therefore this additional factor of *Rht* contributing to FHB susceptibility observed in wheat would not be expected to have an effect in Bd.

6.3 Major FHB effect identified on Bd4

In wheat, resistance is generally polygenic and the result of minor individual contributing effects. I identified a single major FHB effect on Bd chromosome four. Buerstmayr et al. (2020) reviewed wheat FHB QTL studies to date, reporting almost 500 unique QTL, of which 20 % were described as major QTL by publishing authors. Major QTL in wheat located on 3BS and 6BL, have been Mendelised to Fhb1 and Fhb2 respectively, both derived from Sumai-3 (Cuthbert et al., 2007, Cuthbert et al., 2006). Fhb2, Fhb4 and Fhb5 QTL have been refined to 2.2, 0.14 and 0.09 cM intervals respectively, with Wangshuibai the source of resistance (Jia et al., 2018). The major QTL here identified on Bd4 is therefore extremely rare compared to the situation in wheat.

6.4 Association of FHB with lemma trichomes

Chapter 3 described the identification of coincident QTL on the long arm of Bd chromosome four, associated with both a major effect FHB susceptibility and lemma trichome presence/ absence, and highly suggestive of a causal relationship. This observed genetic association adds significance to previous reports of physical interaction of infecting *Fusarium* hyphae with trichome projections and basal cells across a range of monocot species, including Bd, barley and wheat (Peraldi et al., 2011, Imboden et al., 2018, Jansen et al., 2005, Liu and Liu, 2016, Nguyen et al., 2016b, Nguyen et al., 2016a, Wang et al., 2015). In the Bd material assessed, lack of lemma trichomes is assumed to directly result in lower susceptibility to FHB, therefore lemma trichomes are acting as a Type I susceptibility factor.

No orthologues of known *Arabidopsis* genes within the highly studied trichome initiation or development pathways were localised near to the QTL in Bd. It is likely therefore that the trichome locus is novel. Fine-mapping of the trichome QTL identified

on the long arm of Bd chromosome four was continued from work by Jan Bettgenhaeuser and Daniel Woods, who together using two independent RIL populations, ABR6 x Bd21 and Bd21 x Bd1-1, had defined a physical region containing 17 candidate genes associated with the presence/ absence of lemma trichomes. I refined this to a 53.4 kb interval containing five annotated genes in Bd21 (v3.1), by resolving historical recombination events in the ABR6 x Bd21 population, described in Chapter 4. In doing so, with all plants heterozygous across the interval possessing lemma trichomes, it was clear that the presence of lemma trichomes is a dominant trait, with loss-of-function in ABR6 resulting in lemma trichome absence.

As part of the project, it was clear that higher quality sequence data was required for accession ABR6. To this end, I carried out long-read based nanopore re-sequencing of the whole ABR6 genome, and in doing so advanced the sequence quality for ABR6. The long reads obtained allowed confident structural assembly whilst the small genome size meant that high coverage could easily be obtained to overcome any shortfalls in read call accuracy (Leggett and Clark, 2017). The power created from this data was invaluable for confidently comparing gene content and sequence variation between ABR6 and Bd21. It was complemented by the availability of long-read based genome assembly for Bd1-1 (v1.1) and together these datasets demonstrate the potential weakness of reliance upon Illumina style sequencing data.

A critical loss of protein domain in the ATP-dependent CLP protease (Bradi4g22650) was identified, which lies within the physical candidate interval, and was supported by expression analysis by qPCR in which no transcript was detected within the protease domain for either of the trichomeless accessions, ABR6 and Bd1-1. Furthermore, tissue specificity of expression of Bradi4g22650, being completely absent in leaf tissue, is compatible with the observed lemma-specific trichome phenotype. Bessho-Uehara et al. (2016) describe a protease SLP1 that is required to cleave and mature RAE2, a process that is required for awn development in rice. Also

in rice, Jin et al. (2016) described a similar processing pathway required for maturation of developmental proteins. Bradi4g22650 could therefore play a biologically plausible role in trichome development in Bd.

No mutants were available within the protease domain of Bradi4g22650, either from functional genomics resources or CRISPR mutagenesis, which was unsuccessful. Validation of the putative role of Bradi4g22650 in lemma trichome development is required and could be achieved by pursuing T-DNA mutants, or through repeating CRISPR mutagenesis. A thorough guide to CRISPR-Cas9 mutagenesis in Bd has since been published (Hus et al., 2020).

Without obtaining functional mutants that result in the loss of lemma trichomes in Bd, it was not possible to assess the hypothesis that the absence of lemma trichomes provides a level of Type I resistance to FHB. Cultivated wheat varieties do not possess lemma trichomes in the way that Bd does. Instead, wheat lemmas possess smaller prickle cells. It is possible that prickle cells are also providing points of infection, independent of the well characterised entry route via reproductive organs, therefore acting as a susceptibility factor. Peraldi (Unpublished) observed that Bd lemma prickle cells were points of infection in detached lemma inoculations. This observation indicates that understanding of the genes involved in the initiation and development of trichome/prickle cells in Bd may provide a route for translation into wheat.

Looking beyond the project, translation of this work exploring trichome FHB relationship into wheat is the ultimate aim. Orthologues of highest identity for the most promising candidate, ATP-dependent CLP protease gene (Bradi4g22650) were identified and listed in Table 6-1, although identity was low at the protein level, only 29-43%. The wheat TILLING resource can be used to assess the effect of loss-of-function of these orthologues on interaction with FHB; this would require backcrossing to reduce background mutations and crossing of TILLING lines depending on

redundancy. For the putative role of trichomes as FHB infection points, this will involve the examination of the effect of loss-of-function in trichome precursor genes, to identify any pleiotropic effects, as well as any direct change in lemma anatomy.

6.5 DON sensitivity

The greatest potential for preventing DON contamination of grain lies in the field, by limiting accumulation through reducing *Fusarium* infection. The greatest opportunity for this can be found in the potential for generating genetically resistant varieties and cultivars. The most widely studied mechanism of protection against DON is glucosylation to produce DON-3-O-glucoside by UDP-glucosyltransferase (UGT) proteins (Poppenberger et al., 2003). Overexpression of a wheat UGT gene has been shown to increase resistance to FHB and reduce grain DON content (Xing et al., 2018). Gaining understanding into molecular mechanisms by which DON manipulates plant host defences on a cellular level would allow for more targeted approaches to the development of control methods. This ideal approach would require better understanding of the role that DON plays during infection and colonisation, of which very little is known. Previously only noted to accumulate at later stages of infection, Boenisch and Schafer (2011) demonstrated that the DON biosynthetic pathway is induced in hyphal infection structures but is not required for their development or success of initial infection.

Previous work within the Nicholson group suggested a putative function of DON as an auxin transport inhibitor, a hypothesis based upon observations of alterations in root development, root hair development and gravitropism in response to DON treatment in both *Arabidopsis* and *Bd* (Steed and Nicholson, Unpublished). Auxins and abscisic acid are essential regulators of plant responses to stress, with exogenous auxin shown to prime plant defences and decrease susceptibility to FHB

(*F. culmorum*) (Petti, Reiber et al. 2012). Haidoulis and Nicholson (2020) confirmed an increased resistance to FHB and Fusarium root rot upon exogenous application of auxin in Bd. Limiting the transport of this defensive signal might therefore be a plausible strategy of *Fusarium* to evade the initiation of systematic defence response. There are many sources of evidence suggestive of a putative role of auxin in DON sensitivity, but the mechanism is unclear.

Exploitation of natural diversity formed the initial basis for characterising DON sensitivity, leading to the use of the Bd2-3 x Bd21 mapping population for the identification of loci associated with DON responsiveness and was described in Chapter 5. Root assays were used to assess DON sensitivity of Bd accessions in a high-throughput manner whilst allowing non-destructive monitoring of roots over time. *In planta* studies characterising the role of DON as a protein synthesis inhibitor have typically used higher concentrations of DON (McLaughlin et al., 1977, Rocha et al., 2005). Most accessions showed a quantitative elongation in response to a low concentration of DON, relative to controls. Accessions Bd2-3 and Koz-3 exhibited inhibition of the primary root and induction of secondary, branching roots in response to DON; this response is highly unusual and there are no prior reports of similar responses. No other chemical agents tested fully mimicked the DON phenotype in Bd2-3, but much more expansive investigation is required to confirm the specificity of the phenotype. The techniques developed in this thesis will allow this question to be addressed in future studies.

6.6 Major DON sensitivity effect identified on Bd1

This differential response, for which the Bd2-3 x Bd21 RIL population had segregated, was used to identify genetic loci associated with DON sensitivity. A locus on the long arm of Bd chromosome one was identified by two independent methods, by

conventional mapping and bulked segregant analysis by sequencing, as having a major impact on DON response. Phenotyping of DON sensitivity within the Bd2-3 x Bd21 was not as straightforward as initially expected or stable as might be assumed for an apparent simple, single gene trait. Whilst this presented a constant challenge during analysis of experiments, the power of any associations, especially those resulting from BSA analysis, are made even more compelling, with the understanding that, had the phenotyping been completely accurate, the associations would be that much greater as the genotyping pools would have been pure (Trick et al., 2012).

A high-confidence candidate interval of 56 genes was defined using BSA data. DON responsive RNAseq data was used to identify those genes exhibiting differential DON responsiveness in Bd21 and Bd2-3 in the associated region. The most plausible of these candidate genes for underlying DON sensitivity are listed in Table 6-1. Within the 56 gene interval, no genes were present that were related to glucosyltransferases, or other genes previously identified as affecting the phytotoxicity of DON (Walter and Doohan, 2011). Therefore, my data identifies a potentially novel, tissue independent, mechanism for DON sensitivity.

It may also be possible to further refine the physical region associated with the DON sensitivity trait through exploitation of the remaining SNP variation present to delineate the locations of recombination events in Bd2-3 x Bd21 RILs that provide the left and right borders of the candidate interval. KASP markers designed for this purpose were inconclusive, therefore direct sequencing of markers in the three Bd2-3 x Bd21 RILs containing recombination events between markers Bd1L_69696725 and Bd1L_69743518 could be used to limit the number of candidate genes.

As with the trichome factor, once validated in Bd, the next steps for investigating the role of the DON sensitivity factor should then focus on assessment of any orthologous genes in wheat, using the TILLING platform. Similar methodology for root assays in wheat has been successfully adapted from those here used. This work would first

require further refinement of candidate genes, as described. Wheat orthologues for were identified for the most promising current candidate genes: F-box (SNEEZY orthologue), CASP-like protein ALD-1 (defence related) and RNA binding protein pumilio-related (Bradi1g71460, Bradi1g71465, Bradi1g71530 and Bradi1g71624 respectively, Table 6-1). There is an extremely high level of synteny between the candidate interval in Bd chromosome one with the loci of orthologues on group four chromosomes of wheat (Table 6-1). Similar assessment of DON sensitivity should be made in mutant material for these orthologues using adaptation of root assays and well established DON point application head assays, for example as described by Hales et al. (2020b).

Since the inception of this project rapid advances in wheat genetic resources have been made; TILLING mutant resources are available in tetraploid durum wheat cv 'Kronos' and hexaploid bread wheat cv 'Cadenza'. By the end of this PhD project, chromosome level, high quality reference genome for bread wheat cv 'Chinese Spring' as well as reference-quality genome sequences for multiple wheat lines also becoming available (Walkowiak et al., 2020, Alonge et al., 2020, Appels et al., 2018, Clavijo et al., 2017). These genetic resources will greatly improve the ease of translation of the findings of this thesis into crop species.

Table 6-1 Wheat orthologues of *Bd* candidate genes

Candidate gene	Gene Type	Trait	Wheat Orthologues (IWGSC)
Bradi4g22650	ATP-dependent CLP protease	Lemma Trichome	TraesCS3A02G422900 TraesCS3B02G458500 TraesCS3D02G418100
Bradi1g71460	F- box, SNEEZY orthologue	DON	TraesCS4A02G042900 TraesCS4B02G263400 TraesCS4D02G263600
Bradi1g71465	CASP-like protein	DON	TraesCS4A02G043000 TraesCS4B02G263500 TraesCS4D02G263800
Bradi1g71530	ALD-1, defence related	DON	TraesCS4A02G043800 TraesCS4B02G264500 TraesCS4D02G264500
Bradi1g71624	RNA binding protein pumilio-related	DON	TraesCS4A02G039400 TraesCS4B02G266100 TraesCS4D02G266000

References

- Alexandratos, N. & Bruinsma, J. 2012. World agriculture towards 2030/2050: the 2012 revision. ESA Working paper Rome, FAO.
- Alonge, M., Shumate, A., Puiu, D., Zimin, A. V. & Salzberg, S. L. 2020. Chromosome-Scale Assembly of the Bread Wheat Genome Reveals Thousands of Additional Gene Copies. *Genetics*, 216, 599-608.
- Andrews, S. 2010. *FastQC: a quality control tool for high throughput sequence data* [Online]. Available: <http://www.bioinformatics.babraham.ac.uk/projects/fastqc> [Accessed October 24, 2019].
- Appels, R., Eversole, K., Stein, N., Feuillet, C., Keller, B., Rogers, J., Pozniak, C. J., Choulet, F., Distelfeld, A., Poland, J., Ronen, G., Sharpe, A. G., Barad, O., Baruch, K., Keeble-Gagnère, G., Mascher, M., Ben-Zvi, G., Josselin, A.-A., Himmelbach, A., Balfourier, F., Gutierrez-Gonzalez, J., Hayden, M., Koh, C., Muehlbauer, G., Pasam, R. K., Paux, E., Rigault, P., Tibbits, J., Tiwari, V., Spannagl, M., Lang, D., Gundlach, H., Haberer, G., Mayer, K. F. X., Ormanbekova, D., Prade, V., Šimková, H., Wicker, T., Swarbreck, D., Rimbart, H., Felder, M., Guilhot, N., Kaithakottil, G., Keilwagen, J., Leroy, P., Lux, T., Twardziok, S., Venturini, L., Juhász, A., Abrouk, M., Fischer, I., Uauy, C., Borrill, P., Ramirez-Gonzalez, R. H., Arnaud, D., Chalabi, S., Chalhoub, B., Cory, A., Datla, R., Davey, M. W., Jacobs, J., Robinson, S. J., Steuernagel, B., van Ex, F., Wulff, B. B. H., Benhamed, M., Bendahmane, A., Concia, L., Latrasse, D., Bartoš, J., Bellec, A., Berges, H., Doležel, J., Frenkel, Z., Gill, B., Korol, A., Letellier, T., Olsen, O.-A., Singh, K., Valárik, M., van der Vossen, E., Vautrin, S., Weining, S., Fahima, T., Glikson, V., Raats, D., Číhalíková, J., Toegelová, H., Vrána, J., Sourdille, P., Darrier, B., Barabaschi, D., Cattivelli, L., Hernandez, P., Galvez, S., Budak, H., Jones, J. D. G., Witek, K., Yu, G., Small, I., et al. 2018. Shifting the limits in wheat research and breeding using a fully annotated reference genome. *Science*, 361, eaar7191.
- Arendsee, Z. W., Li, L. & Wurtele, E. S. 2014. Coming of age: orphan genes in plants. *Trends in Plant Science*, 19, 698-708.
- Ariizumi, T., Lawrence, P. K. & Steber, C. M. 2011. The role of two f-box proteins, SLEEPY1 and SNEEZY, in Arabidopsis gibberellin signaling. *Plant Physiol*, 155, 765-75.
- Ariizumi, T. & Steber, C. M. 2011. Mutations in the F-box gene SNEEZY result in decreased Arabidopsis GA signaling. *Plant Signal Behav*, 6, 831-3.
- Bai, G. & Shaner, G. 2004. Management and resistance in wheat and barley to fusarium head blight. *Annu Rev Phytopathol*, 42, 135-61.
- Bai, G. H., Desjardins, A. E. & Plattner, R. D. 2002. Deoxynivalenol-nonproducing fusarium graminearum causes initial infection, but does not cause disease spread in wheat spikes. *Mycopathologia*, 153, 91-98.
- Baluška, F., Parker, J. S. & Barlow, P. W. 1993. A role for gibberellic acid in orienting microtubules and regulating cell growth polarity in the maize root cortex. *Planta*, 191, 149-157.
- Banik, M., Liu, S., Yu, K., Poysa, V. & Park, S. J. 2008. Molecular TILLING and EcoTILLING: effective tools for mutant gene detection in plants. *Genes Genomes Genomics*, 1, 123-132.
- Barkley, N. A. & Wang, M. L. 2008. Application of TILLING and EcoTILLING as Reverse Genetic Approaches to Elucidate the Function of Genes in Plants and Animals. *Current Genomics*, 9, 212-226.
- Beccari, G., Covarelli, L. & Nicholson, P. 2011. Infection processes and soft wheat response to root rot and crown rot caused by *Fusarium culmorum*. *Plant Pathology*, 60, 671-684.

- Bessho-Uehara, K., Wang, D. R., Furuta, T., Minami, A., Nagai, K., Gamuyao, R., Asano, K., Angeles-Shim, R. B., Shimizu, Y., Ayano, M., Komeda, N., Doi, K., Miura, K., Toda, Y., Kinoshita, T., Okuda, S., Higashiyama, T., Nomoto, M., Tada, Y., Shinohara, H., Matsubayashi, Y., Greenberg, A., Wu, J., Yasui, H., Yoshimura, A., Mori, H., McCouch, S. R. & Ashikari, M. 2016. Loss of function at RAE2, a previously unidentified EPFL, is required for awnlessness in cultivated Asian rice. *Proceedings of the National Academy of Sciences*, 113, 8969.
- Bettgenhaeuser, J. Unpublished. F8 genetic map for ABR6 x Bd21 recombinant inbred line population.
- Bettgenhaeuser, J., Corke, F. M., Opanowicz, M., Green, P., Hernandez-Pinzon, I., Doonan, J. H. & Moscou, M. J. 2017. Natural variation in Brachypodium links vernalization and flowering time loci as major flowering determinants. *Plant Physiol.*
- Bettgenhaeuser, J., Gardiner, M., Spanner, R., Green, P., Hernandez-Pinzon, I., Hubbard, A., Ayliffe, M. & Moscou, M. J. 2018. The genetic architecture of colonization resistance in Brachypodium distachyon to non-adapted stripe rust (*Puccinia striiformis*) isolates. *Plos Genetics*, 14.
- Bettgenhaeuser, J., Woods, D. P. & Moscou, M. Unpublished. Fine mapping of trichomeless phenotype in ABR6 x Bd21 and Bd21 x Bd1-1 recombinant inbred line populations of Brachypodium distachyon.
- Blümke, A., Sode, B., Ellinger, D. & Voigt, C. A. 2015. Reduced susceptibility to Fusarium head blight in Brachypodium distachyon through priming with the Fusarium mycotoxin deoxynivalenol. *Molecular plant pathology*, 16, 472-483.
- Boenisch, M. J. & Schafer, W. 2011. Fusarium graminearum forms mycotoxin producing infection structures on wheat. *Bmc Plant Biology*, 11.
- Bolger, A. M., Lohse, M. & Usadel, B. 2014. Trimmomatic: a flexible trimmer for Illumina sequence data. *Bioinformatics*, 30, 2114-20.
- Boutigny, A. L., Richard-Forget, F. & Barreau, C. 2008. Natural mechanisms for cereal resistance to the accumulation of Fusarium trichothecenes. *European Journal of Plant Pathology*, 121, 411-423.
- Bragg, J. N., Wu, J., Gordon, S. P., Guttman, M. E., Thilmony, R., Lazo, G. R., Gu, Y. Q. & Vogel, J. P. 2012. Generation and Characterization of the Western Regional Research Center Brachypodium T-DNA Insertional Mutant Collection. *PLOS ONE*, 7, e41916.
- Brauer, E. K., Rocheleau, H., Balcerzak, M., Pan, Y., Fauteux, F., Liu, Z., Wang, L., Zheng, W. & Ouellet, T. 2019. Transcriptional and hormonal profiling of Fusarium graminearum-infected wheat reveals an association between auxin and susceptibility. *Physiological and Molecular Plant Pathology*, 107, 33-39.
- Broman, K. W., Wu, H., Sen, S. & Churchill, G. A. 2003. R/qtl: QTL mapping in experimental crosses. *Bioinformatics*, 19, 889-90.
- Brown, J. K. 2002. Yield penalties of disease resistance in crops. *Curr Opin Plant Biol*, 5, 339-44.
- Brown, N. A., Urban, M., van de Meene, A. M. & Hammond-Kosack, K. E. 2010. The infection biology of Fusarium graminearum: defining the pathways of spikelet to spikelet colonisation in wheat ears. *Fungal Biol*, 114, 555-71.
- Buerstmayr, H., Ban, T. & Anderson, J. A. 2009. QTL mapping and marker-assisted selection for Fusarium head blight resistance in wheat: a review. *Plant Breeding*, 128, 1-26.
- Buerstmayr, H., Lemmens, M., Schmolke, M., Zimmermann, G., Hartl, L., Mascher, F., Trottet, M., Gosman, N. E. & Nicholson, P. 2008. Multi-environment evaluation of level and stability of FHB resistance among parental lines and

- selected offspring derived from several European winter wheat mapping populations. *Plant Breeding*, 127, 325-332.
- Buerstmayr, M. & Buerstmayr, H. 2016. The semidwarfing alleles Rht-D1b and Rht-B1b show marked differences in their associations with anther-retention in wheat heads and with Fusarium head blight susceptibility. *Phytopathology*, 106, 1544-1552.
- Buerstmayr, M., Huber, K., Heckmann, J., Steiner, B., Nelson, J. C. & Buerstmayr, H. 2012. Mapping of QTL for Fusarium head blight resistance and morphological and developmental traits in three backcross populations derived from *Triticum dicoccum* × *Triticum durum*. *Theoretical and Applied Genetics*, 125, 1751-1765.
- Buerstmayr, M., Steiner, B. & Buerstmayr, H. 2020. Breeding for Fusarium head blight resistance in wheat-Progress and challenges. *Plant Breeding*, 139, 429-454.
- Burt, C., Steed, A., Gosman, N., Lemmens, M., Bird, N., Ramirez-Gonzalez, R., Holdgate, S. & Nicholson, P. 2015. Mapping a Type 1 FHB resistance on chromosome 4AS of *Triticum macha* and deployment in combination with two Type 2 resistances. *Theoretical and Applied Genetics*, 128, 1725-1738.
- Cassman, K. G., Dobermann, A., Walters, D. T. & Yang, H. 2003. Meeting cereal demand while protecting natural resources and improving environmental quality. *Annual Review of Environment and Resources*, 28, 315-358.
- Catalan, P., Chalhoub, B., Chochois, V., Garvin, D. F., Hasterok, R., Manzaneda, A. J., Mur, L. A. J., Pecchioni, N., Rasmussen, S. K., Vogel, J. P. & Voxeur, A. 2014. Update on the genomics and basic biology of Brachypodium International Brachypodium Initiative (IBI). *Trends in Plant Science*, 19, 414-418.
- Causier, B., Ashworth, M., Guo, W. & Davies, B. 2012. The TOPLESS interactome: a framework for gene repression in *Arabidopsis*. *Plant physiology*, 158, 423-438.
- Chen, W., Li, X., Tian, L., Wu, P., Li, M., Jiang, H., Chen, Y. & Wu, G. 2014. Knockdown of LjALD1, AGD2-like defense response protein 1, influences plant growth and nodulation in *Lotus japonicus*. *Journal of Integrative Plant Biology*, 56.
- Chu, C., Niu, Z., Zhong, S., Chao, S., Friesen, T. L., Halley, S., Elias, E. M., Dong, Y., Faris, J. D. & Xu, S. S. 2011. Identification and molecular mapping of two QTLs with major effects for resistance to Fusarium head blight in wheat. *Theoretical and Applied Genetics*, 123, 1107.
- Churchill, G. A. & Doerge, R. W. 1994. Empirical threshold values for quantitative trait mapping. *Genetics*, 138, 963-71.
- Clavijo, B. J., Venturini, L., Schudoma, C., Accinelli, G. G., Kaithakottil, G., Wright, J., Borrill, P., Kettleborough, G., Heavens, D., Chapman, H., Lipscombe, J., Barker, T., Lu, F.-H., McKenzie, N., Raats, D., Ramirez-Gonzalez, R. H., Coince, A., Peel, N., Percival-Alwyn, L., Duncan, O., Trösch, J., Yu, G., Bolser, D. M., Namaati, G., Kerhornou, A., Spannagl, M., Gundlach, H., Haberer, G., Davey, R. P., Fosker, C., Palma, F. D., Phillips, A. L., Millar, A. H., Kersey, P. J., Uauy, C., Krasileva, K. V., Swarbreck, D., Bevan, M. W. & Clark, M. D. 2017. An improved assembly and annotation of the allohexaploid wheat genome identifies complete families of agronomic genes and provides genomic evidence for chromosomal translocations. *Genome Research*, 27, 885-896.
- Cox, N. & Smith, L. M. 2019. A Novel Upstream Regulator of Trichome Development Inhibitors. *Plant Physiology*, 181, 1398-1400.

- Cundliffe, E., Cannon, M. & Davies, J. 1974. Mechanism of inhibition of eukaryotic protein synthesis by trichothecene fungal toxins. *Proc Natl Acad Sci U S A*, 71, 30-4.
- Cundliffe, E. & Davies, J. E. 1977. Inhibition of Initiation, Elongation, and Termination of Eukaryotic Protein Synthesis by Trichothecene Fungal Toxins. *Antimicrobial Agents and Chemotherapy*, 11, 491-499.
- Cuthbert, P. A., Somers, D. J. & Brulé-Babel, A. 2007. Mapping of Fhb2 on chromosome 6BS: a gene controlling Fusarium head blight field resistance in bread wheat (*Triticum aestivum* L.). *Theoretical and Applied Genetics*, 114, 429-437.
- Cuthbert, P. A., Somers, D. J., Thomas, J., Cloutier, S. & Brulé-Babel, A. 2006. Fine mapping Fhb1, a major gene controlling fusarium head blight resistance in bread wheat (*Triticum aestivum* L.). *Theoretical and Applied Genetics*, 112, 1465.
- Dalmais, M., Antelme, S., Ho-Yue-Kuang, S., Wang, Y., Darracq, O., d'Yvoire, M. B., Cézard, L., Légée, F., Blondet, E., Oria, N., Troadec, C., Brunaud, V., Jouanin, L., Höfte, H., Bendahmane, A., Lapierre, C. & Sibout, R. 2013a. A TILLING Platform for Functional Genomics in *Brachypodium distachyon*. *PLoS one*, 8, e65503-e65503.
- Dalmais, M., Antelme, S., Ho-Yue-Kuang, S., Wang, Y., Darracq, O., d'Yvoire, M. B., Cézard, L., Légée, F., Blondet, E., Oria, N., Troadec, C., Brunaud, V., Jouanin, L., Höfte, H., Bendahmane, A., Lapierre, C. & Sibout, R. 2013b. A TILLING Platform for Functional Genomics in *Brachypodium distachyon*. *PLOS ONE*, 8, e65503.
- Danecek, P., Auton, A., Abecasis, G., Albers, C. A., Banks, E., DePristo, M. A., Handsaker, R. E., Lunter, G., Marth, G. T., Sherry, S. T., McVean, G., Durbin, R. & Group, G. P. A. 2011. The variant call format and VCFtools. *Bioinformatics*, 27, 2156-2158.
- Davidson, R. M., Gowda, M., Moghe, G., Lin, H., Vaillancourt, B., Shiu, S.-H., Jiang, N. & Robin Buell, C. 2012. Comparative transcriptomics of three Poaceae species reveals patterns of gene expression evolution. *The Plant journal : for cell and molecular biology*, 71, 492-502.
- de los Reyes, B. G. 2019. Genomic and epigenomic bases of transgressive segregation – New breeding paradigm for novel plant phenotypes. *Plant Science*, 288, 110213.
- Dell'Acqua, M., Zuccolo, A., Tuna, M., Gianfranceschi, L. & Pè, M. E. 2014. Targeting environmental adaptation in the monocot model *Brachypodium distachyon*: a multi-faceted approach. *BMC Genomics*, 15, 801.
- Della Coletta, R., Hirsch, C. N., Rouse, M. N., Lorenz, A. & Garvin, D. F. 2019. Genomic Dissection of Nonhost Resistance to Wheat Stem Rust in *Brachypodium distachyon*. *Mol Plant Microbe Interact*, 32, 392-400.
- Derbyshire, P. & Byrne, M. E. 2013. MORE SPIKELETS1 Is Required for Spikelet Fate in the Inflorescence of *Brachypodium*. *Plant Physiology*, 161, 1291-1302.
- Desjardins, A. E., Proctor, R., Bai, G., McCormick, S., Shaner, G., Buechley, G. & Hohn, T. 1996. Reduced virulence of trichothecene-nonproducing mutants of *Gibberella zeae* in wheat field tests.
- Desmond, O. J., Manners, J. M., Stephens, A. E., MaClean, D. J., Schenk, P. M., Gardiner, D. M., Munn, A. L. & Kazan, K. 2008. The Fusarium mycotoxin deoxynivalenol elicits hydrogen peroxide production, programmed cell death and defence responses in wheat. *Molecular Plant Pathology*, 9, 435-445.
- Dill-Macky, R. & Jones, R. 2000. The effect of previous crop residues and tillage on Fusarium head blight of wheat. *Plant disease*, 84, 71-76.

- Dinolfo, M. I., Martínez, M., Nogueira, M. S., Nicholson, P. & Stenglein, S. A. 2020. Evaluation of interaction between *Brachypodium distachyon* roots and *Fusarium* species. *European Journal of Plant Pathology*.
- Draeger, R., Gosman, N., Steed, A., Chandler, E., Thomsett, M., Srinivasachary, Schondelmaier, J., Buerstmayr, H., Lemmens, M., Schmolke, M., Mesterhazy, A. & Nicholson, P. 2007. Identification of QTLs for resistance to *Fusarium* head blight, DON accumulation and associated traits in the winter wheat variety Arina. *Theoretical and Applied Genetics*, 115, 617-625.
- Draper, J., Mur, L. A. J., Jenkins, G., Ghosh-Biswas, G. C., Bablak, P., Hasterok, R. & Routledge, A. P. M. 2001. *Brachypodium distachyon*. A new model system for functional genomics in grasses. *Plant Physiology*, 127, 1539-1555.
- Escriva, L., Font, G. & Manyes, L. 2015. In vivo toxicity studies of fusarium mycotoxins in the last decade: A review. *Food and Chemical Toxicology*, 78, 185-206.
- Eudes, F., Comeau, A., Rioux, S. & Collin, J. 2000. Phytotoxicity of eight mycotoxins associated with the fusariosis of wheat spikelets. *Canadian Journal of Plant Pathology*, 22, 286-292.
- Fernández-Marcos, M., Desvoves, B., Manzano, C., Liberman, L. M., Benfey, P. N., del Pozo, J. C. & Gutierrez, C. 2017. Control of *Arabidopsis* lateral root primordium boundaries by MYB36. *New Phytologist*, 213, 105-112.
- Filiz, E., Ozdemir, B. S., Budak, F., Vogel, J. P., Tuna, M. & Budak, H. 2009. Molecular, morphological, and cytological analysis of diverse *Brachypodium distachyon* inbred lines. *Genome*, 52, 876-890.
- Fitzgerald, T. L., Powell, J. J., Schneebeli, K., Hsia, M. M., Gardiner, D. M., Bragg, J. N., McIntyre, C. L., Manners, J. M., Ayliffe, M., Watt, M., Vogel, J. P., Henry, R. J. & Kazan, K. 2015. *Brachypodium* as an emerging model for cereal-pathogen interactions. *Annals of Botany*, 115, 717-731.
- Flavell, R. 2009. Role of model plant species. *Methods Mol Biol*, 513, 1-18.
- Foroud, N. A., Ouellet, T., Laroche, A., Oosterveen, B., Jordan, M. C., Ellis, B. E. & Eudes, F. 2012. Differential transcriptome analyses of three wheat genotypes reveal different host response pathways associated with *Fusarium* head blight and trichothecene resistance. *Plant Pathology*, 61, 296-314.
- Fu, X., Richards, D. E., Fleck, B., Xie, D., Burton, N. & Harberd, N. P. 2004. The *Arabidopsis* mutant *sleepy1gar2-1* protein promotes plant growth by increasing the affinity of the SCF^{SLY1} E3 ubiquitin ligase for DELLA protein substrates. *Plant Cell*, 16, 1406-18.
- Gan, L., Xia, K., Chen, J.-G. & Wang, S. 2011. Functional characterization of TRICHOMELESS2, a new single-repeat R3 MYB transcription factor in the regulation of trichome patterning in *Arabidopsis*. *BMC Plant Biology*, 11, 176.
- Garrison, E. & Marth, G. 2012. *Haplotype-based variant detection from short-read sequencing.*, arXiv preprint arXiv:1207.3907 [q-bio.GN].
- Garvin, D. F., Gu, Y.-Q., Hasterok, R., Hazen, S. P., Jenkins, G., Mockler, T. C., Mur, L. A. & Vogel, J. P. 2008. Development of genetic and genomic research resources for, a new model system for grass crop research. *Crop Science*, 48, S-69-S-84.
- Gilbert, B., Bettgenhaeuser, J., Upadhyaya, N., Soliveres, M., Singh, D., Park, R. F., Moscou, M. J. & Ayliffe, M. 2018. Components of *Brachypodium distachyon* resistance to nonadapted wheat stripe rust pathogens are simply inherited. *Plos Genetics*, 14.
- Girin, T., David, L. C., Chardin, C., Sibout, R., Krapp, A., Ferrario-Méry, S. & Daniel-Vedele, F. 2014. *Brachypodium*: a promising hub between model species and cereals. *Journal of Experimental Botany*, 65, 5683-5696.
- Goddard, R., Peraldi, A., Ridout, C. & Nicholson, P. 2014. Enhanced disease resistance caused by BRI1 mutation is conserved between *Brachypodium*

- distachyon and barley (*Hordeum vulgare*). *Mol Plant Microbe Interact*, 27, 1095-106.
- Goddard, R., Steed, A., Scheeren, P. L., Maciel, J. L. N., Caierão, E., Torres, G. A. M., Consoli, L., Santana, F. M., Fernandes, J. M. C. & Simmonds, J. 2021. Identification of *Fusarium* head blight resistance loci in two Brazilian wheat mapping populations. *Plos one*, 16, e0248184.
- Goodstein, D. M., Shu, S., Howson, R., Neupane, R., Hayes, R. D., Fazo, J., Mitros, T., Dirks, W., Hellsten, U., Putnam, N. & Rokhsar, D. S. 2012. Phytozome: a comparative platform for green plant genomics. *Nucleic acids research*, 40, D1178-D1186.
- Gordon, S. P., Contreras-Moreira, B., Woods, D. P., Marais, D. L. D., Burgess, D., Shu, S. Q., Stritt, C., Roulin, A. C., Schackwitz, W., Tyler, L., Martin, J., Lipzen, A., Dochy, N., Phillips, J., Barry, K., Geuten, K., Budak, H., Juenger, T. E., Amasino, R., Caicedo, A. L., Goodstein, D., Davidson, P., Mur, L. A. J., Figueroa, M., Freeling, M., Catalan, P. & Vogel, J. P. 2017. Extensive gene content variation in the *Brachypodium distachyon* pan-genome correlates with population structure. *Nature Communications*, 8.
- Gordon, S. P., Priest, H., Des Marais, D. L., Schackwitz, W., Figueroa, M., Martin, J., Bragg, J. N., Tyler, L., Lee, C.-R., Bryant, D., Wang, W., Messing, J., Manzaneda, A. J., Barry, K., Garvin, D. F., Budak, H., Tuna, M., Mitchell-Olds, T., Pfender, W. F., Juenger, T. E., Mockler, T. C. & Vogel, J. P. 2014. Genome diversity in *Brachypodium distachyon*: deep sequencing of highly diverse inbred lines. *The Plant Journal*, 79, 361-374.
- Gosman, N., Chandler, E., Thomsett, M., Draeger, R. & Nicholson, P. 2005. Analysis of the relationship between parameters of resistance to *Fusarium* head blight and in vitro tolerance to deoxynivalenol of the winter wheat cultivar WEK0609. *European Journal of Plant Pathology*, 111, 57-66.
- Goswami, R. S. & Kistler, H. C. 2004. Heading for disaster: *Fusarium graminearum* on cereal crops. *Molecular Plant Pathology*, 5, 515-525.
- Gregory, P. J. & George, T. S. 2011. Feeding nine billion: the challenge to sustainable crop production. *Journal of Experimental Botany*, 62, 5233-5239.
- Haidoulis, J. F. & Nicholson, P. 2020. Different effects of phytohormones on *Fusarium* head blight and *Fusarium* root rot resistance in *Brachypodium distachyon*. *Journal of Plant Interactions*, 15, 335-344.
- Hales, B., Steed, A., Giovannelli, V., Burt, C., Lemmens, M., Molnar-Lang, M. & Nicholson, P. 2020a. Type II *Fusarium* head blight susceptibility conferred by a region on wheat chromosome 4D. *Journal of Experimental Botany*, 71, 4703-4714.
- Hales, B., Steed, A., Giovannelli, V., Burt, C., Lemmens, M., Molnár-Láng, M. & Nicholson, P. 2020b. Type II *Fusarium* head blight susceptibility factor identified in wheat. *bioRxiv*, 2020.02.06.937425.
- He, F., Zhang, R., Zhao, J., Qi, T., Kang, Z. & Guo, J. 2019. Host-Induced Silencing of *Fusarium graminearum* Genes Enhances the Resistance of *Brachypodium distachyon* to *Fusarium* Head Blight. *Frontiers in Plant Science*, 10.
- He, X., Singh, P. K., Dreisigacker, S., Singh, S., Lillemo, M. & Duveiller, E. 2016. Dwarfing Genes Rht-B1b and Rht-D1b Are Associated with Both Type I FHB Susceptibility and Low Anther Extrusion in Two Bread Wheat Populations. *PLOS ONE*, 11, e0162499.
- Hedden, P. 2003. The genes of the Green Revolution. *Trends in Genetics*, 19, 5-9.
- Hong, S. Y., Seo, P. J., Yang, M. S., Xiang, F. & Park, C. M. 2008. Exploring valid reference genes for gene expression studies in *Brachypodium distachyon* by real-time PCR. *BMC Plant Biol*, 8, 112.

- Hsia, M. M., O'Malley, R., Cartwright, A., Nieu, R., Gordon, S. P., Kelly, S., Williams, T. G., Wood, D. F., Zhao, Y., Bragg, J., Jordan, M., Pauly, M., Ecker, J. R., Gu, Y. & Vogel, J. P. 2017. Sequencing and functional validation of the JGI Brachypodium distachyon T-DNA collection. *The Plant Journal*, 91, 361-370.
- Hueza, I. M., Raspantini, P. C. F., Raspantini, L. E. R., Latorre, A. O. & Górniak, S. L. 2014. Zearalenone, an Estrogenic Mycotoxin, Is an Immunotoxic Compound. *Toxins*, 6, 1080-1095.
- Huo, N., Vogel, J. P., Lazo, G. R., You, F. M., Ma, Y., McMahon, S., Dvorak, J., Anderson, O. D., Luo, M. C. & Gu, Y. Q. 2009. Structural characterization of Brachypodium genome and its syntenic relationship with rice and wheat. *Plant Mol Biol*, 70, 47-61.
- Hus, K., Betekhtin, A., Pinski, A., Rojek-Jelonek, M., Grzebelus, E., Nibau, C., Gao, M. J., Jaeger, K. E., Jenkins, G., Doonan, J. H. & Hasterok, R. 2020. A CRISPR/Cas9-Based Mutagenesis Protocol for Brachypodium distachyon and Its Allopolyploid Relative, Brachypodium hybridum. *Frontiers in Plant Science*, 11.
- Ilgen, P., Maier, F. J. & Schafer, W. 2008. Monitoring the induction of trichothecene mycotoxins of Fusarium graminearum using GFP during wheat head infection and in culture. *Cereal Research Communications*, 36, 503-505.
- Imboden, L., Afton, D. & Trail, F. 2018. Surface interactions of Fusarium graminearum on barley. *Molecular Plant Pathology*, 19, 1332-1342.
- International Brachypodium, I. 2010. Genome sequencing and analysis of the model grass Brachypodium distachyon. *Nature*, 463, 763-8.
- Jansen, C., von Wettstein, D., Schäfer, W., Kogel, K.-H., Felk, A. & Maier, F. J. 2005. Infection patterns in barley and wheat spikes inoculated with wild-type and trichodiene synthase gene disrupted Fusarium graminearum. *Proceedings of the National Academy of Sciences of the United States of America*, 102, 16892-16897.
- Jeger, M. J. & Viljanen-Rollinson, S. L. H. 2001. The use of the area under the disease-progress curve (AUDPC) to assess quantitative disease resistance in crop cultivars. *Theoretical and Applied Genetics*, 102, 32-40.
- Jia, H., Zhou, J., Xue, S., Li, G., Yan, H., Ran, C., Zhang, Y., Shi, J., Jia, L. & Wang, X. 2018. A journey to understand wheat Fusarium head blight resistance in the Chinese wheat landrace Wangshuibai. *The Crop Journal*, 6, 48-59.
- Jin, J., Hua, L., Zhu, Z., Tan, L., Zhao, X., Zhang, W., Liu, F., Fu, Y., Cai, H., Sun, X., Gu, P., Xie, D. & Sun, C. 2016. GAD1 Encodes a Secreted Peptide That Regulates Grain Number, Grain Length, and Awn Development in Rice Domestication. *Plant Cell*, 28, 2453-2463.
- Johnson, C. S., Kolevski, B. & Smyth, D. R. 2002. TRANSPARENT TESTA GLABRA2, a Trichome and Seed Coat Development Gene of Arabidopsis, Encodes a WRKY Transcription Factor. *The Plant Cell*, 14, 1359-1375.
- Kamran, A., Iqbal, M. & Spaner, D. 2014. Flowering time in wheat (*Triticum aestivum* L.): a key factor for global adaptability. *Euphytica*, 197, 1-26.
- Kang, Z. & Buchenauer, H. 1999. Immunocytochemical localization of fusarium toxins in infected wheat spikes by Fusarium culmorum. *Physiological and Molecular Plant Pathology*, 55, 275-288.
- Kang, Z. & Buchenauer, H. 2000. Ultrastructural and Cytochemical Studies on Cellulose, Xylan and Pectin Degradation in Wheat Spikes Infected by Fusarium culmorum. *Journal of Phytopathology*, 148, 263-275.
- Kazan, K., Gardiner, D. M. & Manners, J. M. 2012. On the trail of a cereal killer: recent advances in Fusarium graminearum pathogenomics and host resistance. *Molecular Plant Pathology*, 13, 399-413.

- Kersey, P. J., Allen, J. E., Allot, A., Barba, M., Boddu, S., Bolt, B. J., Carvalho-Silva, D., Christensen, M., Davis, P., Grabmueller, C., Kumar, N., Liu, Z., Maurel, T., Moore, B., McDowall, M. D., Maheswari, U., Naamati, G., Newman, V., Ong, C. K., Paulini, M., Pedro, H., Perry, E., Russell, M., Sparrow, H., Tapanari, E., Taylor, K., Vullo, A., Williams, G., Zadissia, A., Olson, A., Stein, J., Wei, S., Tello-Ruiz, M., Ware, D., Luciani, A., Potter, S., Finn, R. D., Urban, M., Hammond-Kosack, K. E., Bolser, D. M., De Silva, N., Howe, K. L., Langridge, N., Maslen, G., Staines, D. M. & Yates, A. 2017. Ensembl Genomes 2018: an integrated omics infrastructure for non-vertebrate species. *Nucleic Acids Research*, 46, D802-D808.
- Kim, D., Langmead, B. & Salzberg, S. L. 2015. HISAT: a fast spliced aligner with low memory requirements. *Nature Methods*, 12, 357-360.
- Kimura, M., Takahashi-Ando, N., Nishiuchi, T., Ohsato, S., Tokai, T., Ochiai, N., Fujimura, M., Kudo, T., Hamamoto, H. & Yamaguchi, I. 2006. Molecular biology and biotechnology for reduction of Fusarium mycotoxin contamination. *Pesticide Biochemistry and Physiology*, 86, 117-123.
- Kind, S., Schurack, S., Hinsch, J. & Tudzynski, P. 2018. Brachypodium distachyon as alternative model host system for the ergot fungus Claviceps purpurea. *Molecular plant pathology*, 19, 1005-1011.
- Kobayashi, K., Baba, S., Obayashi, T., Sato, M., Toyooka, K., Keränen, M., Aro, E.-M., Fukaki, H., Ohta, H., Sugimoto, K. & Masuda, T. 2012. Regulation of Root Greening by Light and Auxin/Cytokinin Signaling in Arabidopsis. *The Plant Cell*, 24, 1081-1095.
- Kolmogorov, M., Yuan, J., Lin, Y. & Pevzner, P. A. 2019. Assembly of long, error-prone reads using repeat graphs. *Nature Biotechnology*, 37, 540-546.
- Kulik, T., Abarenkov, K., Busko, M., Bilska, K., van Diepeningen, A. D., Ostrowska-Kolodziejczak, A., Krawczyk, K., Brankovics, B., Stenglein, S., Sawicki, J. & Perkowski, J. 2017. ToxGen: an improved reference database for the identification of type B-trichothecene genotypes in Fusarium. *PeerJ*, 5.
- Lagudah, E. S. & Krattinger, S. G. 2019. A new player contributing to durable Fusarium resistance. *Nature genetics*, 51, 1070-1071.
- Langevin, F., Eudes, F. & Comeau, A. 2004. Effect of Trichothecenes Produced by Fusarium graminearum during Fusarium Head Blight Development in Six Cereal Species. *European Journal of Plant Pathology*, 110, 735-746.
- Lee, H. G. & Seo, P. J. 2019. MYB96 recruits the HDA15 protein to suppress negative regulators of ABA signaling in Arabidopsis. *Nature Communications*, 10, 1713.
- Lee, K.-H., Utku, A., Qi, L. & Wang, H. 2018. The α -Aurora Kinases Function in Vascular Development in Arabidopsis. *Plant and Cell Physiology*, 60, 188-201.
- Leggett, R. M. & Clark, M. D. 2017. A world of opportunities with nanopore sequencing. *Journal of Experimental Botany*, 68, 5419-5429.
- Lemmens, M., Scholz, U., Berthiller, F., Dall'Asta, C., Koutnik, A., Schuhmacher, R., Adam, G., Buerstmayr, H., Mesterhazy, A., Krska, R. & Ruckebauer, P. 2005. The ability to detoxify the mycotoxin deoxynivalenol colocalizes with a major quantitative trait locus for fusarium head blight resistance in wheat. *Molecular Plant-Microbe Interactions*, 18, 1318-1324.
- Leslie, J. F. & Logrieco, A. 2014. *Mycotoxin Reduction in Grain Chains*, Wiley.
- Li, B., Liu, D. J. & Leal, S. M. 2013. Identifying rare variants associated with complex traits via sequencing. *Current protocols in human genetics*, Chapter 1, 10.1002/0471142905.hg0126s78-1.26.

- Li, G., Zhou, J., Jia, H., Gao, Z., Fan, M., Luo, Y., Zhao, P., Xue, S., Li, N. & Yuan, Y. 2019. Mutation of a histidine-rich calcium-binding-protein gene in wheat confers resistance to Fusarium head blight. *Nature Genetics*, 51, 1106-1112.
- Li, H., Handsaker, B., Wysoker, A., Fennell, T., Ruan, J., Homer, N., Marth, G., Abecasis, G. & Durbin, R. 2009. The sequence alignment/map format and SAMtools. *Bioinformatics*, 25.
- Liu, C. & Zhang, T. 2017. Expansion and stress responses of the AP2/EREBP superfamily in cotton. *BMC Genomics*, 18, 118.
- Liu, S., Griffey, C. A., Hall, M. D., McKendry, A. L., Chen, J., Brooks, W. S., Brown-Guedira, G., Van Sanford, D. & Schmale, D. G. 2013. Molecular characterization of field resistance to Fusarium head blight in two US soft red winter wheat cultivars. *Theoretical and Applied Genetics*, 126, 2485-2498.
- Liu, X. & Liu, C. 2016. Effects of Drought-Stress on Fusarium Crown Rot Development in Barley. *PloS one*, 11, e0167304-e0167304.
- Lobet, G., Pagès, L. & Draye, X. 2011. A Novel Image-Analysis Toolbox Enabling Quantitative Analysis of Root System Architecture. *Plant Physiology*, 157, 29-39.
- Lu, Q., Lillemo, M., Skjinner, H., He, X., Shi, J., Ji, F., Dong, Y. & Bjørnstad, Å. 2013. Anther extrusion and plant height are associated with Type I resistance to Fusarium head blight in bread wheat line 'Shanghai-3/Catbird'. *Theoretical and Applied Genetics*, 126, 317-334.
- Luo, K., Rocheleau, H., Qi, P. F., Zheng, Y. L., Zhao, H. Y. & Ouellet, T. 2016. Indole-3-acetic acid in Fusarium graminearum: Identification of biosynthetic pathways and characterization of physiological effects. *Fungal Biol*, 120, 1135-45.
- Machado, A., Wu, Y., Yang, Y., Llewellyn, D. J. & Dennis, E. S. 2009. The MYB transcription factor GhMYB25 regulates early fibre and trichome development. *The Plant Journal*, 59, 52-62.
- Madden, L., Bradley, C., Dalla Lana da Silva, F. & Paul, P. Meta-analysis of 19 years of fungicide trials for the control of Fusarium head blight of wheat. Proceedings of the 2014 National Fusarium Head Blight Forum. US Wheat & Barley Scab Initiative, East Lansing, MI, 2014. 17-18.
- Madeira, F., Park, Y. M., Lee, J., Buso, N., Gur, T., Madhusoodanan, N., Basutkar, P., Tivey, A. R. N., Potter, S. C., Finn, R. D. & Lopez, R. 2019. The EMBL-EBI search and sequence analysis tools APIs in 2019. *Nucleic acids research*.
- Maes, L., Inzé, D. & Goossens, A. 2008. Functional Specialization of the TRANSPARENT TESTA GLABRA1 Network Allows Differential Hormonal Control of Laminal and Marginal Trichome Initiation in Arabidopsis Rosette Leaves. *Plant Physiology*, 148, 1453-1464.
- Marburger, D. A., Conley, S. P., Esker, P. D., Lauer, J. G. & Ané, J. M. 2015. Yield response to crop/genotype rotations and fungicide use to manage Fusarium-related diseases. *Crop Science*, 55, 889-898.
- Marhavý, P., Montesinos, J. C., Abuzeineh, A., Van Damme, D., Vermeer, J. E., Duclercq, J., Rakusová, H., Nováková, P., Friml, J. & Geldner, N. 2016. Targeted cell elimination reveals an auxin-guided biphasic mode of lateral root initiation. *Genes & development*, 30, 471-483.
- Marin, S., Ramos, A. J., Cano-Sancho, G. & Sanchis, V. 2013. Mycotoxins: Occurrence, toxicology, and exposure assessment. *Food and Chemical Toxicology*, 60, 218-237.
- Masuda, D., Ishida, M., Yamaguchi, K., Yamaguchi, I., Kimura, M. & Nishiuchi, T. 2007. Phytotoxic effects of trichothecenes on the growth and morphology of Arabidopsis thaliana. *Journal of Experimental Botany*, 58, 1617-1626.

- McLaughlin, C., Vaughn, M., Campbell, J., Wei, C., Stafford, M. & Hansen, B. 1977. Mycotoxins in human and animal health.
- McMullen, M. P. & Stack, R. W. 2011. Fusarium head blight (scab) of small grains.
- Mesterhazy, A. 1995. Types and components of resistance to Fusarium head blight of wheat. *Plant breeding*, 114, 377-386.
- Michelmore, R. W., Paran, I. & Kesseli, R. V. 1991. Identification of markers linked to disease-resistance genes by bulked segregant analysis: a rapid method to detect markers in specific genomic regions by using segregating populations. *Proceedings of the National Academy of Sciences*, 88, 9828-9832.
- Mishra, S., Srivastava, S., Dewangan, J., Divakar, A. & Rath, S. K. 2020. Global occurrence of deoxynivalenol in food commodities and exposure risk assessment in humans in the last decade: a survey. *Critical Reviews in Food Science and Nutrition*, 60, 1346-1374.
- Morel, J.-B. & Dangl, J. L. 1997. The hypersensitive response and the induction of cell death in plants. *Cell Death & Differentiation*, 4, 671-683.
- Nazari, L., Pattori, E., Manstretta, V., Terzi, V., Morcia, C., Somma, S., Moretti, A., Ritieni, A. & Rossi, V. 2018. Effect of temperature on growth, wheat head infection, and nivalenol production by *Fusarium poae*. *Food microbiology*, 76, 83-90.
- Nguyen, T., Dehne, H. W. & Steiner, U. 2016a. Maize leaf trichomes represent an entry point of infection for *Fusarium* species. *Fungal Biology*, 120.
- Nguyen, T. T. X., Dehne, H. W. & Steiner, U. 2016b. Histopathological assessment of the infection of maize leaves by *Fusarium graminearum*, *F. proliferatum*, and *F. verticillioides*. *Fungal Biology*, 120, 1094-1104.
- Nicholson, P. 2009. *Fusarium* and *Fusarium*-cereal interactions. eLS.
- Nielsen, L., Justesen, A. & Jensen, J. 2013. *Microdochium nivale* and *Microdochium majus* in seed samples of Danish small grain cereals. *Crop protection*, 43, 192-200.
- O'Donnell, K., Ward, T. J., Geiser, D. M., Corby Kistler, H. & Aoki, T. 2004. Genealogical concordance between the mating type locus and seven other nuclear genes supports formal recognition of nine phylogenetically distinct species within the *Fusarium graminearum* clade. *Fungal Genet Biol*, 41, 600-23.
- Oerke, E. C. 2005. Crop losses to pests. *The Journal of Agricultural Science*, 144, 31-43.
- Oliveros, J. C. 2007-2015. *Venny. An interactive tool for comparing lists with Venn's diagrams.* [Online]. Available: <https://bioinfogp.cnb.csic.es/tools/venny/index.html> [Accessed].
- Olsen, O., Wang, X. & von Wettstein, D. 1993. Sodium azide mutagenesis: preferential generation of A.T-->G.C transitions in the barley Ant18 gene. *Proceedings of the National Academy of Sciences of the United States of America*, 90, 8043-8047.
- Orton, E. S., Rudd, J. J. & Brown, J. K. M. 2017. Early molecular signatures of responses of wheat to *Zymoseptoria tritici* in compatible and incompatible interactions. *Plant Pathology*, 66, 450-459.
- Overvoorde, P., Fukaki, H. & Beeckman, T. 2010. Auxin Control of Root Development. *Cold Spring Harbor Perspectives in Biology*, 2.
- Pacheco-Villalobos, D., Diaz-Moreno, S. M., van der Schuren, A., Tamaki, T., Kang, Y. H., Gujas, B., Novak, O., Jaspert, N., Li, Z. N., Wolf, S., Oecking, C., Ljung, K., Bulone, V. & Hardtke, C. S. 2016. The Effects of High Steady State Auxin Levels on Root Cell Elongation in *Brachypodium*. *Plant Cell*, 28, 1009-1024.
- Pacheco-Villalobos, D., Sankar, M., Ljung, K. & Hardtke, C. S. 2013. Disturbed Local Auxin Homeostasis Enhances Cellular Anisotropy and Reveals Alternative

- Wiring of Auxin-ethylene Crosstalk in *Brachypodium distachyon* Seminal Roots. *Plos Genetics*, 9.
- Packa, D. 1991. Cytogenetic changes in plant cells as influenced by mycotoxins. *Mycotoxin Research*, 7, 150-155.
- Pallotta, M., Warner, P., Fox, R., Kuchel, H., Jefferies, S. & Langridge, P. Marker assisted wheat breeding in the southern region of Australia. Proceedings of the 10th international wheat genetics symposium, Paestum, Italy, 2003. Istituto Sperimentale per la Cerealicoltura Roma, Italy, 789-791.
- Papatheodorou, I., Moreno, P., Manning, J., Fuentes, A. M.-P., George, N., Fexova, S., Fonseca, N. A., Füllgrabe, A., Green, M., Huang, N., Huerta, L., Iqbal, H., Jianu, M., Mohammed, S., Zhao, L., Jarnuczak, A. F., Jupp, S., Marioni, J., Meyer, K., Petryszak, R., Prada Medina, C. A., Talavera-López, C., Teichmann, S., Vizcaino, J. A. & Brazma, A. 2019. Expression Atlas update: from tissues to single cells. *Nucleic Acids Research*, 48, D77-D83.
- Parry, D. W., Jenkinson, P. & McLeod, L. 1995. Fusarium ear blight (scab) in small grain cereals—a review. *Plant Pathology*, 44, 207-238.
- Pasquet, J. C., Chaouch, S., Macadre, C., Balzergue, S., Huguet, S., Martin-Magniette, M. L., Bellvert, F., Deguercy, X., Thareau, V., Heintz, D., Saindrenan, P. & Dufresne, M. 2014. Differential gene expression and metabolomic analyses of *Brachypodium distachyon* infected by deoxynivalenol producing and non-producing strains of *Fusarium graminearum*. *Bmc Genomics*, 15.
- Pattanaik, S., Patra, B., Singh, S. K. & Yuan, L. 2014. An overview of the gene regulatory network controlling trichome development in the model plant, *Arabidopsis*. *Frontiers in Plant Science*, 5.
- Paul, P., Lipps, P., Hershman, D., McMullen, M., Draper, M. & Madden, L. 2008. Efficacy of triazole-based fungicides for Fusarium head blight and deoxynivalenol control in wheat: A multivariate meta-analysis. *Phytopathology*, 98, 999-1011.
- Peraldi, A. 2012. *Brachypodium distachyon* as a genetic model pathosystem to study resistance against fungal pathogens of small grain cereals. PhD, University of East Anglia.
- Peraldi, A. Unpublished. Infection of *Brachypodium distachyon* detached lemma with *Fusarium graminearum*. JIC.
- Peraldi, A., Beccari, G., Steed, A. & Nicholson, P. 2011. *Brachypodium distachyon*: a new pathosystem to study Fusarium head blight and other Fusarium diseases of wheat. *Bmc Plant Biology*, 11.
- Perochon, A., Jia, J. G., Kahla, A., Arunachalam, C., Scofield, S. R., Bowden, S., Wallington, E. & Doohan, F. M. 2015. TaFROG Encodes a Pooideae Orphan Protein That Interacts with SnRK1 and Enhances Resistance to the Mycotoxigenic Fungus *Fusarium graminearum*. *Plant Physiology*, 169, 2895-2906.
- Poppenberger, B., Berthiller, F., Lucyshyn, D., Sieberer, T., Schuhmacher, R., Krska, R., Kuchler, K., Glössl, J., Luschig, C. & Adam, G. 2003. Detoxification of the Fusarium Mycotoxin Deoxynivalenol by a UDP-glucosyltransferase from *Arabidopsis thaliana*. *Journal of Biological Chemistry*, 278, 47905-47914.
- Powell, D., Milton, M., A., P. & Santos, K. 2019. drpowell/degust 4.1.1. Zenodo.
- Prat, N., Guilbert, C., Prah, U., Wachter, E., Steiner, B., Langin, T., Robert, O. & Buerstmayr, H. 2017. QTL mapping of Fusarium head blight resistance in three related durum wheat populations. *Theoretical and Applied Genetics*, 130, 13-27.
- Prăvălie, R., Patriche, C., Borrelli, P., Panagos, P., Roșca, B., Dumitrașcu, M., Nita, I.-A., Săvulescu, I., Birsan, M.-V. & Bandoc, G. 2021. Arable lands under the

- pressure of multiple land degradation processes. A global perspective. *Environmental Research*, 194, 110697.
- Preger, V., Tango, N., Marchand, C., Lemaire, S. D., Carbonera, D., Di Valentin, M., Costa, A., Pupillo, P. & Trost, P. 2009. Auxin-responsive genes AIR12 code for a new family of plasma membrane b-type cytochromes specific to flowering plants. *Plant Physiol*, 150, 606-20.
- Qi, T., Song, S., Ren, Q., Wu, D., Huang, H., Chen, Y., Fan, M., Peng, W., Ren, C. & Xie, D. 2011. The Jasmonate-ZIM-Domain Proteins Interact with the WD-Repeat/bHLH/MYB Complexes to Regulate Jasmonate-Mediated Anthocyanin Accumulation and Trichome Initiation in *Arabidopsis thaliana*. *The Plant Cell*, 23, 1795-1814.
- Rawat, N., Pumphrey, M. O., Liu, S., Zhang, X., Tiwari, V. K., Ando, K., Trick, H. N., Bockus, W. W., Akhunov, E. & Anderson, J. A. 2016. Wheat Fhb1 encodes a chimeric lectin with agglutinin domains and a pore-forming toxin-like domain conferring resistance to *Fusarium* head blight. *Nature genetics*, 48, 1576-1580.
- Ream, T. S., Woods, D. P., Schwartz, C. J., Sanabria, C. P., Mahoy, J. A., Walters, E. M., Kaeppler, H. F. & Amasino, R. M. 2014. Interaction of Photoperiod and Vernalization Determines Flowering Time of *Brachypodium distachyon*. *Plant Physiology*, 164, 694-709.
- Rittenour, W. R. & Harris, S. D. 2010. An in vitro method for the analysis of infection-related morphogenesis in *Fusarium graminearum*. *Mol Plant Pathol*, 11, 361-9.
- Rocha, O., Ansari, K. & Doohan, F. M. 2005. Effects of trichothecene mycotoxins on eukaryotic cells: A review. *Food Additives & Contaminants*, 22, 369-378.
- Roppolo, D., Boeckmann, B., Pfister, A., Boutet, E., Rubio, M. C., Dénervaud-Tendon, V., Vermeer, J. E. M., Gheyselinck, J., Xenarios, I. & Geldner, N. 2014. Functional and Evolutionary Analysis of the CASPARIAN STRIP MEMBRANE DOMAIN PROTEIN Family. *Plant Physiology*, 165, 1709-1722.
- Ruijter, J. M., Ramakers, C., Hoogaars, W. M., Karlen, Y., Bakker, O., van den Hoff, M. J. & Moorman, A. F. 2009. Amplification efficiency: linking baseline and bias in the analysis of quantitative PCR data. *Nucleic Acids Res*, 37, e45.
- Santos, M. A., Gonzalez-Penades, L. & Nicholson, P. Unpublished. RNAseq dataset of DON responsive genes at 6 h and 24 h post application in root tissue of wheat variety Hobbit Sib. John Innes Centre.
- Saville, R. J., Gosman, N., Burt, C. J., Makepeace, J., Steed, A., Corbitt, M., Chandler, E., Brown, J. K., Boulton, M. I. & Nicholson, P. 2012. The 'Green Revolution' dwarfing genes play a role in disease resistance in *Triticum aestivum* and *Hordeum vulgare*. *J Exp Bot*, 63, 1271-83.
- Scarpino, V., Reyneri, A., Sulyok, M., Krska, R. & Blandino, M. 2015. Effect of fungicide application to control *Fusarium* head blight and 20 *Fusarium* and *Alternaria* mycotoxins in winter wheat (*Triticum aestivum* L.). *World Mycotoxin J*, 8, 499-510.
- Schaller, A. 2004. A cut above the rest: the regulatory function of plant proteases. *Planta*, 220, 183-197.
- Schellmann, S., Schnittger, A., Kirik, V., Wada, T., Okada, K., Beermann, A., Thumfahrt, J., Jürgens, G. & Hülskamp, M. 2002. TRIPTYCHON and CAPRICE mediate lateral inhibition during trichome and root hair patterning in *Arabidopsis*. *The EMBO journal*, 21, 5036-5046.
- Scherm, B., Balmas, V., Spanu, F., Pani, G., Delogu, G., Pasquali, M. & Migheli, Q. 2013. *Fusarium culmorum*: causal agent of foot and root rot and head blight on wheat. *Molecular Plant Pathology*, 14, 323-341.

- Schmidt, M. H. W., Vogel, A., Denton, A. K., Istace, B., Wormit, A., van de Geest, H., Bolger, M. E., Alseekh, S., Maß, J., Pfaff, C., Schurr, U., Chetelat, R., Maumus, F., Aury, J.-M., Koren, S., Fernie, A. R., Zamir, D., Bolger, A. M. & Usadel, B. 2017. De Novo Assembly of a New *Solanum pennellii* Accession Using Nanopore Sequencing. *The Plant cell*, 29, 2336-2348.
- Schneebeil, K., Mathesius, U. & Watt, M. 2015. *Brachypodium distachyon* is a pathosystem model for the study of the wheat disease *rhizoctonia* root rot. *Plant Pathology*, 64, 91-100.
- Schnittger, A., Folkers, U., Schwab, B., Jürgens, G. & Hülskamp, M. 1999. Generation of a spacing pattern: the role of TRIPTYCHON in trichome patterning in *Arabidopsis*. *The Plant Cell*, 11, 1105-1116.
- Schroeder, H. W. & Christensen, J. J. 1963. Factors affecting resistance of Wheat to scab caused by *Gibberella zeae*. *Phytopathology*, 53, 831-838.
- Schwartz, C. J., Doyle, M. R., Manzaneda, A. J., Rey, P. J., Mitchell-Olds, T. & Amasino, R. M. 2010. Natural Variation of Flowering Time and Vernalization Responsiveness in *Brachypodium distachyon*. *Bioenergy Research*, 3, 38-46.
- Sen, S. & Churchill, G. A. 2001. A Statistical Framework for Quantitative Trait Mapping. *Genetics*, 159, 371-387.
- Sibout, R., Proost, S., Hansen, B. O., Vaid, N., Giorgi, F. M., Ho-Yue-Kuang, S., Legée, F., Cézar, L., Bouchabké-Coussa, O., Soulhat, C., Provart, N., Pasha, A., Le Bris, P., Roujol, D., Hofte, H., Jamet, E., Lapierre, C., Persson, S. & Mutwil, M. 2017. Expression atlas and comparative coexpression network analyses reveal important genes involved in the formation of lignified cell wall in *Brachypodium distachyon*. *New Phytologist*, 215, 1009-1025.
- Smith, W. G. 1884. *Diseases of field and garden crops: Chiefly such as are caused by fungi*, Macmillan and Company.
- Snijders, C. 2004. Resistance in wheat to *Fusarium* infection and trichothecene formation. *Toxicology Letters*, 153, 37-46.
- Solovyev, V., Kosarev, P., Seledsov, I. & Vorobyev, D. 2006. Automatic annotation of eukaryotic genes, pseudogenes and promoters. *Genome Biol*, 7 Suppl 1, S10.1-12.
- Song, J. T., Lu, H. & Greenberg, J. T. 2004. Divergent Roles in *Arabidopsis thaliana* Development and Defense of Two Homologous Genes, ABERRANT GROWTH AND DEATH2 and AGD2-LIKE DEFENSE RESPONSE PROTEIN1, Encoding Novel Aminotransferases. *The Plant Cell*, 16, 353-366.
- Srinivasachary, Gosman, N., Steed, A., Hollins, T. W., Bayles, R., Jennings, P. & Nicholson, P. 2009. Semi-dwarfing Rht-B1 and Rht-D1 loci of wheat differ significantly in their influence on resistance to *Fusarium* head blight. *Theoretical and Applied Genetics*, 118, 695-702.
- Srinivasachary, Gosman, N., Steed, A., Simmonds, J., Leverington-Waite, M., Wang, Y., Snape, J. & Nicholson, P. 2008a. Susceptibility to *Fusarium* head blight is associated with the Rht-D1b semi-dwarfing allele in wheat. *Theor Appl Genet*, 116, 1145-53.
- Srinivasachary, Gosman, N., Steed, A., Simmonds, J., Leverington-Waite, M., Wang, Y., Snape, J. & Nicholson, P. 2008b. Susceptibility to *Fusarium* head blight is associated with the Rht-D1b semi-dwarfing allele in wheat. *Theoretical and Applied Genetics*, 116, 1145-1153.
- Stanke, M. & Morgenstern, B. 2005. AUGUSTUS: a web server for gene prediction in eukaryotes that allows user-defined constraints. *Nucleic acids research*, 33, W465-W467.
- Starkey, D. E., Ward, T. J., Aoki, T., Gale, L. R., Kistler, H. C., Geiser, D. M., Suga, H., Toth, B., Varga, J. & O'Donnell, K. 2007. Global molecular surveillance

- reveals novel *Fusarium* head blight species and trichothecene toxin diversity. *Fungal Genet Biol*, 44, 1191-204.
- Steed, A. & Nicholson, P. Unpublished. Characterising the effect of low concentrations of DON on the growth of *Arabidopsis* roots. JIC.
- Steiner, B., Buerstmayr, M., Michel, S., Schweiger, W., Lemmens, M. & Buerstmayr, H. 2017. Breeding strategies and advances in line selection for *Fusarium* head blight resistance in wheat. *Tropical Plant Pathology*, 42, 165-174.
- Steiner, B., Buerstmayr, M., Wagner, C., Danler, A., Eshonkulov, B., Ehn, M. & Buerstmayr, H. 2019. Fine-mapping of the *Fusarium* head blight resistance QTL Qfhs.ifa-5A identifies two resistance QTL associated with anther extrusion. *Theoretical and Applied Genetics*, 132, 2039-2053.
- Stephenson, P., Baker, D., Girin, T., Perez, A., Amoah, S., King, G. J. & Ostergaard, L. 2010. A rich TILLING resource for studying gene function in *Brassica rapa*. *BMC Plant Biol*, 10, 62.
- Strader, L. C., Ritchie, S., Soule, J. D., McGinnis, K. M. & Steber, C. M. 2004. Recessive-interfering mutations in the gibberellin signaling gene SLEEPY1 are rescued by overexpression of its homologue, SNEEZY. *Proc Natl Acad Sci U S A*, 101, 12771-6.
- Su, P., Zhao, L., Li, W., Zhao, J., Yan, J., Ma, X., Li, A., Wang, H. & Kong, L. 2021. Integrated metabolo-transcriptomics and functional characterization reveals that the wheat auxin receptor TIR1 negatively regulates defense against *Fusarium graminearum*. *Journal of Integrative Plant Biology*, 63, 340-352.
- Su, P. S., Guo, X. X., Fan, Y. H., Wang, L., Yu, G. H., Ge, W. Y., Zhao, L. F., Ma, X., Wu, J. J., Li, A. F., Wang, H. W. & Kong, L. R. 2018a. Application of *Brachypodium* genotypes to the analysis of type II resistance to *Fusarium* head blight (FHB). *Plant Science*, 272, 255-266.
- Su, Z., Bernardo, A., Tian, B., Chen, H., Wang, S., Ma, H., Cai, S., Liu, D., Zhang, D. & Li, T. 2019. A deletion mutation in TaHRC confers Fhb1 resistance to *Fusarium* head blight in wheat. *Nature genetics*, 51, 1099-1105.
- Su, Z., Jin, S., Zhang, D. & Bai, G. 2018b. Development and validation of diagnostic markers for Fhb1 region, a major QTL for *Fusarium* head blight resistance in wheat. *Theoretical and Applied Genetics*, 131, 2371-2380.
- Sutton, J. C. 1982. Epidemiology of wheat head blight and maize ear rot caused by *Fusarium graminearum*. *Canadian Journal of Plant Pathology*, 4, 195-209.
- Thole, V., Peraldi, A., Worland, B., Nicholson, P., Doonan, J. H. & Vain, P. 2012. T-DNA mutagenesis in *Brachypodium distachyon*. *J Exp Bot*, 63, 567-76.
- Tian, F., Bradbury, P. J., Brown, P. J., Hung, H., Sun, Q., Flint-Garcia, S., Rocheford, T. R., McMullen, M. D., Holland, J. B. & Buckler, E. S. 2011. Genome-wide association study of leaf architecture in the maize nested association mapping population. *Nat Genet*, 43, 159-162.
- Tian, Y., Tan, Y. L., Liu, N., Liao, Y. C., Sun, C. P., Wang, S. X. & Wu, A. B. 2016. Functional Agents to Biologically Control Deoxynivalenol Contamination in Cereal Grains. *Frontiers in Microbiology*, 7.
- Tillmann, M., von Tiedemann, A. & Winter, M. 2017. Crop rotation effects on incidence and diversity of *Fusarium* species colonizing stem bases and grains of winter wheat. *Journal of Plant Diseases and Protection*, 124, 121-130.
- Tominaga-Wada, R., Nukumizu, Y., Sato, S. & Wada, T. 2013. Control of plant trichome and root-hair development by a tomato (*Solanum lycopersicum*) R3 MYB transcription factor. *PLoS One*, 8, e54019.
- Trail, F. 2009. For blighted waves of grain: *Fusarium graminearum* in the postgenomics era. *Plant physiology*, 149, 103-110.
- Trick, M., Adamski, N. M., Mugford, S. G., Jiang, C.-C., Febrer, M. & Uauy, C. 2012. Combining SNP discovery from next-generation sequencing data with bulked

- segregant analysis (BSA) to fine-map genes in polyploid wheat. *BMC Plant Biology*, 12, 14.
- Tyler, L., Lee, S. J., Young, N. D., Delulio, G. A., Benavente, E., Reagon, M., Sysopha, J., Baldini, R. M., Troia, A., Hazen, S. P. & Caicedo, A. L. 2016. Population Structure in the Model Grass *Brachypodium distachyon* Is Highly Correlated with Flowering Differences across Broad Geographic Areas. *Plant Genome*, 9.
- Urban, M., Daniels, S., Mott, E. & Hammond-Kosack, K. 2002. Arabidopsis is susceptible to the cereal ear blight fungal pathogens *Fusarium graminearum* and *Fusarium culmorum*. *The Plant Journal*, 32, 961-973.
- Vadde, B. V. L., Challa, K. R., Sunkara, P., Hegde, A. S. & Nath, U. 2019. The TCP4 Transcription Factor Directly Activates TRICHOMELESS1 and Suppresses Trichome Initiation. *Plant Physiology*, 181, 1587-1599.
- Vain, P. 2011. *Brachypodium* as a model system for grass research. *Journal of Cereal Science*, 54, 1-7.
- van der Schuren, A., Voiniciuc, C., Bragg, J., Ljung, K., Vogel, J., Pauly, M. & Hardtke, C. S. 2018. Broad spectrum developmental role of *Brachypodium* AUX1. *New Phytologist*, 219, 1216-1223.
- Vogel, J. P., Tuna, M., Budak, H., Huo, N., Gu, Y. Q. & Steinwand, M. A. 2009. Development of SSR markers and analysis of diversity in Turkish populations of *Brachypodium distachyon*. *BMC Plant Biol*, 9, 88.
- Wagacha, J. M. & Muthomi, J. W. 2007. *Fusarium culmorum*: Infection process, mechanisms of mycotoxin production and their role in pathogenesis in wheat. *Crop Protection*, 26, 877-885.
- Walkowiak, S., Gao, L., Monat, C., Haberer, G., Kassa, M. T., Brinton, J., Ramirez-Gonzalez, R. H., Kolodziej, M. C., Delorean, E., Thambugala, D., Klymiuk, V., Byrns, B., Gundlach, H., Bandi, V., Siri, J. N., Nilsen, K., Aquino, C., Himmelbach, A., Copetti, D., Ban, T., Venturini, L., Bevan, M., Clavijo, B., Koo, D.-H., Ens, J., Wiebe, K., N'Diaye, A., Fritz, A. K., Gutwin, C., Fiebig, A., Fosker, C., Fu, B. X., Accinelli, G. G., Gardner, K. A., Fradgley, N., Gutierrez-Gonzalez, J., Halstead-Nussloch, G., Hatakeyama, M., Koh, C. S., Deek, J., Costamagna, A. C., Fobert, P., Heavens, D., Kanamori, H., Kawaura, K., Kobayashi, F., Krasileva, K., Kuo, T., McKenzie, N., Murata, K., Nabeka, Y., Paape, T., Padmarasu, S., Percival-Alwyn, L., Kagale, S., Scholz, U., Sese, J., Juliana, P., Singh, R., Shimizu-Inatsugi, R., Swarbreck, D., Cockram, J., Budak, H., Tameshige, T., Tanaka, T., Tsuji, H., Wright, J., Wu, J., Steuernagel, B., Small, I., Cloutier, S., Keeble-Gagnère, G., Muehlbauer, G., Tibbets, J., Nasuda, S., Melonek, J., Hucl, P. J., Sharpe, A. G., Clark, M., Legg, E., Bharti, A., Langridge, P., Hall, A., Uauy, C., Mascher, M., Krattinger, S. G., Handa, H., Shimizu, K. K., Distelfeld, A., Chalmers, K., Keller, B., Mayer, K. F. X., Poland, J., Stein, N., McCartney, C. A., Spannagl, M., Wicker, T. & Pozniak, C. J. 2020. Multiple wheat genomes reveal global variation in modern breeding. *Nature*.
- Walter, S. & Doohan, F. 2011. Transcript profiling of the phytotoxic response of wheat to the *Fusarium* mycotoxin deoxynivalenol. *Mycotoxin Research*, 27, 221-230.
- Wang, Q., Vera Buxa, S., Furch, A., Friedt, W. & Gottwald, S. 2015. Insights Into *Triticum aestivum* Seedling Root Rot Caused by *Fusarium graminearum*. *Molecular Plant-Microbe Interactions*, 28, 1288-1303.
- Wang, X., Zhang, Y., Wang, L., Pan, Z., He, S., Gao, Q., Chen, B., Gong, W. & Du, X. 2020. Casparian strip membrane domain proteins in *Gossypium arboreum*: genome-wide identification and negative regulation of lateral root growth. *BMC genomics*, 21, 1-16.

- Watanabe, S., Tsukamoto, C., Oshita, T., Yamada, T., Anai, T. & Kaga, A. 2017. Identification of quantitative trait loci for flowering time by a combination of restriction site-associated DNA sequencing and bulked segregant analysis in soybean. *Breeding science*, 67, 277-285.
- Wester, K., Digiuni, S., Geier, F., Timmer, J., Fleck, C. & Hülkamp, M. 2009. Functional diversity of R3 single-repeat genes in trichome development. *Development*, 136, 1487-1496.
- Wickham, H. 2016. *ggplot2: Elegant Graphics for Data Analysis*, Springer-Verlag New York.
- Wilson, W., Dahl, B. & Nganje, W. 2018. Economic costs of fusarium head blight, scab and deoxynivalenol. *World Mycotoxin Journal*, 11, 291-302.
- Woods, D. P., Bednarek, R., Bouche, F., Gordon, S. P., Vogel, J. P., Garvin, D. F. & Amasino, R. M. 2017a. Genetic Architecture of Flowering-Time Variation in *Brachypodium distachyon*. *Plant Physiology*, 173, 269-279.
- Woods, D. P., Ream, T. S., Bouche, F., Lee, J., Thrower, N., Wilkerson, C. & Amasino, R. M. 2017b. Establishment of a vernalization requirement in *Brachypodium distachyon* requires REPRESSOR OF VERNALIZATION1. *Proceedings of the National Academy of Sciences of the United States of America*, 114, 6623-6628.
- Xing, L., Gao, L., Chen, Q., Pei, H., Di, Z., Xiao, J., Wang, H., Ma, L., Chen, P. & Cao, A. 2018. Over-expressing a UDP-glucosyltransferase gene (Ta-UGT 3) enhances Fusarium Head Blight resistance of wheat. *Plant Growth Regulation*, 84, 561-571.
- Xu, X.-M., Parry, D., Nicholson, P., Thomsett, M., Simpson, D., Edwards, S., Cooke, B., Doohan, F., Brennan, J. & Moretti, A. 2005. Predominance and association of pathogenic fungi causing Fusarium ear blight in wheat in four European countries. *European Journal of Plant Pathology*, 112, 143-154.
- Xu, X. & Nicholson, P. 2009. Community ecology of fungal pathogens causing wheat head blight. *Annu Rev Phytopathol*, 47, 83-103.
- Yuen, G. Y. & Schoneweis, S. D. 2007. Strategies for managing Fusarium head blight and deoxynivalenol accumulation in wheat. *International journal of food microbiology*, 119, 126-130.
- Zhang, Z., Schwartz, S., Wagner, L. & Miller, W. 2000. A greedy algorithm for aligning DNA sequences. *J Comput Biol*, 7, 203-14.
- Zhong, S., Ali, S., Leng, Y., Wang, R. & Garvin, D. F. 2015. *Brachypodium distachyon*-*Cochliobolus sativus* Pathosystem is a New Model for Studying Plant-Fungal Interactions in Cereal Crops. *Phytopathology*, 105, 482-9.
- Zimmermann, R., Sakai, H. & Hochholdinger, F. 2010. The Gibberellic Acid Stimulated-Like Gene Family in Maize and Its Role in Lateral Root Development. *Plant Physiology*, 152, 356-365.

Appendix

Pot position	1	2	3	4	5	6	7	8	9	10	11	12
1	BdTR11A	Foz1	BdTR13b	Adi-10	BdTR12c	BdTR11I	Kah-6	Bd2-3	BdTR11A	Gaz-8	Adi-2	Sig2
2	Adi-4	Adi-12	Sig2	BdTR10C	Koz-3	Bd1-1	BdTR13a	Adi-12	Tek-4	BdTR11I	Adi-12	BdTR10C
3	Koz-1	BdTR5I	Bd3-1_r	Bd3-1_r	Gaz-8	Bis-1	Bd3-1_r	BdTR13n	Bd18-1	Koz-5	BdTR10d	BdTR5a
4	Bd18-1	ABR7	Gaz-8	BdTR13b	Bd2-3	Tek-4	Gaz-2	Uni2	Bd21Control	Mig3	BdTR3m	Tek-4
5	Gaz-2	Uni2	Bd2-3	Kah-1	BdTR10d	BdTR1I	Adi-2	BdTR11e	BdTR3m	BdTR5I	Per1	BdTR1I
6	Gaz-1	ABR8	Bis-1	ABR8	Adi-4	Luc1	BdTR9m	BdTR10d	ABR8	ABR7	Adi-9	Adi-15
7	Koz-5	Kah-1	ABR4	BdTR5I	BdTR3m	Adi-15	Gaz-8	BdTR2B	ABR7	BdTR2G	Kah-6	Kah-1
8	BdTR3m	Mig3	BdTR12b	BdTR11G	Jer1	ABR2	Mon3	BdTR7a	BdTR12c	Bis-1	ABR6_r	Bd3-1_r
9	BdTR7a	Bd21Control	BdTR11G	Per1	ABR6_r	ABR4	Adi-10	BdTR11I	Bd1-1	Jer1	Uni2	BdTR12c
10	BdTR10d	Koz-3	BdTR13C	BdTR12b	BdTR7a	Adi-12	Kah-5	ABR4	Bis-1	Adi-4	Bd21Control	Adi-10
11	BdTR13a	Kah-6	ABR2	BdTR2B	Kah-5	Koz-5	ABR2	Kah-1	ABR6_r	BdTR11A	BdTR11G	BdTR13n
12	Per1	BdTR2G	Bd1-1	Bd18-1	BdTR13n	BdTR5a	Jer1	Adi-15	Adi-9	BdTR2B	Luc1	Kah-5
13	BdTR11I	BdTR11e	Adi-10	Gaz-1	Adi-9	Uni2	Per1	BdTR12b	BdTR13b	BdTR13C	BdTR7a	ABR4
14	BdTR9m	BdTR12c	Jer1	BdTR13a	BdTR11e	BdTR2G	BdTR9K	Gaz-1	Adi-4	BdTR13a	BdTR12b	Koz-1
15	Bd21-3	Tek-4	Adi-15	Gaz-2	BdTR13C	Bd21-3	Bd21-3	BdTR11G	BdTR1I	Bd1-1	BdTR9K	Koz-3
16	Luc1	Mon3	BdTR1I	ABR7	BdTR9m	BdTR9K	Koz-3	BdTR10C	Sig2	ABR8	BdTR13b	Bd18-1
17	BdTR13n	Kah-5	Adi-9	Sig2	Bd21Control	Kah-6	Foz1	BdTR5a	Luc1	Gaz-1	Mon3	BdTR11e
18	BdTR5a	BdTR10C	Adi-2	Mon3	Adi-2	Koz-1	Koz-5	BdTR13C	BdTR5I	Foz1	ABR2	BdTR9m
19	BdTR2B	BdTR9K	ABR6_r	Foz1	Mig3	BdTR11A	BdTR2G	Mig3	Koz-1	Bd2-3	Gaz-2	Bd21-3

Supplementary Figure 1 Experimental design for glasshouse characterisation experiment of 54 diverse *Brachypodium distachyon* accessions. Incomplete Block Design generated using Gendex software (IBD module)

Rep1					
Tray1	Tray2	Tray3	Tray4	Tray5	Tray6
96	49	95	21	32	128
98	8	122	7	94	47
141	62	131	Bd21	0	37
65	112	44	108	17	13
106	22	89	118	121	91
5	56	9	129	125	ABR6
127	42	105	111	103	97
115	78	114	30	16	107
45	109	51	72	110	117
Bd21	Bd21	Bd21	Bd21	Bd21	Bd21
ABR6	ABR6	ABR6	ABR6	ABR6	ABR6
34	31	2	14	50	6
19	0	26	70	1	67
123	73	33	41	63	116
46	15	18	48	113	61
60	119	126	101	88	20
28	93	104	92	43	71
11	124	64	23	25	100
90	102	59	77	58	36
76	24	75	54	74	29

Rep2					
Tray1	Tray2	Tray3	Tray4	Tray5	Tray6
97	23	19	127	101	44
5	37	89	45	115	21
59	94	30	121	95	112
125	122	48	7	36	74
108	128	117	77	129	6
64	0	11	22	88	60
90	54	42	29	1	91
31	70	131	113	71	50
141	114	107	15	123	14
Bd21	Bd21	Bd21	Bd21	Bd21	Bd21
ABR6	ABR6	ABR6	ABR6	ABR6	ABR6
20	100	58	51	47	126
103	17	116	110	9	ABR6
118	8	63	67	62	65
43	105	2	93	0	109
26	46	25	75	41	119
13	16	102	33	24	104
49	76	72	61	106	32
111	78	96	Bd21	56	92
73	34	124	98	18	28

Rep3					
Tray1	Tray2	Tray3	Tray4	Tray5	Tray6
102	48	101	43	0	141
131	56	37	63	96	6
73	98	2	107	109	42
88	76	50	31	1	106
112	121	67	54	100	118
36	95	28	24	116	89
70	91	72	90	33	126
17	20	123	104	71	30
105	25	59	47	21	113
Bd21	Bd21	Bd21	Bd21	Bd21	Bd21
ABR6	ABR6	ABR6	ABR6	ABR6	ABR6
5	11	78	94	77	46
15	Bd21	0	19	129	16
60	64	110	127	65	61
125	32	97	114	58	18
92	44	124	7	122	93
117	128	22	75	49	103
29	8	111	9	26	74
41	108	14	ABR6	13	62
51	115	34	119	45	23

Supplementary Figure 2 Alpha experimental design for characterisation experiment of ABR6 x Bd21 RIL population. Experimental replicate four used the layout for Rep1. 0 = Blank

Supplementary Table 1 *Brachypodium distachyon* accessions characterised by glasshouse trial. Source ID refers to number given in The Sainsbury Laboratory collection database; Rep refers to source plant after bulking of original material ('-' were sourced directly from TSL collection). *Detailed latitude/longitude location listed in (Filiz et al., 2009), (Gordon et al., 2017).

Accession	Source ID (TSL)	Geographic origin of collection	Bulking Rep/ Source
ABR2	00563	Hérault, France	3
ABR4	00575	Arén, Huesca, Spain	4
ABR6	00588	Los Arcos, Navarra, Spain	2
ABR7	02332	Otero, Valladolid, Spain	4
ABR8	02340	Siena, Italy	-
Adi-10	00311	Adiyaman, Turkey	3
Adi-12	00323	Adiyaman, Turkey	2
Adi-15	00343	Adiyaman, Turkey	3
Adi-2	00263	Adiyaman, Turkey	3
Adi-4	00275	Adiyaman, Turkey	3
Adi-9	00305	Adiyaman, Turkey	2
Bd1-1	02251	Soma, Manisa, Turkey	4
Bd18-1	02254	Kaman, Kirşehir, Turkey	3
Bd21-3	00253	near Salakudin, Iraq	2
Bd21	00246	near Salakudin, Iraq	2
Bd2-3	02252	Iraq	4
Bd3-1	02253	Iraq	3
BdTR10C	01931	Turkey*	3
BdTR10d	01932	Turkey*	2
BdTR11A	01943	Turkey*	2
BdTR11e	01947	Turkey*	3
BdTR11G	01949	Kirklareli, Turkey*	2
BdTR11I	01951	Turkey*	1
BdTR12c	01954	Turkey*	3
BdTR13a	01955	Ankara, Turkey*	1
BdTR13b	01956	Turkey*	3
BdTR13C	01988	Ankara, Turkey*	3
BdTR13n	01998	Turkey*	3
BdTR1i	01866	Aydin, Turkey*	3
BdTR2B	01872	Turkey*	2
BdTR2G	01877	Ankara, Turkey*	3
BdTR3m	01896	Turkey*	1

Supplementary Table 2 (continued) *Brachypodium distachyon* accessions characterised by glasshouse trial. Source ID refers to number given in The Sainsbury Laboratory collection database; Rep refers to source plant after bulking of original material ('-' were sourced directly from TSL collection). *Detailed latitude/longitude location listed in (Filiz et al., 2009), (Gordon et al., 2017).

Accession	Source ID (TSL)	Geographic origin of collection	Bulking Rep/ Source
BdTR5a	01903	Turkey*	4
BdTR5l	01911	Turkey*	4
BdTR7a		Yozgat, Turkey*	-
BdTR9K	01927	Eskişehir, Turkey*	2
BdTR9m	01928	Turkey*	2
Bis-1	00366	Bismil, Turkey	4
Foz1	00683	Foz de Lumbier, Navarra, Spain	1
Gaz-1	00372	Gaziantep, Turkey	4
Gaz-2	00377	Gaziantep, Turkey	4
Gaz-8	00413	Gaziantep, Turkey	4
Jer1	00695	Huesca, Spain	2
Kah-1	00425	Kahta, Turkey	3
Kah-5	00450	Kahta, Turkey	-
Kah-6	00455	Kahta, Turkey	2
Koz-1	00461	Kozluk, Turkey	4
Koz-3	00475	Kozluk, Turkey	3
Koz-5	00485	Kozluk, Turkey	4
Luc1	00701	Ermita de Santa Lucía, Berdún, Huesca, Spain	3
Mig3	00707	Huesca, Spain	4
Mon3	00725	Zaragoza, Spain	4
Per1	00743	Navarra, Spain	2
Sig2	00779	Zaragoza, Spain	4
Uni2	00791	Huesca, Spain	2

Supplementary Table 2 Standard compost mixes used by Horticultural Services at the John Innes centre, used in a 1:1 ratio in the preparation of potting medium for *Brachypodium distachyon*

Cereal mix	Peat and Sand
40 % Medium Grade Peat	85 % Fine Peat
40 % Sterilised Soil	15 % Grit
20 % Horticultural Grit	2.7 kg/m ³ Osmocote 3-4 months
1.3 kg/m ³ PG Mix 14-16-18 + Te Base Fertiliser	Wetting Agent
1 kg/m ³ Osmocote Mini 16-8-11 2mg + Te 0.02 % B	4 kg/m ³ Maglime
Wetting Agent	1 kg PG Mix
3 kg/m ³ Maglime	
300 g/m ³ Exemptor	

Supplementary Table 3 F-test statistics for qPCR expression for trichome candidate genes fine mapped on Bd4L

Gene	Tissue	F-value
Bradi4g22637	Leaves	0.331
	Head	0.503
Bradi4g22641	Leaves	0.148
	Head	0.073
Bradi4g22645	Leaves	0.132
	Head	0.035
Bradi4g22650	Leaves	n/a
	Head	0.022
Bradi4g22650	Leaves	0.728
	Head	0.146

Supplementary Table 4 Primer sequences for KASP markers used for initial mapping of DON sensitivity trait to chromosome arm by single marker association

Chromosome arm	Marker	Identifier	Primer Sequence 5'-3'	T _m
Bd1S	Bd1sD3477318	Bd1sD3477318F1	GAAGGTCGGAGTCAACGGATTCAGTCTCTCGGAAGTGC	59.8
		Bd1sD3477318F2	GAAGGTGACCAAGTTCATGCTTCAGTCTCTCGGAAGTGG	59.6
		Bd1sD3477318R	ACTCATCCCTATGAACGCA	61.2
	Bd1sP25660244	Bd1sP25660244F1	GAAGGTCGGAGTCAACGGATTAAGCATCATGGTCCCGG	66.3
		Bd1sP25660244F2	GAAGGTGACCAAGTTCATGCTAAAGCATCATGGTCCCGA	64.7
		Bd1sP25660244R	CCTGTCTGAGCTCCTGGA	62.4
Bd1L	Bd1L 70039898	Bd1L70039898F1	GAAGGTCGGAGTCAACGGATTGCGACGTAGATCCACCCTC	65.1
		Bd1L70039898F2	GAAGGTGACCAAGTTCATGCTGCGACGTAGATCCACCCTT	64.4
		Bd1L70039898R	TCCATCCAGAGAATCGGC	64.4
Bd2S	Bd2SD3043237	Bd2SD3043237F1	GAAGGTCGGAGTCAACGGATTTGTGGCTGTGGAAGTGGC	66.8
		Bd2SD3043237F2	GAAGGTGACCAAGTTCATGCTTGTGGCTGTGGAAGTGGT	63.6
		Bd2SD3043237R	CCCTACTACATGCCCTCTGC	63.9
Bd2L	Bd2LP39624921	Bd2LP39624921F1	GAAGGTCGGAGTCAACGGATTTGTCCCAGATGGATCTGT	59.5
		Bd2LP39624921F2	GAAGGTGACCAAGTTCATGCTTGTCCCAGATGGATCTGC	63
		Bd2LP39624921R	ATCGTGTGGATGGAGTTG	60.1
Bd3S	Bd3SD25709812	Bd3SD25709812F1	GAAGGTCGGAGTCAACGGATTCACCTGTGGCTCGAAGGA	65.8
		Bd3SD25709813F2	GAAGGTGACCAAGTTCATGCTCACCTGTGGCTCGAAGGC	67.6
		Bd3SD25709814R	TGCTACATGGGTCATCGC	64
Bd3L	Bd3LP36863202	Bd3LP36863202F1	GAAGGTCGGAGTCAACGGATTGGTGCAGGCTCTGGAGAG	64.5
		Bd3LP36863202F2	GAAGGTGACCAAGTTCATGCTGGTGCAGGCTCTGGAGAA	64.8
		Bd3LP36863202R	TCAAGCAGATCGACAGTTGG	64.5
	Bd3LD51834867	Bd3LD51834867F1	GAAGGTCGGAGTCAACGGATTCTCAAAGGAACTGGACC	60.2
		Bd3LD51834867F2	GAAGGTGACCAAGTTCATGCTCTCAAAGGAACTGGACA	59.3
		Bd3LD51834867R	CCAGCTTGACTCTTCGAG	59.4

Supplementary Table 4 Continued Primer sequences for KASP markers used for initial mapping of DON sensitivity trait to chromosome arm by single marker association

Chromosome arm	Marker	Identifier	Primer Sequence 5'-3'	T _m
Bd4(S)	Bd4SD2701106	Bd4SD2701106F1	GAAGGTCGGAGTCAACGGATTTTGCTTCTCTTCGCCCAT	64
		Bd4SD2701106F2	GAAGGTGACCAAGTTCATGCTTTGCTTCTCTTCGCCCAC	64.7
		Bd4SD2701106R	TTTATGGGCCCCAAATGTAA	64
Bd4(S)	Bd4SP10040253	Bd4SP10040253F1	GAAGGTCGGAGTCAACGGATTGAACAGGTCTGGACTTCA	56.6
		Bd4SP10040253F2	GAAGGTGACCAAGTTCATGCTGAACAGGTCTGGACTTCG	58.9
		Bd4SP10040253R	CTTACCCACTCAACTGAATG	57.7
Bd4(L)	Bd4LD43365030	Bd4LD43365030F1	GAAGGTCGGAGTCAACGGATTTTAATGACGCTCCTTGTC	56.8
		Bd4LD43365030F2	GAAGGTGACCAAGTTCATGCTTTAATGACGCTCCTTGTT	56.3
		Bd4LD43365030R	GAGCTCCACAGTTGCAAC	60.2
Bd5(S)	Bd5SP2052726	Bd5SP2052726F1	GAAGGTCGGAGTCAACGGATTGCATAATGCATTGGCGAG	63.3
		Bd5SP2052726F2	GAAGGTGACCAAGTTCATGCTGCATAATGCATTGGCGAA	63.7
		Bd5SP2052726R	GTCCCACTGCCTGTCAGAAT	64.6
Bd5(L)	Bd5LP17775550	Bd5LP17775550F1	GAAGGTCGGAGTCAACGGATTGGAACAGCGAACCTTCAG	61.6
		Bd5LP17775550F2	GAAGGTGACCAAGTTCATGCTGGAACAGCGAACCTTCAC	61.4
		Bd5LP17775550R	GCCTGCATTATTGCTTCG	62.4
	Bd5LD25964048	Bd5LD25964048F1	GAAGGTCGGAGTCAACGGATTTTAGAGCGACTCCAATGA	57.5
		Bd5LD25964048F2	GAAGGTGACCAAGTTCATGCTTTAGAGCGACTCCAATGG	59.5
		Bd5LD25964048R	AAGGTGTGGTTGGATGAAG	60.5

Supplementary Table 5 Primer sequences for KASP markers used for mapping of DON sensitivity trait on Bd1L

Bd1L marker position	Identifier	Primer Sequence 5'-3'	T _m
Bd1L 50961826	Bd1L50961826F1	GAAGGTCGGAGTCAACGGATTTACAAAGCCGCAACAAG	64.2
	Bd1L50961826F2	GAAGGTGACCAAGTTCATGCTTCACAAAGCCGCAACAAT	63.4
	Bd1L50961826R	GCAAATATGCCAGGAGTCGT	64.3
Bd1L 63558055	Bd1L63558055F1	GAAGGTCGGAGTCAACGGATTGGGACAGGATCGTCCTCC	65.1
	Bd1L63558055F2	GAAGGTGACCAAGTTCATGCTGGGACAGGATCGTCCTCG	66.3
	Bd1L63558055R	TACGCGAACAAGTCGTCTGA	65
Bd1L 66077182	Bd1L66077182F1	GAAGGTCGGAGTCAACGGATTTTGCCTGGAACCTGTAATAGA	61.5
	Bd1L66077182F2	GAAGGTGACCAAGTTCATGCTTTGCCTGGAACCTGTAATAGG	63.1
	Bd1L66077182R	GCTCCTCCCATCGATTTTC	62.7
Bd1L 67231892	Bd1L67231892F1	GAAGGTCGGAGTCAACGGATTGCTACGCTGTACGTTCCAATAA	63.2
	Bd1L67231892F2	GAAGGTGACCAAGTTCATGCTGCTACGCTGTACGTTCCAATAC	62.8
	Bd1L67231892R2	ATACCATTTCGAGAACAGGGAG	62.3
Bd1L 67755382	Bd1L67755382F1	GAAGGTCGGAGTCAACGGATTGGAGTGGTCATAACTCGTGCA	65.4
	Bd1L67755382F2	GAAGGTGACCAAGTTCATGCTGGAGTGGTCATAACTCGTGCG	67.1
	Bd1L67755382R1	CAGGTTCACTGCTTTGCTTG	64
Bd1L 68322255	Bd1L68322255R1	GAAGGTCGGAGTCAACGGATTGCAATTTGACATCGGCCAGT	67.5
	Bd1L68322255R2	GAAGGTGACCAAGTTCATGCTGCAATTTGACATCGGCCAGA	68.6
	Bd1L68322255F1	TTTGGTGTCCGTCCCTGC	67.8
Bd1L 68481897	Bd1L68481897F1	GAAGGTCGGAGTCAACGGATTGCATTCACACCAACCAAAGTA	62.8
	Bd1L68481897F2	GAAGGTGACCAAGTTCATGCTGCATTCACACCAACCAAAGTG	65.7
	Bd1L68481897R1	CTGCTTCAGAGAGTGTCCC	60.7
Bd1L 68688411	Bd1L68688411F1	GAAGGTCGGAGTCAACGGATTGGACGGTGCATTAGACTAAAT	60
	Bd1L68688411F2	GAAGGTGACCAAGTTCATGCTGGACGGTGCATTAGACTAAAC	60.5
	Bd1L68688411R	GGACTCCGAAAGAAGTATGG	60.6

Supplementary Table 5 Continued Primer sequences for KASP markers used for mapping of DON sensitivity trait on Bd1L

Bd1L marker position	Identifier	Primer Sequence 5'-3'	T _m
Bd1L 68992730	Bd1L68992730F1	GAAGGTCGGAGTCAACGGATTTTGACACGATGCACTCGTAAC	64.2
	Bd1L68992730F2	GAAGGTGACCAAGTTCATGCTTTGACACGATGCACTCGTAAT	63.5
	Bd1L68992730R1	TGCAGGATTCTTGTGCTCTG	64.7
Bd1L 69118233	Bd1L69118233F1	GAAGGTCGGAGTCAACGGATTTTCCAGTGTAGCAGCCTCTG	63.7
	Bd1L69118233F2	GAAGGTGACCAAGTTCATGCTTTCCAGTGTAGCAGCCTCTC	62.7
	Bd1L69118233R1	ACCACGGAAGAAAGGAACTC	62.5
Bd1L 69245412	Bd1L69245412F1	GAAGGTCGGAGTCAACGGATTAACGTCCCCGACTTCTGC	65.8
	Bd1L69245412F2	GAAGGTGACCAAGTTCATGCTAACGTCCCCGACTTCTGG	65.6
	Bd1L69245412R	GTGCACCAATCGCTTGATAA	64
Bd1L 70039898	Bd1L70039898F1	GAAGGTCGGAGTCAACGGATTGCGACGTAGATCCACCCTC	65.1
	Bd1L70039898F2	GAAGGTGACCAAGTTCATGCTGCGACGTAGATCCACCCTT	64.4
	Bd1L70039898R	TCCATCCAGAGAATCGGC	64.4
Bd1L 70410887	Bd1L70410887F1	GAAGGTCGGAGTCAACGGATTCCAGCAATCACGACCTGTAAC	64.8
	Bd1L70410887F2	GAAGGTGACCAAGTTCATGCTCCAGCAATCACGACCTGTAAT	64.2
	Bd1L70410887R	GCTGGACAGCTCTCTTCATCT	63.1
Bd1L 70589328	Bd1L70589328F1	GAAGGTCGGAGTCAACGGATTGTCCATAGTATACTCCCTCCA	57.6
	Bd1L70589328F2	GAAGGTGACCAAGTTCATGCTGTCCATAGTATACTCCCTCCG	59.5
	Bd1L70589328R1	TGACTCAAATTTGCCCAACA	64.5
Bd1L 70657141	Bd1L70657141F1	GAAGGTCGGAGTCAACGGATTGCGGTGAACTGATATTTGTT	59.6
	Bd1L70657141F2	GAAGGTGACCAAGTTCATGCTGCGGTGAACTGATATTTGTG	61.1
	Bd1L70657141R	AAATCGCTTTGTGGCAAT	61.2
Bd1L 70689962	Bd1L70689962F1	GAAGGTCGGAGTCAACGGATTCACACCAAGTAGAGAAATGAA	57.4
	Bd1L70689962F2	GAAGGTGACCAAGTTCATGCTCACACCAAGTAGAGAAATGAG	57
	Bd1L70689962R1	GATCAAGAAAGGGAATGGA	59.6

Supplementary Table 5 Continued Primer sequences for KASP markers used for mapping of DON sensitivity trait on Bd1L

Bd1L marker position	Identifier	Primer Sequence 5'-3'	T _m
Bd1L 70875643	Bd1L70875643F1	GAAGGTCGGAGTCAACGGATTCTCCCAAGTTGCTGGATTGT	64.4
	Bd1L70875643F2	GAAGGTGACCAAGTTCATGCTCTCCCAAGTTGCTGGATTGC	67.2
	Bd1L70875643R1	CCGTGCCTCCGATCCATA	67.5
Bd1L 70957617	Bd1L70957617F1	GAAGGTCGGAGTCAACGGATTGGAAAAATCAGCCCACCA	64
	Bd1L70957617F2	GAAGGTGACCAAGTTCATGCTGGAAAAATCAGCCCACCG	65.8
	Bd1L70957617R	CTCTGCCGATTGGTCTTCTC	64.3
Bd1LD 71418888	Bd1L71418888F1	GAAGGTCGGAGTCAACGGATTTCCATGCTTGTGACATGGTG	66.3
	Bd1L71418888F2	GAAGGTGACCAAGTTCATGCTTCCATGCTTGTGACATGGTT	64.6
	Bd1L71418888R	CTCCATATAAAGCATGGCACT	61
Bd1L 72052958	Bd1L72052958F1	GAAGGTCGGAGTCAACGGATTGCCCTAATAATGCCCGCTA	64
	Bd1L72052958F2	GAAGGTGACCAAGTTCATGCTGCCCTAATAATGCCCGCTG	66.7
	Bd1L72052958R	CGACCTGTGAAGCTTGTTCTC	64.3
Bd1L 72672681	Bd1L72672681F1	GAAGGTCGGAGTCAACGGATTGGTTGTCTAGAGTACGGCGTA	61.2
	Bd1L72672681F2	GAAGGTGACCAAGTTCATGCT GGTTGTCTAGAGTACGGCGTG	64
	Bd1L72672681R	ACTGAACCCGTCGTCAAAAC	64.3
Bd1L 73243490	Bd1L73243490F1	GAAGGTCGGAGTCAACGGATTGGGGCTGAATGCAAAGCT	65.7
	Bd1L73243490F2	GAAGGTGACCAAGTTCATGCTGGGGCTGAATGCAAAGCA	67.7
	Bd1L73243490R	GAAGAACAGCAACTCACCGTT	63.6
Bd1L 74037836	Bd1L74037836F1	GAAGGTCGGAGTCAACGGATTTGATCGGACGGCTCTCA	65.1
	Bd1L74037836F2	GAAGGTGACCAAGTTCATGCTTTGATCGGACGGCTCTCT	64.2
	Bd1L74037836R	AGCCAGTGGGGTCATGTTAG	64.3

Supplementary Table 6 KASP primers for fine-mapping of BSA Bd1L peak associated with DON sensitivity in Bd2-3xBd21 F7 high-confidence RILs

Bd1L marker position	Identifier	Primer Sequence 5'-3'	T _m
Bd1L_69245412	Bd1_69316550_F1	GAAGGTCGGAGTCAACGGATTTTCTCTGAGTTGCCAGATTCT	61.1
	Bd1_69316550_F2	GAAGGTGACCAAGTTCATGCTTTCTCTGAGTTGCCAGATTCC	63.7
	Bd1_69316550_R	CCCACCGGTGTTGTAAATA	62.4
Bd1L_69674361	Bd1_69674361_F1	GAAGGTCGGAGTCAACGGATTGCTTTGCGGATAGATGGC	63.8
	Bd1_69674361_F2	GAAGGTGACCAAGTTCATGCTGCTTTGCGGATAGATGGT	60.8
	Bd1_69674361_R	ATGGTACAGGCTGCCTACTG	62.2
Bd1L_69696725	Bd1L_69696725_F1	GAAGGTCGGAGTCAACGGATTCCTCAGCAGCACAAAGC	61.6
	Bd1L_69696725_F2	GAAGGTGACCAAGTTCATGCTGCACTCAGCAGCACAAAGT	62.4
	Bd1L_69696725_R	CTTGGCTACCAATTAACCCT	60
Bd1L_69718309	Bd1L_69718309_F1	GAAGGTCGGAGTCAACGGATTTTAATACTTGGACGCCATACC	60.7
	Bd1L_69718309_F2	GAAGGTGACCAAGTTCATGCTTTAATACTTGGACGCCATACA	60
	Bd1L_69718309_R	TAGGATTCTGGACAAACGAT	59.1
Bd1L_69743518	Bd1L69743518_F1	GAAGGTCGGAGTCAACGGATTATATATGCTGGGACGAAGGAA	62.6
	Bd1L69743518_F2	GAAGGTGACCAAGTTCATGCTATATATGCTGGGACGAAGGAC	62.1
	Bd1L69743518_R	GAGTGCCCTGTAGGTTAGGC	63.0
Bd1L_69756524	Bd1L_69756524_F1	GAAGGTCGGAGTCAACGGATTTGGATGATTACTAGAGGTGGC	61
	Bd1L_69756524_F2	GAAGGTGACCAAGTTCATGCTTGGATGATTACTAGAGGTGGT	58.1
	Bd1L_69756524_R	CTCCGGTGAATAGAGTTACAC	58.3
Bd1L_69775755	Bd1_69775755_F1	GAAGGTCGGAGTCAACGGATTTTATTGGTCCACTAAACGCCG	65.9
	Bd1_69775755_F2	GAAGGTGACCAAGTTCATGCTTTATTGGTCCACTAAACGCCA	64.4
	Bd1_69775755_R	CTTGGAGTGCATACGCAAGT	63.3

Supplementary Table 7 DON induced phenotypes of Bd2-3 x Bd21 RILs

RIL	10uM DON	20uM DON
1	Bd21	Intermediate
3	Intermediate	Bd2-3
4	Bd2-3	Intermediate
5	Bd2-3	Bd21
7	Bd2-3	Bd2-3
9	Bd2-3	Bd2-3
10	Bd21	Intermediate
11	Bd21	Bd2-3
12	Bd21	Intermediate
13	Intermediate	Bd21
14	Intermediate	Bd21
15	Intermediate	Intermediate
16	Bd21	Bd2-3
17	Bd2-3	Bd2-3
18	Bd2-3	Bd2-3
19	Bd21	Bd2-3
20	Bd21	Intermediate
21	Bd2-3	Bd2-3
22	Bd21	Bd21
23	Bd21	Bd21
24	Bd21	Intermediate
25	Bd2-3	Intermediate
26	Bd21	Bd21
27	Bd21	Bd21
28	Bd21	Intermediate
29	Bd21	Bd2-3
30	*	Bd2-3
31	*	Bd2-3
32	*	Bd2-3
34	*	Intermediate
35	Bd21	Intermediate
36	Bd2-3	Bd2-3
37	*	Bd2-3
38	Bd21	Bd2-3
39	Bd21	Intermediate
40	Intermediate	Bd2-3
41	Bd21	Bd21
42	Bd2-3	Bd2-3
43	Bd21	Bd2-3

Supplementary Table 7 continued DON induced phenotypes of Bd2-3 x Bd21 RILs

RIL	10uM DON	20uM DON
44	Bd21	Intermediate
45	*	*
46	Bd21	Bd2-3
47	Bd2-3	Bd2-3
48	Intermediate	Intermediate
49	Bd21	Bd2-3
50	Bd2-3	Bd2-3
51	Bd21	Bd21
52	Bd2-3	Bd2-3
53	Bd2-3	Bd21
54	*	Bd21
55	*	Bd2-3
56	Bd21	Bd2-3
57	Bd21	Intermediate
58	Bd21	Bd2-3
59	Intermediate	Intermediate
60	Bd21	Bd2-3
61	Bd21	Bd2-3
62	*	Bd2-3
63	Bd21	Bd2-3
64	Bd21	Bd2-3
65	Bd2-3	Intermediate
67	Bd21	Intermediate
68	Bd2-3	Intermediate
70	Bd21	Bd2-3
71	Bd2-3	Bd2-3
73	Bd2-3	Bd2-3
75	*	Bd2-3
76	Bd2-3	Bd2-3
77	Bd21	Bd2-3
78	Intermediate	Bd2-3
79	Bd21	Bd21
80	Bd21	Intermediate
81	Intermediate	Bd2-3
82	Bd2-3	Bd2-3
83	Bd2-3	Bd2-3
85	Bd2-3	Bd2-3
86	Bd21	Intermediate
88	Intermediate	Bd21

Supplementary Table 7 continued DON induced phenotypes of Bd2-3 x Bd21 RILs

RIL	10uM DON	20uM DON
89	Bd21	Intermediate
90	Bd21	Bd2-3
91	Bd21	Bd2-3
92	Bd2-3	Bd2-3
93	Bd2-3	Bd2-3
94	Bd2-3	Bd2-3
96	Bd2-3	Bd2-3
97	Bd21	Bd2-3
98	Intermediate	Bd2-3
99	Intermediate	Bd2-3
100	Bd21	Bd21
101	Bd21	Intermediate
102	Bd2-3	Bd2-3
104	Bd21	Intermediate
105	Bd2-3	Bd2-3
107	Bd21	Bd21
108	Bd21	Bd21
109	Bd21	Bd21
111	Bd21	Intermediate
112	Bd21	Intermediate
113	Intermediate	Bd2-3
114	Bd21	Intermediate
115	Bd2-3	Bd2-3
116	Bd21	Bd21
117	Bd21	Bd21
118	Bd2-3	Bd21
119	Bd2-3	Bd21
120	Bd2-3	Bd2-3
121	Bd21	Bd2-3
122	Bd2-3	Bd2-3
123	Intermediate	Bd2-3
124	Bd21	Bd21
125	Bd21	Bd21
126	Bd21	Bd21
127	Bd21	Bd21
128	Bd21	Bd21
129	Bd21	Bd21
130	Bd21	Bd21

Supplementary Table 7 continued DON induced phenotypes of Bd2-3 x Bd21 RILs

RIL	10uM DON	20uM DON
131	Bd21	Bd21
132	Bd21	Bd21
133	*	Bd21
134	Bd21	Bd21
136	Bd2-3	Bd21
137	Bd2-3	Intermediate
138	*	Bd2-3
139	Intermediate	Intermediate
140	Bd21	Bd2-3
142	Bd21	Bd21
144	Bd2-3	Bd21
145	Bd2-3	Intermediate
146	Bd21	Bd21
147	Bd2-3	Bd2-3
148	Intermediate	Intermediate
149	Bd21	Bd21
150	Bd2-3	Intermediate
151	Intermediate	Bd2-3
152	Intermediate	Bd21
153	Bd21	Bd2-3
154	Bd2-3	Bd2-3
155	Bd21	Bd21
156	Bd21	Bd21
157	Bd2-3	Bd2-3
158	Bd21	Bd21
159	Bd2-3	Bd2-3
161	Bd21	Intermediate
162	Bd21	Bd21
163	Bd2-3	Intermediate
164	Bd21	Intermediate
165	Bd21	Intermediate
166	Intermediate	Intermediate
167	*	Intermediate
169	Bd2-3	Bd2-3
171	Bd2-3	Bd21
172	Intermediate	Bd21
173	Bd21	Bd21